ZAE BAYERN

Technische Universität München

Sononucleation of Inorganic Phase Change Materials

Dissertation
von
Eva Günther

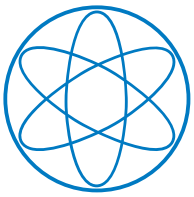

Physik-Department

TECHNISCHE UNIVERSITÄT MÜNCHEN

Lehrstuhl E19, Physik-Department
Bayerisches Zentrum für Angewandte Energieforschung e. V.

Sononucleation of inorganic phase change materials

Eva Doris Günther

Vollständiger Abdruck der von der Fakultät für Physik der Technischen Universität München zur Erlangung des akademischen Grades eines

Doktors der Naturwissenschaften (Dr. rer. nat.)

genehmigten Dissertation.

Vorsitzender:

Univ.-Prof. Dr. Martin Zacharias

Prüfer der Dissertation:

1. Univ.-Prof. Dr. Ulrich Stimming
2. Univ.-Prof. Dr. Wolfgang Voigt, Technische Universität Bergakademie Freiberg

Die Dissertation wurde am 25.08.2009 bei der Technischen Universität München eingereicht und durch die Fakultät für Physik am 20.01.2011 angenommen.

Abstract – Kurzfassung

Abstract

Many inorganic phase change materials, and particularly salt hydrates, show strong subcooling, which has negative effects on their performance as heat or cold storage materials. In this work, a suggested reduction of subcooling by ultrasonic treatment ("sononucleation") was investigated. The nucleation temperature as function of pressure was experimentally quantified up to 800 MPa for three salt hydrates. Various experiments showed that sononucleation is an effective, robust and reliable technique for solidifying water, but ineffective for solidifying salt hydrates. Contrary to what is proposed in literature, it is shown that peak pressures during cavitation in the ultrasonic field cannot be made responsible for sononucleation. Instead, sononucleation could be explained by a surface mechanism, which is effective in pure substances or solutions, but not in salt hydrates.

Kurzfassung

Viele anorganische Phasenwechselmaterialien, insbesondere Salyhydrate, zeigen deutliche Unterkühlung. Unterkühlung verzögert die Kristallisation und behindert den Einsatz der Materialien als Energiespeichermedien. In dieser Arbeit wurde die Auslösung der Kristallisation mit Hilfe von Ultraschall (Sononukleation) untersucht. Die Nukleationsdruckkurve $T_n(p)$ der Salzhydrate wurde experimentell im Bereich bis 800 MPa quantifiziert. Ultraschall wurde im Experiment als effektive und robuste Nukleationsmethode für Wasser bestätigt, aber als wirkungslos für die Salzhydrate befunden. Es wurde gezeigt, dass die durch Kavitation im Ultraschallfeld erzeugte Druckspitzen die Sononukleation im Wasser nicht auslösen können. Ein Oberflächenmechanismus kann aber die experimentellen Beobachtungen in den verschiedenen Stoffsystemen zufriedenstellend erklären.

Contents

1. Background and motivation

In this chapter, the background and motivation of this work is presented. First, thermal energy storage as an important technology in the energy supply and demand system is introduced. The advantage of latent heat storage compared to sensible heat storage is explained next. Then, materials used as latent heat storage media are introduced with their specific advantages and limitations. In particular, the problem of subcooling and nucleation in inorganic phase change materials is presented, and the need for new solutions is demonstrated.

1.1. Thermal energy storage (TES)

Energy storage is a main approach to manage mismatch between power demand and supply. The storage of energy in form of heat or cold is called *thermal energy storage*. Although other forms of energy storage such as electro-chemical (e.g. in batteries), electrical (e.g. in capacitors) or potential (e.g. in reservoirs for hydropower plants) are more widely-used and well-known today, thermal energy storage is an important technology and a key concept in energy efficient systems.

1.1.1. Relevance of TES

From one perspective, energy storage is a very interesting technology for conventional power generation. An illustration is given in figure 1.1a. To provide a varying power supply in an energy infrastructure without storages, either the loads of power plants are varied, or whole power plants are switched on and off. In general, power plants running in partial load have lower efficiencies than when running in full load. For plants running on fossil fuel, a lower efficiency is equivalent to a higher emission of the greenhouse gas CO_2 per generated kWh. Energy from power plants which are idle most of the time and running only during peak hours is very expensive due to high relative investment costs. In countries like Japan, off-peak power is cheaper by up to a factor of five when compared to peak power [1]. If peaks in the energy demand, like for example the large cooling load during hot hours of the day, are satisfied from a storage, the time profile of power generation can be smoothed and the peak in power generation can be significantly reduced.

From another perspective, energy storage is used to adapt a given energy supply to a different demand curve, as sketched in figure 1.1b. A good example is solar thermal power, where the primary power supply is highly fluctuating. With the help of storage

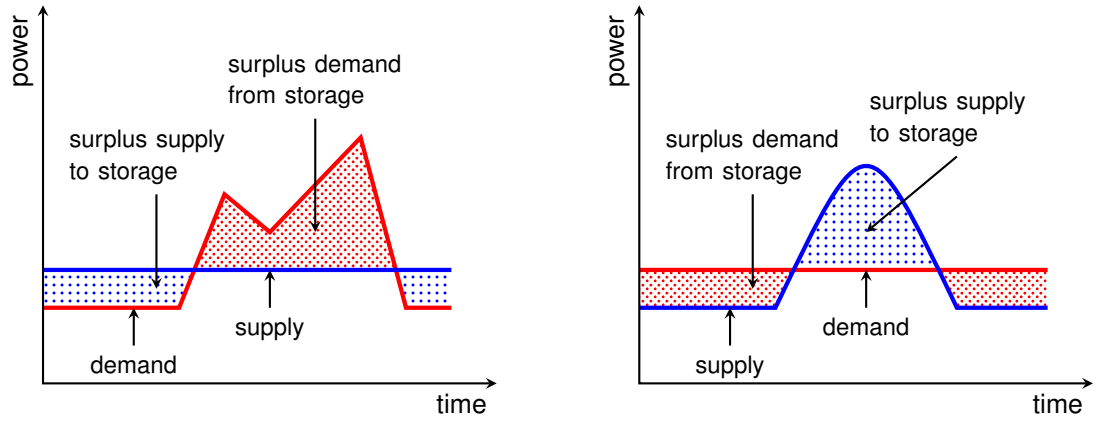

(a) supply management **(b)** demand management

Figure 1.1.: Storage technology is used to manage mismatch between demand and supply.

technology, the supply can be adapted to a more continuous demand.

With the help of thermal energy storage and peak-shifting, energy efficiency in conventional technologies can be greatly improved, and renewable energy sources can be used [2]. While peak shifting is a general storage topic, a more specifically thermal energy storage topic is the use of waste heat. Heat is a by-product of all irreversible energy conversions. In German energy production, the losses sum up to about 45% of the energy delivered to the consumers, as shown in figure 1.2.

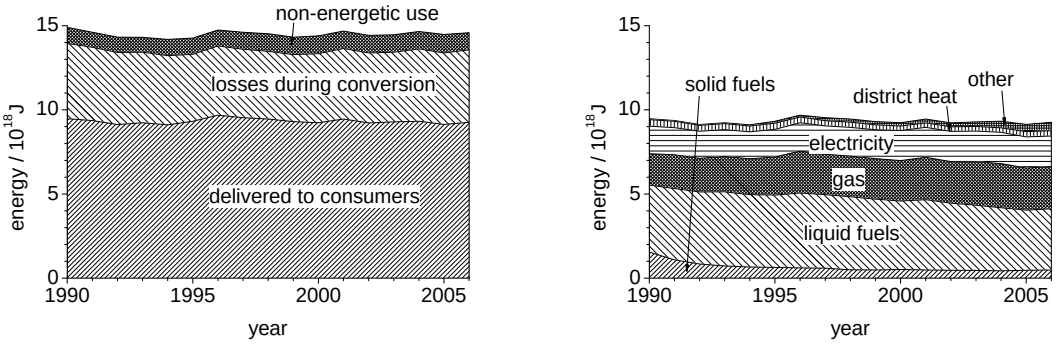

(a) **(b)**

Figure 1.2.: Amount of primary energy (a) and forms of secondary energy as delivered to the consumer (b). Graphs based on data for Germany [3].

While the main amount of energy is transported via the electric grid or directly delivered as fuel and gas as shown in figure 1.2b, the final use of energy is often thermal. The demand for heat covers about two thirds of the total energy demand in Germany, as shown in figure 1.3b.

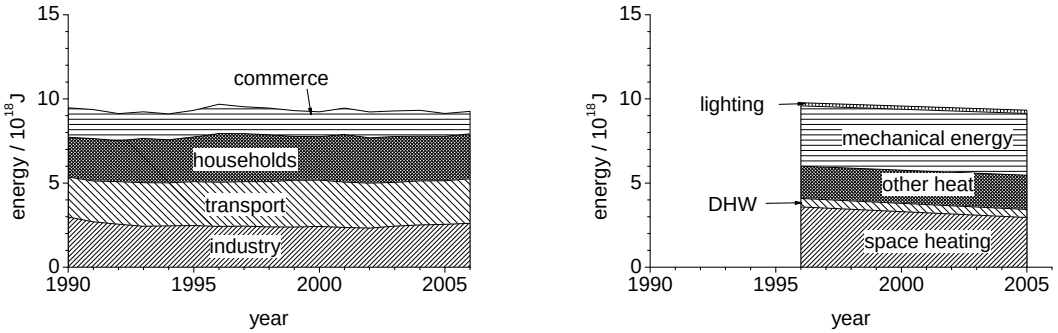

Figure 1.3.: Energy distribution to the four sectors (a) and use of energy by application (b) [DHW: domestic hot water]. Graphs based on data for Germany [3].

Generation of heat by combustion of fossil fuels could be reduced by a great extend if more "waste" heat was used. For this efficient and sustainable use of energy, thermal energy storage is a key technology. Comprehensive overviews of various TES technologies and applications are given in literature [4, 5].

In the last years with rising fuel costs and augmented awareness of global warming, thermal energy storage as a tool to increase efficiency has gained significant interest. Media covering and public awareness has increased, and public funding has started to explicitly support thermal energy storage. In the 7th research framework of the European Union, out of a 32 billion euros budget for research funding in the "collaborative projects" program, 2.3 billion euros are reserved for energy research. For example, the program "Renewables for heating and cooling" aims to support "technologies and devices (including storage technologies) to increase the potential of active and passive heating and cooling from renewable energy sources" [6]. Compared to other storage technologies such as thermo-chemical or hydrogen storage, thermal storage is rather well developed. Sensible heat storage is already implemented in a large quantity today, ice storage is commercial and widely used [7, 8, 9], while latent heat storage using different storage media than water/ice is basically found in the prototype state and in demonstration plants, except for a few products.

1.1.2. Sensible and latent heat storage

The most common storage technology for thermal storage today is *sensible heat storage*. To charge the storage, the storage material is heated, and to discharge the storage, it is cooled. The temperature of the storage medium is a measure for the charge state of the storage: the stored heat can be "sensed" directly, hence the name "sensible heat" storage. The most common storage materials are water, concrete, gravel and soil.

Sensible heat storage is a well-known and established technology. However, in some

situations, sensible heat storage is not an ideal solution. If only a small temperature span is available between charging and discharging temperatures, the storage capacity is not very high. In such a case, latent heat storage is a good alternative. In the following examplary calculation illustrated by figure 1.4, the storage capacity of sensible heat storage is compared to that of latent heat storage.

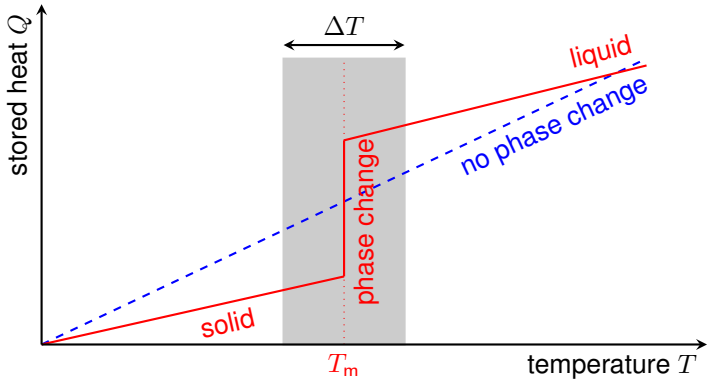

Figure 1.4.: Storage capacity as function of temperature for a sensible (– – – –) and a latent heat storage medium (——).

The storage capacity ΔQ of a sensible heat storage material is determined by the specific heat capacity of the storage material $c_p(T)$, the mass of the storage material m, and the usable temperature span $\Delta T = T_2 - T_1$ to

$$\Delta Q = \int_{T_1}^{T_2} \cdot c_p(\tau) \cdot m \cdot \mathrm{d}\tau \tag{1.1a}$$

which is, for a constant c_p

$$\Delta Q = \Delta T \cdot c_p \cdot m \tag{1.1b}$$

For a material that undergoes a phase change with the latent heat Δh_pc at the melting temperature T_m (where $T_1 < T_\mathrm{m} < T_2$), the stored heat is given by

$$\Delta Q_\mathrm{PCM} = \left((T_\mathrm{m} - T_1) \cdot c_{p,\mathrm{solid}} + \Delta h_\mathrm{pc} + (T_2 - T_\mathrm{m}) \cdot c_{p,\mathrm{liquid}} \right) m \tag{1.2}$$

In the temperature range of about 5-95 °C, the most popular material for sensible heat storage is water. In that case, latent heat storage systems have to compete with a simple water tank. Most phase change materials have a smaller c_p than water, are more expensive, and some are corrosive or toxic. Thus, only if the inferior sensible term of equation (1.2) is overcompensated by the latent term by a factor large enough to justify increased expenses, latent heat storage is the better choice. That means, if

$$(T_2 - T_1) \cdot c_{p,\mathrm{water}} - (T_m - T_1) \cdot c_{p,\mathrm{PCM,solid}} - (T_2 - T_m) \cdot c_{p,\mathrm{PCM,liquid}} \ll \Delta h_\mathrm{pc} \tag{1.3}$$

latent heat storage should be considered. For an average specific heat capacity of solid and liquid PCM, typically $c_{p,\mathrm{PCM}} \approx 2.5\,\mathrm{J/gK}$, this means

$$\Delta h_{\mathrm{pc}}/(T_2 - T_1) \gg 1.7\,\mathrm{J/g} \tag{1.4}$$

Phase change enthalpies of salt hydrates are typically in the range of 150-220 J/g, so latent heat storage for temperature ranges in the 20 K order of magnitude is already considerably advantageous to leave some space for constructional efforts.

Put aside the storage capacity, the charging and discharging power characteristics of a storage are different if sensible or latent storage is used. In principle, the charging power is dependent on material properties and the temperature gradient between heat supply and storage material. If a constant charging temperature is used, the temperature gradient in a sensible heat storage decreases as heat is supplied to the storage. For a latent heat storage, the gradient changes much less, because the main amount of heat is supplied while the material undergoes the phase change at the phase change temperature. This is why latent heat storage is particularly advantageous for thermal buffering. If a system is carefully designed, good buffering can be achieved passively without need for additional regulation devices.

1.2. Phase change materials (PCM)

Materials that are used as storage material in latent heat storages are called *phase change materials (PCM)*. In this section, material classes that are used as PCM are shortly introduced. It is outlined why the group of salt hydrates is in the focus of current research in PCM technology, including this work.

A material that can be used as PCM has to fulfill a number of requirements. The most obvious are a high storage density and a suitable melting temperature, as well as a good thermal conductivity and stability under thermal cycling. However, in order to be suitable for commercial applications, a PCM also should be non-corrosive, non-toxic and safe for handling, as well as cheap and abundant. Chances to discover a PCM that would fulfill all requirements are very low, and compromises of advantageous and disadvantageous properties have to be made [10].

An extensive review of available PCM and candidates was done in the 1980s by Lane [11, 12], and recently by Zalba et al. [13]. The most common material classes that are nowadays used as PCM can be roughly divided into organic and inorganic PCM.

1.2.1. Organic PCM

The chemical structures of three groups of organic PCM are shown in figure 1.5.

The basic form of organic PCM are *paraffins*, linear alkanes of the chemical structure $\mathrm{C_nH_{2n+2}}$. Depending on the chain length n, the melting temperature varies. Typical values of paraffins used as PCM are $n = 14-20$ with $T_{\mathrm{m}} = 6\,^{\circ}\mathrm{C} - 38\,^{\circ}\mathrm{C}$. Another group of

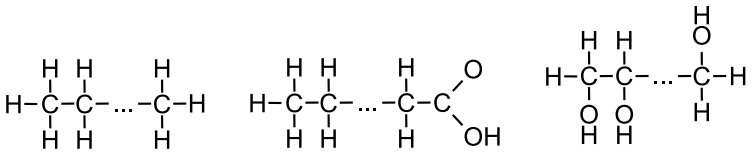

(a) alkane **(b)** fatty acid **(c)** sugar alcohol

Figure 1.5.: Common organic PCM are alkanes, fatty acids, sugar alcohols or mixtures thereof.

organic PCM are *fatty acids*. Their chemical structure is similar to that of the paraffins, but a final methyl group is replaced by a carboxyl group. Another popular group for the use as PCM are *sugar alcohols*. Here, one of the two hydrogen atoms bond to the carbon atoms in the back chain of the alkanes is replaced by a hydroxyl group.

Paraffins are produced from crude oil, and therefore their price is strongly affected by the oil market. Fatty acids are also gained from agricultural products. In general, organic PCM are flammable and have a low density, i.e. require a large volume, which is disadvantageous in particular in building applications.

1.2.2. Inorganic PCM

Three decades ago, when Lane published his fundamental book about thermal energy storage with PCM [11, 12], the corrosive properties of inorganic PCM were a major problem that often ruled out inorganic PCM completely. Due to advances in plastic technology and a better understanding of corrosion chemistry, expensive construction materials such as stainless steel can now be substituted by cheaper plastic materials. In this new situation, inorganic PCM promise higher storage capacities at lower material costs compared to organic PCM. This is why inorganic PCM are in the focus of current research in latent heat storage.

The most prominent inorganic PCM is water with the phase change temperature 0 °C. Pure materials like water have a distinct melting temperature, because they crystallize in a regular lattice where the bond strength between all molecules is the same, as sketched in figure 1.6a.

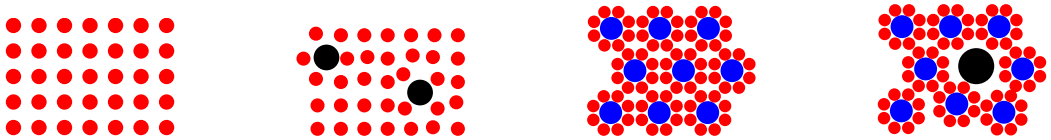

(a) pure water **(b)** water with impurities **(c)** pure salt hydrate **(d)** salt hydrate with impurities

Figure 1.6.: Crystal structure of different inorganic PCM, schematic. Impurities disturb the crystal grid and lower the melting temperature of pure substances.

The addition of a second substance to a pure substance disturbs the crystal structure of the solid as sketched in figure 1.6b. The intermolecular bonds are weaker and the melting temperature is lowered. Using this principle, various salts are added to water in order to change the melting temperature. When the number of ions that are integrated in the crystal lattice is high enough compared to the water molecules, at some point a lattice different from the ice lattice forms. The salt ions and the water molecules can form a salt hydrate. Some common salt hydrates are $CaCl_2 \cdot 6\,H_2O$, $Na_2SO_4 \cdot 10\,H_2O$ and $NaOAc \cdot 3\,H_2O$.

In stoichiometric salt hydrates, again a regular pattern is formed as shown in figure 1.6c. The bonds in a salt hydrate are stronger than the hydrogen bonds in water, but weaker than the ionic bonds in salts. This is why the melting temperature of salt hydrates is situated between that of pure water and that of pure salts. Again, the melting temperature can be lowered, if another soluted substance disturbs the crystal lattice of the salt hydrate, as sketched in figure 1.6d. Impurities do not only lower the melting temperature, but also decrease the melting enthalpy. This is why this kind of shifting of the melting temperature of a PCM cannot be done without a reduction of the storage capacity.

1.3. Subcooling and nucleation in latent heat storages

Subcooling refers to the cooling of a material below its phase change temperature but without the phase change actually taking place. In the case of a solid/liquid phase change, the liquid is cooled below the melting temperature without solidification of the material.

1.3.1. Effect of subcooling on storage performance

If subcooling occurs in the PCM of a latent heat storage, the storage material behaves similar to a sensible storage material, and the storage capacity is reduced. In figure 1.7, the effect of subcooling is shown in a heat versus temperature plot.

The subcooled state is a metastable state. The further a material is subcooled below the melting temperature, the more it deviates from its equilibrium state. At some point, the phase change is triggered – this is called the *nucleation* of the solid phase – and the systems returns to the equilibrium state. The reasons for subcooling and the mechanisms of nucleation will be discussed in detail in section 2.1. Here, a short numerical study is presented as an introduction to subcooling from the application point of view. The simulation tool was developed in the context of the LWSNet project to allow simulation of PCM including subcooling, crystal growth and heat transfer effects [14].

The principle effects of subcooling in PCM are shown in figure 1.8b to figure 1.9b. In figure 1.8a, the geometry that was used for the simulated temperature profiles is sketched. A liquid PCM is cooled on one side by a heat exchanger at constant

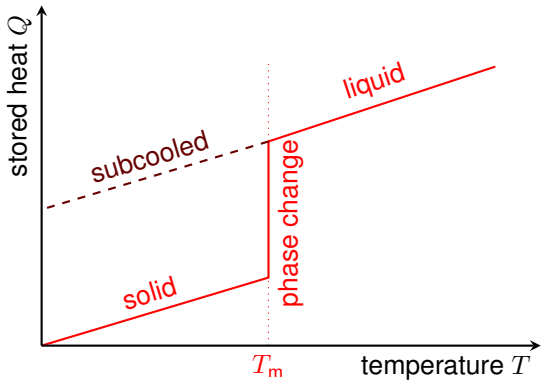

Figure 1.7.: If subcooling occurs, the phase change does not take place and the release of the latent heat is suppressed. The PCM behaves like a sensible heat storage material with reduced storage capacity.

temperature T_{hx}, where $T_{hx} < T_m$. The temperature is calculated for equidistant points inside the PCM, marked by ×. For each of these points, the temperature is plotted as a function of time in figure 1.8b to figure 1.9b.

In the reference case without subcooling, as shown in figure 1.8b, a characteristic plateau is formed at the melting temperature T_m.

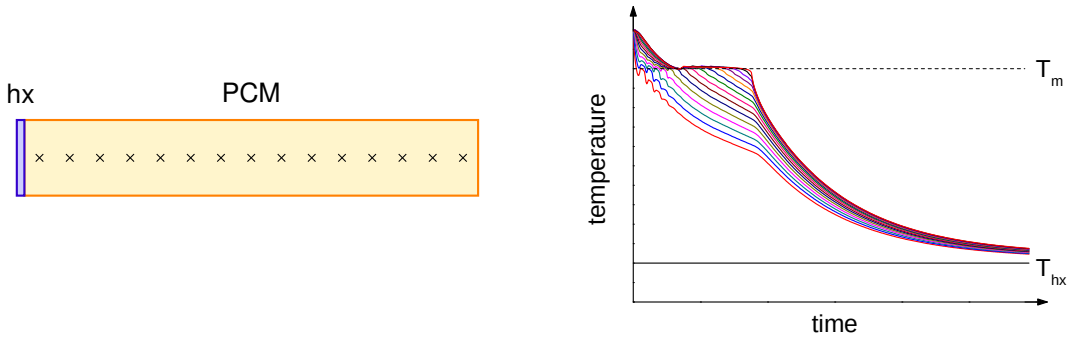

(a) geometry **(b)** reference case

Figure 1.8.: Simulation of temperature inside a PCM that is cooled via a constant temperature heat exchanger – sketch of the geometry of the simulation (a) and reference case without subcooling (b).

If subcooling occurs, the unloading characteristics of a heat storage can be considerably altered. The crystallization process is initialized only at a lower temperature T_n. Depending on the boundary conditions, the plateau is shortened as in figure 1.9a or lowered, i.e. the solidification takes place at a reduced temperature compared to the melting temperature as in figure 1.9b.

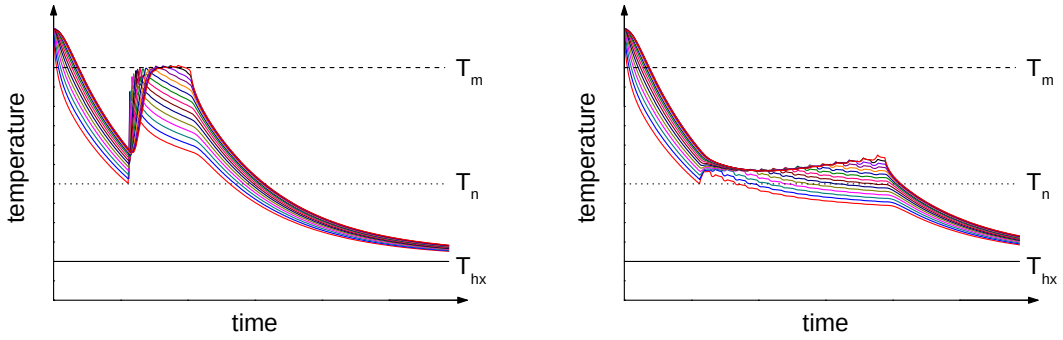

(a) shortened plateau **(b)** shifted plateau

Figure 1.9.: Simulation of temperature inside a PCM that is cooled via a constant temperature heat exchanger – two cases with subcooling. If the phase change starts only at a lower temperature T_n, the plateau is shortened (a) or reduced in temperature (b), depending on the boundary conditions.

The shortened or lowered plateau leads to a significantly changed discharging power compared to a situation without subcooling. In some cases, the heat release of the PCM is spread over a longer time span. If the necessary cold is available only for a limited time span, which is typical for renewable sources of cold [15], a complete solidification of the storage material may be inhibited. The usable storage capacity can then be reduced as a consequence of subcooling [16].

1.3.2. Reduction of subcooling

Undesired subcooling in PCM is currently reduced with the help of *nucleating agents*, also called *nucleators*. These addititves remain solid at all times and act as centers of crystal growth for the material that undergoes the phase change. However, it is not clearly understood how exactly this works on a molecular scale. This is why a reliable theoretic prediction or a systematic synthetic production of suitable nucleation agents is still not possible. The current practice is to look for suitable materials by empiric studies that involve thousands of candidate agents for one PCM. Using a high-throughput method as developed by Rudolph [17], such an exhaustive nucleator search is now possible, but still this is no guarantee for success.

There are many substances with a high phase change enthalpy, that cannot be used as PCM because of their strong subcooling and missing nucleation agents. Even for PCM where a suitable nucleating agent is known, subcooling remains a cause for problems. It has to be assured that the nucleator is present in every volume element; this is particularly difficult for microencapsulated PCM. Furthermore, if the nucleator melts only once, like during a malfunction of the storage, the nucleator will loose its

nucleation capability. This means, the melting temperature of the nucleator has to be considerably higher than that of the PCM. Additionally, the nucleator should be not soluble in the PCM. If it is, a larger quantity of the nucleator is needed in order to have some solid material that can act as growth center. The solved nucleator then acts as an impurity in the storage material, reducing the storage capacity and altering the phase change temperature. A nucleating agent can be toxic and corrosive, and it can be a rare or expensive material. Summing it up, nucleation agents are prone to cause trouble in the design and operation of latent heat storages. A completely different approach to reduce subcooling in PCM that could offer an alternative to nucleation agents is therefore much sought-after.

1.3.3. Aim of this work

In the light of the current situation as lined out so far, alternative concepts to reduce subcooling in inorganic PCM are required for a wider use of these interesting materials. Particularly a nucleation method based on physical mechanisms is of great interest. A physical method could be less selective to specific materials than the currently used nucleating agents. There are some hints that ultrasound can be used to trigger the phase change in a metastable liquid. Cavitation and high pressure effects are believed to play an important role in this context. Although there are a range of investigations on this effect called *sononucleation*, no systematic study with regard to the potential of this method for PCM has been carried out yet.

The aims of this work are therefore

- ▷ to give an overview of the current knowledge about subcooling and sononucleation,
- ▷ to quantify the effect of pressure on the nucleation of salt hydrates,
- ▷ to quantify the effect of sonic treatment on the nucleation of salt hydrates,
- ▷ to carry out an in-depth analysis of the physical mechanisms involved in sononucleation,
- ▷ to discuss the technical potential of sononucleation for inorganic PCM.

2. Theory and context

In this chapter, thermodynamic concepts concerning phases, phase changes and nucleation are introduced. As nomenclature in the context of this work is often ambiguous, a thorough definition of the terms used in this text is given. Then, the state of the current knowledge is analyzed and open questions with regard to the ultrasonic nucleation of salt hydrates are identified. Based on this, the problem to be solved in this work is defined.

2.1. Theory of phase change and nucleation

Most pure substances exist in three phases, namely the solid, liquid and gaseous phases. Depending on the boundary conditions of a system, one specific phase is thermodynamically preferred. Phase transitions are a reaction of the system to a change in boundary conditions. The fundamental works by Gibbs [18] and Boltzmann [19], published about a hundred years ago, are the basis of modern thermodynamics. A comprehensive interpretation for today's readers is given by Atkins [20] or Gerthsen [21]. The nucleation theory deals with the initial formation of a new phase. The main references used here are the books of Skripov [22], of Kurz and Fisher [23], and of Kashchiev [24]. A recent discussion of kinetic and thermodynamic theories of nucleation is published by Schmelzer [25]. Considering sononucleation of PCM, the phase transitions liquid-solid (solidification) and liquid-gaseous (cavitation) are of interest. A good overview of cavitation theory and applications is given by Brennen [26].

2.1.1. Stable phases – equilibrium thermodynamics

A phase is defined as "a form of matter that is uniform throughout in chemical composition and physical state" [20]. The three main physical phases are called solid, liquid and gaseous phases [1]. Transitions between these phases are called melting/solidification, evaporation/condensation and sublimation/desublimation, see figure 2.1. In some cases, a substance will chemically decompose at a temperature below the evaporation or even melting temperature, such that less than three stable phases may exist. Some substances form a number of different crystal lattices, corresponding to a number of distinct solid phases. Solid-solid phase transitions are called recrystallizations. For

[1] The plasma phase is usually accessible only under extreme conditions.

non-pure materials, in addition to physical phases, more phases can exist which are distinct in their chemical compositions.

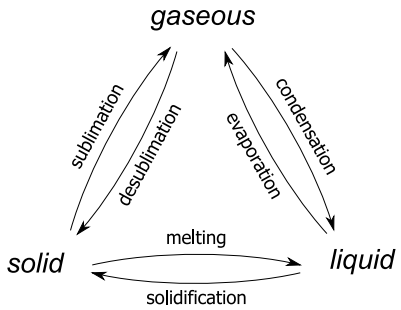

Figure 2.1.: Names of phase transitions of a pure substance.

Phases and phase transitions

The phase that a thermodynamic system actually adopts depends on the boundary conditions. A system can be determined by different sets of boundary conditions. The boundary conditions of a closed isobaric isothermal system, i.e. a system without mass exchange but in mechanical and thermal contact with its surroundings [2] , are pressure p, temperature T and number of particles N.

Particles in thermodynamic theory can be very different things such as molecules, atoms, ions, electrons, photons, phonons and so on. For the nucleation of salt hydrates, particles are in most cases molecules or ions. Thus, in any case, quantum effects can be disregarded as justified in section B.1. For simplicity, the general nucleation theory in this chapter does not specify the nature of the particles further; a more detailed discussion of this issue is given in section 4.1.2.

According to the second principle of thermodynamics, a system spontaneously tends to maximize its entropy. The entropy S of a closed system is written as

$$S = k_\mathrm{B} \ln \Omega \tag{2.1}$$

where Ω is the relation of the number of all possible microscopic configurations corresponding to the macroscopic configuration to the number of all possible microscopic configurations of the system, and $k_\mathrm{B} = 1.38066 \cdot 10^{-23}\,\mathrm{J/K}$ is Boltzmann's constant.

At any given fixed temperature, a closed isobaric system spontaneously tends to minimize its Gibb's free energy G. This means that any change of state that is associated with a reduction of Gibb's energy will occur without external force, if the path from the first to the second state is not blocked.

[2] A thermal contact to the surrounding is obviously required to charge and discharge a heat storage. An isobaric storage is chosen in most cases, because it is much easier to handle than an isochoric storage.

The Gibb's free energy is

$$G = H - TS \tag{2.2a}$$

For the solid, liquid and gaseous phases, the enthalpies are

$$H_{\mathrm{sol}} < H_{\mathrm{liq}} < H_{\mathrm{gas}} \tag{2.2b}$$

and the entropies are

$$S_{\mathrm{sol}} < S_{\mathrm{liq}} < S_{\mathrm{gas}} \tag{2.2c}$$

Thus, the $G(T)$ curves of the phases intersect. In thermodynamic equilibrium, G is minimized and a change of phases at certain temperatures is implied, as shown in figure 2.2.

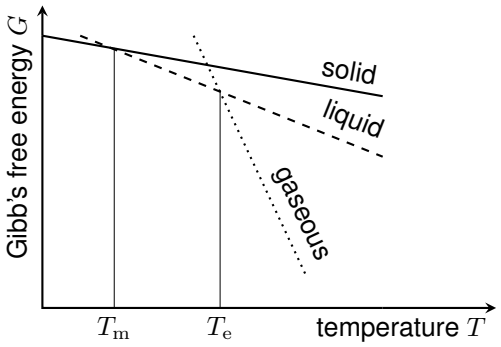

Figure 2.2.: The slope of the $G(T)$-curves for the three phases, schematic. The equilibrium transition temperatures for melting T_{m} and evaporation T_{e} are marked.

Considering the liquid-solid transition and using the abbreviation $\Delta = \Delta^{\mathrm{solid}}_{\mathrm{liquid}}$, the difference in G is

$$\Delta G = \Delta H - T\Delta S \tag{2.3}$$

Here, ΔH is the phase change enthalpy (also called melting enthalpy or latent heat) and ΔS is the phase change entropy.

For reversible processes in thermodynamic equilibrium, $\Delta G = 0$ and the transition takes place at a fixed melting temperature T_{m}

$$\Delta H = T_{\mathrm{m}}\Delta S \tag{2.4}$$

The reverse phase change, in this case the solidification, takes place at the same temperature. Therefore, the melting temperature is also called solidification temperature T_{s}. However, the equality $T_{\mathrm{m}} = T_{\mathrm{s}}$ can be violated for phase changes which take place not in thermodynamic equilibrium.

Phase rule

Gibbs' phase rule defines the number of free variables F as a function of the number of phases in equilibrium P, and the number of components of the system C.

$$F = C - P + 2 \tag{2.5}$$

This equation is deduced from the definition of the thermodynamic equilibrium as the state in which the chemical potentials μ are equal for each phase. The deduction can be found for example in [20, page 196].

For a one-component system with the variables pressure p and temperature T, a phase diagram is sketched in figure 2.3.

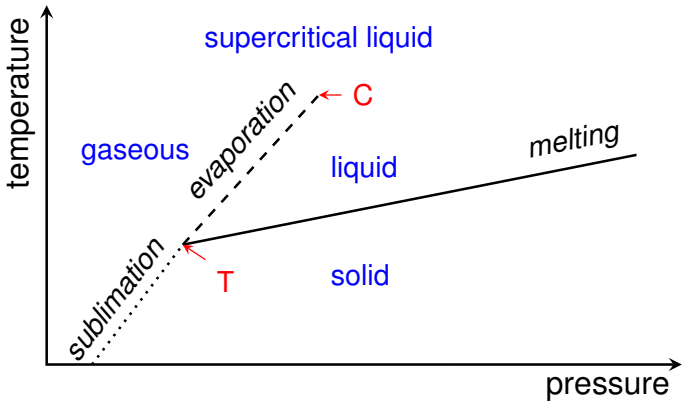

Figure 2.3.: Sketch of a phase diagram of a pure substance. The region of the phases and the lines of coexistence are shown. The triple point (T) and the critical point (C) are marked.

The number of free variables for $C = 1$ is $F = 1 - P + 2 = 3 - P$. It follows directly that three phases $P = 3$ can coexist only at one specific state $F = 0$, and that two phases $P = 2$ can coexist with one degree of freedom $F = 1$ remaining. For example the coexistence of the solid and liquid phases is found at one fixed temperature for any given pressure. This line of coexistence in the (T, p)-plane is called the *melting curve*. Similarly, the *sublimation curve* marks the border between solid and gaseous phases, and the *evaporation curve* is the border between liquid and gaseous phases in this diagram. At the triple point and at the critical point, three phases are in equilibrium.

For a two-component system, the number of free variables is $F = 2 - P + 2 = 4 - P$. Here, the coexistence of two phases leaves two free variables, e.g. temperature and pressure. This makes the situation for systems of two or more components much more complex. The regions of coexistence, melting temperatures and phase separation are read from *phase diagrams*. Phase diagrams are a key tool in material science. An introduction to phase diagrams in general is given by Atkins [20], and in particular to phase diagrams of PCM with many examples is given by Lane [12].

Phase change temperature as a function of pressure

The slope of the lines of coexistence in the phase diagram as shown in figure 2.3, also called *phase boundaries*, can be extrapolated from the phase change data at one given pressure. A coexistence of two phases is given if their chemical potentials μ are equal

$$\mu_1 = \mu_2 \tag{2.6a}$$

Using the total differential of the chemical potential of a phase i, in the mole-specific representation

$$\mathrm{d}\mu_i = -s_i \mathrm{d}T + v_i \mathrm{d}p \tag{2.6b}$$

and considering the difference between two phases Δ, the phase boundary is thus characterized by

$$\frac{\mathrm{d}p}{\mathrm{d}T} = \frac{\Delta s}{\Delta v} \tag{2.6c}$$

Together with equation (2.4), the phase boundary is then described by the *Clapeyron equation*

$$\frac{\mathrm{d}p}{\mathrm{d}T} = \frac{\Delta h}{T \Delta v} \tag{2.7}$$

This general relation is applied to the phase change solid-liquid in order to determine the melting curve. Assuming that the specific volume change during the phase change Δv as well as the phase change enthalpy Δh are independent of pressure, one gets for the slope of the melting curve

$$p_\mathrm{m}(T) = p_\mathrm{m}^0 + \frac{\Delta h}{\Delta v} \cdot \ln\left(\frac{T}{T_\mathrm{m}^0}\right) \tag{2.8a}$$

or, with the pressure as free variable

$$T_\mathrm{m}(p) = T_\mathrm{m}^0 \cdot \exp\left[\left(p - p_\mathrm{m}^0\right) \frac{\Delta v}{\Delta h}\right] \tag{2.8b}$$

For small changes in temperature, the fraction in the argument of the logarithmic function, in the right side of 2.8a, is close to 1. The logarithm can then be approximated by a linear function, and we get

$$p_\mathrm{m}(T) \approx p_\mathrm{m}^0 + \frac{\Delta h}{\Delta v T_\mathrm{m}^0} \left(T - T_\mathrm{m}^0\right) \tag{2.9a}$$

or, with the pressure as free variable

$$T_\mathrm{m}(p) \approx T_\mathrm{m}^0 + \frac{T_\mathrm{m}^0 \Delta v}{\Delta h} \left(p - p_\mathrm{m}^0\right) \tag{2.9b}$$

The inclination of the melting curve is thus approximated by $T_\mathrm{m}^0 \Delta v / \Delta h$.

2.1.2. Subcooling – stabilizing the mother phase

At the beginning of a phase transition, the new phase is starts to form from the old phase, the *mother phase*. This formation spreads from a starting point, the *nucleus*, i.e. a very small piece of the new phase. The nucleation theory deals with the events that lead to the formation of a nucleus that is able to grow. The typical size of such a nucleus is in the range of a few to a few hundreds of particles. Due to this microscopic scale, surface effects play a key role in nucleation theory.

Surface energy

In section 2.1.1, phases in thermodynamic equilibrium were considered, and situations that lead to a phase transformation have been introduced. In the course of any phase transition, there is a situation where two phases are simultaneously present in a system. The two phases meet at an interface, and this interface is associated with a *surface energy*.

The surface energy is caused by variations of the intermolecular bonding, as sketched in figure 2.4.

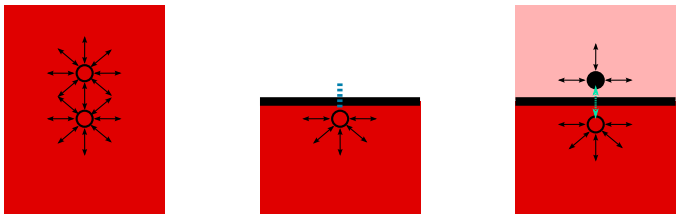

(a) bulk **(b)** surface **(c)** interface

Figure 2.4.: Sketch of bonds affected by a surface or interface. In the bulk material, each particle has a number of bonds – indicated by arrows – to neighboring particles (a). On a surface, on one side of the particle, the neighbors are removed, and no bonds can be established (b). At an interface, new bonds associated with a different energy can be established to particles on the other side (c).

If not mentioned explicitly, literature values of surface energy refer to an ideal surface, i.e. the interface between sample substance and vacuum. The surface energy is the energy required to remove intermolecular bonds on one side of a particle, as it is the case when the particle is located at the surface of a sample volume and not in the bulk. At an interface, new bonds can be created to molecules in the neighbor phase. These new bonds have in general a different energy than the inner-phase bonds, and thus the interface energy is in general non-zero.

In fact, although the term *surface energy* or *surface tension* is commonly used, in most real situations rather *interfaces* are relevant. Particularly in sononucleation, many different types of interfaces can be present: The interface between the liquid

and solid phases is the primary interface relevant for any solidification process. The interface between the liquid and gaseous phases governs the nucleation of gas bubbles under ultrasonic treatment. Considering a situation where a cavitation bubble causes solidification, also the solid and gaseous phases meet at an interface. In addition, in real systems impurities may be present and interfaces between the various phases of the system's components are possibly relevant, too. In that case, the interfaces have to be specified both by their physical state and their chemical composition.

For nucleation problems, the contact angle between a foreign substance and the phase to be nucleated indicates possible nucleating substrates: If the angle is smaller than 180°, a good wettability is given, and the interface with the substrate is energetically favored over the interface between the two phases of the sample material. However, wettability tests are not possible for solid materials, and more sophisticated epitaxial investigations are required [17].

Curved surfaces

Generally speaking, if the curvature is not mentioned explicitly, the surface tension refers to a plane surface. For nucleation problems, surfaces of small particles are considered. Thus, plane surfaces are a rough approximation and curvature effects can become important. In figure 2.5, a sketch of particles with a plane and a curved surface is given as illustration.

(a) plane surface **(b)** curved surface

Figure 2.5.: Sketch of the effect of curvature on surface tension.

In this simplified example, a particle can establish bonds to eight nearest neighbors in the bulk. At a plane interface only five of them remain, and in a curved geometry, even less neighbors are within reach.

In sononucleation, solidification but also evaporation and condensation processes are relevant. The surface energy for evaporation and condensation is different when curvature effects are considered, see figure 2.6.

The impact of the droplet size (i.e. curvature) on the surface tension is explained by introducing the concept of a surface layer of finite thickness [27, 28]. A particle of the droplet is considered part of the surface layer as long as its surroundings is significantly influenced by the near interface to the surrounding medium.

For spheric droplets, the curvature is expressed as a function of the radius. The

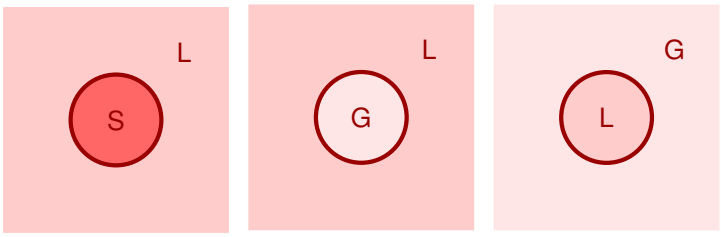

(a) solidification **(b)** evaporation **(c)** condensation

Figure 2.6.: Sketch of different configurations of interfaces during the nucleation of a new phase. Nuclei of the solid (S), gaseous (G) and liquid (L) phases are sketched.

Laplace equation relates vapor pressures on the inside and outside of curved surfaces

$$p_{\text{in}} = p_{\text{out}} + \frac{2\sigma}{r} \tag{2.10}$$

Using this equation, the relevance of curvature effects for a given geometry can be estimated. For example, the ratio of the vapor pressures over the plane and in a droplet is about 1.001 for a water droplet of radius 1 μm and 3 for a droplet of radius 1 nm [20]. In this case, surfaces of particles well below 1 μm should therefore not be considered plane. Of course, this is just an order of magnitude and specific to this system.

Considering a small solid phase, the concept of a spheric particle is a strong simplification. The energetic benefit of the solid phase is connected to the location and arrangement of the particles, that cannot move freely like in a liquid or gas. This is why solids grow in crystal shapes, in principle. However, for lack of detailed data, solid particles are often assumed as spheres anyway. For small droplets, the amount of particles that are part of the surface layer can become significant with respect to the particles inside the droplet. Then, the surface tension decreases considerably compared to flat surfaces.

Nucleation barrier

To simplify nomenclature, the following discussion refers to solidification. Nonetheless, the introduced principles apply as well to the other phase changes.

Starting from a stable liquid phase, when the temperature or pressure of a system change in such a way that the solid phase becomes the stable phase, a phase transition would reduce the systems free energy and could happen spontaneously. Considering a volume V, the phase transition is associated with an energetic change of

$$\Delta G_V = \Delta g_V \cdot V < 0 \tag{2.11}$$

A second energetic contribution arises from the created interface between the mother phase and the new phase. For a surface area A of the new phase, this sec-

ond term is

$$\Delta G_A = \Delta g_A \cdot A > 0 \tag{2.12}$$

The total change in G is thus the sum of these two terms.

If the shape of the solid phase is known, volume and surface can be related one to the other. Assuming the most favorable case of a spheric nucleus of radius r, the total energetic change is

$$\Delta G(r) = \frac{4}{3}\pi r^3 \Delta g_V + 4\pi r^2 \Delta g_A \tag{2.13a}$$

For small radii, the surface tension is a function of the curvature and can be approximated by

$$\sigma(r) = \sigma_0 \exp(-a\delta/r) \tag{2.13b}$$

where $a\delta$ parametrizes the thickness of the interface [28].

Taking this into account, one can rewrite equation (2.13a) to

$$\Delta G(r) = 4/3\pi r^3 \Delta g_v + 4\pi r^2 \sigma_0 \exp(-a\delta/r) \tag{2.13c}$$

Critical radius

The agglomerate of particles in the emerging new phase is in general called a *cluster*. Depending on the cluster size, two very different situations are possible. This can be seen directly when looking at the shape of $\Delta G(r)$ as plotted in figure 2.7.

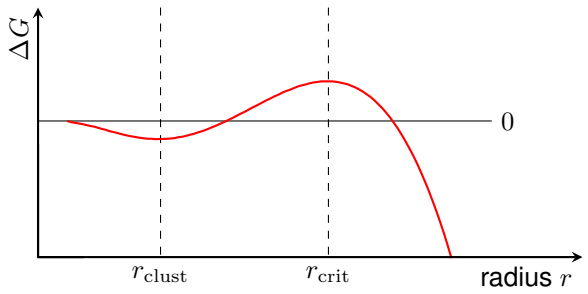

Figure 2.7.: The maximum in $\Delta G(r)$ defines the critical radius r_{crit}, the local minimum the stable cluster radius r_{clust}.

Recalling that thermodynamic processes are spontaneous if they are associated with a decreasing G, the two extrema of ΔG correspond to a stable and an unstable cluster:

- ▷ For radii $r \approx r_{\text{clust}}$, a change in r corresponds to an increased ΔG. A cluster of size r_{clust} is thus stabilized.

▷ For radii $r \approx r_{\text{crit}}$, a change in r corresponds to a reduction in ΔG. These clusters are not stable and can either shrink to smaller, stabilized clusters of r_{clust}, or they can grow unrestricted and thus reach a macroscopic size.

When neglecting curvature effects, the local minimum disappears and there are no stabilized clusters.

Clusters are thus classified according to their radius as *subcritical clusters* ($r < r_{\text{crit}}$) or *supercritical clusters* ($r > r_{\text{crit}}$). Another commonly used notation is to speak of *embryos* for subcritical clusters and *nuclei* for supercritical clusters. For the successful nucleation of a new phase, at least one supercritical nucleus is required. The maximum in $\Delta G(r)$ has to be overcome for the phase transition to take place. This maximum at r_{crit} is thus called the *nucleation barrier*. The nucleation barrier and the *critical radius* r_{crit} are key parameters in nucleation theory. Just like ΔG, the critical radius is a function of temperature and pressure, which is important for sononucleation as lined out below.

An approximation that is attributed to Turnbull [29] relates the Gibb's entropy to the melting enthalpy per unit volume of crystal, Δh_v as

$$\Delta g_v = \Delta h_v \left(1 - \frac{T}{T_{\text{m}}}\right) \tag{2.14}$$

Using the melting curve from equation (2.9b), and assuming again a phase change enthalpy invariant with pressure, the nucleation barrier equation (2.13a) can be rewritten as a function of radius, pressure and temperature. While in equation (2.14), Δh_v refers to melting and is specific to the crystal volume, the phase change enthalpy Δh in equation (2.9b) refers to crystallization and is mole-specific, such that

$$\Delta h_v = -\Delta h \cdot \rho_{\text{cm}} \tag{2.15}$$

where ρ_{cm} relates the mole-specific to the crystal volume specific enthalpy. Then, the nucleation barrier is

$$\Delta G(r, p, T) = 4/3\pi r^3 \Delta h \rho_{\text{cm}} \left(\frac{T}{T_{\text{m}}(p)} - 1\right) + 4\pi r^2 \sigma_0 \tag{2.16}$$

An increased subcooling reduces $T/T_{\text{m}}(p)$, i.e. decreases the factor in the first pair of brackets, and thereby reduces the height of the barrier. The increased subcooling can be achieved by a rise in $T_{\text{m}}(p)$ or a reduction of T.

In the following calculation, curvature effects of subcritical nuclei are disregarded for simplification. The critical radius is defined as the value of r where ΔG has its maximum. Using equation (2.13a) and substituting factors invariant with respect to r with constants a, b, the extrema of $\Delta G(r)$ are found where

$$\frac{\partial}{\partial r}\left(ar^3 + br^2\right) = 0 \tag{2.17a}$$

The non-zero solution is then the critical radius

$$r_{\mathrm{crit}} = -\frac{2b}{3a} \tag{2.17b}$$

or, resubstituting a and b,

$$r_{\mathrm{crit}}(p,T) = \frac{2\sigma_o}{\Delta h\,\rho_{\mathrm{cm}}}\left(\frac{T}{T_{\mathrm{m}}^o\left(1+\Delta v/\Delta h\left(p-p_{\mathrm{m}}^0\right)\right)}-1\right)^{-1} \tag{2.17c}$$

Two tendencies can be read directly from this equation: The radius of the critical nucleus decreases for decreased temperature, and it decreases for increasing pressure. Some illustrating graphs are presented in section B.2.

So far, the principle concept of the nucleation barrier and the role of the critical nucleus for nucleation have been lined out. In addition, when the critical radius is quantified, it can be set in relation to other length scales relevant for sononucleation, such that possible interactions e.g. with sound waves or cavitation bubbles can be estimated. For water, all parameters of equation (2.17c) are known and the critical radius is about 16 nm at 10 K subcooling, as lined out in detail in the appendix.

2.1.3. Nucleation 1 – general concepts

The nucleation barrier can be overcome spontaneously, i.e. without explicit triggering. The probability of such a spontaneous nucleation is described by statistic thermodynamics and depends on the boundary conditions. Theses boundary conditions can deliberately be changed in order to improve nucleation. Of particular interest in the context of sononucleation is nucleation triggered by pressure. While the formation of the critical cluster is a microscopic phenomenon, the main macroscopic characteristic that can be observed in experiment is the nucleation rate.

Spontaneous nucleation

Thermodynamics describes not single particles, but the sum of all particles in a system. The state of an individual particle can differ considerably from the average state of the system. This is important in the context of nucleation problems.

The amount of fluctuation is described by the entropy: if all particles are found in exactly the same energetic state, the total energy of the system is equally distributed to all particles. There is only one possible configuration, and the entropy is zero. This situation is possible only at a temperature of 0 K, as for higher temperatures, the entropy is always positive. The energetic states of the particles are distributed over a certain range. The individual particles interchange energy by inelastic collisions. In an ideal monoatomic gas, all energy is movement, i.e. kinetic energy. For more complex constituents and systems, forms of internal energy such as molecular vibrations or

phononic excitations in solids also play a role. A discussion of energies rather than velocities is therefore more general.

The distribution of the energetic states of the particles in a system is described by statistical thermodynamics. For systems far above the absolute zero in temperature, quantum effects can be neglected and the energetic distribution can be considered continuous.

The mean energy of a particle with f degrees of freedom in a system at the temperature T is given by

$$E = 1/2 f k_B T \tag{2.18}$$

The total energy of a system of N particles sums up to $E = N/2 f k_B T$.

The energetic distribution of the individual particles has to minimize the total entropy of the system according to the second law of thermodynamics. The distribution of the energetic states of the particles in an ideal gas is described by the Maxwell-Boltzmann partition function

$$f(E,T) = \sqrt{\frac{E}{\pi (k_B T)^3}} \exp(-E/k_B T) \tag{2.19}$$

This equation is generally used in nucleation theory, although in fact this form of the partition function is only valid for gases. As no formulation is known that would describe liquid salt hydrates with better precision, this formula will be used for the following explanations nonetheless. Limitations of this approach are discussed in more detail in section 4.1.2.

A sketch of the energy partition function for three temperatures is shown in figure 2.8.

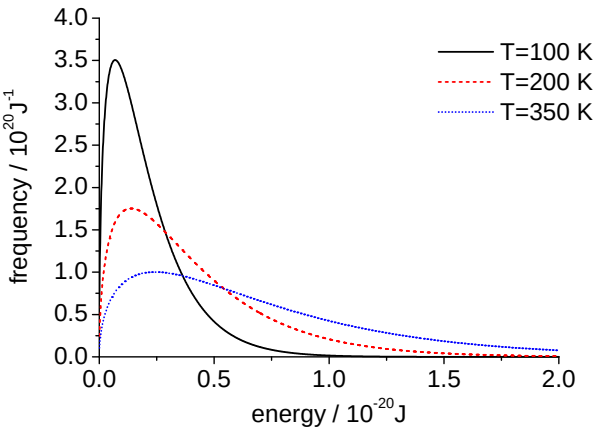

Figure 2.8.: Sketch of the partition function of a thermodynamic system for three temperatures.

The main points that can be read from this graph are:

- ▷ The lower the temperature of the system, the lower is the mean energy of the particles.
- ▷ The distribution is denser for lower temperatures, i.e. the energies of the single particles differ less.
- ▷ The maximum energy is much more sensible to the system temperature than the mean energy.

Only particles with a kinetic energy of $E \geq E_0$ can surpass an energetic barrier E_0. The relative number of these particles with $E \geq E_0$ is thus given by

$$n(E_0) = 1 - \int_0^{E_0} f(E,T)\mathrm{d}E \tag{2.20}$$

Considering for example an energy of e.g. $1.5 \cdot 10^{-20}$ J in figure 2.8, there are no particles with this energy for the lowest shown temperature, some few particles for the medium temperature, and a considerable fraction of the particles for the highest shown temperature. Discrete energy levels are relevant only for very low temperatures and are not shown in this graph.

So far, an elevated temperature seems favorable for the surpassing of an energetic barrier. In nucleation theory, however, the energetic barrier itself is dependent on the temperature. For temperatures close to the melting temperature, the nucleation barrier is high, but also the particles have good mobility and high energies. For temperatures far below the melting temperature, the nucleation barrier is low, but the movement of particles is slower and may be hindered because their kinetic energy is reduced with respect to the intermolecular forces. In an extreme case, the formation of an amorphous solid phase, i.e. a glass, can occur and nucleation of the solid phase is altogether blocked.

Nucleation by pressure

The basic idea of nucleation by pressure is to decrease the nucleation barrier by applying pressure, while preserving an energetic distribution with some high energy particles. Like this, a situation is created where particles may surpass the nucleation barrier at a temperature close to the atmospheric melting temperature. This corresponds effectively to a suppression of subcooling. This is illustrated in figures 2.9 and 2.10.

In figure 2.9, the nucleation barrier is plotted for $NaOAc \cdot 3\,H_2O$ using data suggested by Rogerson and Cardoso [30]. The critical radius at normal conditions is about 45 nm. A compression by several 100 MPa is expected to show a similar effect on the barrier as cooling to 250 K where nucleation at atmospheric pressure is reported.

In figure 2.10, a sketch of equation (2.20) is shown for a material with rising melting curve at two temperatures. The peak heights of the nucleation barrier are indicated for different boundary conditions, where $T_1 < T_2$ and $p_1 < p_2$. The number of particles

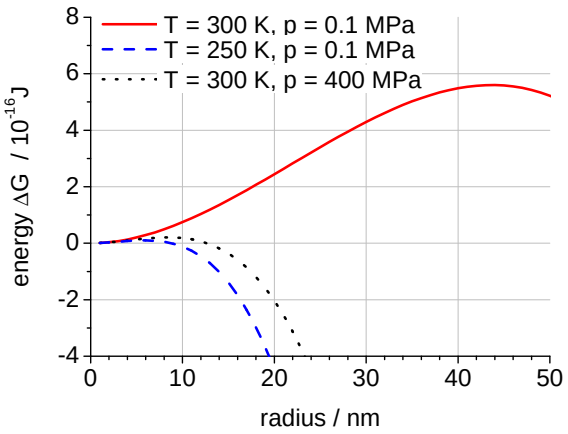

Figure 2.9.: The form of the nucleation barrier for different boundary conditions. Here, data for $NaOAc \cdot 3\,H_2O$ was used from Rogerson and Cardoso [30].

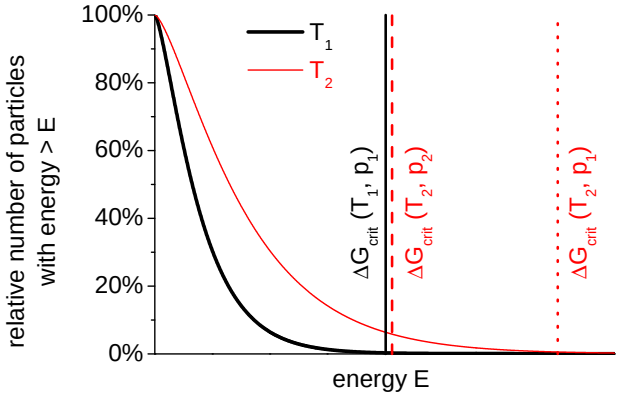

Figure 2.10.: The height of the nucleation barrier ΔG_{crit} depends on temperature and pressure. Compared to the reference case (——), the number of particles that can surpass the barrier is much increased for high temperature / high pressure (– – – –), but not for high temperature alone (·····).

that can surpass an energetic barrier in general is dependent from temperature (availability of particles with sufficient energy) and form of the energy barrier (definition of "sufficient" energy). For a nucleation barrier, the barrier itself is dependent from temperature and pressure. As shown in figure 2.9, the value of $\Delta G_{\text{crit}}(T_1, p_1)$ can also be reached at a higher temperature when the pressure is raised, too. In that case, the barrier is reduced by pressure, but the number of particles with sufficient energy is not changed. This is the basic idea of nucleation by pressure.

Nucleation rate

A significant ratio of particles whose energy is high enough to surpass the nucleation barrier is a necessary condition for nucleation to occur. The other main condition is that the attachment of the particles on the surface of the new phase actually happens. The surface may be blocked by geometric obstacles, only few growth sites remaining accessible, or the movement of the particles may be hindered or blocked by a high viscosity of the mother phase.

The nucleation rate is the product of the average number of critical nuclei present in the sample N_{crit} and the transition rate f_{crit} for critical clusters to grow to supercritical clusters. For simplicity, specific values are considered.

$$j = f_{\text{crit}} \cdot n_{\text{crit}} \tag{2.21}$$

The average number of critical nuclei present per volume at any time (under stable conditions) is derived from the Boltzmann distribution equation (2.20). Using $\Delta G_{\text{crit}} = \Delta G(r(n_{\text{crit}}))$, i.e. the work needed to grow a critical nucleus as given by equation (2.13a) and equation (2.17c), the number of critical nuclei is

$$n_{\text{crit}} = n_0 \cdot \exp[-\Delta G_{\text{crit}} / k_{\text{B}} T] \tag{2.22}$$

where n_0 is the number of particles per unit volume. Due to the exponential term, the nucleation rate increases first slowly and then strongly for falling temperature. The temperature where the nucleation rate becomes macroscopically significant is called the *nucleation temperature*.

If the transition rate is dominated by diffusion, then, considering a spherically symmetrical system in steady state [20], the flux J' towards the nucleus is proportional to the concentration gradient and

$$J' = \frac{D\gamma}{r} \tag{2.23}$$

where D is the diffusion coefficient, γ the concentration in the liquid phase, and r the radius of the solid sphere.

The rate of attachment f is the product of the surface $4\pi r^2$ and the flux J', so

$$f_{\text{crit}} = 4\pi r_{\text{crit}} D\gamma \tag{2.24}$$

and thus

$$j = 4\pi r_{\text{crit}} D\gamma \cdot n_0 \exp[-\Delta G_{\text{crit}} / k_{\text{B}} T] \tag{2.25}$$

This expression is preferably applied to nucleation problems in supersaturated systems.

In homogeneous systems, there is no concentration gradient and diffusion is not the governing time factor. Instead, the attachment rate is kinetically controlled, i.e. a correct microscopic orientation of the molecule at the surface is required for attachment. This concept is more appropriate for solidification of PCM.

The particle has to overcome an effective energetic barrier of magnitude E_{att} for attachment. So the transition rate is another Boltzmann term

$$f_{\text{crit}} = \beta \exp[-E_{\text{att}} / k_{\text{B}} T] \tag{2.26}$$

and the nucleation rate becomes

$$j = \beta n_0 \exp[-(\Delta G + E_{\text{att}}) / k_{\text{B}} T] \tag{2.27}$$

In classic solid state physics, there are more and less preferred sites where the new molecule can join the solid body that are associated with different E. The value of the β-factor characterizes the kinetics of attachment, and depends on the type of hindrance. This variable is controversially discussed in literature; more details are given in section 4.1.1.

In the most favorable situation, i.e. negligible attachment hindrance $E \ll \Delta G_{\text{crit}}$, the nucleation rate is

$$j = \beta \cdot n_0 \exp(-\Delta G_{\text{crit}} / k_{\text{B}} T) \tag{2.28}$$

Nucleation sites

In *homogeneous nucleation*, every particle in the system can act as nucleation site, and n is equal to the number of particles in the system. In *heterogeneous nucleation*, the nucleation is triggered at preferred nucleation sites, such as container surfaces or foreign particles. The nucleation barrier ΔG is reduced, but at the same time the nucleation sites n are dramatically decreased.

In a real system, typically a number of different types of nucleation sites associated with different barriers and different kinetics will be present. Then, the nucleation rate is

$$j = \sum_i n_i \beta_i \exp(-\Delta G_i / k_{\text{B}} T) \tag{2.29}$$

2.1.4. Nucleation 2 – more types of nucleation

So far, the nucleation of the solid phase from a liquid mother phase was considered. In sononucleation, also the nucleation of the gaseous phase and nucleation in multi-components-systems are relevant, that will be addressed in this section.

Cavitation – nucleation of the gaseous phase

The formation of the gaseous phase from the liquid is called “boiling” (under roughly isobaric conditions) or “cavitation” (under roughly isothermal conditions) [26]. In liquids that are treated with ultrasound, neither strictly isothermal nor isobaric conditions can be expected, but usually the main focus lies on the change in pressure and the general convention is to speak of cavitation.

For a given temperature, the vapor phase is thermodynamically stable for pressures below the saturation vapor pressure $p < p_{\mathrm{sat}}$. However, similar to nucleation of the solid phase, for cavitation actually to happen, a nucleation barrier has to be overcome. Equation (2.13a) can be directly applied to cavitation, with Δ now referring to the liquid and gaseous states. The pressure at which cavitation actually occurs is called the *tensile strength* of the liquid, or the *cavitation threshold*. Again, a nucleation rate for cavitation bubbles can be defined, and a distinction between thermodynamic and kinetic values is needed. The transition liquid-vapor is distinct from the transition liquid-solid in several ways.

- ▷ First of all, the main difference between liquid and vapor phases is the mean intermolecular distance, while for the liquid and solid phases, the main difference is the variable or fixed relative position of the molecules. A consequence is that for the nucleation of the solid phase, diffusion, orientation and attachment processes have a strong impact the nucleus growth, while for the nucleation of cavitation, a mere energetic view describes the process quite precisely. This is why evaporation and condensation are far more symmetric than melting and solidification.
- ▷ Second, nucleation sites for heterogeneous nucleation are different in the two cases. The interface tension between different gases is negligible, which is not the case for interfaces between different solids. So, for cavitation, basically any gas bubble will be a good seed, independent from its chemical composition.
- ▷ Third, nucleation of the vapor phase is clearly favored for higher energies, i.e. it can be enhanced by adding energy. For example, cosmic radiation may trigger cavitation even in a highly purified liquid [26, 31]. The enhancement of nucleation of the solid phase is more complex, because the nucleation barrier grows for higher energies.

Once a vapor bubble is nucleated, the bubble expands quickly due to the large density change of evaporation. If this happens within the bulk liquid phase, the surrounding liquid cannot give way to the increasing volume of the bubble immediately, and creates a counteracting pressure. The bubble expansion comes to a halt when the equilibrium vapor pressure is reached.

When a microbubble passes a valve or turbine, or in an ultrasonic field, the external pressure increases again after the nucleation of the bubble. In such a situation, the bubble will collapse. Due to the inertia of the bulk liquid, the phase front does not come to a halt at the original bubble radius, but moves further in the direction of the

bubble center, creating a high pressure peak. Subsequently, if dissipation mechanisms are disregarded, the bubble rebounds and collapses again and again, as sketched in figure 2.11.

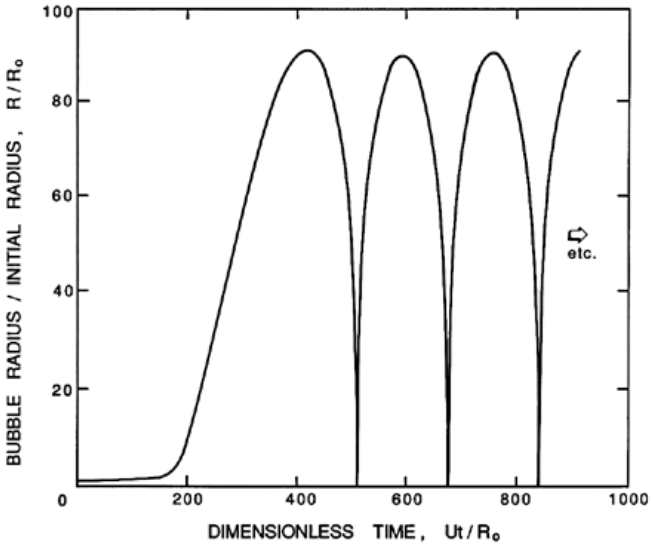

Figure 2.11.: Following its nucleation, a cavitation bubble expands and collapses. The nucleus enters a low-pressure region at a dimensionless time of 0. The original outer pressure is restored at a dimensionless time of 500, and the bubble collapses. Graph from Brennen [26].

Precipitation – nucleation in non-pure systems

As a first approach, treating PCM as pure systems is helpful to understand basic mechanisms. However, in reality, impurities often play an important role in nucleation problems. Also, nucleation literature often refers to impure systems without explicit mention. The term *supersaturation* is often used interchangeably with subcooling: The solubility of substances is a function of temperature and pressure, where the solubility is higher for higher temperatures [32]. Thus, a cooling below the solubility limit leads to a metastable state where the solution is subcooled, or supersaturated. A main difference is however, that during the formation of a stable system by precipitation, a concentration gradient is formed, and diffusion processes may become important. The supersaturation of both solid or gaseous diluted substances play a role in the context of sononucleation.

Salt hydrates consist of water and salt, but are not to be confused with salt solutions. The phase change considered is melting/solidification of the salt hydrate and not dissolution/precipitation of the salt in water. Impurities in this context are foreign substances, such as solid particles (dust, dirt), liquid material (e.g. excess water), gaseous

substances (e.g. dissolved air). In any case, the concentration of the impurities is very low compared to the material that is actively taking part in the phase change.

Diffusion enhancing techniques are important for impure systems, but not for pure systems. One example of such a technique is stirring. Heat dissipating techniques are however effective in both types of systems. As stirring may also enhance heat transfer by improved convection, it is not useful to experimentally separate the two kind of systems.

2.1.5. Summary

To summarize the theory section, a short overview of the most commonly used expressions (which are unfortunately not used consistently in literature) is given here for further reference in this text.

subcooling – supersaturation The term subcooling refers to cooling below an equilibrium phase change temperature, without the phase change taking place. Similarly, supersaturation refers to a thermodynamic state beyond the solubility limit, without the solute precipitating from the solvent. In the case of a temperature dependent solubility, subcooling and supersaturation can coincide. Other commonly used expressions are undercooling, supercooling or hypercooling and oversaturation, respectively.

pure material – non pure material A pure material in this context is a chemically uniform system, where concentration gradients are impossible. In non-pure materials, components may separate (on a microscopic or macroscopic scale) and form concentration gradients.

particle – cluster – embryo – nucleus A particle is the smallest mobile unit of the considered system, for salt hydrates this is in most cases an ion or a molecule. While cluster unspecifically denotes any agglomerate of particles, an embryo is of a radius smaller than the critical radius, and a nucleus is able to grow, i.e. of a radius larger than the critical radius. In case of doubt, *amorphous* / *crystalline* and *subcritical* / *supercritical* can be used for clarification.

homogeneous – heterogeneous nucleation Homogeneous and heterogeneous refer to the chemical constitution of the system. For homogeneous nucleation, the nucleus is of the same substance as the nucleated phase, while for heterogeneous nucleation, it is a different substance.

primary nucleation – secondary nucleation Primary nucleation refers to the nucleation of a new phase from a one-phase starting situation, while secondary nucleation refers to a situation where already two phases are present, and e.g. small parts of the new phase like dendrite's tips are broken and act as seeds for further nucleation.

spontaneous – triggered nucleation If nucleation occurs in a metastable system as a consequence of thermal fluctuations, this is called spontaneous nucleation. The probability of a nucleation event as function of time refers to invariant boundary conditions, i.e. constant pressure and temperature. Triggered nucleation occurs as a reaction to rapid changes in the boundary conditions, i.e. as a reaction to insonication or rapid cooling.

2.2. Context

In this section, the scientific context of this work is presented. Background information from different fields of science is required to line out the current state of knowledge in sononucleation of salt hydrates. First, reported data on the melting and nucleation temperatures is summarized. Next, various nucleation mechanisms and their fields of relevance are introduced. Then, ultrasound and the action of ultrasound on liquids is presented. Last, previous studies on sononucleation are analyzed.

2.2.1. Melting and nucleation temperatures

Melting temperatures T_m and melting curves $T_\mathrm{m}(p)$

The melting temperature at atmospheric pressure is one key property of any material that exhibits a solid/liquid phase transition. The determination of this property is carried out as a standard procedure to assure the identity and purity of a material. Data are widely available for most materials [33, 34, 35], particularly for phase change materials [12].

As to the melting curve, i.e. the pressure dependency of the melting temperature, the situation is different, varying with respect to the specific kind of material. Some early works on organic materials melting at low temperatures were done by Bridgman [36, 37, 38] in the context of a theoretical discussion about the nature of the solid and liquid states. Water has gained much attention both in a theoretic and applied context, and its melting curve is well established [39, 40]. High pressure data is available also for other materials which are of practical importance in different fields of science, such as in metallurgy [41, 42], geophysics [43] or food processing [44]. Typical experimental setups are piston-cylinder and anvil cells for adiabatic experiments, and shock wave experiments for very high pressures during short times [45].

As to salt hydrates, there is however no prominent high pressure application, and the number of investigated materials is therefore comparatively low. Tammann has published melting curves of some salt hydrates in 1922 [46], among them $CaCl_2 \cdot 6\,H_2O$ for pressures up to 250 MPa. A more recent investigation of some salt hydrates was published in 1989 by Barrett [47]. Among other, data is reported for $NaOAc \cdot 3\,H_2O$ in the pressure range of 0.1 to 80 MPa. His method comprised the trapping of a seed crystal between two clamped pieces of material with a known hardness, and subsequent

determination of the maximum temperature at which the seed's nucleation capability survived a heat treatment. The melting pressure of the sample at that temperature equal to the pressure exerted by the clamping material. Repeated measurements with different clamping materials were used to determine a melting curve.

Nucleation temperatures T_n

Data on the nucleation of solids under high pressures is particularly available for geologic materials [43] and for water [48, 49]. A collection of both theoretic and experimental current research of nucleation and solidification is found in [50]. For atmospheric pressure, the group of commonly investigated materials includes metals and alloys [51, 52], glasses [29], and solutions [53]. However, special attention as to the definition of the nucleation temperature has to be paid when referring to literature values. Due to the nucleation temperature being not a thermodynamic property, experimental conditions can have a strong influence on the determined value. Therefore, repeated experiments and a statistical analysis should be carried out. An apparatus for statistical studies of heterogeneous nucleation for small samples is described by Seeley [54]. A recent critic discussion of the repeatability in freezing experiments is given by Vali [55]. In a review by Avedisian about experiments on superheating of liquids, a valuable discussion of various methods and their suitability to approach homogeneous nucleation is presented [56]. This is also of interest in the context of subcooling, because similar considerations apply from nucleation theory for both kinds of nucleation. The experimental techniques used are pulse heating, isobaric droplet heating, isothermal decompression, the capillary tubes and the bulb methods. One important conclusion is that an uncertainty in the nucleation rate changing of three to four orders of magnitude is reflected in the nucleation temperature by only about 1 K.

As to salt hydrates, the second tome of Lane's book on PCM for thermal energy storage [12] indicates nucleation temperatures for most listed materials, but usually with a large uncertainty. Particularly for $NaOAc \cdot 3\,H_2O$, data is also found in the works of Wada [57] and Rogerson [30]. With respect to the materials investigated in this work, the following data are reported:

- ▷ $KF \cdot 4\,H_2O$: The maximum observed subcooling is reported in the range of 15 K to 24 K, i.e. the nucleation temperature is in the range of 267.5 K to 276.5 K.
- ▷ $CaCl_2 \cdot 6\,H_2O$: The theoretically expected nucleation temperature is 243 K, i.e. at 60 K subcooling; experimentally observed values in analytical grade samples are 273 K to 283 K nucleation temperature, i.e. at 20 K to 30 K subcooling.
- ▷ $NaOAc \cdot 3\,H_2O$: Subcooling without additives is reported to be about 23 K. Nucleation in samples diluted with 10wt% water was observed in the range 248 K to 255 K, i.e. at a subcooling of 76 K to 83 K.

In the work of Rogerson, a prediction of the nucleation rate based on some assumptions is presented as shown in figure 2.12. Regions of instantaneous and negligible

nucleation rates are sketched for NaOAc·3 H_2O in the T-p-plane.

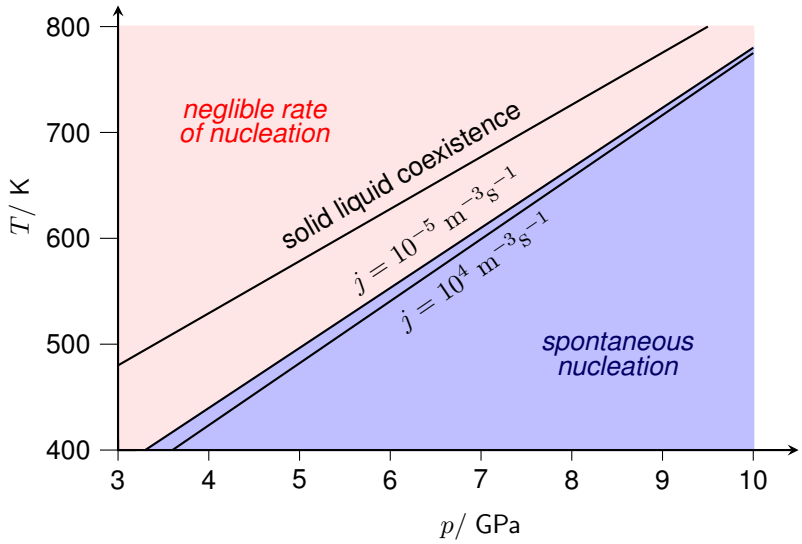

Figure 2.12.: Instantaneous and negligible nucleation rates for NaOAc·3 H_2O in the T-p-plane – graph after Rogerson [30].

The nucleation curve confined by the two regions is then associated with an uncertainty in temperature of about 10 K and in pressure of about 200 MPa. Similar to the conclusions of Avedisian [56] mentioned above, this moderate uncertainty corresponds to a change in the nucleation rate by 9 orders of magnitude. It is however puzzling that the authors chose to plot only a high pressure region starting at 3 GPa. Extrapolating the curves to normal pressure, the distance between the solid liquid coexistence line (equilibrium melting curve) and the nucleation curve seems to be more than 100 K, which is considerably larger than what is observed in experiment, as lined out above.

2.2.2. Nucleation mechanisms

In order to improve solidification, the nucleation of the solid phase is often triggered externally. There are different mechanisms and methods to do this. In order to quantify the effect of a trigger mechanism, a comparison to non-triggered nucleation is desirable. However, in practice, real non-triggered nucleation is hard to observe, and a comparison is rather done between different triggering mechanisms. Therefore, in the context of this work about sononucleation, it is important to know also other possible trigger mechanisms. Those other mechanisms can then be experimentally excluded or considered in the analysis of the results.

Nucleation in water plays a role in very different applications, and different concepts of the effective mechanisms are discussed in literature. For salt hydrates, only a small number of publications exist, and the focus of published work is mainly practical. In

addition to nucleation mechanisms, the concept of antinucleation is also introduced in this section.

Nucleation of water – ice and snow

The properties of water are of enormous importance in many different contexts. The nucleation of its solid phase is of relevance in technical, meteorological and biological systems, for example. Different boundary conditions and nucleating mechanisms are expected for these different systems.

Nucleation of ice in a technical context The experimental nucleation temperature of water is reported in a wide interval. The lowest experimentally observed nucleation temperature is 235 K. In varying setups and measurement methods, almost any temperature between this limit and the melting temperature is found to be a "nucleation temperature" of water [56, 58].

Under laboratory conditions, nucleation on sample containers is an important issue. Levitation techniques (avoiding interface with solids) and microemulsions (isolation of heterogeneous nuclei) are used to study quasi-homogeneous nucleation. In addition, a wide choice of additives can be studied with respect to their nucleating activity in laboratory experiments.

The nucleation activity of glass test tubes was recently investigated by Heneghan et al. [59]. They determined the limits of subcooling of pure water in glass and coated glass containers, as well as water with silver iodide (AgI) as nucleator in the same setup. An increase in subcooling was observed if the glass container was coated with a hydrophobic layer only when the nucleator was absent. Their conclusions are that nucleation takes place on the glass surface, or on the nucleator crystal surface.

The role of liquid-air interface on the nucleation of ice was studied by Shaw et al. [60]. The authors observed that nucleation agents act more effectively on a subcooled water droplet when the seed is in contact with the surface of the droplet than when the seed is completely immersed in the droplet. They conclude that the nucleation is favored by the liquid-air interface, and suggest that this is generally the case, not only for water. In a molecular dynamics simulation of alcohol monolayer-water droplet systems [61], it was found that the water layer immediately below the monolayer surfaces adopts ice-like lattice parameters and thus serves as template for ice nucleation.

The production of ice e.g. in ice storage systems profits economically and energetically, if efficient nucleation of ice is possible. A group around Prof. Egolf, chair at the University of Applied Sciences of Western Switzerland, has investigated a novel ice slurry production process [62]. A refrigerant evaporates within a water tank, chilling the surrounding liquid and producing ice. The refrigerant used in this system is a hydrocarbon called R600a. It has an evaporation temperature of 261 K under atmospheric pressure, and very low solubility in water of 0.0054 wt.%. The evaporation temperature of the refrigerant was chosen to satisfy a quick heat transfer to the liquid, as well as a

good energetic efficiency of the system. The authors state that in their system, spontaneous nucleation occurs that is caused by gas expansion. Still, nucleation agents are added to the water. While there is no explicit statement about this, apparently the nucleation agent reduces the required subcooling that can then be easily reached by expansive cooling.

The suppression of subcooling in water is a problem that seems to be technically solved. Expansion cooling and heterogeneous nucleation using solid seeds, in particular AgI, are established methods. Also interfaces to air are considered nucleation enhancing.

Nucleation of ice in living nature Many living organisms have to deal with temperatures below 0 °C, and therefore with the phenomenom of freezing and frost damage. Frost damage is caused by a mechanical or an osmotic effect, or both. While frost damage on cells is harmful for the organism that gets damaged, it may be advantageous for a parasitic organism. Also, freezing of dead leaves or water in a cavity of a plant as sketched in figure 2.13 can protect living parts of the organism by heating with the released latent heat. Species that have developed nucleation strategies are found among trees, insects, fish and bacteria [63]. A detailed study on the thermal cycling

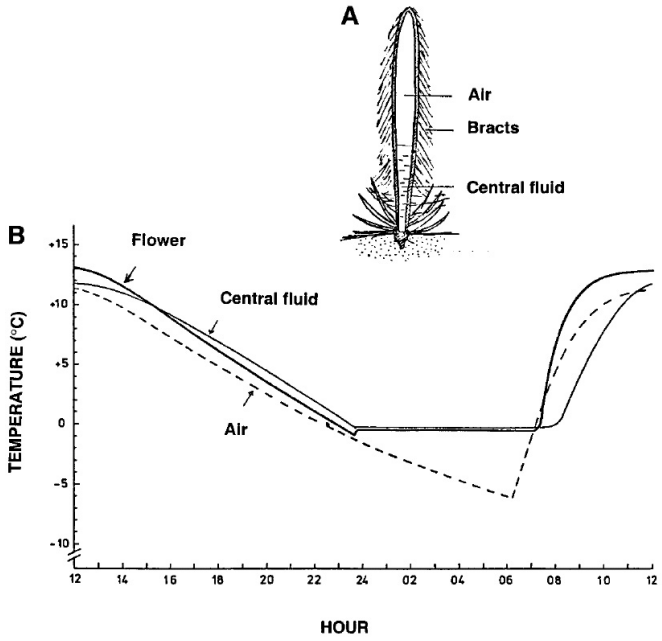

Figure 2.13.: Freezing protection by the use of latent heat from a water reservoir by an alpine plant – graph by Zachariassen [63].

stability of bacteria as nucleating agents for ice was published by Tsuchiya et al. [64].

These bacteria act as effective nucleating agents already at very low subcooling, they are cheap and non-toxic, and are therefore used e.g. in snowmaking machines.

Nucleation of ice in the meteorological context – snow, hail and clouds Another field where nucleation plays a major role is meteorology. For example, the nucleation of ice particles during the formation of cirrus clouds is very important for climate and weather models and not yet fully understood. An extensive review of phase change problems of atmospheric particles was done by Martin [65]. A compact introduction on nucleation theory with a focus on atmospheric ice nucleation is given by Vali [66].

Investigations of the nucleation of snow have attracted much attention: in theory, the conditions in cloud droplets are particularly unfavorable for nucleation of the solid phase, coming close to homogeneous nucleation. Very small, separated volumes of evaporated, i.e. comparatively pure water lead to high degrees of subcooling and a difficult nucleation of precipitation. Silver iodide is used on a large scale for artificial precipitation in so-called "weather modification programs" such as the Nevada State Cloud Seeding Program [67].

It was discovered several decades ago, that natural snowfall is influenced by aerosol particles, and that organic matter has a better nucleation effect than inorganic matter [68]. Tests on decaying organic matter revealed particularly good nucleation activity of "actively decomposing poplar mulch", treated under aerobic conditions. The authors suggest to substitute inorganic seeds, that are commonly used for technical snow, by this very effective and nontoxic material. A discussion of the nucleation mechanism is not provided in this article. A recent paper by Christner et al. [69] comes again to the conclusion that particles of biologic origin play an important role in the nucleation of atmospheric snow. The authors state that the nucleation temperature of inorganic nucleation agents for snow is at about 261 K, while biologic agents are found in snow that was nucleated at about 266 K to 269 K. Here, too, explanations or theories on how the nucleation works are missing.

One theory that suggests a biologic motivation of improved nucleation in meteorology is lined out by Morris et al. [70]. The so-called *bioprecipitation* is believed to be caused by ice nucleating bacteria, which profit from an enhanced water cycle: they are transported into clouds, incite precipitation and thereby cause favorable conditions for their growth on plant surfaces. The bacteria are believed to produce proteins that serve as structural templates for the water in the subcooled liquid, which line up along the protein and thus form supercritical ice nuclei.

The unfavorable conditions for nucleation of snow from aerosol water droplets are also an important issue in the context of technical snow makers. Subcooling is the main obstacle that has to be overcome when producing artificial snow. Where nucleating agents cannot be used due to environmental concerns, other nucleation mechanisms are needed [71]. There are basically two types of snow makers [72, 73]. The older type is the high pressure snow maker. The snow is produced by classic expansion

cooling, where the nucleation of every snow flake is done via low temperatures. The newer type is the low pressure snow maker. Here, only few ice crystals are nucleated by low temperatures, and those crystals are then used as homogeneous agents to seed the subcooled water and produce snow. In this case, the growing of the flakes is slower, and therefore, large fans are needed that blow the water over several meters through the air (nucleation by seeding with high-pressure produced nuclei). In a patent claiming a nozzle head of snow maker lance [74], the nucleation of ice is explicitly mentioned. Unfortunately, what exactly happens at the nozzle is not explained in detail. An expansion cooling mechanism could be active in that case.

Nucleation of salt hydrates

Nucleation of salt hydrates is usually investigated in the context of their application in thermal storage systems. In most cases, the effectiveness of different nucleating agents is studied. While the general idea is that agents with similar crystal structure are effective, also exceptions to this rule have been observed.

One problem in this context is, that usually only effective nucleating agents are investigated in some detail. Their absence in a sample does not guarantee for a nucleator-free sample, and weaker, unknown nucleating agents could still be present. Known nucleators for the materials in this study are reported in [12, 57]:

- ▷ $KF \cdot 4\,H_2O$: Subcooling is reduced to 9.5 K using pumic stone as nucleator. No more effective nucleator is known.
- ▷ $CaCl_2 \cdot 6\,H_2O$: BaI_2 and SrI_2 are “effective” nucleators (not quantified).
- ▷ $NaOAc \cdot 3\,H_2O$: Subcooling is reduced to about 4 K using $Na_4P_2O_7 \cdot 10\,H_2O$ as nucleator.

The work by Rogerson et al. [75] investigates the mechanical trigger mechanism in heat packs based on $NaOAc \cdot 3\,H_2O$. When a small metallic disk that is immersed in the PCM is flexed, the solidification is triggered. The authors proved that solid crystallites trapped in micro cracks of the metallic trigger survive the heating of the pack, and act as seed crystals when the trigger is flexed and the cracks are widened.

Rudolph has developed a high-throughput screening method to find nucleating agents for PCM [17] and carried out some tests on $NaOAc \cdot 3\,H_2O$. Subsequently, the group around Prof. Voigt [76] has continued his work and searched agents for a number of different salt hydrates. In spite of the enormous number of tested material combinations, only very few successful pairs were found. A recent ambitious attempt to predict nucleation agents based on crystallographic and other available data has not yet led to the results that were hoped for [77].

Antinucleation

A lowering of the nucleation temperature is called *antinucleation*. One way to achieve antinucleation is to deactivate nucleation agents or preferred nucleation sites, thus forcing homogeneous nucleation at much lower temperatures and stabilizing the subcooled state. Another method is to inhibit growth of supercritical nuclei.

Remarkable antinucleation capacity of antarctic fish larvae were studied by Cziko et al. [78]. For fish of the *Pagothenia borchgrevinki* species, the serum melting temperature is above the surrounding water temperature. Therefore, their hypo-osmotic serum is in a stable subcooled state, except for a situation where the antinucleation mechanisms fail. Then, the serum will crystallize and the fish will die. The adsorption-inhibition theory tries to explain the antinucleation found in fish serum. In figure 2.14, this theory is illustrated. Antifreeze proteins are thought to be adsorbed on the surface

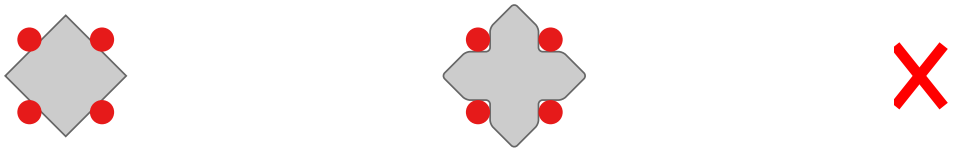

(a) before growth

(b) growing crystallite with curved surface

(c) further growth is blocked

Figure 2.14.: Antifreeze proteins are supposed to attach to the surface of a crystallite (a) where they lead to an increased curvature when the crystal grows (b) and thus block further growth and macroscopic solidification.

of small ice crystals. Crystal growth then leads to increased curvature of the ice surface. This increased curvature increases the surface to volume ratio of the ice crystal, which then is no longer supercritical and cannot continue growing. Proteins are still found in the liquid, and are supposed to be sticky only below the melting temperature of ice.

Investigations of larvae have shown a corelation between the shape of the gill surface and the subcooling capabilities. Ice nucleates less on larvae with a smooth gill surface compared to larvae with a more structured gill surface. The size of the structures is in the order of 10 μm, see figure 2.15. Thus, not only proteins but also larger structures seem to be able to inhibit nucleation in fish.

Antinucleation is also observed in a non-biologic context, as for example in geology [79]. In PCM technology, a microencapsulattion of the PCM material is known to reduce the nucleation temperature in some cases [80]. This is explained by a reduced sample volume (each droplet must be nucleated separately) and the deactivation of nucleation sites by their local isolation. This effect is also observed in emulsions such as butter [81].

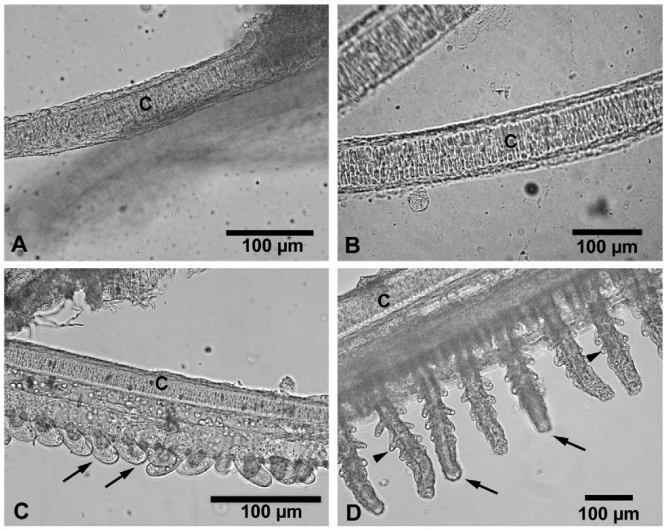

Figure 2.15.: The gill surface of antarctic fish larvae are different for individuals with different antinucleation capabilities – figure by Cziko [78].

2.2.3. Physical conditions in insonicated liquids

Ultrasound is a periodic sound pressure with frequencies beyond human hearing, usually in the range 20-100 kHz. The properties of an ultrasonic field are determined by the sound generator, the insonicated medium, and the geometry of the sample. The sound generator is characterized by frequency, and amplitude or sonic power. The insonicated medium determines the speed of sound and thereby the wavelength.

The wavelength λ is

$$\lambda = \frac{c}{\nu} \tag{2.30}$$

where c denotes the speed of sound and ν the frequency. The speed of sound in water is about 1480 m/s [82] and ultrasonic wavelengths are thus in the range of 15 mm to 75 mm, approximately. The geometry of the sample determines if standing waves are generated or not. For laboratory installations, standing wave setups are often preferred: the location of zero and maximum amplitudes is known, easing interpretation of experimental observations. For non-laboratory applications, standing wave setups are rarely found.

If cavitation occurs, the thermodynamic conditions in the sample are more complex. The books of Neppiras [83] and of Franc [84] give a good introduction to the topic of acoustic cavitation. The current state of knowledge and discussion is sketched in the following sections, with a special focus on what is known about the boundary conditions that apply for sononucleation.

Pressure

Minimum pressure The pressure amplitude of the ultrasonic field itself is determined by the parameters of the ultrasonic generator, and the tensile strength of the liquid. When cavitation occurs, pressure peaks during bubble collapse may exceed the pressures of the ultrasonic field by orders of magnitude.

In figure 2.16, a schematic definition of pressure ranges relevant in the context of sononucleation is given.

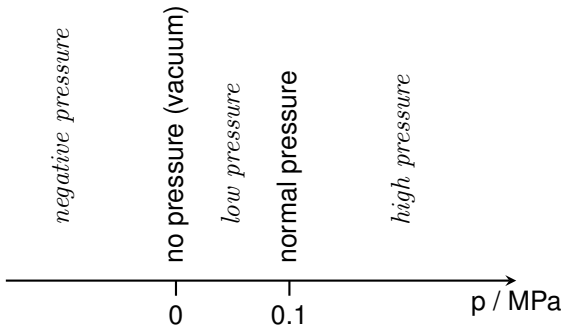

Figure 2.16.: Definition of pressure ranges.

The pressure in an ultrasonic field $p(t)$ oscillates around the atmospheric pressure p_0 with an amplitude p_{US} determined by the power of the sound generator.

$$p(t) = p_0 \pm p_{US} \sin 2\pi\nu\, t \tag{2.31}$$

If the amplitude p_{US} is larger than atmospheric pressure p_0, in theory also negative pressures can be reached. However, there is a lower limit to the pressure which is given by the cavitation threshold of the liquid p_{cav}. For periodic sound waves like in equation (2.31), this lower limit implies an upper limit, i.e.

$$p_{max} = p_0 + (p_0 - p_{cav}) \tag{2.32}$$

However, if the cavitation threshold is passed, and transient cavitation occurs, collapsing cavitation bubbles cause shock waves. The maximum pressure of these shock waves can then exceed the periodic maximum pressure by orders of magnitude.

Similar to the nucleation of the solid phase, also the nucleation of the vapor phase is strongly influenced by impurities. Again, dynamic experiments yield much higher nucleation limits than do static experiments. Also, surface effects are important. An early theoretic analysis of the effect of surface tension on bubble dynamics was carried out by Epstein in 1950 [85]. The author lines out, that stable gas bubbles exist only because of surface effects. Not only impurities, but also cosmic radiation reduces the cavitation threshold in experiment. A study by Sette and Wanderlingh [31] on water samples showed that samples shielded from cosmic radiation have a higher

cavitation threshold. A recent careful study of the cavitation onset in water was carried out by Herbert et al. [86]. They used focused ultrasonic waves and studied different variation of parameters of their setup, such as gas content, temperature of the sample, amplitude of the sound pressure. They argue that the theoretically predicted cavitation threshold of about -120 MPa is not reached by far in experiment because of invalid extrapolations and / or because of impurities in the samples. In their experiments as shown in figure 2.17, at most -27 MPa were reached.

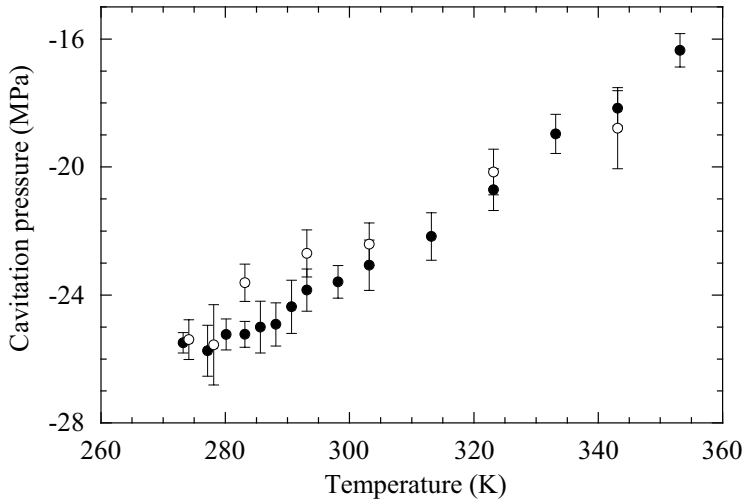

Figure 2.17.: Temperature dependency of the cavitation threshold in water as reported by Herbert [86]; open and filled symbols denote two sets of experiments. There could be a bend upwards for temperatures below 277 K, and thus for subcooled water, but this is not clearly visible from the available data.

The general disagreement of theoretic expectations and experimental data on the cavitation threshold is addressed by Lubetkin [87]. The author suggests that the surface activities of solved gases are not appropriately included in theory. The discrepancies in measured tensile strength of water are the topic of a recent review by Mørch [88], too. The author's conclusion is that presence or absence of surfaces, and their structure, has a great impact on the nucleation of gas bubbles. Reported values for the tensile strength range from about -0.15 MPa to -30 MPa. A strong temperature dependence of the tensile strength is observed, with a maximum at around 283 K.

The experimental determination of the cavitation threshold in shock-wave experiments is difficult. Staudenraus and Eisenmenger [89] present a special hydrophone to measure ultrasonic and shock-wave pressures in water. In figure 2.18, a pressure shock in water is shown. They observe a negative pressure of about -7.2 MPa during about 8 μs after the shock. Then, cavitation is nucleated and the pressure rises again. The maximum pressures during the cavitation bubble collapse is then only about 5 MPa.

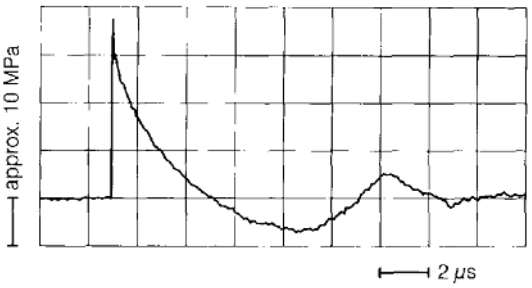

Figure 2.18.: Pressure during a shock as measured by Staudenraus et al. [89]. An electromagnetic shock causes a high pressure peak, that is followed by a strong negative pressure of about -7.2 MPa during about 4 μs. Only then, cavitation develops.

The cavitation threshold also plays a role in a biologic context: A recent publication suggests that Dolphins' speed is limited by the onset of cavitation and associated injuries [90]. Whether cavitation is a limiting factor in the vertical water transport in trees is controversly discussed [91, 92]. The actual value of the cavitation threshold does not seem to be well established in biology either.

Data for subcooled water is not reported in any work, presumably because the nucleation of the solid phase makes such experiments difficult. Considering the highly dynamic conditions in an ultrasonic field, probably a value similar to the highest reported value of -30 MPa is appropriate for cavitation triggered by ultrasound. Judging from the published works, a more negative pressure is very unlikely to occur, but less negative pressures can easily be .

Maximum pressure As to the maximum pressure during cavitation bubble collapse, it is highly sensitive to impurities, particularly dissolved gases. If gases are present in an insonicated sample, cavitation bubbles are more readily filled with them than with vapor of the liquid. During the bubble collapse, the re-dissolution of the gases exhibits another, usually slower, kinetics than does the condensation of vapor.

Pressures of several hundred MPa are supposted to be reached during cavitation bubble collapse in water according to Trilling [93]. This estimation is based on some simplistic assumptions, such as a nonviscous, nonconducting, perfect gas, which is initally at rest inside the bubble. The results from simplistic bubble collapse calculations may however be quite misleading [26]. Reasons are that the finite compressibility of the liquid has to be considered, the collapsing bubble may lose its spherical form, and mass transport effects become significant. A better prediction of the pressure profile during bubble collapse is therefore dependent on a very precise knowledge of material data and boundary conditions.

Heterogeneous nucleation of gas from liquid on solid surfaces was investigated by Qi [94], who clearly states that theory does not predict experiments with good precision. A study on the role of dissolved gases on cavitation in water was published by Behrend

and Schubert [95]. “On the one hand, gases were found to be indispensable for the onset of cavitation at typical conditions in practice. Gas molecules or micro-bubbles provide the basis for bubble formation and growth. On the other hand, however, an increasing content of gas in the liquid increases the gas/vapor ratio inside the bubbles. Due to the dissolution kinetics, the gas acts as a buffer, cushioning the collapse of the bubbles and, thereby, reducing the shock wave intensity. ” In experiments, a clear effect of hydrostatic pressure on the cavitation intensity could not be observed. The authors argue that both the number of cavitation bubbles and the intensity of each bubble collapse is influenced by hydrostatic pressure, but cannot be independently investigated. The role of the bubble content was also discussed by Brennen [26] in the context of jet formation and nonspherical bubble shape during collapse. “Stable oscillations are more likly with predominantly gas-filled bublles while bubbles which contain mostly vapor will more readlily exhibit transient acoustic cavitation.” The accumulation of inert gas in sonoluminescing bubbles was studied by Lohse and Hilgenfeldt [96]. Different solubilities and diffusivities cause an accumulation of non-dissociating products of sonochemical reactions. Very interesting in the context of sononucleation is the asymmetric behavior of bubble growth and bubble collapse. As a tendency, the movement of dissolved gas from the liquid to the bubble is quicker than from the bubble to the liquid. This would result in a buffering of the bubble collapse, and reduce the associated pressure peaks.

A study of water samples with different surface active additives [97] showed that stable and transient cavitation have distinct acoustic emission spectra. The authors of this study conclude that charged additives have a significant effect on cavitation behavior. The individual cavitation bubbles are repulsed by electrostatic forces, coalescence is avoided and transient cavitation is reduced.

In the context of this work, the presented references lead to the conclusion, that, unfortunately, the pressure peaks during cavitation bubble collapse have to be considered very sensitive to the sonicated material. Literature values from single bubble experiments are to be used with precaution.

Temperature

Ultrasound is a form of mechanical energy and thus provides heat to the insonicated liquid. If no cavitation occurs, the liquid is mixed on the length scale of the soundwave. Beyond the cavitation threshold, the situation becomes more complex.

An experimental approach to determine temperatures in the ultrasonic field is sonochemistry. Substances are found in sonicated samples, that are formed only under extreme thermodynamic conditions. An analysis of the chemical composition of the sonicated sample is done to assess the physical conditions during the sonication.

Sonochemistry in water was investigated by Suslick [98], who comes to the conclusion that several thousand K are commonly reached in the water samples when cavitation occurs. Studies that use sonochemical methods to determine the tempera-

tures of cavitation collapse in silicon oil and alkane solvents were published by Flint and Suslick [99]. A methyl radical recombination method was used in aqueous tert-butyl alcohol solutions in a similar study Ciawi et al. [100]. The maximum temperatures are estimated to approximately 5000 K.

The role of the liquid compressional viscosity in the dynamics of a sonoluminescing bubble was investigated by Moshaii et al. [101]. They describe the hydrodynamics of single bubble sonoluminescence in water with the help of a modified Rayleigh-Plesset equation, and study the variaton of compressiblitiy and viscosity of the liquid. The authors suggest that the peak pressure was significantly overestimated in earlier works, as shown in figure 2.19. They expect about 8000 K as peak temperatures during the bubble collapse.

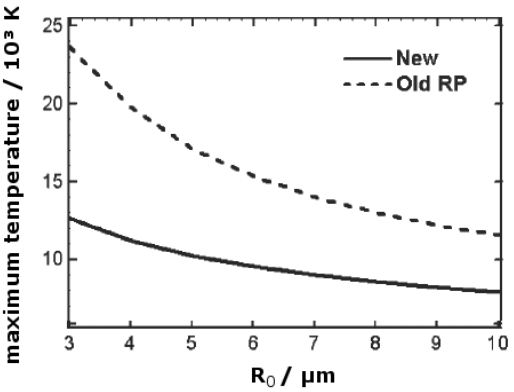

Figure 2.19.: The new calculation of Moshii et al. [101] from 2004 suggest that the peak pressure was significantly overestimated in earlier works. According to the corrected model, during the collapse of 10 μm bubbles, peak temperatures of about 8000 K are predicted.

Various sensors for the measurement of temperature in insonicated liquids were studied by Faid et al. [102]. They detected an elevation of the temperature by a couple of degrees only. One possible explanation for this observation might be, that the sensor covers a small region on a macroscopic scale, but not with respect to the cavitation bubbles. Then, the measured temperature is an integral over a very steep gradient and only a small heating effect is detected.

Concluding from these the works on the temperature in cavitating liquids, very high temperatures of several thousand K are to be expected. However, these temperatures are strongly localized, dependent on the bubble collapse dynamics, and their value is not well established.

2.2.4. Investigations of sononucleation

In this section, an overview of published investigations of sononucleation is given. In the vast majority, these investigations cover sononucleation of water / ice, but there

are also a considerable number of studies concerning sononucleation of solutions, a few works concerning PCM, and some more "exotic" materials.

Sononucleation of water

The main reference for sononucleation of water is the early work of Hickling [103] entitled *Nucleation of freezing by cavity collapse and its relation to cavitation damage*. "[It is proposed] (a) that the sub-cooling may easily reach the critical level for the homogeneous nucleation of freezing; (b) that, once it is initiated, the growth of ice particles is very rapid." Since then, investigations of ultrasonic nucleation of subcooled water were carried out by many groups. Most of the more recent works were carried out in China and Japan, where ice storage is a common technique [104, 105, 106, 107, 108]. Although the investigations have a different focus, all authors agree that ultrasonic treatment of water is an effective nucleation method. Nucleation in the sample volume and explicitly not on the container wall was observed by Zhang [106].

Despite the intense research, it is striking that Lee and Wang [109] conclude in their review and discussion of published sononucleation literature that the proposed mechanisms for water are not plausible, and do not suggest any alternate mechanisms.

Sononucleation from solutions

The nucleation from solutions is mainly of interest for the pharmaceutical industry. Here, products of synthesis are produced in supersaturated solutions. The required high purity of the drugs is prohibitive for the use of foreign seeds. A constant quality and grain size is very important for the further processing. Therefore, large subcooling and subsequent uncontrolled crystal growth is not favored.

Recent experiments at the chair of Prof. Schembecker, university of Dortmund [110], have shown that ultrasound can effectively nucleate supersaturated solutions. Sononucleation was found to be insensitive to a variation in sonic frequency, amplitude, as well as to the pH and viscosity of the sample liquid. Surprisingly, experiments without ultrasound and just passing small air bubbles through the sample have resulted in improved nucleation, too. A nucleation activity of bubbles was also observed previously in organic materials [111].

Acetylsalicylic acid (aspirin) in supersaturated solutions was investigated by Miyasaka et al. [112]. The influence of ultrasound on nucleation phenomena was studied with the goal to control the crystal size of the solid precipitate. The setup was similar to that used in the study of $Na_2HPO_4 \cdot 12\,H_2O$ discussed above. As shown in figure 2.20, depending on the intensity of the ultrasound, the authors suggest that the sonication actually enhances or inhibits nucleation. They argue that a minimum energy supply by the ultrasound is needed to overcome the nucleation barrier, and that too strong ultrasound can break up subcritical nuclei.

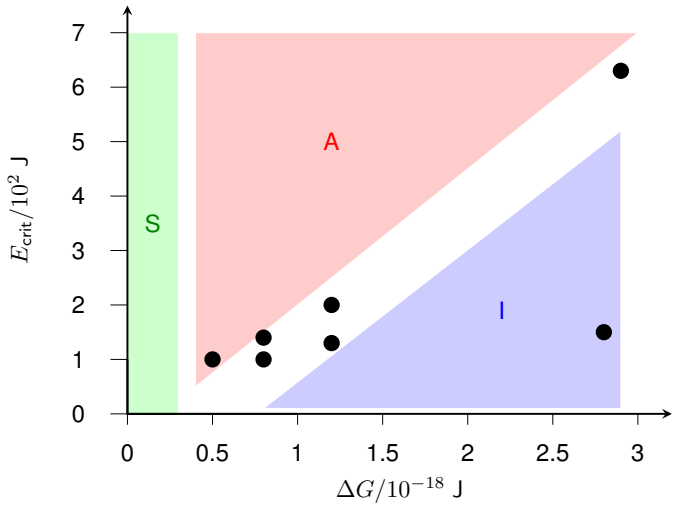

Figure 2.20.: Nucleation is spontaneous for small nucleation barrier ΔG and any ultrasound intensity E, marked by the green region (S) in this plot after Miyasaka et al. [112]. Most reported sononucleation experiments (•) are not clearly attributed to the regions of enhanced nucleation (A) or inhibited nucleation (I).

The authors explicitly speak of primary nucleation, which was detected visually. An interesting point is the finding that "the ultrasonic energy needed to activate primary nucleation decreases with a decrease in the energy necessary to form a stable nucleus.". This implies that the ultrasonic energy is directly used to enhance the nucleus growth. There is no mention whatsoever of cavitation phenomena in this work.

A study on *ammonium sulphated solutions* is reported by Virone et al. in their publication entitled "Primary nucleation induced by ultrasonic cavitation" [113] They observe a quicker nucleation in insonicated samples at otherwise similar conditions. Their attempt to establish a correlation between the collapse pressure of the cavitating bubbles and the nucleation rate was however not successful. The authors attribute this discrepancy to a large number of uncertainties. In fact, particularly their assumption that an underestimated pressure amplitude and an overestimated bubble size cancel out with respect to the nucleation rate is not convincing.

In their recent investigation of crystallization of *2,4-dinitrotoluene* from solution [114], Chen and Huang attribute a "significantly accelerated crystal formation" to an elevation of mass transfer rate for crystal growth. The concept of induced nucleation is not pursued any further in this work.

Sononucleation of PCM

Studies on substances that are used as PCM are reported for $Na_2HPO_4 \cdot 12\,H_2O$ [115], $NaOAc \cdot 3\,H_2O$ [116], and erythritol [117].

A theoretic analysis of a special case of sononucleation was done by Rogerson and

Cardoso concerning $NaOAc \cdot 3\,H_2O$ in heat packs [116]. The authors confronted cavitation theory with nucleation theory, considering a rough estimate of the nucleation pressure based on room pressure data only, and the time available for nucleation process during a cavitation pressure peak. They conclude that, in the best case, "a minimum initial pressure for nucleation of at least 100 bar [sic! must be 10 kbar = 1 GPa, see figure 2.12] at any temperature" is needed.

A study of sononucleation in $Na_2HPO_4 \cdot 12\,H_2O$ was conducted by Miyasaka et al. [115]. They observed a clear reduction of subcooling by ultrasonic treatment, as shown in figure 2.21. Also, a faster heat release of the crystallizing PCM was detected when

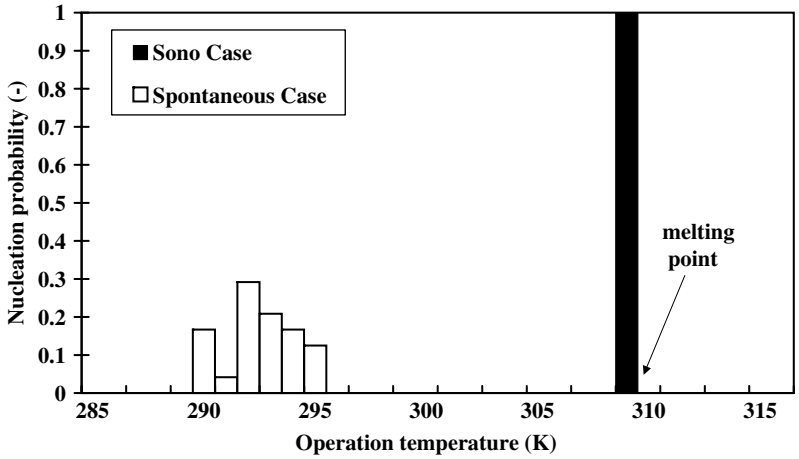

Figure 2.21.: An experimental investigation on disodium hydrogen phosphate dodecahydrate showed strongly reduced subcooling under ultrasonic treatment; figure from Miyasaka et al. [115].

the sample was insonicated. The authors propose that "ultrasound irradiation caused the implosions of cavities. These implosions then caused primary nucleation, which in turn generated heat." As to the imploding cavities and their sort of impact on nucleation, it is suggested that they provide localized energy which is needed for the nucleation.

Ultrasonic treatment of erythritol was investigated by Matsuda et al. [118]. While erythritol is no salt hydrate, this study is still one of the few documented studies of sononucleation on PCM. The authors report that subcooling was reduced from 60 K without treatment to about 23 K with ultrasonic treatment, as shown in figure 2.22.

Sononucleation of other materials

Organic materials Günther and Zeil [119] investigated crystallization speeds of glycerine and benzophenone in the ultrasonic field. Both benzophenone and glycerine could not be nucleated by ultrasound. The authors found that the speed of formation

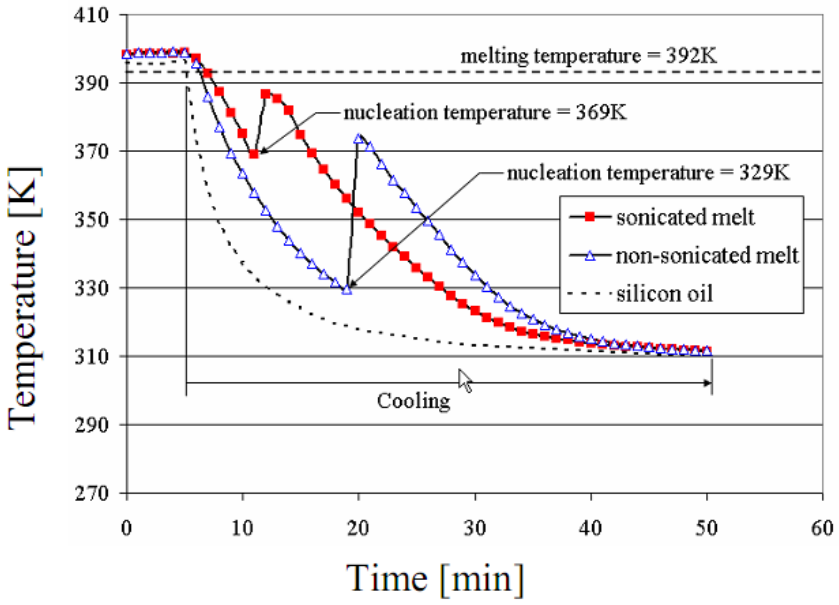

Figure 2.22.: Reduced subcooling was observed in erythritol treated with ultrasound of 30 kHz and 50 W. Figure from Matsuda et al. [118].

of the solid phase was improved for subcooled benzophenone, but decreased for subcooled glycerine. The authors reason that the energy that is brought into the sample via the ultrasound increases the sample temperature and thereby reduces crystallization speed. In the case of benzophenone, enhanced removal of latent heat from the phase front is believed to speed up the crystallization process. The transport induced by the ultrasound is only visible if the phase front movement is slower than the sonophoretic movement. It was proved that dissolved gases play a dominant role in the effect of ultrasonic irradiation.

There is a patent concerning sononucleation of organic materials, in particular of triglyceride oil [120]. These materials are reported to nucleate by ultrasonic irradiation even when the cavitation threshold is explicitly not surpassed. The inventors state that the general believe in cavitation of the mechanism promoting sononucleation is a prejudice, and nucleation of fats in the ultrasonic field can also occur without transient cavitation. The problem of transient cavitation is that the high temperatures during bubble collapse cause some chemical reactions that badly influence the taste of the treated fat.

Metals Sononucleation of germanium, gallium, silicon and bismuth was studied by Hickling in the 1960ies [103]. He observed no nucleation in the ultrasonic field, although those materials have a similar melting curve as water, which was successfully nucleated by US. However, the turn upward in the melting curve is found at much

higher pressures, e.g. for bismuth at 1.8 GPa (for water, at 200 MPa).

A second early work about sononucleation of metals was published by Hunt and Jackson [121]. Their sample materials were nickel and cobalt. They suggest that, during the growth of the solid phase, negative pressures are created by the volumetric shrinking. These negative pressures would nucleate continuously more solid phase, and this would be the predominant mode of crystal growth.

Overview of proposed mechanisms of sononucleation

The early works of Hickling, Hunt and Jackson introduced potential nucleation mechanisms, that were discussed from then on. All of those mechanisms are based on an increased subcooling, which then leads to statistical nucleation. The proposed mechanisms are:

- ▷ evaporative cooling during bubble expansion
- ▷ high pressure during bubble collapse, leading to a melting point elevation
- ▷ adiabatic cooling during decompression at bubble collapse, i.e. the shrinking volume of the bubble puts tensile stress on the surrounding liquid, and in an adiabatic situation leads to cooling.

More recent works [122] suggest that ultrasound does not improve homogeneous nucleation by a thermodynamic mechanism, but that rather the collapse of cavitation bubbles creates nucleation sites for heterogeneous nucleation.

2.2.5. Summary of the scientific context of this work

In short, the consequences of the available reports for this work are the following:

- ▷ Nucleating agents are very specific to a target substance: if no data is available for one substance, a transfer from another substance is at least very risky.
- ▷ In addition to effective seeds, so-called nucleating agents, many weakly nucleating materials exist. However, they are not easily identified and usually unknown.
- ▷ Nucleation can also be hindered by additives, not only improved (antinucleation).
- ▷ Sononucleation is experimentally established for water, but the mechanism is controversely discussed.
- ▷ Both volume and surface mechanisms have to be considered for sononucleation.
- ▷ Accelerated crystal formation from solutions is observed for several substances, but it is not clear if this is sononucleation.
- ▷ The physical state generated by ultrasound and cavitation in liquids is possibly very sensible to the sonicated liquid.
- ▷ The thermodynamic conditions during cavitation are not well established, and the physical interpretation of sonoluminescence is an open question.

3. Experimental work

In this chapter, the experimental work is presented. At first, the general considerations are lined out, i.e. the sample substances are presented and the common design principles of nucleation experiments are discussed. This part is followed by the description of the individual experiments. As a number of different experiments were carried out, each experimental setup is described and the corresponding results are summarized in a separate section. The discussion of the overall results is done in chapter 4.

3.1. General considerations

Before the actual experiments and their results are presented in detail, some general considerations are lined out in this section. The choice of the sample substances and the container materials, as well as the time scales used in the nucleation experiments are explained.

3.1.1. Sample substances

In this work, water and three inorganic PCM from the material class of salt hydrates were used as samples. The selected salt hydrates are sodium acetate trihydrate, calcium chloride hexahydrate and potassium fluoride tetrahydrate, written as $NaOAc \cdot 3\,H_2O$, $CaCl_2 \cdot 6\,H_2O$ and $KF \cdot 4\,H_2O$, respectively. The material purity as declared by the supplier is listed in table 3.1.

Table 3.1.: The purity of the salt hydrates as declared by the suppliers refers to the hydrated salt (^{h}) or the dried salt (^{d}). The purity of water is given as declared by the purifying apparatus (ion exchanger: resistivity; microfilter: pore size).

	purity in %	supplier
$KF \cdot 4\,H_2O$	$> 98.5\,^d$	Sigma-Aldrich
$CaCl_2 \cdot 6\,H_2O$	$97 - 103\,^h$	Merck
$NaOAc \cdot 3\,H_2O$	$99.5 - 101\,^h$	Merck

	resistivity $M\Omega\ cm^{-1}$	pore size μm
H_2O	> 0.1	< 0.22

The thermodynamic and crystallographic properties of the materials, as well as the motivation for their choice are discussed in the following pages.

Basic properties of the sample materials

Some basic properties of the sample materials are shown in the following tables and graphs. Thermodynamic data is listed in table 3.2. Here, the specific volume change was determined from the densities ρ in the liquid and solid states as $\Delta v = \rho_{\text{liquid}}^{-1} - \rho_{\text{solid}}^{-1}$. This value is used to predict the slope of the melting curve according to equation (2.9b).

The phase diagrams of the salt/water systems are shown in figure 3.1. Crystallographic and structural data is represented in table 3.3, figure 3.2 and figure 3.3.

Table 3.2.: Thermodynamic data at normal pressure as given in [12, 123] and as determined by own measurements (*a*). Values are given for the specific volume change (Δv), phase change enthalpy (Δh), melting temperature at normal pressure (T_{m}^0), and the specific heat capacity of the liquid and solid phases ($c_{p,\text{liquid/solid}}$).

	Δv / cm^3g^{-1}	Δh / Jg^{-1}	T_{m}^0 / K	$c_{p,\text{liquid}}$ / $\text{Jg}^{-1}\text{K}^{-1}$	$c_{p,\text{solid}}$ / $\text{Jg}^{-1}\text{K}^{-1}$
H_2O	−0.087	334	273.15	4.22	2.10
$KF \cdot 4\,H_2O$	0.0038	231	291.5	2.39	1.84
$CaCl_2 \cdot 6\,H_2O$	0.085	191	302.8	2.2	1.4
$NaOAc \cdot 3\,H_2O$	0.092	226	331		2.79
	0.051[a]	230[a]		3.5[a]	

Table 3.3.: Crystallographic data from [12, 124, 125]. Values are given for the lengths of the unit cell (a, b, c), the monoclinic angle (β), the numbers of molecules in the unit cell (Z), and the coordination number (N_c).

material	lattice, space group	unit cell lengths /Å a	b	c	β/°	Z	N_c
H_2O (ice Ih)	hexagonal $P6_3/mmc$	4.5181		7.3560		4	
$KF \cdot 4\,H_2O$	monoclinic $P2_1/c$	6.80	13.29	6.64	90.67	4	
$CaCl_2 \cdot 6\,H_2O$	trigonal P321	7.860		3.87			9
$NaOAc \cdot 3\,H_2O$	monoclinic C2/c	12.321	10.425	10.380	111.72	8	

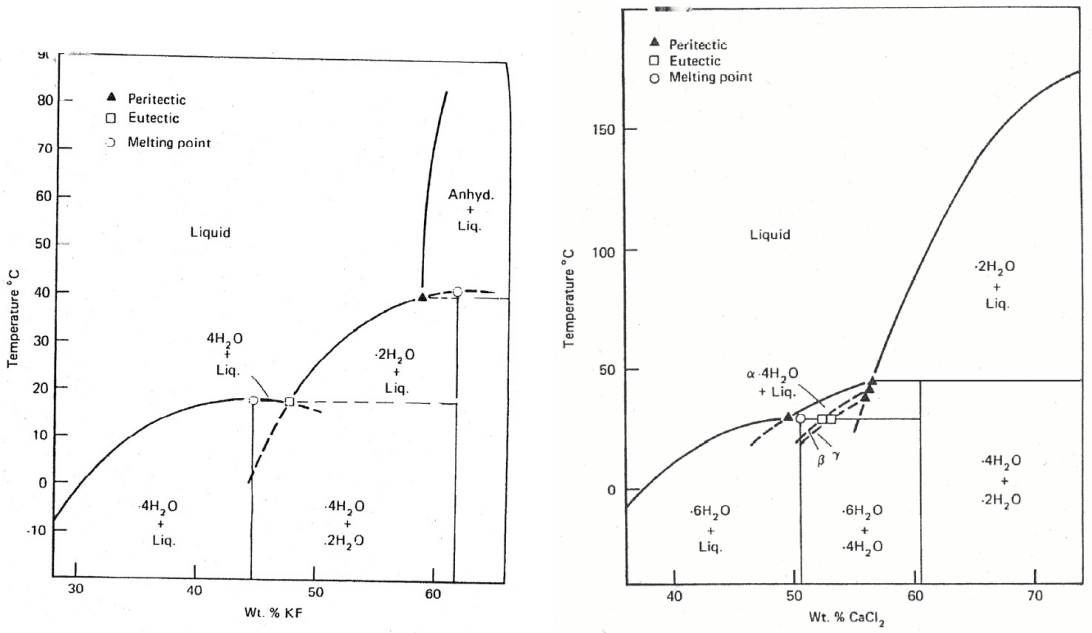

(a) water / KF

(b) water / $CaCl_2$

(c) water / NaOAc

Figure 3.1.: Phase diagrams of the water-salt systems of the investigated substances, graphs from [12]. For water as a pure substance there is no phase diagram provided.

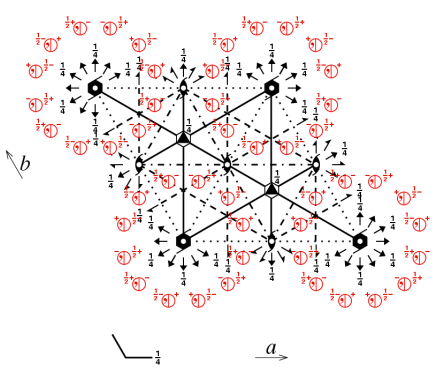

(a) P63mmc (water ice Ih)

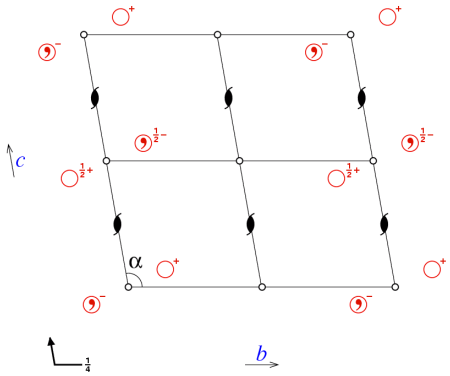

(b) P21c ($KF \cdot 4\,H_2O$)

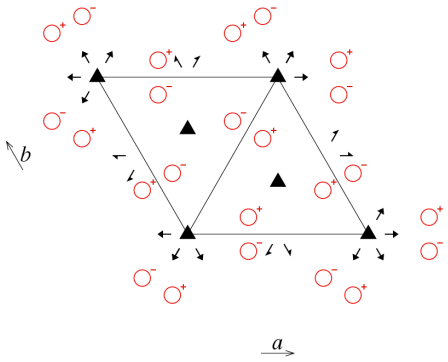

(c) P321 ($CaCl_2 \cdot 6\,H_2O$)

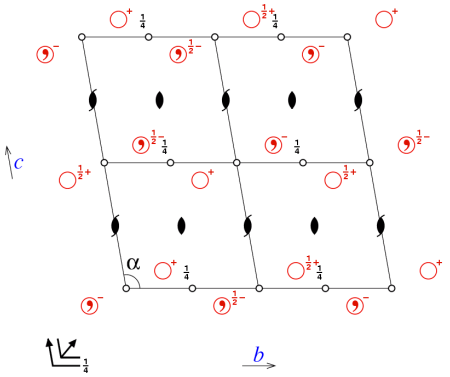

(d) C2/c ($NaOAc \cdot 3\,H_2O$)

Figure 3.2.: Space group diagrams that show the symmetry relations of the investigated solids. Graphs from [126].

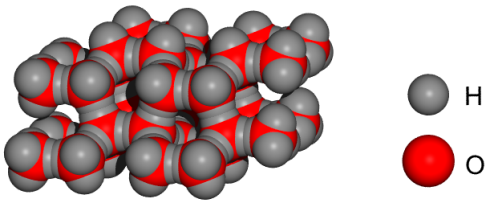

(a) ice Ih

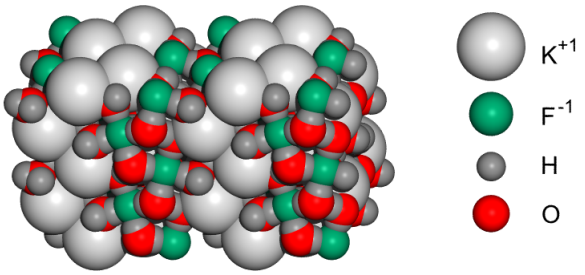

(b) $KF \cdot 4\,H_2O$

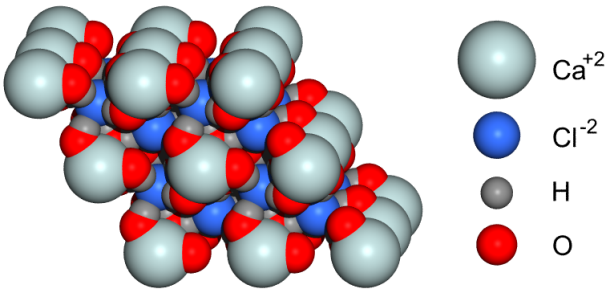

(c) $CaCl_2 \cdot 6\,H_2O$

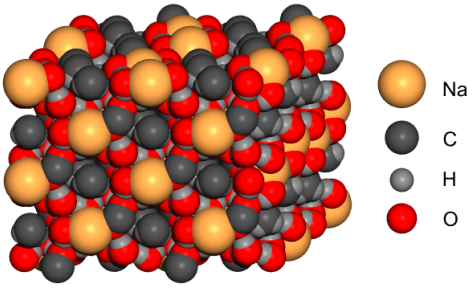

(d) $NaOAc \cdot 3\,H_2O$

Figure 3.3.: Crystal structures, ball plots. Plots generated with the softwares `Diamond` [127] and `POV-Ray` [128] based on data from [124, 125, 129, 130, 131].

Key characteristics of the sample materials

For this work a group of four sample substance was chosen. Ideally, the samples shall allow a systematic analysis of aspects that have an impact on nucleation, and additionally be of some practical relevance, as lined out in the following.

Purity A high purity of the sample substance is desired in nucleation experiments to avoid heterogeneous nucleation and thus acquire data which is representative for the sample substance itself. If absolute purity is not obtainable in practice, another approach is to use samples with well-determined purity and thus avoid unspecified impurities, which could provide additional, uncontrolled and thus random nucleation sites. In this work, water and salt hydrates are used as sample substances. While water as a single-component substance can be readily purified, this is more difficult for the salt hydrates. In particular, the correct water content of the hydrates is a potential problem. Chemical purity with respect to the salt component can be assured by using analytical grade salts. However, while purity in an analytical context might be high, even low concentrations of some contaminants may alter the nucleation behavior. Therefore, only samples from one lot were used throughout this work to assure well-defined impurities. In order to study the influence of impurities, some intentionally non-pure samples were investigated, too.

Phase change behavior Using the phase diagrams in figure 3.1, the expected melting and solidification behavior of the samples can be analyzed. A simple phase change without separation of components is expected for water as a pure material, and for $KF \cdot 4\,H_2O$ as a congruent melting salt hydrate. For $CaCl_2 \cdot 6\,H_2O$ and $NaOAc \cdot 3\,H_2O$, the situation is more complex. These salt hydrates can form different hydrates and salt solutions above the maximum stable temperature of their solids, showing an incongruent melting. Incongruent melting is very common among inorganic PCM. For nucleation, incongruent melting is expected to pose no particular experimental difficulties. Still, the phase diagrams might look different at high pressures due to a possibly changed solubility of the components.

Crystal structure The crystal structure of the samples is relevant for dynamic nucleation experiments, because it has an impact on the speed of crystal growth. Salt hydrates in general have a complicated crystal structure with many atoms in the unit cell, and $NaOAc \cdot 3\,H_2O$ has a particularly complex arrangement of the atoms in the crystal, as shown in figure 3.4. It can be seen that four sodium ions are found in very close proximity. $KF \cdot 4\,H_2O$ apparantly also has its anions closely grouped, as seen in figure 3.3b. This is a rather unusual pattern. $CaCl_2 \cdot 6\,H_2O$ shows a more balanced arrangement of the molecules in the crystal. In contrast to the salt hydrates, water with its two-atomic molecules has a very regular pattern.

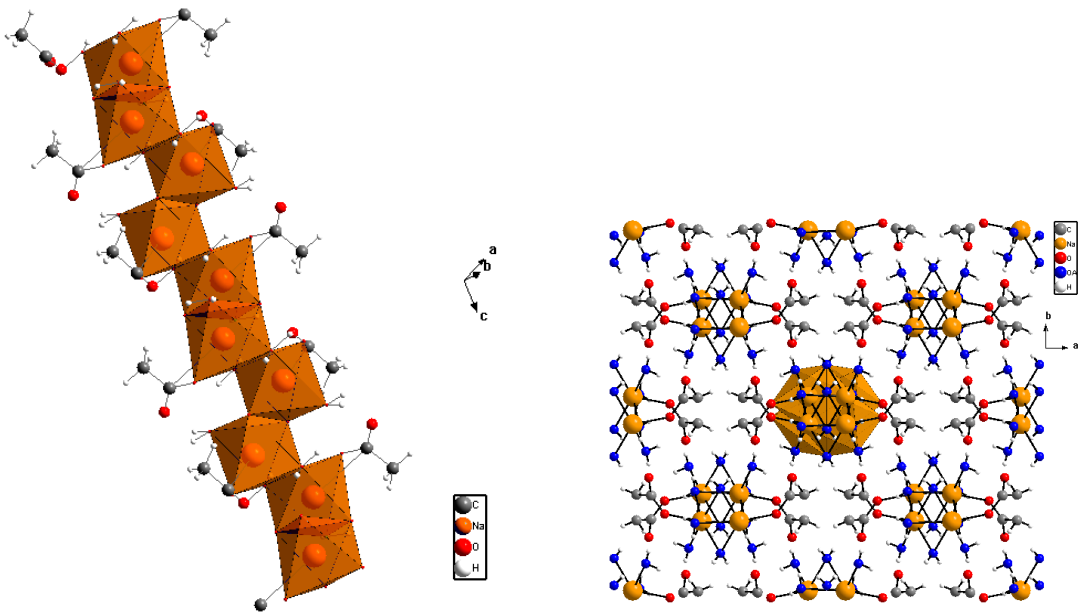

(a) **(b)**

Figure 3.4.: The structure of the $NaOAc \cdot 3\,H_2O$ crystal is comparatively complicated. The molecular arrangement in the solid phase is shown here from two different perspectives. Graphs by courtesy of Prof. Voigt [76].

Expected pressure effect From thermodynamic theory, the slope of the melting curve as function of pressure in equation (2.9b) depends on the volume change and phase change enthalpy. The volume change differs much more among the four materials than does the phase change enthalpy. Thus, the effect of pressure on the melting and subcooling behavior is expected to be large for materials with large volume change on phase change. This is the case for water, $CaCl_2 \cdot 6\,H_2O$ and $NaOAc \cdot 3\,H_2O$; for $KF \cdot 4\,H_2O$, the volume change is extremely small. This material is therefore thought to be comparatively insensitive to pressure changes, and therefore can serve as a counter sample in this work.

Reported subcooling The sample substances should subcool readily and considerably in order to allow an experimental assessment of factors that influence their nucleation temperature. Strong subcooling of at least 10 K is reported for all four substances in this work, with $NaOAc \cdot 3\,H_2O$ showing an outstanding value of about 80 K. An easy accessibility of the subcooled state is therefore assured for all samples. Nucleating agents are known for $NaOAc \cdot 3\,H_2O$ and $CaCl_2 \cdot 6\,H_2O$, which reduce the subcooling to a few K, which can be helpful in some experiments.

Reported sononucleation Successful sononucleation was reported for water. Ultrasonic experiments are reported for $NaOAc \cdot 3\,H_2O$, but no sononucleation was observed. For the other materials, no experimental data is known.

In summary, the chosen substances all have their advantages and disadvantages as samples in this work. Water is unusual in two main aspects: First, it is a pure material, which is rarely the case for any other PCM, but which simplifies its theoretic description. Second, water exhibits a density anomaly and its melting curve falls with pressure. The main reason to include this material is however that sononucleation for waters seems to be well established. $NaOAc \cdot 3\,H_2O$ and $CaCl_2 \cdot 6\,H_2O$ are typical for PCM in that they have a rather complicated phase diagram and a moderate volume expansion upon melting. $NaOAc \cdot 3\,H_2O$ is unusual with regard to its crystal structure, its tendency to lose water, and its large reported subcooling, but it is very commonly applied as PCM. Also, the work of Rogerson and Cardoso [30, 116, 75] provides a detailed theoretic study on the nucleation in heat packs based on this PCM. $KF \cdot 4\,H_2O$ has very similar densities in the liquid and solid states, which is exceptional. The phase diagram of $KF \cdot 4\,H_2O$ is however typical for salt hydrates, with several stable hydrates. All three salt hydrates are expected to be well accessible in their subcooled state in experiment.

3.1.2. Containers

The choice of the sample containers is very important in nucleation experiments. The two main experimental conditions that are determined by the containers are the outer surface of the sample, and the sample volume.

From nucleation theory, heterogeneous nucleation is known to lower the nucleation barrier or increase the nucleation temperature. In order to assess the nucleation temperature of a sample, nucleation on the container wall should be avoided wherever possible. There are a number of possible container arrangements with different expected nucleation activity, but also different experimental limitations.

Effect of change in water content A change in water content alters the melting and freezing behavior of a substance, and may change its equilibrium phase change temperature. Excess water in salt hydrates usually lowers the melting temperature and leads to incongruent melting behavior. In equilibrium, at temperatures below the stoichiometric melting temperature, the solid salt hydrate and a water-rich liquid phase are present. The composition of the phases can be read from the phase diagrams shown in figure 3.1. Considering the subcooled melt, it contains some additional water, that cannot become part of the solid phase. As a consequence, during the solidification process water molecules have to move away from the phase boundary by diffusion, a process that slows solidification down. The hindered growth process could induce a higher subcooling: the interface and volume terms that determine the nucleation barrier are unchanged, but the nucleation rate is reduced due to a necessary water diffusion. While this effect is assumed to be of moderate importance for slow processes, in shock experiments such as in ultrasonic cavitation it could become prominent. In a salt hydrate with excess water, during repeated freezing / melting cycles, water accumulates on top of a denser salt hydrate layer. Depending on the geometry of the sample and the kinetics of thermal cycling, the phase separation can be more or less complete. If complete phase separation occurs, a layer of salthydrate of standard composition and standard phase change temperature, and a layer of brine are formed. The brine does not take part in the phase change and is considered thermally inactive (only sensible heat effect). If the phase separation is blocked, i.e. by stirring of the sample or osmotic effects, the diffusion process has to take place during every phase change again and again. Analogous considerations are valid for an increased salt content by water loss. Phase separation effects can usually be detected by a visual inspection of the sample, if the sample container is transparent.

Levitation techniques Levitation techniques can be used to avoid a contact between sample and container. The liquid sample is confined by external forces, which counteract the gravitational force and thereby keep the sample without ground contact. There are different methods of levitation classified by this counteracting force, namely electrostatic [132, 133], optic [134], acoustic [135] and (electro)magnetic [136, 137] levitation. The choice of the levitation technique depends on the sample material and the investigated property. All in common is however that the sample is quite small, with typical droplet diameters ranging from μm to mm. While the missing solid container in levitated samples is of advantage as it avoids an external solid surface, it is at the

same time also of disadvantage, as it offers no barrier to mass transfer. In the context of subcooling of salt hydrates, levitated drops are unsuitable samples for various reasons. First, the large specific surface of a small levitated drop is unprotected from particles in the surrounding gas which could act as nucleation agents. Second, the water content will inevitably vary during an experiment, i. e. either increase if water vapor is available in the surrounding gas, or decrease if the experiment is carried out in a dried gas or vacuum. The chemical composition of the sample is then not well defined during the experiment and the acquired data is of very limited use. Additionally, evaporation or solution of water from or into the sample will alter the sample temperature. Third, the maximum volume that can be levitated is very small compared to the sample volume of the high pressure cell that serves as reference, as lined out below in "Sample volume". Due to these fundamental difficulties, levitation techniques were not used in this work.

Glass container Glass is a transparent solid with a high vapor and gas diffusion resistance, which qualifies it as a standard container material. Also, it has a very good stability against most chemicals and it has a smooth surface, so it can be cleaned from possible nucleating particles efficiently. As an amorphous material, it probably is at most a very weak nucleating agent itself. However, one main drawback of glass as a container material is its low resistance to mechanical stress. When subcooled liquids solidify, this can happen very rapidly and the volume change causes a significant stress on the container. Depending on the experimental setup, it is sometimes not possible to observe multiple solidification-melting cycles of one sample in one container if the container breaks. If multiple nucleation experiments of one sample are needed for statistical evaluation, glass containers are therefore not always suitable. In this work, glass containers of standard test tube size (approximately 15 ml) were used wherever possible. The uncovered surface of the sample which is in direct contact to the surrounding gas still offers an area for exchange of water, but it is small compared to the volume of the sample. If the test tube is closed, in the long run a chemical equilibrium is established in the gas volume above the sample, and the overall sample composition will only change to a very small extend.

Plastic container Containers made of plastics offer much better tolerance to mechanical stress than do glass containers, and enough transparency to observe the sample visually. However, the diffusion resistance of most plastics is not very high. Particularly in a setup where a highly concentrated salt solution is on one side of the plastics barrier, and distilled water is on the other side (as when using a water bath to keep a sample at a constant temperature), transmission of water by diffusion can be significant. The main factor which determines the amount of transmitted water is the time span of the experiment. Plastic containers therefore can be used for short experiments, but should be avoided for long time experiments, particularly at elevated temperatures. Polypropylene (PP), teflon (PTFE) and high density polyethylene (HDPE) are compati-

ble with the heat transfer fluids used in the thermostatic bath as well as with the chosen sample materials within the needed temperature range. The situation with respect to an exchange of matter with gas above the sample is similar to that described above for the glass containers.

Metallic container Metallic containers offer very good mechanical resistance, but they are opaque and thus prohibit a direct visual observation of the sample. In addition, chemical reactions with salt hydrates specific for each metal/PCM combination are to be expected as reported by Cabeza et al. [138]. Compatibility data is not available for all materials, and chemical reactions therefore cannot be excluded without preliminary lengthy corrosion tests. Even worse for nucleation experiments, metallic surfaces are not smooth on a microscopic scale, and are considered to show significant nucleation activity in some cases [75]. This was considered prohibitive and therefore, in this work, no metallic containers were used.

Sample volume In order to be able to compare as directly as possible nucleation data at room pressure, high pressure and under ultrasonic treatment, similar sample volumes should be used in all setups. The setup of the high pressure experiments is invariable, and thus determines the sample volume in the other experiments, too. Nucleation experiments reported in literature are often carried out with the help of a differential scanning calorimeter (DSC). This instrument is a standard equipment for thermal analysis [139, 140]. The sample volume in DSC instruments is typically less than 40 μl. The sample volume in the high pressure cell is about 10 ml, and therefore, DSC experiments were not used in this work but substituted with an own test stand for larger samples.

3.1.3. Time scales in nucleation experiments

Waiting time and sample size

Strictly speaking, nucleation theory defines a nucleation rate, but not a nucleation temperature. This is because the thermodynamic process of overcoming the nucleation barrier is governed by statistics. The nucleation rate is given in units of nucleation events per volume and time as a function of temperature and pressure.

If the speed of crystal growth is fast compared to the sample dimensions, the whole sample solidifies quickly after a single nucleation event has taken place. For a fixed waiting time, the larger the sample volume, the lower is the required ratio of nucleation events per volume. Similarly, the longer the waiting time, the lower is the required nucleation rate per time. Thus, a nucleation probability (as function of temperature) can only be given for a fixed sample volume and waiting time. A perfectly fixed sample volume and waiting time is difficult to achieve in experiment, and the sensitivity of

an experiment on variations in these values should be estimated. In figure 3.5, two example functions of the nucleation rate vs. temperature are sketched.

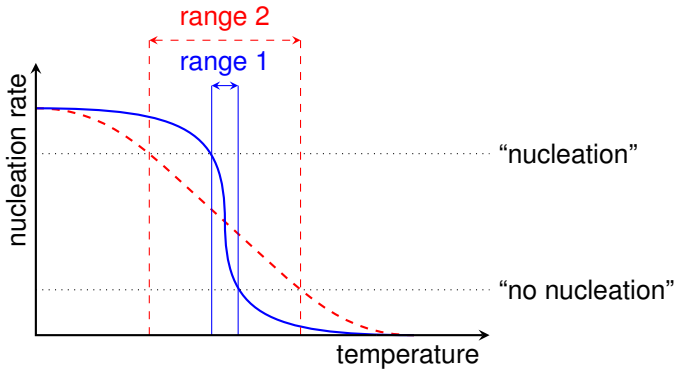

Figure 3.5.: For a given waiting time and sample size, the temperature range between observation of "no nucleation" and "nucleation" depends on the slope of the nucleation rate.

Two levels of the nucleation rate, indicated with horizontal lines, correspond to the experimental diagnosis "nucleation" and "no nucleation" for a given waiting time and sample volume; those are the observation thresholds. The intersections of these lines with the nucleation rate designate the corresponding nucleation temperatures. It can be seen, that the resolution of the nucleation temperature depends on the slope of the nucleation rate. If we change the levels of the observation thresholds, i.e. the sample size or waiting time, the variation of the nucleation temperature is different in the two cases. If the nucleation rate changes fast in a narrow temperature interval (solid line), the observed nucleation temperature is almost independent from the experimental setup. If the nucleation rate is less sensible to the temperature (dashed line), the nucleation temperature varies much more with a varying setup. Therefore, a certain variation of the setup should be carried out in nucleation experiments to assure a low sensitivity of the results with respect to small parameter variations.

Heat transport, cooling rates and temperature measurement

In any experiment where heat transfer shall be obtained without mass transfer, a thermal gradient is required. This is the case for the PCM samples in the nucleation experiments. If a thermal gradient is present in the sample, the sample has no defined single temperature. In the case of a static gradient, the nucleation takes place most probably at the coldest part of the sample. Quantitatively, the nucleation probability is defined by the nucleation rate as function of temperature as sketched in figure 3.5. If the nucleation rate shows a strong increase within the temperature interval that is present in the sample, a nucleation in the warmer part of the sample is highly improbable. The gradient then has primarily an impact on the active volume of the sample. That means, the volume where the nucleation rate is significant is not equal to the sample volume.

The active volume decreases for increasing thermal gradient. In order to minimize this effect, thermal gradients should be reduced as much as possible.

The size of the thermal gradient is determined by the speed of cooling and the heat transfer properties of the setup. The cooling rates in nucleation experiments should be small to keep the gradients small. The thermal conductivity of all sample substances in this work is similar, so similar cooling rates can be used. In the setups as described below, the temperature of the cooling fluid that is in contact with the sample test tube is expected to be uniform along the test tube, and a thermal stratification of the samples is avoided.

In the nucleation experiments, a temperature sensor which is in direct contact with the sample substance could act as nucleation site. Therefore, wherever possible, the sensor is placed outside the sample on the container wall. In principle, this arrangement reduces the accuracy of the temperature measurement, but in fact the effect is small and the temperature in any local point of the sample is anyway not exactly equal to the sample temperature as a whole as lined out above. The main focus of the temperature measurement is to acquire comparable data and detect changes in the nucleation temperature. This can be assured by using the same cooling rates, i.e. creating the same gradients, and measuring at the same spot.

3.2. Determination of the nucleation temperature at normal pressure

As a reference for the investigation of nucleation by high pressure or ultrasonic treatment, the nucleation temperature at normal pressure was determined. Normal pressure is the room pressure of about 0.1 MPa, more exactly it is typically in the range of 96 ± 2 kPa in the laboratory in Garching located at about 480 m above sea level [141].

3.2.1. Setup and procedure

The nucleation temperature is determined from many individual freezing experiments in order to achieve data suitable for statistical analysis. Six samples of one material are subjected in parallel to repeated freezing / melting cycles. Like this, a possible influence of the individual sample and of the cycles can be evaluated. For each sample material, at least 140 nucleation experiments are carried out altogether.

Setup

The general setup of the nucleation experiments is sketched in figure 3.6.

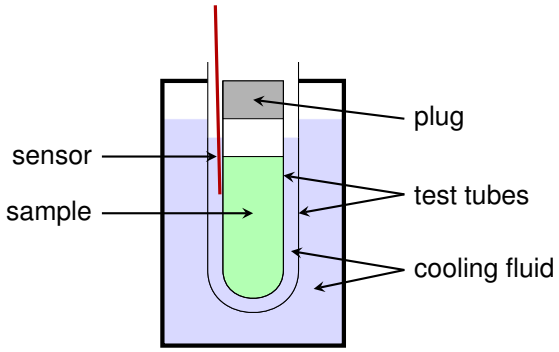

Figure 3.6.: Setup for the determination of the nucleation temperature, schematic.

For each sample, about 8 ml of the sample material are put in a glass test tube. This test tube is sealed with a plug and it is put inside a second, slightly larger test tube. The space between the two tubes is filled with the cooling fluid, and a temperature sensor is placed in the space between the two tubes, to detect the sample temperature. This double wall construction avoids putting the sensor directly inside sample, where it could serve as additional nucleation site. The space between the two tubes is only about 1 mm, and the sensor is in direct contact with the outer surface of the inner tube. Six samples are prepared in this way, and then are placed in a cooling bath.

Procedure

The thermostat controls the bath temperature according to a programmed ramp, heating and cooling the samples in a temperature range from below the nucleation temperature to above the melting temperature. The heating and cooling rates are slow, such that small thermal gradients in the samples are assured, and a correct detection of the sample temperature can be assumed. Typical rates are 0.2 K/min.

When a nucleation event occurs, the sample starts to solidify, setting free the latent heat of the phase change. The samples being phase change materials, this effect is large and the nucleation temperature can be securely detected by a rising temperature. The nucleation temperature is taken as the minimum temperature before a significant deviation of the temperature from the previous smoothly falling slope. As an example, in figure 3.7, the temperatures of six water samples during one heating / cooling cycle are shown. The nucleation events can be identified clearly by a sharp rise in temperature, as marked in the enlarged part shown in figure 3.7b.

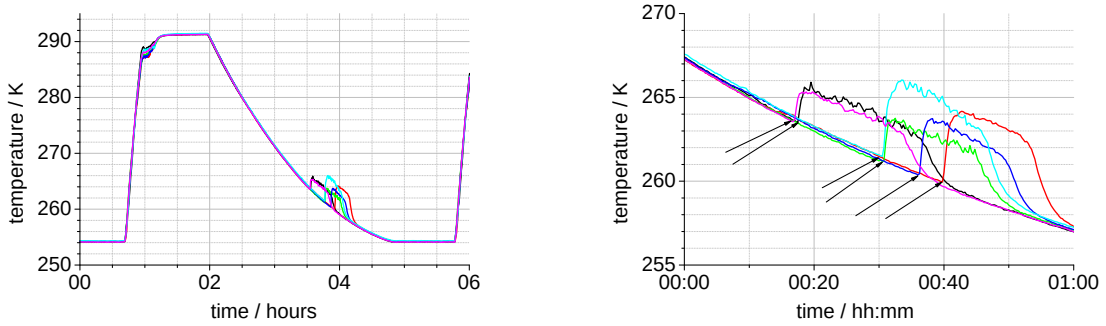

Figure 3.7.: A typical signal of a nucleation experiment is shown in (a). The start of the deviation of the sample temperature from the bath temperature, as marked by arrows in (b), is noted as the nucleation temperature.

It can be seen clearly in figure 3.7b that the maximum temperature after nucleation is not equal to the melting temperature of water. This is due to the position of the sensor with respect to the sample and the cooling power in the given setup.

3.2.2. Results

The results of nucleation experiments are displayed in the following graphs. For each material, the ramp, the time line plot and the histogram plot are displayed.

The ramp shows the temperature program that was used in the experiments. Those are not the programmed temperatures to control the thermostatic bath, but the real

temperatures that were measured during the experiment. In particular, the minimum and maximum temperatures and the actual cooling rates can be read from these graphs.

The time line plot shows the nucleation temperatures of each sample for each cycle. With the help of the time line graphs, the cycling behavior of each sample can be evaluated. If the nucleation temperature changes during cycling systematically, this is a hint for a phase separation. Also, a deactivation or activation of a nucleation seed can be identified from these plots.

Finally, the histogram summarizes the nucleation behavior of a material as a function of temperature only. The histograms show the distribution of observed nucleation events in given temperature intervals on the left y-axis, and the resulting probability to observe a nucleation event at a given temperature on the right y-axis. From the histograms, temperture ranges of low nucleation probability (less than 10%) and high nucleation probabilty (more than 90%) can be easily read.

Water

Experiments were carried out on purified water and tap water. The temperature program used for the experiments on H_2O is shown in figure 3.8. As minimum and maximum temperatures, 255 K and 292 K were chosen.

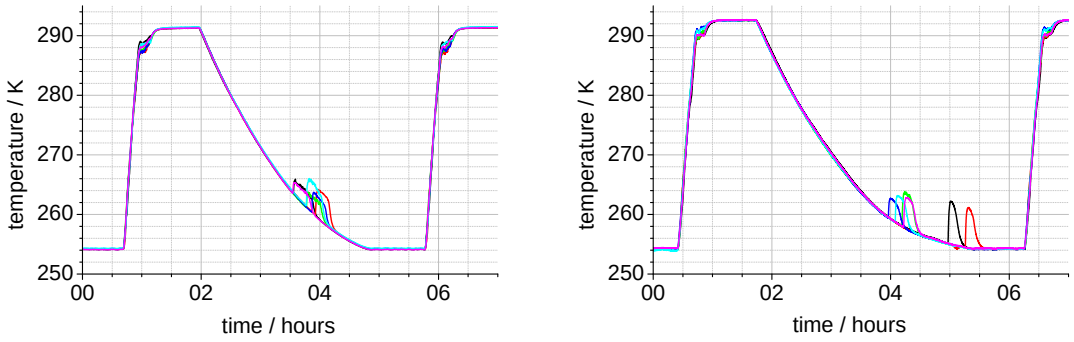

(a) tap water **(b)** purified water

Figure 3.8.: The temperature program used for the nucleation experiments of H_2O. The ramps for tap water (a) and purified water (b) were the same.

The time line of the nucleation temperatures of the individual samples is shown in figure 3.9.

For both materials, the scattering of the nucleation temperatures of the individual samples is small compared to the difference between the samples. There are some samples with significantly less scattering than others. While the general trend of the purified water is a lower nucleation temperature compared to tap water, there are some samples from the two materials that show very similar nucleation temperatures.

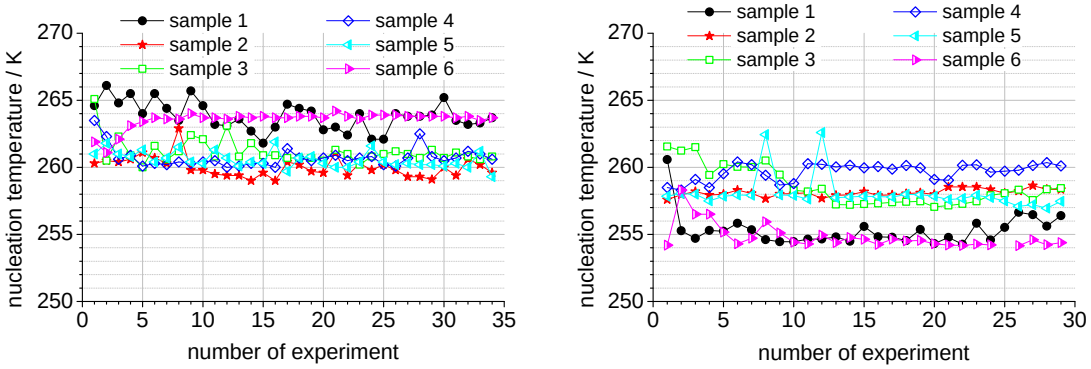

(a) tap water **(b)** purified water

Figure 3.9.: Time lines of the nucleation temperatures of tap water (a) and of purified water (b).

The histograms of the nucleation temperatures of H_2O are shown in figure 3.10.

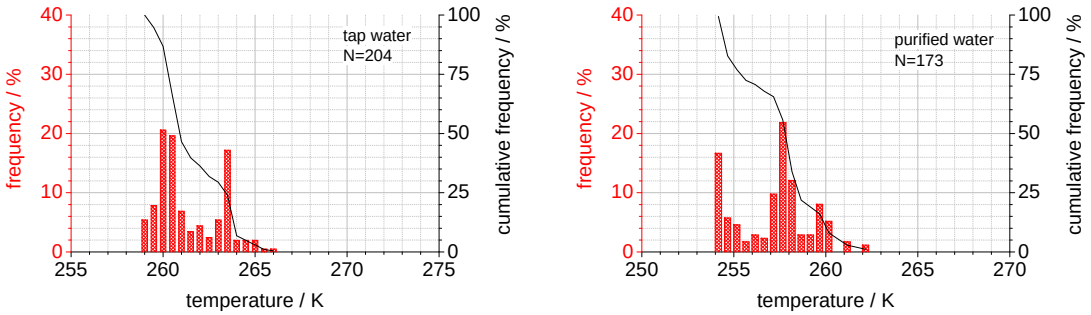

(a) tap water **(b)** purified water

Figure 3.10.: Histogram of the nucleation temperatures of tap water (a) and purified water (b). The number of nucleation events over equal temperature intervals is given on the left axis, the percentage of nucleated samples at a given temperature (the cumulated frequency) is given on the right axis.

The first nucleation events occur at about 266 K in tap water and at about 262 K in purified water. The strongest subcooling was found at 259 K in tap water and at 254 K in purified water.

$KF \cdot 4\,H_2O$

The temperature program used for the experiments on $KF \cdot 4\,H_2O$ is shown in figure 3.11a. The bath temperature was varied between 258 K and 303 K. The time line of the nucleation temperatures of the individual samples is shown in figure 3.11b.

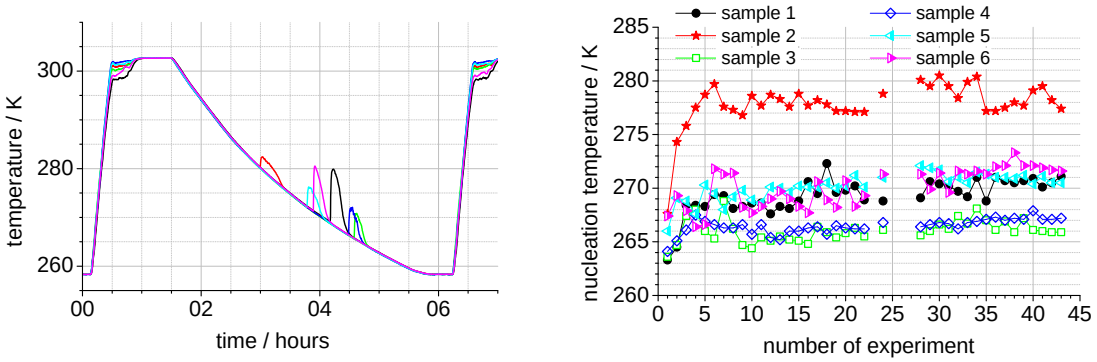

Figure 3.11.: The temperature program used for the nucleation experiments of $KF \cdot 4\,H_2O$ (a) and the determined nucleation temperatures of the individual samples during all cycles (b). Some data points around the 25th cylce are missing due to a temporary failure of the measurement equipment; the cycles were carried out but not recorded.

It can be seen that the nucleation temperatures vary more between the individual samples than between the individual cycles. Also, the very first nucleation temperatures are lower than the following for sample 2.

The histogram of the nucleation temperatures of $KF \cdot 4\,H_2O$ is shown in figure 3.12.

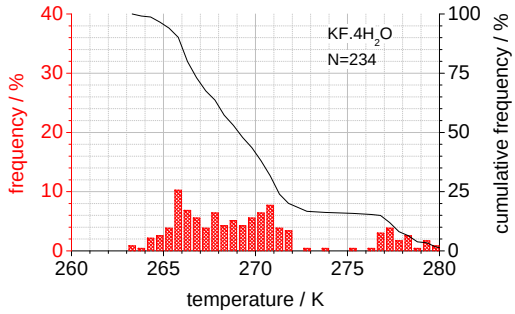

Figure 3.12.: Histogram of the nucleation temperatures of $KF \cdot 4\,H_2O$.

First nucleation events occur at about 281 K, or 12 K subcooling. Most nucleation events, i.e. 20% to 90%, were observed at $269\,K \pm 3\,K$.

$CaCl_2 \cdot 6\,H_2O$

The temperature program used for the experiments on $CaCl_2 \cdot 6\,H_2O$ is shown in figure 3.13a. A high maximum temperature of 328 K was chosen in order to avoid separation effects. The time line of the nucleation temperatures of the individual samples is shown in figure 3.13b.

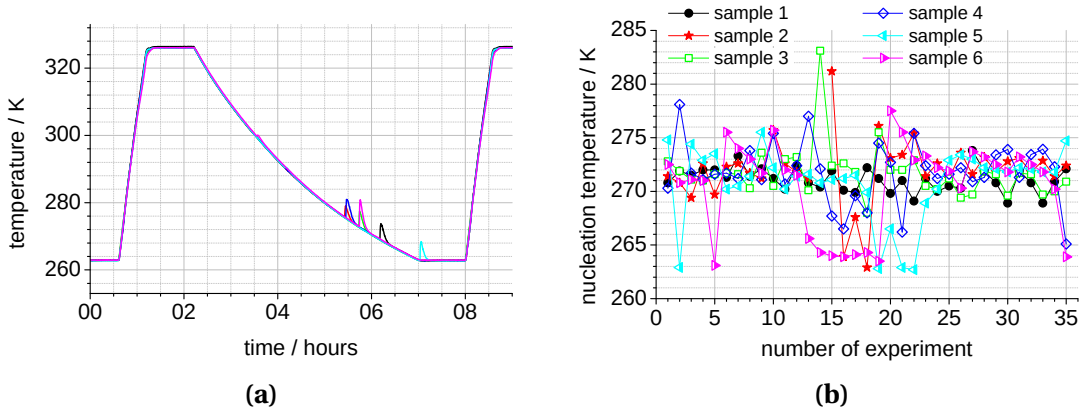

Figure 3.13.: The temperature program used for the nucleation experiments of $CaCl_2 \cdot 6\,H_2O$ (a) and the determined nucleation temperatures of the individual samples during all cycles (b).

All $CaCl_2 \cdot 6\,H_2O$ samples show very similar nucleation behavior, the variance of the cycles being in the same order of magnitude as the variance between the individual samples. Compared to the other investigated materials, the scattering of the nucleation temperatures of each sample is larger.

The histogram of the nucleation temperatures of $CaCl_2 \cdot 6\,H_2O$ is shown in figure 3.14. Very few first nucleation events occur at about 283 K, corresponding to 20 K subcooling.

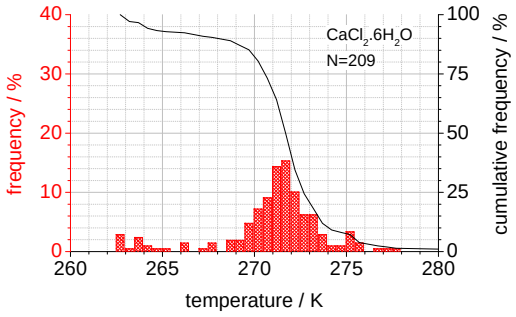

Figure 3.14.: Histogram of the nucleation temperatures of $CaCl_2 \cdot 6\,H_2O$.

The temperature range where most nucleation events were observed is $271\,K \pm 3\,K$.

$NaOAc \cdot 3\,H_2O$

The temperature program used for the experiments on $NaOAc \cdot 3\,H_2O$ is shown in figure 3.15a. During the heating, a slower segment was inserted in the ramp to slowly melt the sample. This was done to decrease mechanic stress of the phase change volume expansion on the glass tubes. However, still some of the glass tubes broke during the experiment, and the measurements were continued with new samples. The new samples are marked A and B in the time line plot in figure 3.15b.

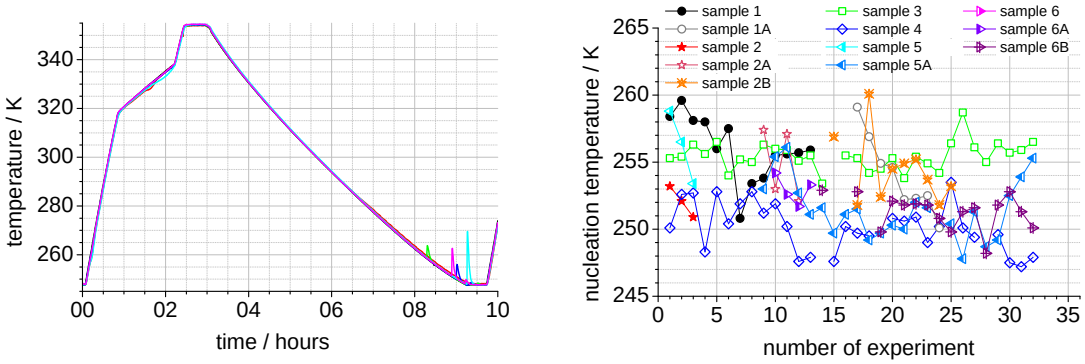

Figure 3.15.: The temperature program used for the nucleation experiments of $NaOAc \cdot 3\,H_2O$ (a) and the determined nucleation temperatures of the individual samples during all cycles (b).

Here, the scattering of the nucleation temperatures is of similar magnitude for the freezing cycles and between the individual samples.

A histogram of the nucleation temperatures of $NaOAc \cdot 3\,H_2O$ is shown in figure 3.16. First nucleation events occur at about 260 K, or 72 K subcooling. Most nucleation events were observed at $252\,K \pm 4\,K$.

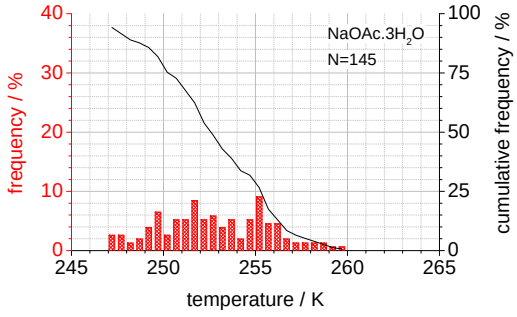

Figure 3.16.: Histogram of the nucleation temperatures of $NaOAc \cdot 3\,H_2O$.

3.3. Determination of melting and nucleation temperatures at high pressures

The maximum pressures that occur during cavitation bubble collapse are believed to be well above 100 MPa, as lined out in section 2.2.3. In order to evaluate the nucleation potential of such high pressures, the nucleation temperature as a function of pressure was determined experimentally. In parallel, the melting curve as a function of pressure was determined as well.

3.3.1. Setup and procedure

Setup

The experiments described in this section were carried out in a high pressure laboratory at the LFP (Lehrstuhl für Fluidmechanik und Prozessautomation, Technical University of Munich), located on the campus in Freising-Weihenstephan [142]. An autoclave suitable for static pressures up to 800 MPa was used for these experiments. The setup is sketched in figure 3.17, and some images are presented in figure 3.18.

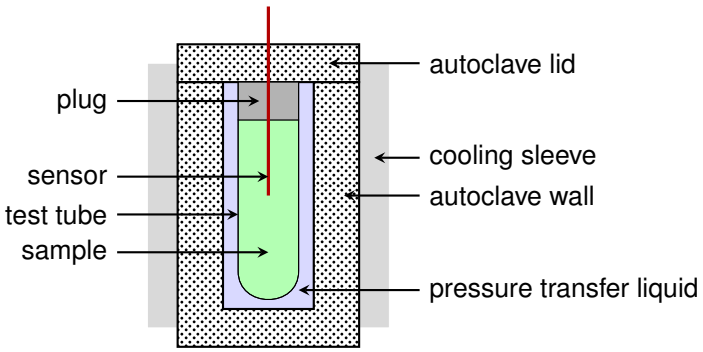

Figure 3.17.: Setup of the high pressure experiments, schematic.

The sample volume is about 10 ml, similar to that of the ambient pressure experiments. Glass could not be used as container material, because it would break when the pressure in the autoclave is changed. Therefore, PTFE test tubes were used instead. A gas cushion above the sample as in the ambient pressure experiments could not be realized here, as it would not allow a transmission of the pressure to the sample. The sample has to fill the test tube completely, and it was in direct contact with the plug which was made of silicone. The pressure is transmitted from the autoclave to the sample via a liquid with low compressibility, in this case ricinus oil.

The temperature of the autoclave is controlled by a thermostatic bath in the range of about 253 K to 368 K. Due to the large thermal mass of the autoclave, the temperature can be changed only slowly. The temperature and pressure of the autoclave is observed

(a)

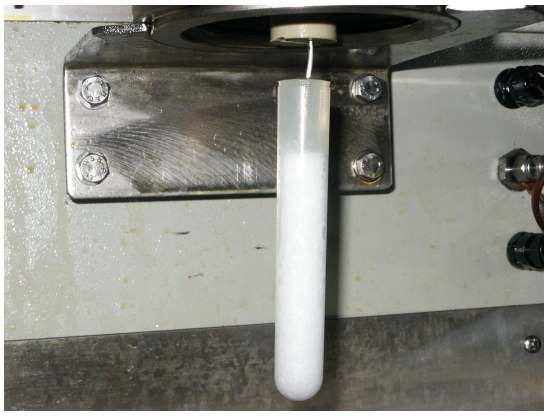

(b)

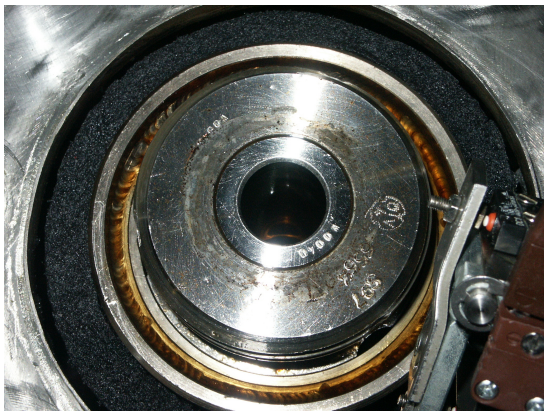

(c)

Figure 3.18.: The high pressure cell: total view (a), a view of the sample tube attached via the temperature sensor to the cell lid (b), and a top view into the open cell of the autoclave (c).

and recorded via computer equipment. The temperature is measured inside the test tube containing the sample by a thermocouple which is fed through the lid of the autoclave, as shown in figure 3.18b. Due to this arrangement, the temperature sensor could not be placed outside the sample but is directly immersed in the sample, in contrast to the other experiments of this work. The sensor was cleaned from solid PCM after each experiment using boiling distilled water.

Procedure

Two types of experimental procedures were used: isobaric cooling and isothermal compression experiments. The pressure change during both kinds of experiments was very slow, so the pressure conditions can be considered as quasi-static. Schematic recordings for both methods are shown in figure 3.19.

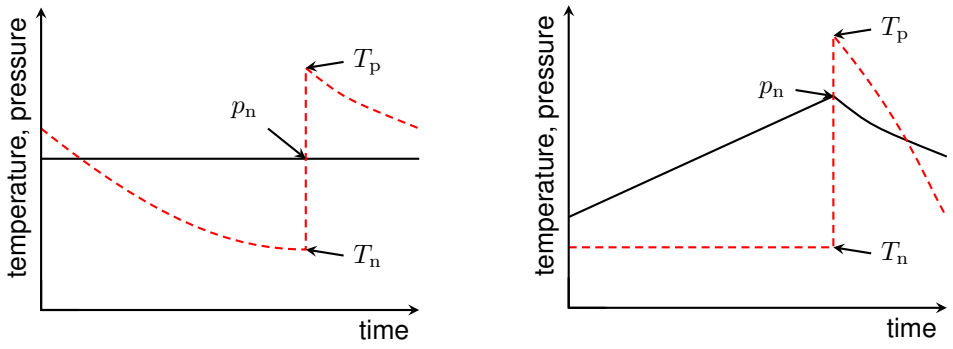

(a) isobaric **(b)** isothermal

Figure 3.19.: Isobaric cooling (a) and isothermal compression (b) experiments, schematic. Temperature (– – – –) and pressure (——) are plotted over time. The nucleation is detected by a sharp increase in temperature. Nucleation temperature T_n, peak temperature T_p and nucleation pressure p_n are indicated.

When the crystallization is triggered, the latent heat is released and the temperature of the sample increases suddenly, the signal showing a clear peak. The temperature immediately before the peak is noted as nucleation temperature. After the peak, the maximum temperature that can be reached is the melting temperature. During the crystallization of the sample, the temperature is stable and a plateau in the recording is formed. Sometimes, if subcooling is very strong, the melting temperature is not reached. This causes a thin peak that quickly falls without showing a plateau. In that case, to detect the melting temperature, isobaric heating instead of cooling experiments should be carried out, or subcooling should be reduced. For the samples of this study, this was necessary only for sodium acetate trihydrate, for which a nucleation agent is known, and thus the more convenient isothermal compression mode could be used.

As a second variable, the pressure in the chamber during the nucleation event is noted. The uncertainty of the pressure is assumed to be given by the pressure interval from about 2 s before the onset of peak to the maximum value of the peak. The time lag of the temperature measurement does not allow a more precise interpretation. For isobaric experiments, the uncertainty is therefore smaller than for isothermal experiments. The uncertainty in temperature is estimated to ±0.5 K.

3.3.2. Results

Typical recordings of the high pressure experiments are shown in figure 3.20.

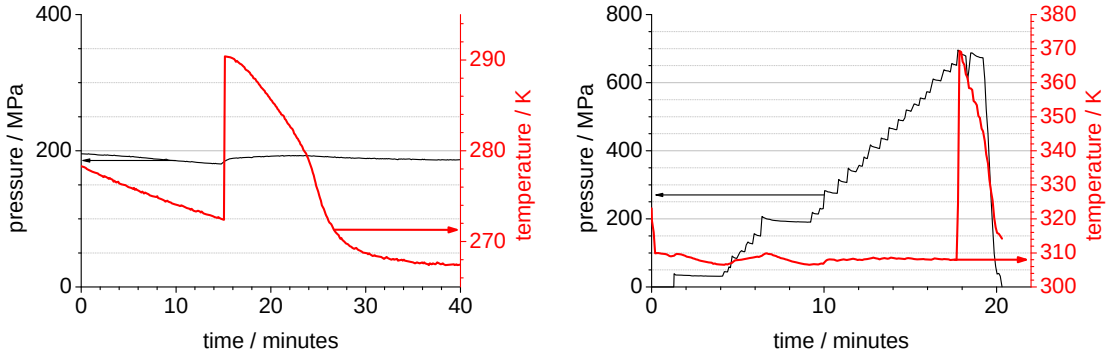

(a) isobaric **(b)** isothermal

Figure 3.20.: Typical recordings from an isobaric (a) and an isothermal (b) measurement.

An isothermal experiment and an isobaric experiment are shown. The nucleation temperature can easily be read from the graphs. The pressure in the isobaric and the temperature in the isothermal experiments is not strictly constant. This is due to the volume contraction of the cooled liquid and the heat generated by the compression, respecptively. However, the change in the "constant" property is small compared to the free variable, and the experiments were carried out slowly to reach near-constant conditions.

$NaOAc \cdot 3\,H_2O$

The crystallization peaks were always initiated at a pressure step, giving clear data for the nucleation curve. Concerning the melting temperature, there were some difficulties in interpreting the data. Surprisingly, the scattering of the maximum recorded temperatures was larger than the scattering of the nucleation temperatures. A possible explanation could be that the maximum achieved temperatures were not correctly detected because of a quickly falling right shoulder of the peak as shown in figure 3.20b, combined with the time lag of the sensor.

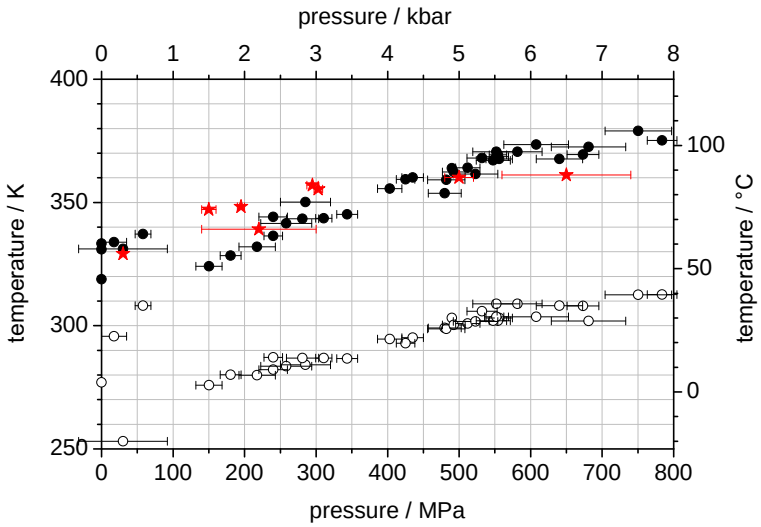

Figure 3.21.: Results of the high pressure measurements on $NaOAc \cdot 3\,H_2O$. Nucleation temperatures (○) and maximum peak temperatures (•) of all experiments are shown. For samples with nucleator, only the maximum peak temperatures are shown (★).

Another possibility is that the maximum achieved temperature is smaller than the melting temperature. With the thermal data of $NaOAc \cdot 3\,H_2O$ as given in table 3.2 it follows that the temperature lift achieved during crystallization is smaller than the subcooling.

$$\Delta T_{\text{cryst}} = \frac{\Delta h}{c_p} = \frac{226\,\text{J/g}}{3.5\,\text{J/gK}} = 65\,\text{K} < \Delta T_{\text{subcool}} \tag{3.1}$$

To estimate the difference between recorded maximum peak temperature and melting temperature, another series of experiments using samples with nucleator were carried out. With the reduced subcooling, the falling side of the peak is less steep, and the melting temperature is achieved and recorded correctly during the crystallization. However, because of the deactivation of the nucleator at high temperatures and the experimental limitations, experiments with nucleator could be carried out only in a reduced pressure range. The results of the experiments with and without nucleating agent are shown in figure 3.21.

In the accessible pressure range, it was found that the peak temperatures from samples without nucleator are about 8 K lower than values from samples with nucleator. Assuming that this distance is constant, i.e. the specific heat and phase change enthalpy do not vary with pressure, the inclination of the melting curve as found by samples without nucleator can be used and the intercept is corrected by 8 K. The crystallization temperature is shifted from about -20 °C at room pressure to about 20 °C at 400 MPa.

Some additional experiments were carried out with samples of increased water content. Small variations in the water content of salt hydrates can occur easily, and

therefore the impact of a changed water content on the pressure curves was studied in this exemplary case. Approximately 10 wt.% of distilled water was added to the samples.

Simply put, the excess water acts as “dead” thermal mass, i. e. its mass does not contribute to the latent heat but is sensibly heated and cooled. Therefore, in equation (3.1), Δh is decreased and the temperature lift is smaller than for the stoichiometric samples. This can be well observed in figure 3.22.

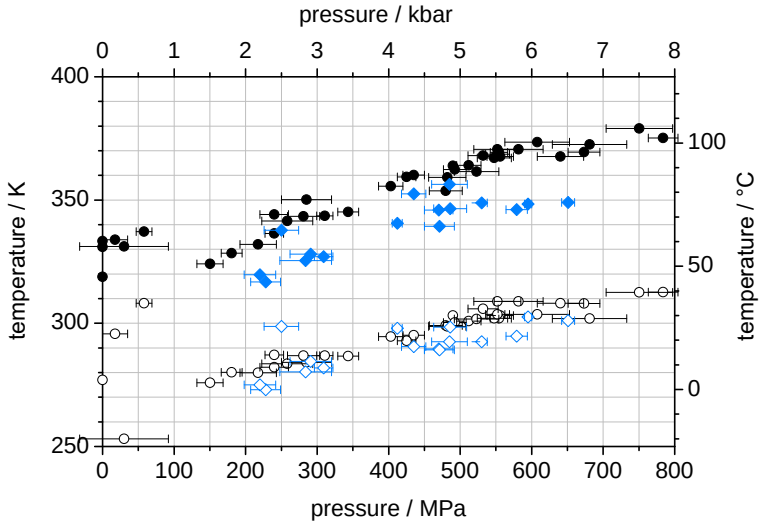

Figure 3.22.: Comparison of results for samples with excess water and the stoichiometric samples. Nucleation temperatures (○ stoichiometric / ◇ excess water) and maximum peak temperatures (• stoichiometric / ♦ excess water) are indicated.

As to the nucleation temperature of the samples with excess water, the change is smaller than for the peak maximum temperatures. With the exception of one experiment at 250 MPa, the nucleation was triggered at higher pressures / lower temperatures. The mean distance of the nucleation curve of the stoichiometric salt hydrate and the curve of the samples with excess water is about 5 K.

$CaCl_2 \cdot 6\,H_2O$

The results of the experiments on $CaCl_2 \cdot 6\,H_2O$ are shown in figure 3.23.

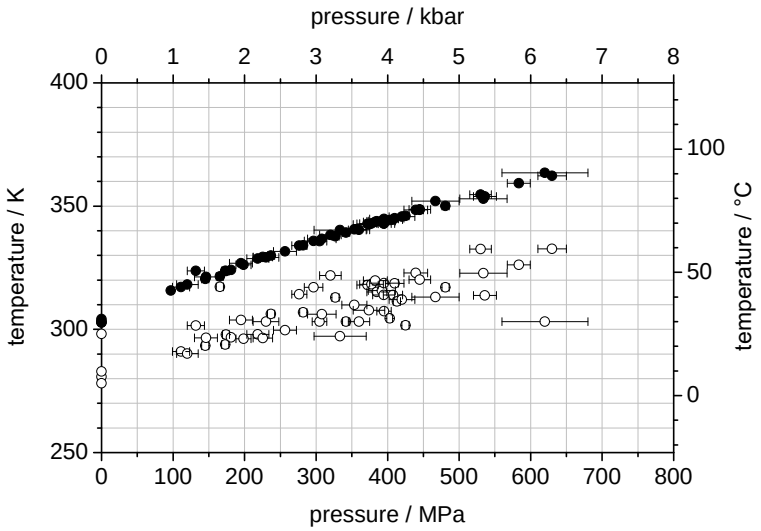

Figure 3.23.: Results of the high pressure measurements on $CaCl_2 \cdot 6\,H_2O$. Nucleation temperatures (○) and maximum peak temperatures (•) are shown.

Here, the maximum temperatures observed in the individual experiments form a very smooth curve. The subcooling is smaller than in the case of $NaOAc \cdot 3\,H_2O$, and the melting temperature is expected to be reached after nucleation in all cases. Using thermal data at room pressure as given in table 3.2, the potential temperature lift from crystallization is larger than the observed subcooling.

$$\Delta T_{\text{cryst}} = \frac{\Delta h}{c_p} = \frac{191\,\text{J/g}}{1.4\,\text{J/gK}} = 136\,\text{K} > \Delta T_{\text{subcool}} \tag{3.2}$$

The nucleation temperatures are much more scattered than the maximum temperatures. This observation corresponds well to the different natures of an equilibrium value (melting temperature) and a statistic value (nucleation temperature). As a general trend, melting and nucleation curves are roughly parallel. The mean subcooling is about 20 K.

$KF \cdot 4\,H_2O$

The results of the experiments on $KF \cdot 4\,H_2O$ are shown in figure 3.24. Here, using isothermal experiments, crystallization was observed only during decompression. Then, using the isobaric method, this behaviour was found to be due to a negative inclination of the melting curve.

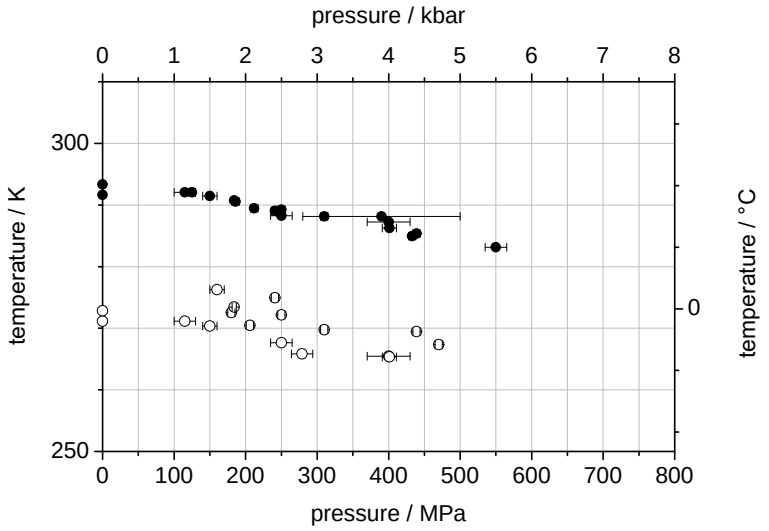

Figure 3.24.: Results of the high pressure measurements on $KF \cdot 4\,H_2O$. Nucleation temperatures (○) and maximum peak temperatures (•) are shown.

Similar to the behaviour of $CaCl_2 \cdot 6\,H_2O$, the melting curve is more distinct than the nucleation curve. And again, the maximum temperature can be set equal to the equilibrium melting temperature because of sufficient latent heat:

$$\Delta T_{\text{cryst}} = \frac{\Delta h}{c_p} = \frac{231\,\text{J/g}}{1.84\,\text{J/gK}} = 128\,\text{K} > \Delta T_{\text{subcool}} \tag{3.3}$$

3.4. Observation of the samples under ultrasonic treatment

After the determination of nucleation and melting temperatures at static pressure and temperatures, the samples were exposed to ultrasound, i.e. highly dynamic pressures and temperatures. The nucleation temperature was determined in a similar way as described in section 3.2.

3.4.1. Setup and procedure

Setup

An ultrasonic generator type *Bandelin GM3100* was used for the observations of the samples under ultrasonic treatment. The instrument's sound frequency is 20 kHz and its maximum power output 100 W. The power output is controllable via the so-called "amplitude" control that can be adjusted in the range 10%-100%.

A titanium sonotrode (ultrasonic horn) with tip diameter 2 mm was used for the experiments. In principle, to avoid a metallic surface in direct contact with the sample material, using a glass sonotrode seemed to be a better option. However, a sonotrode made of glass is very sensible to the mechanical stress. Some preliminary tests were carried out with a glass sonotrode, but it broke during the tests. Therefore, in the experiments reported here, the metallic sonotrode was used throughout.

The setup is sketched in figure 3.25.

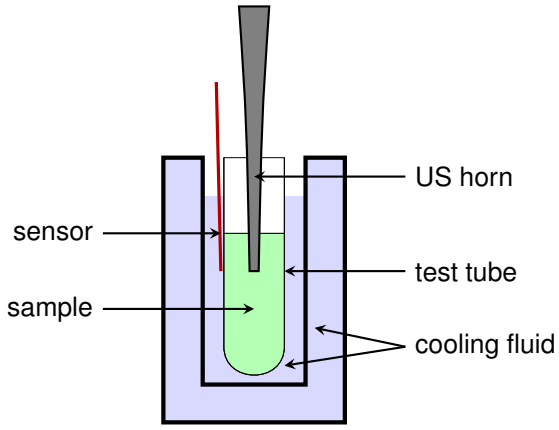

Figure 3.25.: Setup for experiments with ultrasonic treatment.

Glass test tubes as in the static ambient pressure experiments were used here, too. However, only one sample could be investigated at a time. The horn of the ultrasound generator was dipped in the sample. A smaller thermostatic bath was used, which is made of glass and thus allows a direct visual observation of the experiment. A photograph of this transparent thermostatic bath is shown below in figure 3.27b. The

temperature sensor was fixed on the outer surface of the test tube. The gap between the test tube and the bath is larger than in the double wall construction used in the experiments without ultrasound, and an unfixed sensor could easily slip out of the gap when the sample vibrates by the ultrasound.

In addition, in order to investigate the influence of solved gases on ultrasonic nucleation, a setup similar to that shown in figure 3.25 was installed in a chamber that can be evacuated, as shown in figure 3.26.

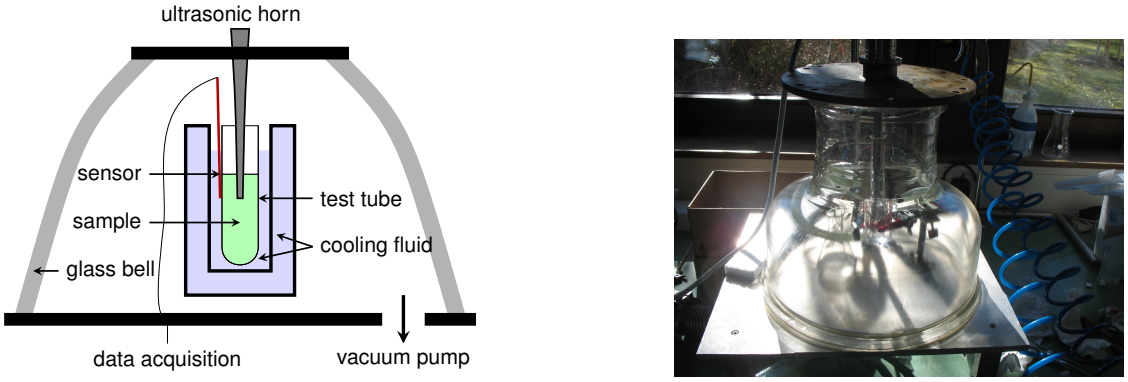

Figure 3.26.: Setup for experiments with ultrasonic treatment in low pressure atmosphere.

The lower limit of the air pressure in the chamber is given by the vapor pressure of the sample, because the liquid sample will then start to evaporate, preventing a further reduction of the air pressure. The evaporation corresponds to a strong cooling of the liquid from its surface, and can cause the sample to freeze. Then, a solid layer is created on the sample surface, as shown in figure 3.27a.

Nucleation of the solid by ultrasound results in a very different appearance of the solid sample: the solid is formed not only on the surface, but all over the sample volume as seen in figure 3.27b. It is therefore assured that sononucleation was not mistaken with nucleation by evaporative cooling on the surface.

To avoid freezing by evaporation, an Erlenmeyer flask with some water was put under the glass bell in the following experiments. As the pressure drops, the water from the flask will evaporate as well, contributing to an increased humidity in the glass bell and thus reduce the evaporation of the sample. The liquid surface of the water in the Erlenmeyer flask is large compared to the sample in the test tube, so the main amount of evaporated water will be provided by the sacrificial water from the flask.

Procedure

Two different modes were used in the experiments:

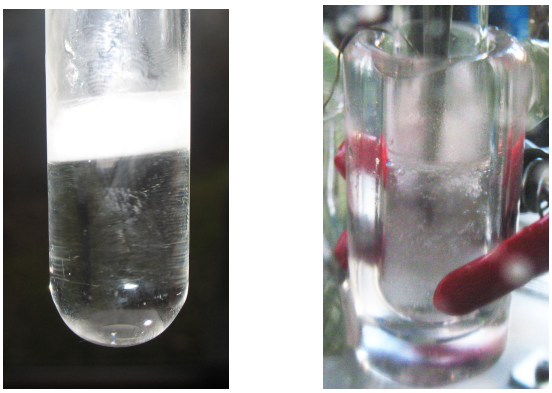

(a) **(b)**

Figure 3.27.: A water sample freezes from the surface when the pressure is reduced quickly below about 50 mbar (a). A sample frozen after insonication has a very different appearance (b).

1. Ultrasound is applied while the sample is kept at a given temperature level (isothermal mode). This mode allows a very clear detection of a possible nucleation effect of the ultrasonic treatment.
2. Ultrasound is applied while the sample temperature is lowered (dynamic mode). Like this, the nucleation temperature is determined as in the case without ultrasound described in section 3.2. A pulsing sonication is used in order to minimize the heating effect of the ultrasound.

Before each experiment, the ultrasonic horn was cleaned by operating the ultrasound with the horn dipped in hot distilled water. In addition, in order to verify the ultrasound as the cause of any observed phenomena, a number of experiments were carried out with the ultrasonic horn just dipped in the sample but not vibrating. A degassing of the sample was carried out by operating the ultrasound before the nucleation experiment at a temperature $T > T_m$. The low pressure atmosphere was used to improve the degassing. Various combinations of pressure and sonication were used as lined out below in the results section.

3.4.2. Results

Cavitation threshold

First of all, it was investigated if the ultrasonic treatment indeed causes cavitation in the liquid samples, and which parameters are relevant. To this goal, isothermal insonication experiments at temperatures above the melting temperature were carried out, varying the amplitude of the ultrasound.

Normal pressure For all sample materials, as soon as ultrasound was applied to the liquid samples, cavitation was observed. Typical cavitation clouds in water for different sonication amplitudes are shown in figure 3.28.

(a) 0% **(b)** 10% **(c)** 30% **(d)** 80%

Figure 3.28.: The cavitation cloud directly below the ultrasonic horn increases with increasing amplitude of the ultrasound.

Only for the lowest possible sound amplitude of 10% (of the maximum ultrasonic generator power of 100 W), cavitation did not occur at once but after some seconds from the start of insonication. The starting point of cavitation could be easily identified by a sharply increased noise and the formation of a bubble cloud below the ultrasonic horn. For higher amplitudes of the ultrasound, the cavitation cloud became larger and the noise increased. A significant difference in the cavitation behavior of the different sample materials was not observed.

Low pressure In the low pressure atmosphere, already at low ultrasonic amplitudes, a strong bubbling of the sample liquid was observed. When insonication was continued, the bubbling decreased within about a minute significantly. When the sample was

exposed to normal pressure after this treatment, cavitation was observed only for increased amplitudes of at least 40%. Similarly, cavitation by low amplitude ultrasonic treatment of the degassed sample was observed when the pressure was reduced again.

Sononucleation of Water

For water, the experiments showed that nucleation was clearly improved compared to the situation without applied ultrasound.

Typical recordings Examples of temperature recordings during dynamic sononucleation experiments of water are shown in figure 3.29.

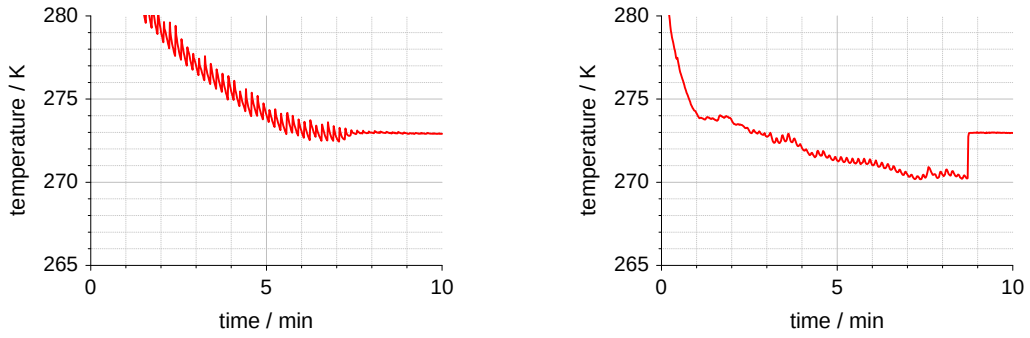

(a) without subcooling **(b)** with subcooling

Figure 3.29.: Examples of temperature recordings during sononucleation experiments on water.

The individual pulses of the ultrasound are clearly visible as many small peaks in temperature as in figure 3.29a. The time interval between the individual peaks corresponds to the pulsing of the ultrasound. The size of the temperature peaks is larger for larger ultrasonic amplitude.

In the first example shown in figure 3.29a, subcooling is completely suppressed. At first, the temperature of the thermostatic bath is slowly falling and the sample temperature decreases. When the sample reaches T_m at about 7:30 minutes, the peaks disappear in the signal, and the temperature remains constant. This is when the sample starts to freeze.

In the second example shown in figure 3.29b, there is some subcooling before the temperature rises to the melting temperature at about 7:50 minutes. Again, the ultrasonic peaks disappear when the sample starts to solidify.

Evaluation The experiments with ultrasound on water were evaluated in the same way as the ambient pressure experiments, and are presented in the following histogram, figure 3.30.

Over 90% of the sononucleation experiments resulted in a nucleation temperature above −2 °C, i.e. subcooling was reduced to 2 K. Compared to the results of the experiments without ultrasonic treatment, as shown in figure 3.10, this is a very clear reduction of subcooling. Without ultrasonic treatment, in over 90% of the experiments a subcooling of at least 9 K (tap water) and 13 K (purified water) was observed.

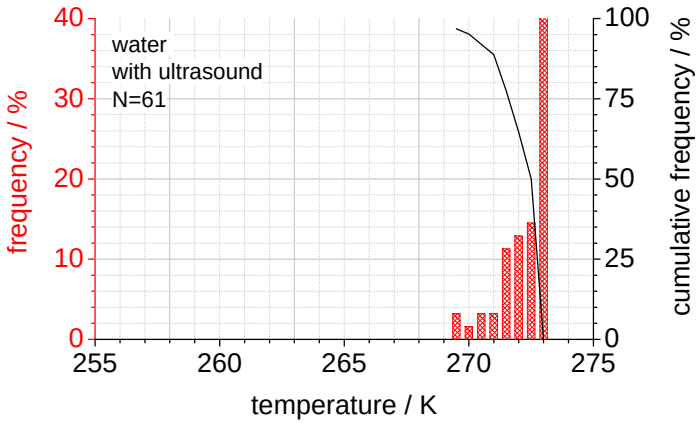

Figure 3.30.: Histogram of the nucleation temperatures of H_2O, for all 61 runs irradiated with ultrasound of variable intensity (see below).

In figure 3.31, the observed nucleation temperature is plotted separately for the different ultrasonic amplitudes.

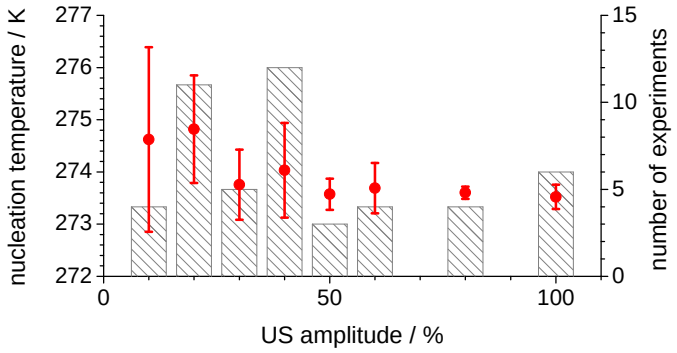

Figure 3.31.: Nucleation temperatures (•) and their variance (left axis) as a function of ultrasonic amplitude for the water experiments at normal pressure. The number of experiments for each amplitude is marked with the bar plots (right axis).

As a general trend, for the amplitudes lower than 50%, the nucleation temperature is higher and varies more. However, from about 30% amplitude on, no further reduction in the nucleation temperature is observed.

To investigate the sononucleation more in detail, a series of experiments were carried out in the setup where the ambient atmosphere could be varied. With the atmospheric pressure as an additional parameter, a different graphic representation is required. In figure 3.32, the results are plotted in a time line graph with the ambient pressure and the ultrasonic amplitude indicated for each experiment. In the graphs, both data from dynamic and isothermal experiments are represented, indicated by different data point markers. The pressure was kept constant at about 80-120 mbar, except for experiments 1 (600 mbar), 2–4 (normal pressure) and 15 (400 mbar). In experiment 15, the pressure was reduced at constant temperature and insonication until cavitation occurred and the nucleation was triggered. In all dynamic experiments with irradiation, nucleation was observed at temperatures higher than 271 K. In all isothermal experiments, nucleation was observed in the temperature range 268 K-271 K, as soon as the ultrasound was applied. In the experiments without application of ultrasound, nucleation was observed at about 260 K-262 K.

In summary, subcooling of water was almost completely suppressed when applying ultrasound of an intensity that leads to cavitation.

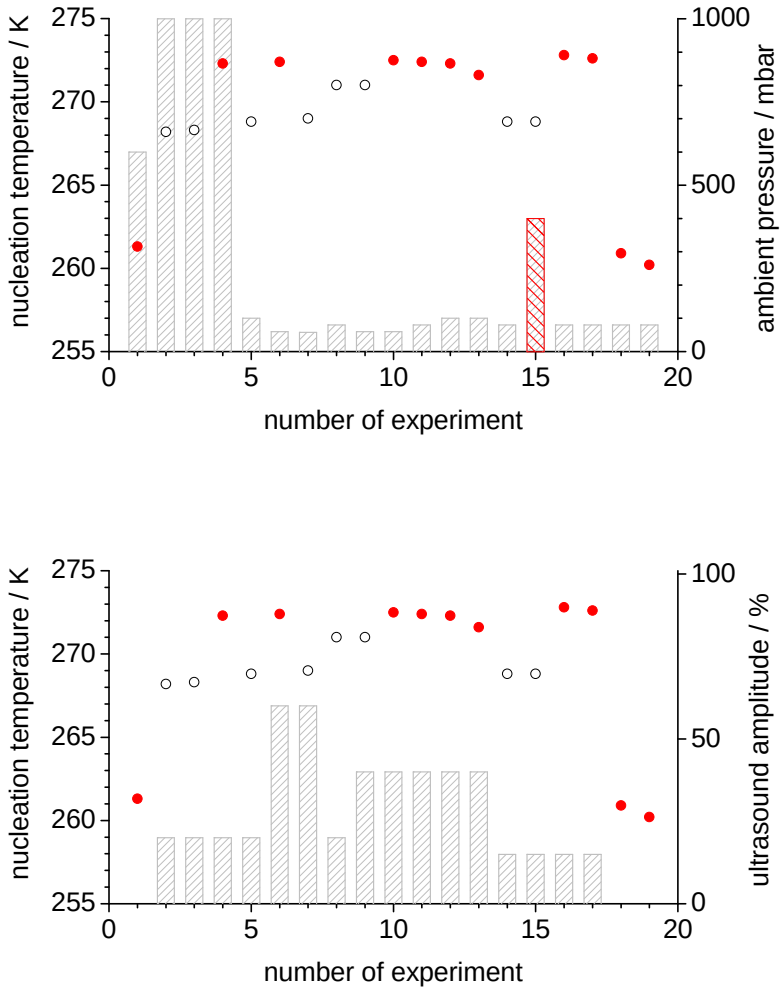

Figure 3.32.: Results of the low pressure experiments on water. The nucleation temperatures (left axis) of the same 19 dynamic (•) and isothermal (○) experiments are plotted in two variants: The bars (rigth axis) indicate the ambient pressures in the upper plot and the ultrasonic amplitude in the lower plot.

Sononucleation of salt hydrates

As described in the section about the cavitation threshold, cavitation was observed in all three salt hydrates as well as in water. Judging from the high pressure and normal pressure experiments, sononucleation is most readily expected for $CaCl_2 \cdot 6\,H_2O$ with its moderate subcooling and comparatively low pressure required to suppress subcooling. The first experiments on salt hydrates were therefore carried out on $CaCl_2 \cdot 6\,H_2O$. In figure 3.33, the result of a series of nucleation experiments on $CaCl_2 \cdot 6\,H_2O$ using varying ultrasonic amplitudes at ambient pressure are shown.

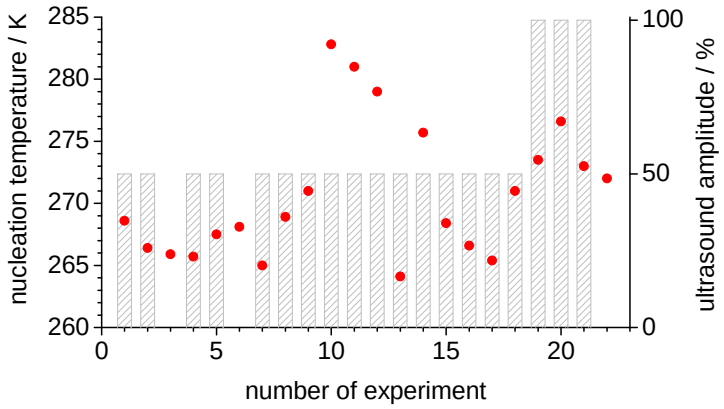

Figure 3.33.: The nucleation temperatures of $CaCl_2 \cdot 6\,H_2O$ observed in dynamic experiments (•, left axis) irradiated with different amplitudes of ultrasound (bars, right axis).

The ultrasound was applied either at half amplitude, full amplitude, or not at all. The nucleation temperatures vary between 265 K and 283 K. The nucleation temperature in the third experiment (no ultrasound applied) is very similar to the temperature observed in the second and fourth experiments (half amplitude). The significantly higher nucleation temperatures observed in experiments 10-12 and 14 all appeared at the same ultrasonic amplitude as the more "typical" nucleation temperatures in the other experiments.

In contrast to the experiments with water, for $CaCl_2 \cdot 6\,H_2O$ there is no correlation between the ultrasonic irradiation and the nucleation temperature. In any case, an almost complete suppression of subcooling like in water can be excluded for this substance.

Second, $NaOAc \cdot 3\,H_2O$ was investigated. In the high pressure experiments, the nucleation curve of this substance was found to be about 5-10 K below that of $CaCl_2 \cdot 6\,H_2O$. First, insonication experiments were carried out at room temperature. Cavitation was clearly observed, but no nucleation was observed at all. Next, the sample was cooled under pulsed ultrasonic irridiation. Nucleation was observed at about the regular

nucleation temperature as determined previously. Considering that the cavitation experiments were carried out at room temperature, corresponding to a large subcooling, a complete suppression of subcooling like observed for water can be clearly excluded for this substance. In summary, there is no experimental hint that ultrasonic treatment would change the nucleation temperature of $NaOAc \cdot 3\,H_2O$.

Finally, some ultrasonic experiments were performed on $KF \cdot 4\,H_2O$. The same procedure as for $NaOAc \cdot 3\,H_2O$ was carried out. Again, cavitation was observed readily, but no improved nucleation.

In summary, for all three salt hydrates, there was no clear effect of the ultrasonic treatment on subcooling observed. While this does not strictly mean that any effect whatsoever is experimentally excluded, a possible effect is small and not usable to efficiently nucleate the salt hydrates at low subcooling.

3.5. Determination of the speed of solidification

The speed of solidification, or speed of crystal growth, is a key parameter in the nucleation theory. For crystallization from solutions, the speed of solidification is governed by diffusive processes. For the salt hydrate samples, the solidification however does not involve concentration gradients or long-distance diffusion. Therefore, the determination of the speed of solidification is comparatively simple for these materials.

3.5.1. Setup and procedure

Setup

The observation of the moving phase front in a solidifying salt hydrate can be detected visually or thermally. While the visual contrast between solid and liquid phase is low, particularly in the case of $KF \cdot 4\,H_2O$, the release of heat during the solidification leads to a well-detectable thermal contrast between the two phases. Initial experiments using a line of thermocouples to observe the moving phase boundary were troublesome, because the setup was difficult to clean from nucleation sites. Therefore, a setup without direct contact between sensors and sample was preferred and realized with an infrared (IR) camera. A high speed, high temperature resolution IR camera was available at ZAE Bayern, division 3 in Erlangen. In figure 3.34, the setup of the experiment is sketched.

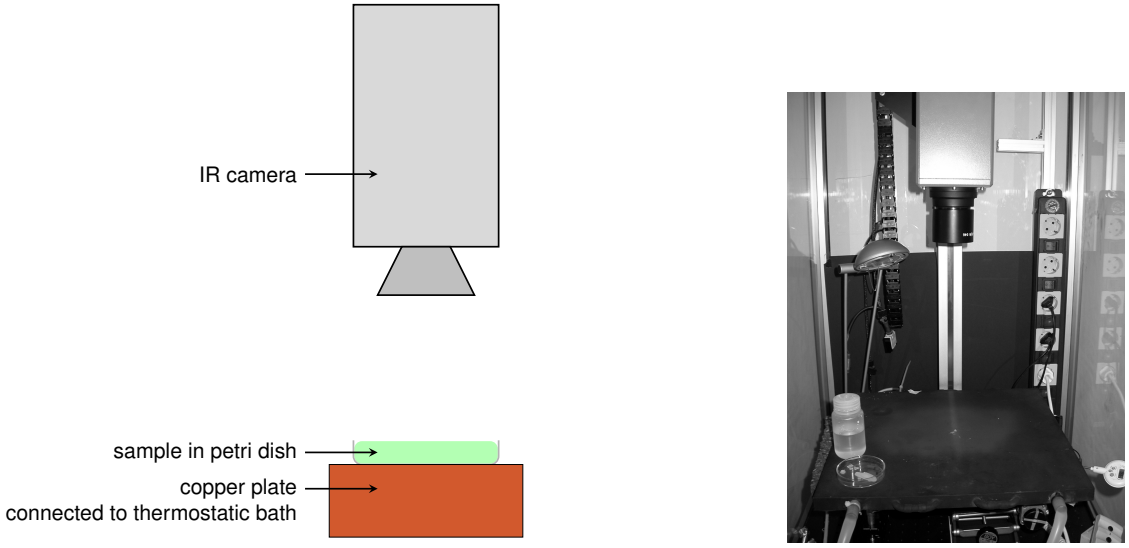

Figure 3.34.: Setup of the solidification speed experiments. The liquid sample is placed in a petri dish on a copper plate. A seed crystal is added to trigger crystallization. The movement of the phase boundary can be clearly observed with a highly sensitive infrared camera.

The instrument used is a model *Taurus 110K SM pro*, manufactured by IRCAM GmbH, Erlangen. The typical temporal resolution is about 1 ms, the temperature resolution

is about 20 mK. The camera is mounted in vertical position above a temperature controlled, blackened copper plate.

Procedure

The sample is heated well above the melting temperature, poured in a petri dish, and placed on the copper plate. The sample in the dish is let stand for a while, allowing to adapt the temperature of the copper plate, which is controlled to a temperature level below the melting temperature of the sample. Next, a seed crystal is placed in the center of the subcooled sample. The subsequent spreading of the solid phase is monitored and registered.

3.5.2. Results

Based on the video registrations, a qualitative analysis of the solidification process, as well as a quantitative analyzsis of the speed of solidification was done. For brevity, not all experiments are represented with images in this section. A complete set of images is provided in the appendix in section B.6.

General observations

The phase front for experiments with initial strong subcooling is smooth, while for little subcooling, the solid phase grows in needles. This general trend was observed for all materials, but was found most distinct for $KF \cdot 4\,H_2O$.

$NaOAc \cdot 3\,H_2O$ Exemplary images of $NaOAc \cdot 3\,H_2O$ are shown in figure 3.35. The solid phase forms a smooth circular area when triggered at strong subcooling as in figure 3.35a. Nucleation at less subcooling leads to the develepment of a more complex phase front as in figure 3.35b.

In addition to the measurement of the solidification speed, a remarkable effect was observed in one experiment shown in figure 3.36: Cooler liquid material at the rim of the petri dish is nucleated when a needle growing in the dish plane reaches the rim. Then, a halo-like structure is formed as the phase front proceedes alongside the rim of the petri dish.

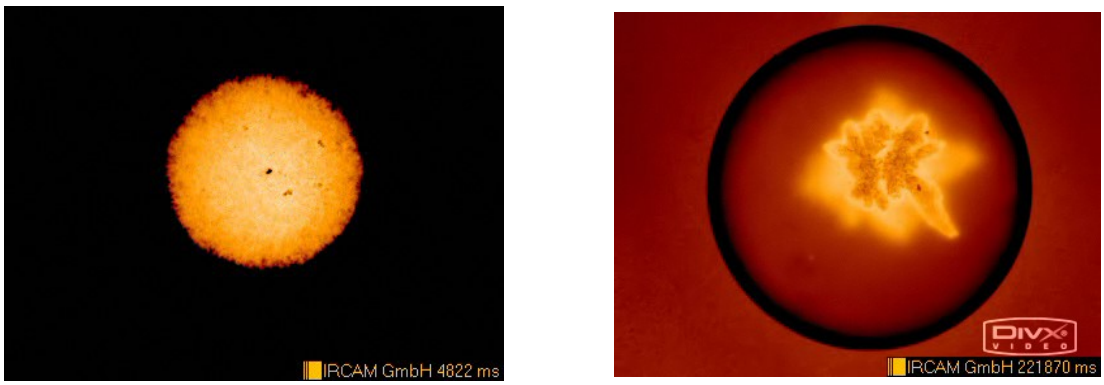

(a) 28 K subcooling **(b)** 4 K subcooling

Figure 3.35.: IR-images of solidifying $NaOAc \cdot 3\,H_2O$ showing different shapes of the phase front for different initial subcooling.

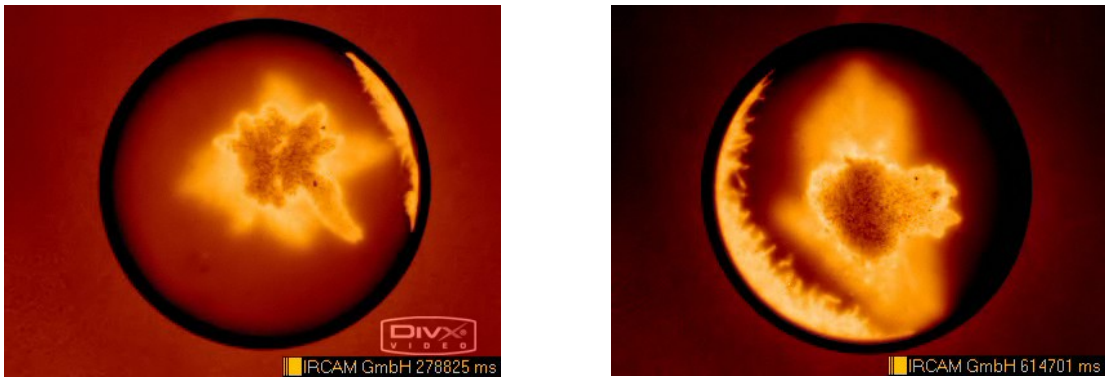

(a) **(b)**

Figure 3.36.: In some cases, cool liquid $NaOAc \cdot 3\,H_2O$ at the rim of the petri dish was nucleated by a growing needle, and forms a halo-like structure.

$CaCl_2 \cdot 6\,H_2O$ Exemplary images of $CaCl_2 \cdot 6\,H_2O$ are shown in figure 3.37. Already for nucleation at the largest subcooling shown in figure 3.37a, the formation of needles can be observed, but the needles are clearly enveloped in a circular shape. The space between the needles becomes wider with decreasing subcooling, as shown in figure 3.37b. For nucleation at small subcooling shown in figure 3.37c, single needles can be clearly identified, and the general shape of the phase front is no longer circular.

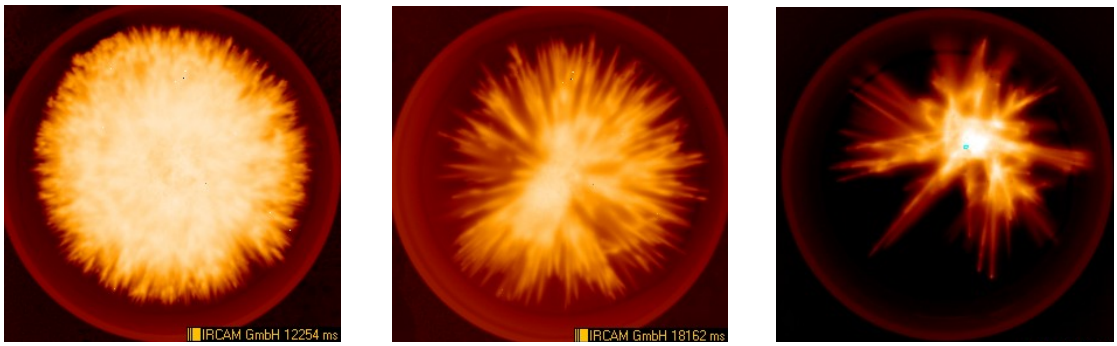

(a) 19 K subcooling **(b)** 14 K subcooling **(c)** 5 K subcooling

Figure 3.37.: IR-images of solidifying $CaCl_2 \cdot 6\,H_2O$ for different initial subcooling.

$KF \cdot 4\,H_2O$ Exemplary images of $KF \cdot 4\,H_2O$ are shown in figure 3.38. For nucleation at moderate subcooling shown in figure 3.38a, forming needles enveloped in a circular shape are observed as for $CaCl_2 \cdot 6\,H_2O$. At less subcooling as shown in figure 3.38b, the single needles become more distinctive. The tip speed of the individual needles is found to vary considerably.

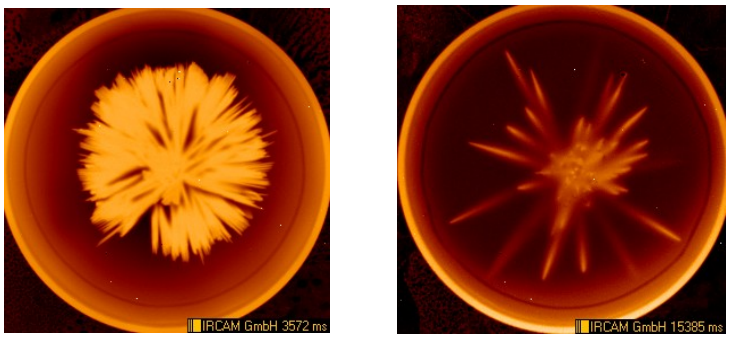

(a) 8 K subcooling **(b)** 3 K subcooling

Figure 3.38.: IR-images of solidifying $KF \cdot 4\,H_2O$ for different initial subcooling.

Speed of solidification

Using a series of still images for each experiment, the speed of solidification was determined as follows: The front position of the solid phase was determined for each image. The distance was related to the time span between two images. It was found that the speed was rather stable during one experiment, and this speed was attributed to the copper plate temperature. Due to the high resolution in time of the IR camera, the uncertainty of the speed depends on the determination of the phase front location only. The progress of the solid phase was determined at different locations of the phase front in order to estimate the error of this variable. The sample bulk temperature was assumed to be equal to that of the copper plate within 1 K.

In figure 3.39, the results of the three salt hydrates are shown. For a better comparison of the substances, the degree of subcooling was chosen as ordinate, referring to the literature value of the melting temperature.

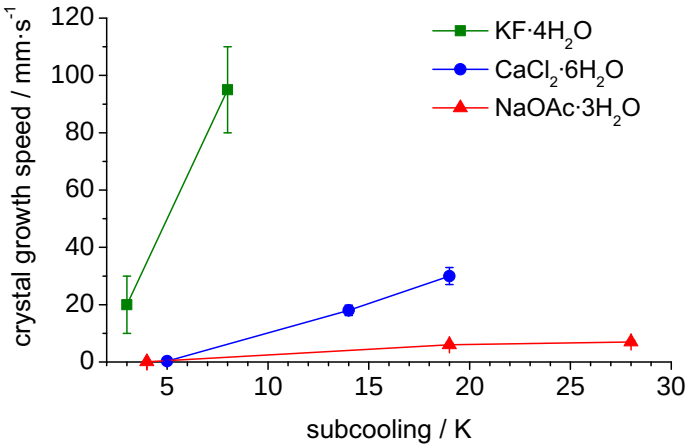

Figure 3.39.: Comparison of the speed of solidification for the three salt hydrates.

$KF \cdot 4\,H_2O$ stands out with an extraordinary fast solidification. $CaCl_2 \cdot 6\,H_2O$ and $NaOAc \cdot 3\,H_2O$ show a much slower speed of solidification. Glass forming effects, i.e. slower crystal growth for large subcooling, was not observed for any sample substance in the investigated temperature range.

4. Discussion

In this chapter, sononucleation of salt hydrates is discussed based on theory and experimental work as described in the previous chapters. First, a critical discussion of the limits of nucleation theory and experiments with respect to sononucleation of salt hydrates is given. Then, the results of the experiments carried out in this work are confronted with literature data and predicitons from theory. Finally, possible explanations for the experimental observations are discussed, and new insights in sononucleation of salt hydrates are summarized.

4.1. General limitations of theory and experiment

The current state of knowledge of nucleation phenomena as introduced in section 2 certainly is not complete and leaves several open questions. These open questions are partly due to a lack of theoretic understanding, and partly due to experimental limitations. These weak points and their relevance with respect to sononucleation of inorganic PCM are discussed in this section.

4.1.1. Small clusters and the early stage of nucleation

The basic idea of nucleation by pressure is that a nucleus which is subcritical at normal conditions turns supercritical under changed pressure and thus grows during a pressure pulse. When the pulse is over, and the nucleus has grown enough to be now supercritical even at normal conditions, it can continue to grow and macroscopic solidification was triggered. The properties of subcritical nuclei and the kinetics of early nucleation are therefore crucial in order to determine the time span of the pulse which is required for successful nucleation.

Role of subcritical nuclei in sononucleation

Nucleation theory puts its focus on the critical nucleus, but for dynamic problems such as sononucleation, also the size distribution and properties of subcritical nuclei is of major importance. This is motivated using an illustration as follows.

In figure 4.1, the nucleation barrier is sketched for two different sets of boundary conditions (i.e. different temperatures or pressures). A nucleus that is subcritical under the first state becomes critical under the second state, if its radius r_a is in the range $r_{crit,2} < r_a < r_{crit,1}$. If the nucleation barrier is changed because of a changed temperature, also the cluster size distribution is changed. Instead, if the nucleation

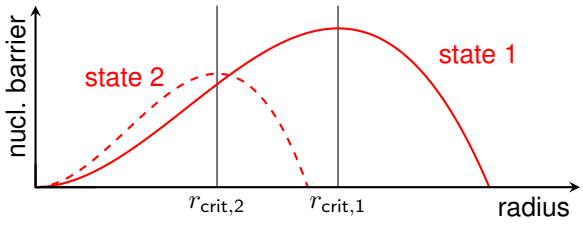

Figure 4.1.: A nucleus of radius r_a where $r_{crit,2} < r_a < r_{crit,1}$ is subcritical with respect to state 1 but supercritical with respect to state 2.

barrier is changed because of a changed pressure, this does not have an impact on the cluster size distribution. Then, the initial size of a nucleus before the pulse is decisive with respect to its further development.

Simplified scenario In a simplified scenario assuming a rectangular pressure pulse, during a time span $\Delta t = t_2 - t_1$ the nucleation barrier changes its shape form state 1 to state 2, as sketched in figure 4.2.

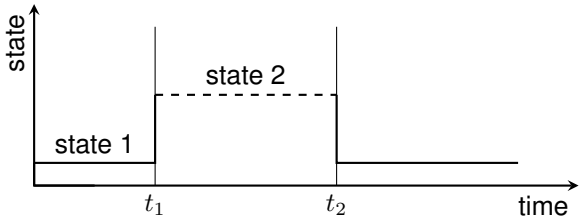

Figure 4.2.: A simplified rectangular pulse.

Depending on the initial cluster size and the length of the pulse, three possible reactions of a subcritical cluster to this pulse exist, as sketched in figure 4.3:

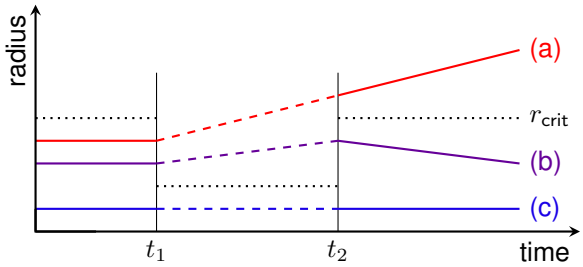

Figure 4.3.: Possible reaction of the cluster size to a pulse in boundary conditions as sketched in figure 4.2.

(a) The cluster becomes supercritical during the pulse of state 2 and growths to a size that is supercritical with respect to state 1. Then, it can continue to grow after the pulse: successful nucleation.

(b) The cluster becomes supercritical during the pulse of state 2, but does not reach a supercritical size with respect to state 1 during the pulse. After the pulse, the cluster is again subcritical and will not grow further: no nucleation.

(c) The cluster is too small to become supercritical during the pulse of state 2. The pulse has no effect on the cluster: no nucleation.

In order to judge what situation is present, the pulse width Δt, the speed of growth during the pulse, and the initial size r_a have to be known. Therefore, information about the subcritical clusters and their growth to supercritical clusters is important to quantitatively describe the process of sononucleation.

More realistic scenario In a more realistic scenario, the situation is more complicated. Due to the different transmission speeds of pressure and heat, the temperature pulse which is caused by compression is not synchronous with the pressure pulse. Thus, even assuming a rectangular pressure pulse, the change in the boundary conditions (T, p) is not rectangular as sketched in figure 4.2. Instead, pressure p, temperature T and critical radius r_{crit} change in a different way, for example as sketched in figure 4.4.

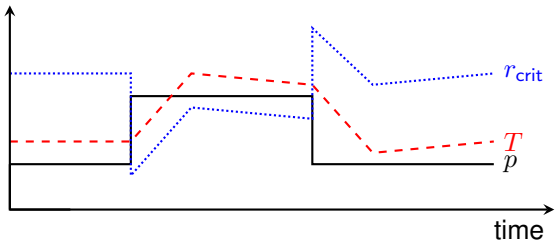

Figure 4.4.: In a more realistic scenario, also the temperature changes during a pressure peak. Thus, the critical radius shows a different form than in the simplified sketch above.

The critical radius now shows a different peak form than in the simplified situation. It is reduced most during the first moment of the pressure peak, where the temperature has not yet increased much. This negative peak is only possible if the pressure transmission is faster than the temperature transmission. Later, the value of the critical radius depends on the reached temperature and pressure values, it might be similar that in the simplified scenario, or it might as well be larger than the critical radius at the initial conditions. Considering that the time span of a cavitation pressure peak is in the range of some μs, and that the critical radius changes constantly during this peak time, one important question is how fast the energetic distribution will adopt to a change in temperature and pressure. In fact, the Boltzmann equation describes

a thermodynamic system in equilibrium, and thus makes no statement about time scales. While statistic thermodynamics explains the general concept, it is thus highly doubtful that it will provide detailed information about a sononucleation process.

Properties of small clusters

Clusters are treated in theory as very small solid particles. However, due to their small size, the assumption of spheric clusters with properties equal to a bulk solid phase is not strictly correct. Particularly for very small clusters of just a couple of particles, the assumption of bulk solid properties must be a rough approximation. For small agglomerates, the bulk values for interface and volume energies are most certainly far from appropriate. Also, the assumption in equation (2.17c) relies on a constant density even for small nuclei – a concept that hardly holds for a tiny solid phase. In a comparative study confronting experiment and theory, the assumption of size-independent properties used in classic nucleation theory was found to fail in describing experiments carried out on a group of glass-forming liquids [29]. Considering the complex processes of solidifying salt hydrates, similar problems have to be expected for this group of materials.

Establishment of the cluster size distribution

Nucleation theory gives a concise explanation why clusters of at least critical radius grow spontaneously. However, how are the subcritical clusters formed, and how is the cluster size distribution established? These questions are important when considering a very short pulse in pressure and temperature, that is, in nucleation barrier and energy distribution. The kinetics of the system's reaction to a change in temperature is therefore a key factor in sononucleation.

- ▷ The most popular explanation is *growth from zero*, i.e. two individual particles meet and form a two-particle cluster, a next particle attaches and so forth until the critical nucleus is formed. However, this would require a tremendous energetic effort for the first two particles.
- ▷ Another option is a *simultaneous collision* of N_{crit} particles with enough energy to form a critical nucleus. The total energy needed is $E \geq E(N_{\mathrm{crit}})$, which corresponds to a mean energy $e \geq E(N_{\mathrm{crit}})/N_{\mathrm{crit}}$. From the energy distribution function, the fraction of suitable particles from the whole volume can be determined. In that case, N_{crit} of those particles have to meet simultaneously in one place. This is possible only for very small nuclei that consist of a few individual particles, or for a nucleation barrier that corresponds approximately to the mean energy.
- ▷ Taking account of curvature effects, it was shown in section 2.1.2 that small subcritical clusters are stable. From these clusters, in fact only some would suffice to form a critical nucleus: A *collision of clusters* might correspond to a "hop over the barrier" instead of taking it slowly over the peak by single-particle attachments.

In such a scenario, it is however most important that the clusters and the nucleus have the same structure of the solid and can join without creating an internal interface.

Nucleation rate in theory and experiment

The exact value of the nucleation rate is clearly a weak point of nucleation theory. In a recent publication, Perez et al. [143] discuss different approaches to model precipitation in solids with the help of the nucleation theory. As to the kinetics of nucleation, they summarize that "many expressions for the condensation rate β^* can be found in the literature, none of them being supported by a clear justification." In this section, possible explanations for this discrepancy are presented.

Solidification and heat transport Temperature must be a major parameter for the cross section of attachment, because vibrations and mobility play a key role. How does the temperature of a critical nucleus of N particles evolve, when the nucleus starts growing? Everything depends on heat transport.

- ▷ Considering a case with instantaneous unlimited heat transport, energy set free by the first particle attaching to the critical nucleus is absorbed by the surrounding (infinite) liquid without heating it up. The temperature and the nucleation barrier are unchanged, the nucleus of $N+1$ particles is supercritical, and it keeps growing without any complications. In this case, the only limiting factor of solidification speed is the attachment rate of the particles to the solid surface.
- ▷ In a case without heat transport, the energy set free by the first particle attaching to the critical nucleus is slightly raising the temperature of the surrounding liquid. The shape of the nucleation barrier is adjusted to this new temperature, that means the maximum of the barrier is shifted toward larger nuclei and the inclination of ΔG for supercritical nuclei is reduced. Depending on the exact relation between temperature induced change in nucleation barrier and temperature change of the system, the present cluster of $N+1$ particles may still be supercritical or now subcritical. In any case, sooner or later, the temperature will rise to the melting temperature where the nucleation barrier is continuously rising and no further growth of the nucleus is possible. The growth is stopped thermally; macroscopic solidification cannot take place without heat transport.

Growth of the critical nucleus and macroscopic growth During the very first steps of nucleation, the situation is almost isothermal with $T = T_\mathrm{n} < T_\mathrm{m}$. This situation cannot be realized in a macroscopic experiment; this is illustrated in figure 4.5. In a macroscopic situation, the phase interface is near to flat. This corresponds to a large exothermic effect of every attaching particle, because the surface area is unchanged and only the volume term in equation (2.13a) applies. Then, to keep the phase boundary

(a) microscopic **(b)** macroscopic

Figure 4.5.: The integration of a new particle into the growing solid has an impact on the surface energy in a microscopic but not in a macroscopic configuration.

at a constant temperature where $T < T_m$, the latent heat has to be removed. In order to avoid mechanic disturbance at the phase boundary, the heat removal can only be done via heat conduction through the sample material itself. Then, the material parameters and the available thermal gradient are determining factors for the heat flux. The gradient is influenced by boundary conditions at the sample surface or heat exchanger interface, and the sample geometry. During solidification, the heat transfer path continuously changes and is a priori unknown. Therefore, a heat exchanger control assuring constant temperature at the phase boundary is not possible. Even if the boundary movement were known, the temperature transport via heat conduction is limited and could probably not cope with the generated heat, at least for fast growing solids.

In summary, an experimentally observable growth speed is not the same as the speed that applies for early stages of nucleation. Can an experimental value at least be used as an upper or lower limit? As lined out above, the attachment of salt hydrate molecules to the solid phase requires the correct orientation of the molecules and a restructuring of the hydrate hull. Whether the correct orientation for integration into the solid is reached faster for high temperatures (better mobility of the constituents) or for lower temperatures (less vibrations and higher sensitivity to local potentials) is hard to decide in theory. Therefore, it is very risky to make a statement whether macroscopic or microscopic growth is faster.

4.1.2. Application of nucleation theory to solidification of inorganic PCM

The application of nucleation theory to solidification of inorganic PCM, i.e. to the solidification of a complex liquid which is associated with a high phase change enthalpy, is particularly difficult, as lined out in this section.

Thermodynamic statistics of liquid salt hydrates

Statistic thermodynamic theory can be readily applied to ideal gases, where small particles interact by elastic collisions only. As to liquid salt hydrates, different particles with different interactions have to be considered.

Internal and kinetic energies The role of internal energy in nucleation theory shows an important difference dependent on the phase change under consideration. In the thermodynamic description of the phase change, the change in enthalpy Δh is the main variable. In a system of constant number of particles $N = \text{const}$, the differential of the specific entropy is

$$\mathrm{d}s = \frac{1}{T}\mathrm{d}u + \frac{p}{T}\mathrm{d}v \tag{4.1a}$$

For an isobaric, isothermal phase change, it follows with equation (2.4)

$$\Delta h = \Delta u + p\Delta v \tag{4.1b}$$

Because of

$$\Delta v_{\text{liq-sol}} \ll \Delta v_{\text{gas-liq}} \tag{4.1c}$$

and

$$\Delta h_{\text{liq-sol}} \lesssim \Delta h_{\text{gas-liq}} \tag{4.1d}$$

the change in internal energy Δu plays a much more important role in solidification than in condensation phase changes. In general, PCM are selected for their exceptional high value of Δh. The change in internal energy corresponds, in the case of salt hydrates, to a rearrangement of the hydrate hull, i.e. a dehydration of ions, a reduction of the coordination number, and/or a "depolymerization" of coordinated water polyhedrons, followed by the arrangement in the crystal lattice. Compared to this, the liquid / gaseous phase change is simply characterized by a mere change in mean intermolecular distance. In summary, structural effects are exceptionally important in solidification of PCM compared to most other phase changes. A simplification or negligence of structural effects in nucleation theory may not show significant effects for most materials, but could have serious consequences for salt hydrates.

The energetic distribution function The initial configuration of a subcooled system before nucleation occurs is generally described by the Boltzmann distribution function as in equation (2.19) in nucleation theory. While this seems to be the generally accepted approach, a quantitative application to nucleation of salt hydrates is not directly possible.

- ▷ First of all, what kind of particles are considered? For salt hydrates, this is not trivial. In the liquid, hydrated ions, ions and water molecules could play a role. Probably a liquid salt hydrate is a mixture of various kinds of particles that attach and detach continuously. How is this reflected in the form of the nucleation barrier?
- ▷ Second, what are the degrees of freedom in a subcooled salt hydrate? The degrees of freedom are required for a quantitative evaluation of the Boltzmann distribution function. From thermodynamic theory, there is no consistent explanation of the degrees of freedom in a liquid. In addition, different kinds of particles as

lined out above could have different degrees of freedom. The movement of the particles in a liquid salt hydrate is surely not well described by elastic collisions, that are applied for an ideal gas, but different particle-particle interactions and respective potentials apply.

▷ A third major problem is that the distribution function applies to equilibrium thermodynamics only, and does not include information about time scales. As lined out above, the time required for the establishment of the particle size distribution is however an important parameter in sononucleation.

Attachment rate in salt hydrates Classical nucleation theory provides solutions for diffusion or attachment controlled growth. In the case of salt hydrates, the chemical composition of the solid and liquid phases is the same, and also the density of the two phases is similar. Therefore, no depletion region is created around the growing nucleus, and diffusion limited kinetics can be ruled out. Theories developed for precipitation problems are therefore not appropriate for solidification of PCM. The other group of problems which are well-established in nucleation theory are condensation processes. Here, the attachment of the particles to the forming nucleus is the step that determines the kinetics. The most simple idea of attachment is full absorption, that means every particle that touches the nucleus is integrated into it. This can be a valid simplification for the condensation from the gaseous phase, but for solidification, the orientation of the molecules has to be considered, too. A theoretical derivation of the cross section of the interaction nucleus - particle is thus not reliable for salt hydrates, and experimental data is missing.

4.1.3. Interpretation of nucleation experiments

In nucleation and sononucleation experiments, the setup and the experimental conditions are very important. Even static nucleation experiments, where “static” refers to nucleation at almost constant boundary conditions, are difficult to carry out and analyze. Depending on the intention of the experimenter, nucleation experiments differ considerably and deliver different information. Contradicting results of static nucleation experiments can be explained fairly well by the influence of heterogeneous nucleation sites and kinetic effects. As to sononucleation experiments, often even more fundamental questions are not clarified. In particular, “successful sononucleation” can refer to quite different situations.

Consistency of experimental values with theoretic models

When comparing experimental data of different setups or research groups, as well as with respect to theoretic predictions, in general there is no convincing agreement.

Many works in literature line out that a prediction of the nucleation rate from theoretic considerations is not successful, while others claim good agreement of experi-

mental and theoretic data. In his recent review of nucleation experiments in protein solutions and colloidal suspensions , Sear states vaguely that if "the nucleation barrier [...] is many kT, then homogeneous nucleation will be slow" [53]. As to the nucleation of water, Hobbs [144, page 465] argues that "it is not possible to obtain an accurate estimate of the nucleation rate [...] due to the fact that the magnitudes of several of the parameters [...] are not known with certainty." The high sensitivity of the predictions made by nucleation theory with respect to input parameters is thus believed to be the cause of a disagreement between experimental and theoretic data. From one point of view, this high sensitivity may lead to the false impression that the theory fails, when the uncertainty of the input parameters is underestimated [145]. From another point of view, nucleation experiments are considered a sensible tool to check thermodynamic data used as input parameters in theory [146]. In more detail, the discrepancy between theoretic and experimental data can be understood when considering the concepts of homogeneous / heterogeneous and kinetic / thermodynamic nucleation temperatures.

Homogeneous and heterogeneous nucleation While most theoretic works on nucleation focus on homogeneous nucleation, experimental works rather deal with heterogeneous nucleation. On the one hand, the experimental determination of the homogeneous nucleation temperature faces many difficulties. On the other hand, the theoretic description of heterogeneous nucleation suffers from a lack of available data input, e.g. a theoretic prediction of the nucleation activity of heterogeneities is currently not possible [17, 77]. In this situation, theoretic predictions for real systems are not reliable, and an experimental validation of theory is possible only in exceptional cases. This is due to two main experimental limitations.

- ▷ First, a very high purity of the sample needs to be given, because any impurity can potentially act as nucleation site. If a filtering or other purification of the sample results in a lower nucleation temperature, it is clear that heterogeneous nucleation agents were removed by the treatment. If however a filtering does not lead to a further depression of the nucleation temperature, all that can be deduced is that no active substances were filtered, and agents may still be present. Also, recrystallization as used in the Czochralski and float zone purification processes, is not suitable to remove finely dispersed nucleation agents from a sample.
- ▷ Second, any surface can potentially act as a nucleation site. Levitation techniques can avoid contact to a solid container surface, but still the interface between drop and surrounding gas is a potential nucleation site. For salt hydrates, levitation techniques are even less suitable, because the missing containment can lead to a change in the water concentration of the sample.

A commonly used technique to approach homogeneous nucleation is to observe the sample material in an emulsion. Heterogeneous seeds are isolated in a few droplets and thus the majority of droplets contains no seeds. The droplet surface is supposed not to act as a crystal seed as it does not offer a template for the crystal structure. There

are however two problems with this technique.

- ▷ First, the high specific surface and high curvature could influence the formation of clusters. The substance surrounding the droplet is not actively favoring nucleation, but it clearly rearranges the molecules of the sample substance at the surface, compared to a situation in the bulk. If surfactants are used to stabilize the emulsion, there is obviously some modification of the surface.
- ▷ Second, the small separated volumes change the nucleation statistics. Crystal growth is restricted to the volume within each droplet. The nucleation rate therefore has to refer to a supercritical nucleus per droplet, which is much more than the commonly used one nucleus per ml.

A recent study by Schmid [147] has shown that subcooling in hexadecane emulsions is much stronger than in macroscopic hexadecane samples, and that the surfactant has a significant influence on the nucleation temperature.

Real homogeneous nucleation therefore is rather to be considered a theoretic concept, and in reality, even carefully designed experiments will be influenced by some sort of heterogeneity. What can be done experimentally is to quantify the influence of varied system parameters with respect to a reference situation on the nucleation process. In this work, the influence of sonic treatment was to be investigated. Literature values of nucleation temperatures were used to chose suitable sample materials, but for the evaluation of a possible ultrasonic effect, reference data was acquired in dedicated experiments.

Kinetic and thermodynamic nucleation temperature A second important issue is to distinguish between kinetic and thermodynamic nucleation temperatures. As lined out in section 2.1.3, nucleation theory rather defines a nucleation rate than a nucleation temperature. The nucleation temperature is commonly defined as the temperature where a nucleation event will occur within a reasonable observation time, i.e.

$$\int_{t_0}^{t_{\text{observation}}} j(T_{\text{n}}, \tau) d\tau \geq 1 \tag{4.2}$$

The nucleation temperature T_{n} therefore refers to an isothermal situation, and is dependent on the sample volume and the observation time.

- ▷ If an experiment is carried out dynamically, i.e. a variation of the temperature or other system parameters is done continuously, the observed nucleation temperature is called the kinetic nucleation temperature. The observation time for one state of the system is very short in that case. A precise measurement of the boundary conditions, under which the nucleation was observed, may be difficult in dynamic setups, too. The main parameters in dynamic setups are the cooling rate and sample geometry, that should always be reported together with the results of the experiments.

- ▷ To achieve a longer observation time, a variation of the system parameters can be done stepwise. After an initial adaption time, thermodynamic equilibrium is obtained for each step, and the observation time of one state can be prolonged as desired. In this case, the resulting nucleation temperature is called the thermodynamic nucleation temperature. Here, the step size and the waiting time are important parameters.

In order to evaluate results from different experimental setups, it is important to have precise information regarding the dynamics of the experiment, in addition to sample purity and sample size. What kind of measurement is suitable to generate useful data strongly depends on the intention of the experiment. If theoretic values shall be verified, a thermodynamic measurement is commonly chosen. If some practical questions of solidification shall be answered, a kinetic measurement is usually more straightforward. However, if the dependency of temperature is much stronger than the dependency of time, a dynamic measurement may be advantageous compared to a step measurement also in theory oriented works. To summarize, some experimental data of the nucleation temperature is available for most materials, but of very different usefulness.

Is reported sononucleation really about nucleation?

From the literature on nucleation experiments as presented in section 2.2, a deep doubt remains on whether all claimed observations of sononucleation really are cases of nucleation triggered by ultrasound.

Doubtful diagnosis Particularly for nucleation from solutions and nucleation of PCM, in fact rather improved solidification was the main focus of the works, and a distinction between nucleation and solidification was omitted in many cases.

- ▷ The study by Miyasaka et al. [115] claimed successful sononucleation of $Na_2HPO_4 \cdot 12\,H_2O$. However, the reported faster heat release during solidification is a strong hint for improved crystallization. Supercritical nuclei could be small enough to pass the visual detection system, which is used to identify nucleation, unseen. Then, the acoustic streaming may enhance diffusion in the supersaturated sample, causing a rapid growth and thus the detection of nuclei that were already previously present. Ultrasound could act by effective mixing, thus improving heat transfer and supporting growth of the stoichiometric solid. The provision of localized energy is not a convincing explanation of nucleation, as lined out above in section 2.1.4.
- ▷ The study by Matsuda et al. [118] reports a reduction of subcooling in erythritol from 60 K without treatment to about 23 K with ultrasonic treatment. The mechanism that leads to this enhanced nucleation is described as “by acoustic streaming and the propagation of sound pressure, etc.”, a statement that is strikingly blurry.

Also, the sonication experiments were carried out in a dynamic setup, and no isothermal tests were done to confirm the nucleation temperature. The necessary subcooling for sononucleation to work is still remarkable. Also, erythritol is an exceptional PCM, that forms two solid phases with close melting temperatures [148]. These two phases must have two distinct interface energies with the liquid. It is possible that one phase is preferred for small clusters, while the other is preferred for larger agglomerates. If the ultrasound leads to a disruption of the clusters of the first phase, this could allow the formation of nuclei of the second phase, and finally crystal growth. This would explain to some extend the needed subcooling, but is a very speculative suggestion.

What could apparent sononucleation really be? By definition, nucleation is the *creation* of supercritical nuclei. If crystal growth is very slow or hindered, for example by temperature or concentration gradients, then a subcooled but already nucleated melt may have the appearance of a non-nucleated melt. Small supercritical nuclei may remain undetected. In such a situation, ultrasonic treatment may seem to "nucleate" the solid phase, although it does not. Figure 4.6 illustrates the following thoughts.

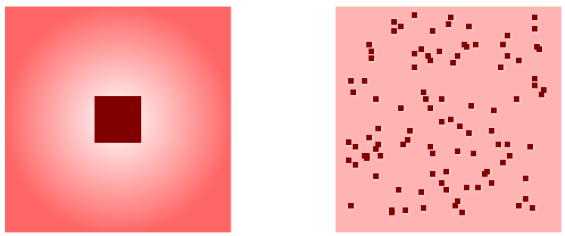

Figure 4.6.: Solidification can be improved by ultrasonic disruption of crystallites and reduction of gradients; see text.

- ▷ Some substances have very different growth speeds of their different crystal faces, with the slowest growing faces constituting the surface of a growing crystal. In such a case, violent mixing may disrupt the small supercritical nuclei, generating new, quickly growing crystal surfaces. As a consequence, a larger amount of the sample solidifies and the solidification finally becomes detectable.
- ▷ A second mechanism is possible for solutions, where ultrasonic mixing of the bulk liquid may very efficiently reduce concentration gradients and like this favor solidification.
- ▷ Third, thermal gradients in the bulk liquid can block crystal growth, considering that the speed of solidification is a function of temperature. These thermal gradients can be efficiently reduced by ultrasonic mixing, too.

How can real nucleation clearly be identified? In order to assure that improved solidification is not mistaken for nucleation, two easy tests can be carried out that indicate problems in crystal growth and thus potential for improved solidification.

- ▷ If the sample is kept for a long time at constant conditions, also slowly growing crystals will eventually reach a dimension where they are detectable.
- ▷ If solid seeds of the sample substance are added to the subcooled melt, and no macroscopic solidification is observed, this is a clear indication of blocked crystal growth.

Unfortunately, these tests were not carried out in all reported sononucleation experiments, in particular those on PCM [118]. For the sample substances used in this study, a quick solidification was observed in the experiments as described in section 3.5, and hindered growth can be excluded at least on a macroscopic level.

Sononucleation and cavitation

Does sononucleation only happen when cavitation is present? In a patent concerning sononucleation of organic materials, in particular fats, successful sononucleation even in the absence of cavitation is claimed [120]. The authors explain that cavitation should be avoided because it is suspected to change the taste of the fat due to sonochemical reactions. But then, "no cavitation" is not to be understood as a strict concept of no cavitation at any time, but rather little production of bad taste during the whole treatment. The overwhelming majority of literature on sononucleation agrees that in fact cavitation is necessary for sononucleation to occur.

Can nucleation by a pressure pulse be studied separately? In order to better understand sononucleation, it would be very helpful to generate a high pressure pulse in a subcooled sample with a different method that does not involve cavitation. This is however not possible. Each shock wave involves a high but also a low pressure period. During this low pressure period, cavitation inevitably will occur as soon as the cavitation threshold is undercut. Therefore, the cavitation threshold also limits the peak pressure that can possibly be applied to a liquid without the occurrence of cavitation. The secondary pressure peaks caused by cavitation are generally much stronger than the primary pressure peaks which cause cavitation. A controlled variation of the pulse regarding peak pressure and pulse width is therefore not possible for pressures beyond the cavitation threshold. The pressures required for a significant change in melting temperature are by orders of magnitude larger than the cavitation threshold in the investigated substances. Two potential approaches are not viable in this case:

- ▷ Properties of the sample substance such as viscosity or surface tension could be varied with additives in order to achieve higher cavitation thresholds or different pressure peaks during cavitation bubble collapse. These additives would however at the same time change the nucleation temperature and crystal growth kinetics.

- ▷ A very acute temporal detection of the primary and secondary pulses and the first appearance of supercritical nuclei could allow to identify the cause of nucleation. This is however very difficult in experiment, in particular as to the detection of just supercritical nuclei in a highly dynamic setup.

4.2. Discussion of new experimental data from this work

In this section, the results of the new experiments are discussed with respect to literature, theory, and consistency among the different methods. First, general issues that apply to all experiments are adressed. Next, the high pressure experiments are discussed in detail, including an estimate of uncertainty, a comparison to literature data and theory, and practical implications of the results. Some light is shed on theoretic limits and experimental hints of low pressure nucleation. Then, the dynamic experiments are addressed and overall conclusions are drawn.

4.2.1. General issues

In this section, issues common to all experiments are addressed. Time scales in nucleation experiments, influence of sample composition, interfaces and sample mass are discussed. In addition, a comparative analysis of statistics in nucleation experiments as presented here and in literature is given.

Time scales

The time scales involved in a phenomenon to be investigated determine the experimental effort, such as to stabilize boundary conditions or to measure thermodynamic data. For a given setup of a nucleation experiment, the macroscopic solidification speed has an important impact on the experimental precision, as do the temporal characteristics of cavitation and nucleation.

Macroscopic solidification speed For subcooling of 5 K or more, typical solidification speeds are in the order of mm/sec for all substances. When coming close to T_m, the speeds slow down very much for all investigated samples. A slower crystal growth for strong subcooling was not observed in the investigated temperature range, i.e. glass forming effects are not expected to be of any relevance. The macroscopic structure of the solidified sample was found to give clear indication of the crystallization speed: larger crystallites were formed during slow crystal growth, while for fast grown solids, the general appearance was more uniform and only small crystallites were formed. This observation is helpful to understand what happens during the high pressure experiments, where no direct visual observation was possible due to the opaque sample container. In the pressure signal, an “instant” pressure drop was observed after nucleation, i.e. the scanning rate of the sensor could not resolve the speed of the pressure change. Similarly, the temperature signal did not resolve the temperature change neither. After the experiment, the solid sample was examined outside the container. The structure was similar to that of the quickly crystallized samples from the ambient pressure test tube experiments. This observation suggests strongly that nucleation

took place quickly and at large subcooling, i.e. it can be assumed that the sample was completely solid after a few seconds at most.

In summary, for the investigated substances, crystal growth from the subcooled melt is fast. There are no hints that the speed of solidification is substantially different at high pressures or that the speed is reduced for very strong subcooling. One important consequence is that a nucleation event happening unnoticed is practically out of the question. A second consequence is that the time span between the very first nucleation and the detection of it is very small. Thus, the detected (macroscopic) nucleation temperature and pressure correspond well to the values during (microscopic) nucleation, as long as at least a moderate scanning rate is used for the measurements. A high experimental effort to precisely stabilize boundary conditions is therefore not required. Of course, the situation is different for a cavitating liquid.

Cavitation and nucleation A second observation about time scales can be drawn from the ultrasonic experiments. The time span observed between the start of insonication and the first observation of cavitation was about 0.5 seconds or less in most cases, and up to a few seconds in some few cases. As a tendency, the latter cavitation onset was observed for low powers of the ultrasonic generator. Once cavitation developed in the liquid, it was observed without interruption during the insonication. The general impression was that the time span before cavitation onset is rather stochastic and no systematic relation could be established. The time span between cavitation onset and nucleation (in configurations where nucleation was observed at all) was very short in all cases, i.e. instantaneous within the precision of measurement. A heating of the bulk volume by the ultrasonic power is therefore not expected.

Sample composition

The uncertainty in the sample composition and its expected and observed impact on nucleation is summarized and discussed in this part.

Uncertainty in sample composition The salt hydrates that were used in this study were obtained from chemical companies and were sold as “analytical grade” materials. The declared impurities of less than 0.01 % are mainly different salts. The nucleation activity of those impurities is a priori unknown. Therefore, material from one lot of one supplier was used throughout all experiments for each substance. In PCM literature, impurities are usually not specified in detail. A comparison of the results to literature data can only be a rough estimate. Water was used as tap water and purified tap water. The purified water was obtained using an ion exchange and micro filter system. While ionic material, i.e. dissolved salts, and dust particles are well removed, very small organic particles are not as efficiently filtered. Biogenic nucleators as introduced in section 2.2.2 could be present in the filtered water. For the salt hydrates, the existence of biogenic nucleators is improbable and not documented. Dissolved gases from atmospheric air such as

carbon-dioxide are not removed by the filtering and purification processes for either of the sample substances.

While not strictly an impurity, a non-stoichiometric water content is a prominent problem for salt hydrates. Most salt hydrates are hygroscopic and tend to take up water from surrounding air — with the exception of $NaOAc \cdot 3\,H_2O$, which tends to lose water — and need to be stored well sealed. In this work, the initial water content of the materials as acquired from the chemicals supplier was successfully verified by Carl Fisher titration. During long time experiments, glass test tubes were used preferably, but had to be substituted with PP containers in some cases. This is due to the very quick volume change, that takes place when a sample is significantly subcooled and suddenly crystallizes. Particularly for the water samples with their large, positive $\Delta\nu$, glass test tubes could not be used. In the high pressure experiments, glass test tubes could also not be used. Here, the effect of water uptake or loss is assumed to be negligible, due to short time of the experiment and the surrounding oily medium in the pressure cell.

Impact on nucleation A possible change in the sample composition should be reflected in the temporal evolution of nucleation temperatures during repeated experiments. For the normal pressure experiments, in general, irregular fluctuations around a mean nucleation temperature without any trend are observed. Only for one sample of $KF \cdot 4\,H_2O$, a distinct change in the nucleation temperature was observed within the first few freezing cycles, as shown in figure 4.7.

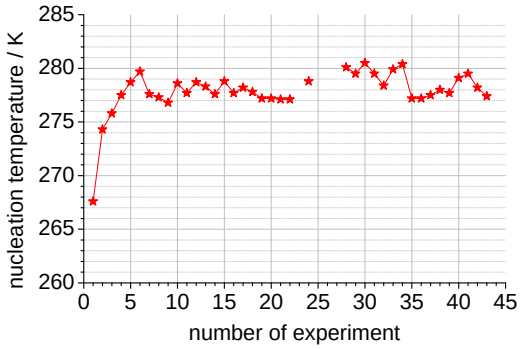

Figure 4.7.: Sample 2 of $KF \cdot 4\,H_2O$ showed a distinct initial change in nucleation temperature.

During the later cycles, this sample shows a significantly higher nucleation temperature than the other samples of the same material. The deviation from the mean nucleation temperature is about 10 K. This behavior is probably due to an initial activation of a nucleation seed; the nature of this nucleation could however not be identified. A slowly but steadily changing nucleation temperature, that would be caused by continuous change in composition, was not observed in any case. When looking at the time line graph of $CaCl_2 \cdot 6\,H_2O$ shown in figure 3.13b, a strong scattering of the nucleation

temperature for each sample is observed particularly during the cycles 14–23. This varied nucleation temperature could be a sign of a temporary phase separation.

Interfaces

In figure 4.8, the sample and its surrounding surfaces are sketched for the various setups. The sample was in direct contact to the sample container in all setups. In the

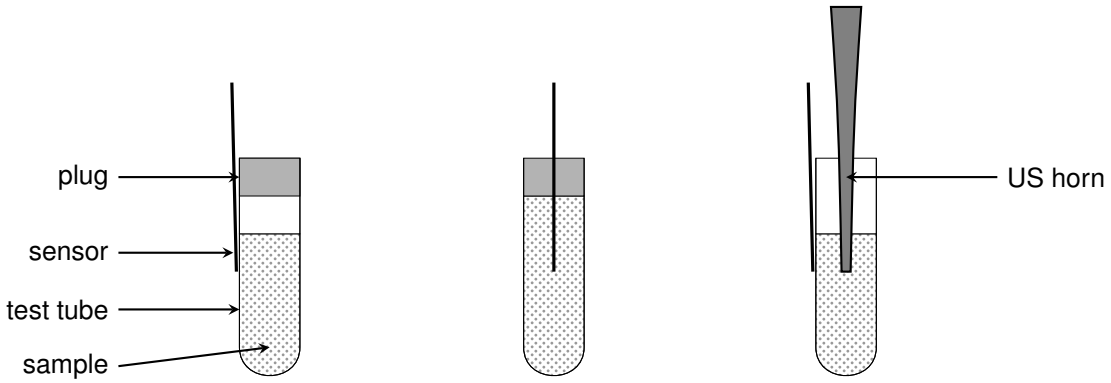

Figure 4.8.: Different surfaces are in direct contact with the sample in the normal pressure (a), high pressure (b), and ultrasonic experiments (c).

normal pressure and ultrasonic setups, an interface with surrounding air was present, while in the high pressure experiments, the tube plug sealed the sample on the top. Here, the temperature sensor provided an additional interface with the sample. This setup was not variable. In the ultrasonic experiments, an additional interface was created by the ultrasonic horn dipped in the sample.

The additional interfaces in the high pressure and ultrasonic experiments are potential nucleation sites. Their actual nucleation activity was assessed by running the experiments at normal pressure or without ultrasonic operation respectively. The reference nucleation temperatures of the three types of experiments (normal pressure, high pressure, ultrasonic) are shown in table 4.1.

Judging from the available data, the influence of the different interfaces on the nucleation temperature is very small. The largest deviation of 4 K is found for $CaCl_2 \cdot 6\,H_2O$ at high and normal pressure. For comparison, the standard deviation of the high pressure nucleation curve is 7.2 K and the range of nucleation temperature in the normal pressure experiments is typically ± 3 K. The difference between nucleation and melting temperatures is in the smallest case 12 K for tap water, and T_n is increased by at least 10 K by the ultrasonic treatment. The influence of the interfaces is thus small enough to allow a clear detection of improved nucleation by pressure or ultrasound.

Table 4.1.: The reference nucleation temperatures T_n^0 as determined in the different setups. Normal pressure: 50% nucleation frequency as read from the histograms; high pressure: nucleation curve extrapolated to normal pressure; ultrasonic: horn dipped in sample without vibrating; missing data: no experiments; t: tap water; p: purified water.

	H_2O	$KF{\cdot}4H_2O$	$CaCl_2{\cdot}6H_2O$	$NaOAc{\cdot}3H_2O$
normal pressure	$261^t/258^p$	268	272	253
high pressure	–	265	268	253
ultrasonic	261^p	–	271	–

Sample mass

The sample mass was similar in all setups. Two sizes of test tubes were used, glass test tubes of about 10 ml for the ambient and ultrasonic experiments, and PP test tubes of about 3 ml for the high pressure experiments. Some ultrasonic experiments were also carried out with the smaller PP test tubes.

For the normal pressure setup, where the large number of experiments should minimize statistical effects, an exemplary evaluation is shown in figure 4.9.

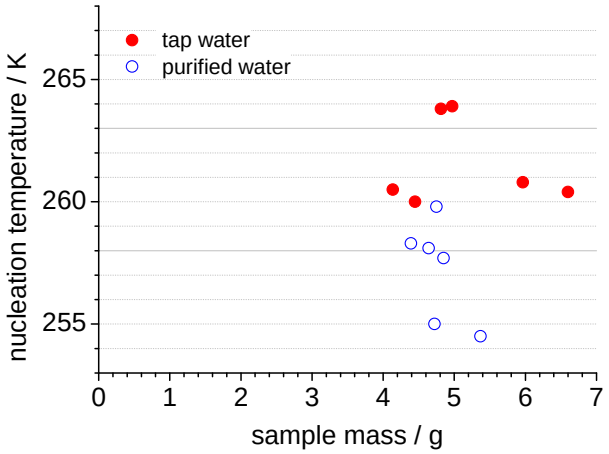

Figure 4.9.: Nucleation temperatures of the individual water samples versus the sample mass. The nucleation temperatures of tap water and purified water are indicated for 50% frequency as read from the histograms.

The nucleation temperatures of the twelve water samples are plotted over the sample mass. A systematic relation between nucleation temperature and sample mass was not detected. Some of the purified water samples show similar nucleation temperatures as some of the tap water samples. The general trend is however that the purified water can be cooled to lower temperatures than the tap water before nucleation occurs, as expected from nucleation theory. This implies that, at least for tap water, the nucleation

sites are part of the sample materials and not the container walls. For both water substances, the general shape of the histograms and thus the nucleation statistics are similar.

Experimental statistics in literature

In figure 4.10, so-called "survival curves" for water are shown from nucleation experiments reported by Vali and Heneghan et al. [55, 59]. The curves indicate the percentage of non-nucleated subcooled water samples in a cooling experiment, corresponding to $1-x$ where x is the value of the histogram curves determined in the ambient pressure experiments of this work.

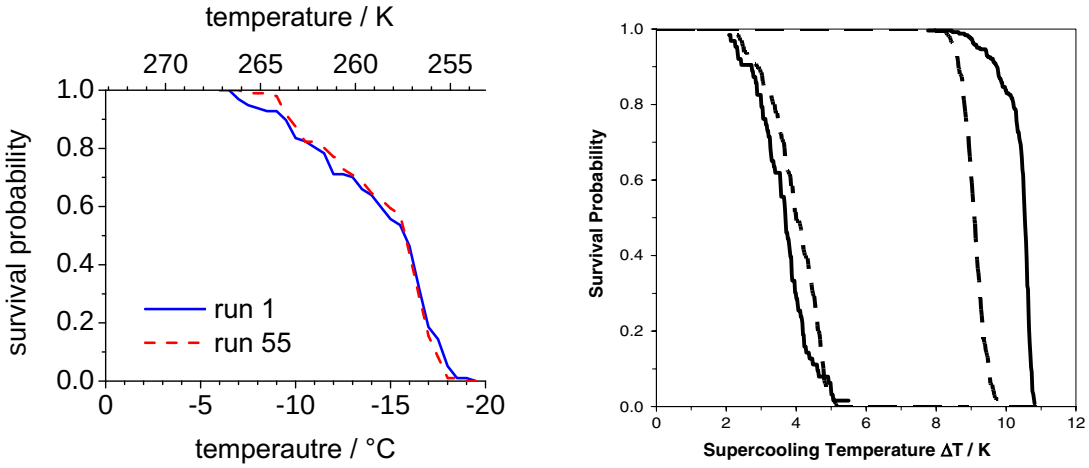

(a) graph based on data from Vali [55]

(b) graph from Heneghan [59]

Figure 4.10.: Survival curve for subcooled water in literature. Vali investigated repeatability of heterogeneous freezing in water with soil samples. Heneghan et al. investigated the effect of coatings; the right dashed line refers to an uncoated glass container.

In table 4.2, the results of Vali and Heneghan et al. are compared to the results of this study.

Table 4.2.: Survival curves of subcooled water, comparison to literature data.

	nucleation temperature /K at ... survival rate			
	10%	40%	60%	90%
this study (tap water)	259.8	260.8	261.5	264
this study (purified water)	254.5	257.5	258	260
Vali	254.5	257	258.5	263.5
Heneghan et al.	263	263.2	263.4	264

The experiments from Heneghan et al. show a steeper survival curve than observed in this study. This is probably due to the very clean and well-defined crucible surface which was the main object of research in their study. The sample volume was about 200 μl. Vali's experiments were carried out on smaller drops of 10 μl. They are not so steep and resemble more the curves of the experiments carried out in this study, although the maximum observed subcooling is significantly larger in Vali's data, which is most probably due to the small sample size. In summary, it seems that the sample size has rather an impact on the maximum subcooling than on the steepness of the survival curves.

For the salt hydrates, survival curves or more generally statistical evaluation of nucleation experiments were not found in literature. In lack of this data, values of the survival curves at 50% from this study are compared to literature data as shown in table 4.3.

Table 4.3.: Nucleation temperatures of salt hydrates. Comparison of results of this work to literature data from Lane [12]. The range in T_n from this work is given as the values of the histogram curves at 20% to 80% frequency.

	nucleation temperature /K		
	$KF \cdot 4\,H_2O$	$CaCl_2 \cdot 6\,H_2O$	$NaOAc \cdot 3\,H_2O$
this study	269 ± 3	272 ± 1.5	253 ± 3
Lane	272 ± 4.5	278 ± 5	251 ± 3.5

The results agree with the literature data within the stated accuracy.

4.2.2. Nucleation by static pressure

An elevation of the melting temperature with increaseing pressure should lead to an elevation in the nucleation temperature. If the maximum degree of subcooling is constant, both curves are parallel. Then, isothermal nucleation by pressure should be possible.

However, this idea is based on two rough assumptions: First, extrapolating the melting curve from 0.1 MPa (normal pressure) to 800 MPa is not very trustworthy. Second, the assumption of the nucleation curve being parallel to the melting curve is also not very trustworthy. Therefore, an experimental verification was carried out for the salt hydrates used in this work as described in section 3.3. The results of the experiments are discussed and compared to the theoretic data and literature values in this section.

The results of the high pressure experiments on the three salt hydrates are shown in figure 4.11. Melting and nucleation temperatures were determined for pressures up to 800 MPa.

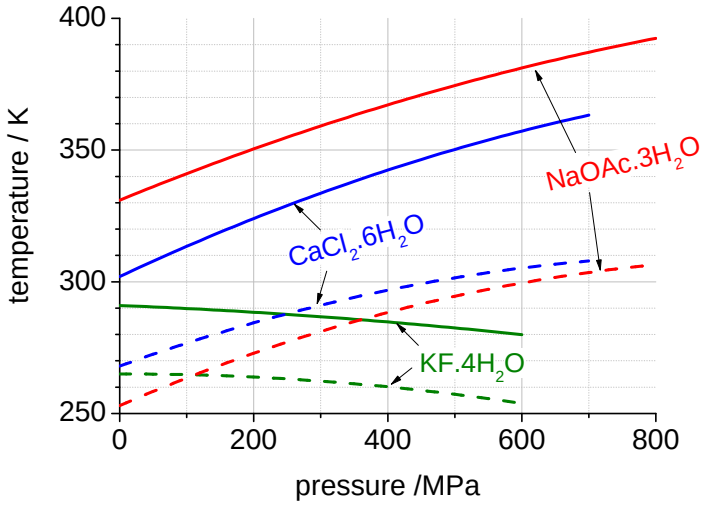

Figure 4.11.: Results of the high pressure experiments on salt hydrates. Interpolated melting (——) and nucleation (– – –) temperatures are shown for $NaOAc \cdot 3\,H_2O$, $CaCl_2 \cdot 6\,H_2O$ and $KF \cdot 4\,H_2O$.

The melting and nucleation curves are parametrized by

$$T_{\mathrm{m,n}}(p) = T_{\mathrm{m,n}}(p = p_0) + a\,p - b\,p^2 \tag{4.3}$$

The coefficients of these fits are listed for the three sample substances in table 4.4.

Table 4.4.: Values of the fit parameters used to interpolate the experimental results of the high pressure experiments by equation (4.3). Values indicated by *m* refer to melting, *n* to nucleating curves.

		a $/10^{-2}\,\mathrm{KMPa^{-1}}$	b $/10^{-5}\,\mathrm{KMPa^{-2}}$
$KF \cdot 4\,H_2O$	*m*	−1.0	−1.4
	n	0.062	−3.2
$CaCl_2 \cdot 6\,H_2O$	*m*	11.9	−4.5
	n	9.2	−5.0
$NaOAc \cdot 3\,H_2O$	*m*	10.4	−3.4
		11	−5.4

Analysis of uncertainty

The uncertainty of the extrapolations from room pressure data is determined according to propagation of errors. Experimental melting and nucleation curves are determined

as parametric fit to the second order polynomial equation (4.3). From this, the standard deviation of the measurement is determined. The evaluation procedure is presented in detail in section B.3. The results are shown in table 4.5.

Table 4.5.: Uncertainties of interpolated melting and nucleation curves (measurement) and extraplated melting curves (theory). σ denotes the standard deviation of the measured data with respect to the interpolation (of the melting m and nucleation n curves), $\delta\Delta T_\mathrm{m}(400\,\mathrm{MPa})$ denotes the theoretic uncertainty of the melting temperature at 400 MPa.

	σ_m / K	σ_n / K	$\delta\Delta T_\mathrm{m}(400\,\mathrm{MPa})$ / K
$KF\cdot 4\,H_2O$	0.74	2.6	0.4
$CaCl_2\cdot 6\,H_2O$	1.1	7.2	4
$NaOAc\cdot 3\,H_2O$	3.8	2.6	4

Measurement vs. theory The curves of the melting temperatures are shown together with extrapolations from normal pressure data according to equation (2.8b) in figure 4.12. This comparison shows that the extrapolation overestimates the pressure dependency of the melting temperature considerably. For $CaCl_2\cdot 6\,H_2O$ and $NaOAc\cdot 3\,H_2O$, there is a similar gap of about 20 K at 400 MPa. This gap is about 10 K for $KF\cdot 4\,H_2O$.

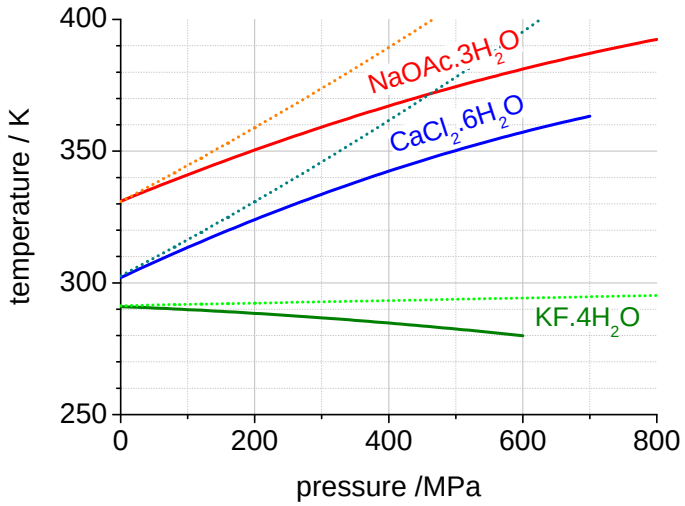

Figure 4.12.: Comparison of interpolated melting curves from high pressure measurement to extrapolations from normal pressure data. Data from table 3.2 was used together with equation (2.8b) for the extrapolations.

Considering the uncertainties of experimental and theoretic curves presented in table 4.5, this observed difference is significant. What could be the reason for this

discrepancy?

Equations 2.8 and 2.9 assume a constant $\Delta v/\Delta h$ in the integration. For very large pressures, the compressibility of a liquid is not constant. For water, it decreases by about 50% from 0.1 MPa to 800 MPa as discussed in section B.4. It can be assumed that the compressibility of the solid is less sensible to pressure than that of the liquid, i.e. Δv decreases with pressure. As to Δh, from equation (2.4) its dependency on the phase change temperature goes with the slope of $T_\mathrm{m} \cdot \Delta s(T_\mathrm{m})$. The change in entropy between liquid and solid states Δs should be rather insensitive to or rising with temperature, because the entropy of the solid is less variable with T than the entropy of the liquid. Thus, for increased melting temperature, Δh increases and the tendency of $\Delta h/\Delta v$ with increasing melting temperature is positive. Then, in equation (2.8a) the right side of the equation is underestimated and the real pressure curve should have a steeper slope than that of the simplified case. In the same way, the melting curve in equation (2.8b) should have a less steep form than predicted based on the simplification. This tendency is confirmed by the experimental results. The simple extrapolation used in the work of Rogerson and Cardoso [30] considerably overestimates the pressure dependency of the melting temperature.

Measurement vs. literature data A comparison of the experimental results from this work to available literature data is shown in figure 4.13. Here, only the melting curves are plotted, because there is no literature data for the nucleation curves available.

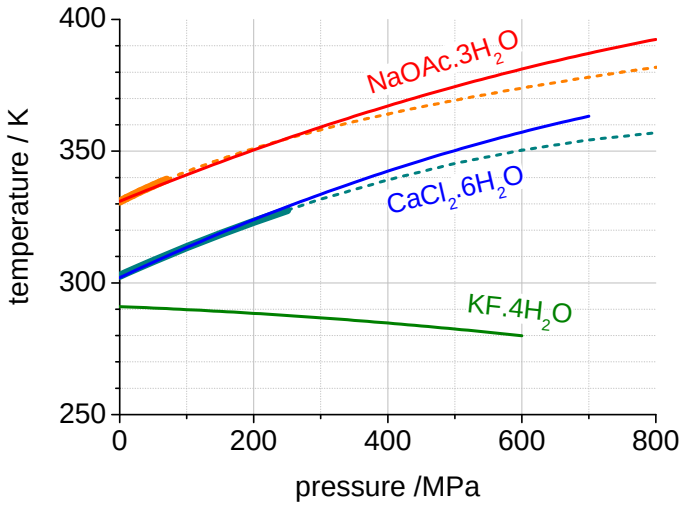

Figure 4.13.: Comparison of measured melting curves (——) to literature data (·····). Experimental data (thick lines) and suggested extrapolations (– – – –) from Barrett and Tammann [47, 46] are shown together with the results from measurement.

Barrett and Tammann [47, 46] report experimental data up to 250 MPa and sug-

gest extrapolations to higher pressures. It can be seen that the results from the high pressure experiments of this study agree very well within the measured range of the reported works. It is remarkable that, in the extended pressure range investigated in this work, the results are fairly well described by the extrapolations from literature. Contrary to the extrapolations from normal pressure only, here the extrapolated curves slightly underestimate the pressure dependency of the melting temperatures. The superior agreement of measured data compared to theoretic data is obvious and implies that high pressure melting of the salt hydrates is not well described by the simplified thermodynamic relations.

Practical consequences

From the experimental results, a first set of practical conclusions regarding nucleation by high pressure can be drawn.

- ▷ The situation for $CaCl_2 \cdot 6\,H_2O$ is quite clear. A compression of the subcooled liquid leads to nucleation. The nucleation pressure depends on the initial degree of subcooling. Considering a tolerable subcooling of for example 1 K, a compression of about 500 MPa is necessary to suppress subcooling. This can be considered good conditions for an application of a high pressure nucleation mechanism.
- ▷ For $NaOAc \cdot 3\,H_2O$, a nucleation at the normal pressure melting temperature was not observed. This is due to the limited maximum accessible pressure of 800 MPa. The observed steepness of the nucleation curve is decreasing with increasing pressure, so a further extrapolation until the nucleation curve reaches the normal pressure melting temperature seems not recommendable. Still, nucleation by pressure could be interesting for $NaOAc \cdot 3\,H_2O$, because this method works very well at room temperature. Nucleation at room temperature would be a strong improvement for $NaOAc \cdot 3\,H_2O$, because the nucleation temperature at ambient pressure at about 253 K(−20 °C) is not readily accessible. In an application, one could implement a cold finger technique where only part of the PCM volume is cooled to room temperature and used for nucleation. The pressure needed to nucleate at 25 °C is about 600 MPa.
- ▷ The experiments on $KF \cdot 4\,H_2O$ clearly showed that a nucleation by isothermal compression is not possible for pressures smaller than 600 MPa. The presence of a solid phase above the normal pressure melting temperature of 291 K is highly improbable for pressures smaller than 1 GPa. Although this result is not encouraging with regard to the potential of a nucleation by pressure method, it is very useful in the context of this work. Due to the insensitivity of the subcooled $KF \cdot 4\,H_2O$ to high pressures, it can be used as a counter sample in the other experiments.

Nucleation at $T > T_m^0$

For $CaCl_2 \cdot 6\,H_2O$, several data points were recorded where $T_n > T_m^0$, i.e. where the nucleation temperature is larger than the melting temperature at ambient pressure. This is very interesting, because it allows some deductions about the speed of pressure stabilization in the setup.

Once the solidification is triggered, the sample volume decreases and the high pressure cell has to react in order to stabilize the set pressure. If this does not happen quickly, it could be that a region above the melting curve is reached in the temperature vs. pressure plane, i.e. a point (T, p) with $T > T_m(p)$. In that case, the solid could melt again, and the phase change is "aborted", which should be visible in the temperature signal. The peak form is however regular, and thus an aborted phase change does apparently not happen. In principle, the solid could be prevented from melting during decompression by adiabatic cooling. However, as latent heat set free by the phase change counteracts external cooling, and only a small volume change and thus little expansion work occurs, this option can be ruled out. This means that the pressure is well stabilized in this apparatus even during the solidification of the sample.

4.2.3. Nucleation under ultrasonic irradiation

In this section, the results of the ultrasonic experiments are discussed. A change in the nucleation temperature was observed for water, but not for the salt hydrates. The impact on the nucleation temperature is therefore discussed for water only.

Effects of ultrasound without cavitation on nucleation

Comparing the length and pressure scales of ultrasonic waves in liquids with the length scales of critical nuclei and the pressure dependency of the nucleation temperature, two first important conclusions can be drawn.

The length scale of critical nuclei is in the range of fractions of micrometers ([30], section B.2), while the length scale of an ultrasonic wave in water or liquids with similar speed of sound is in the range of several centimeters (section 2.2.3). Considering a sinusoidal wave, a variation of roughly 10^{-5} of its amplitude is found along the diameter of a nucleus. The pressure amplitude of an ultrasonic wave without cavitation is limited by the cavitation threshold. As lined out in section 2.2.3, the cavitation threshold is at most 30 MPa. The pressure variation along the diameter of a nucleus is thus at most 300 Pa, corresponding to a very small shear force. Ultrasonic disruption of liquid droplets is a common technique to produce micro-emulsions, which show in fact droplet sizes in the micrometer range. In this case, the emulsification process is commonly agreed to rely on cavitation [95, 149], i.e. this is not a counter-example that significant shear forces act in the ultrasonic field on the micrometer length scale. A rupture of nuclei and thus an anti-nucleation effect of the pressure variation in an ultrasonic field can therefore be ruled out.

Considering the pressure dependency of the nucleation curve of about 0.1 K/MPa as determined in section 4.2.2, the nucleation temperature is changed in the ultrasonic field by about 3 Kat most. This is a noticeable change, but a small value compared to the difference between melting and nucleation temperature in untreated samples which ranges from about 11 K for tap water to 78 K for $NaOAc \cdot 3\,H_2O$. In particular, the nucleation of water under ultrasonic treatment was observed at about 272 K, i.e. the nucleation temperature was in fact changed by almost 10 K. A direct nucleating effect of the pressure variation in the ultrasonic field can be ruled out as well.

In summary, the effect of ultrasonic treatment on nucleation has to be dominated by cavitation processes.

Parameters of the cavitation threshold

Cavitation as such is a nucleation problem, and it only occurs if the cavitation threshold is overcome. From theory, the cavitation threshold is hard to quantify, again because it is highly sensible to impurities.

Liquid properties In theory, material properties of the liquids such as viscosity could have a large impact on the cavitation threshold. This impact is hard to quantify, and exact material data is not available for the salt hydrates.

The maximum pressures obtained in a cavitating liquid depends on the maximum bubble size and its content, as shown in section 2.2.3. Both variables are sensitive to the material. Also, the viscosity of the liquid plays an important role for the collapse kinetics, a larger viscosity damping the oscillation and reducing pressure peaks [26]. The impact on the maximum of the first peak of the bubble collapse is however less strong. As a general rule, the viscosity is large for salt hydrates, and a function of temperature and pressure. Precise experimental values of the subcooled melt are unknown.

In the experiments, no difference in cavitation threshold was visible between the four sample substances. However, in degassed water samples, the cavitation threshold was increased significantly. Thus, dissolved gases apparently play a more important role for the cavitation threshold than the bulk liquid properties.

Pressure At normal pressure, cavitation was observed in all insonication experiments for all ultrasonic amplitudes. After degassing and operating the ultrasound at its minimum amplitude, a situation was created where the ultrasound did not cause cavitation. The degassing was carried out only for water, because for the salt hydrates, a constant chemical composition of the sample could not be guaranteed after degassing.

The pressure levels are sketched for four situations in figure 4.14.

In the reference case, i.e. insonication at normal pressure, cavitation occurs already at the smallest ultrasonic amplitude. When the sample is degassed, the cavitation threshold is reduced. Then, insonication at normal pressure operating the ultrasound

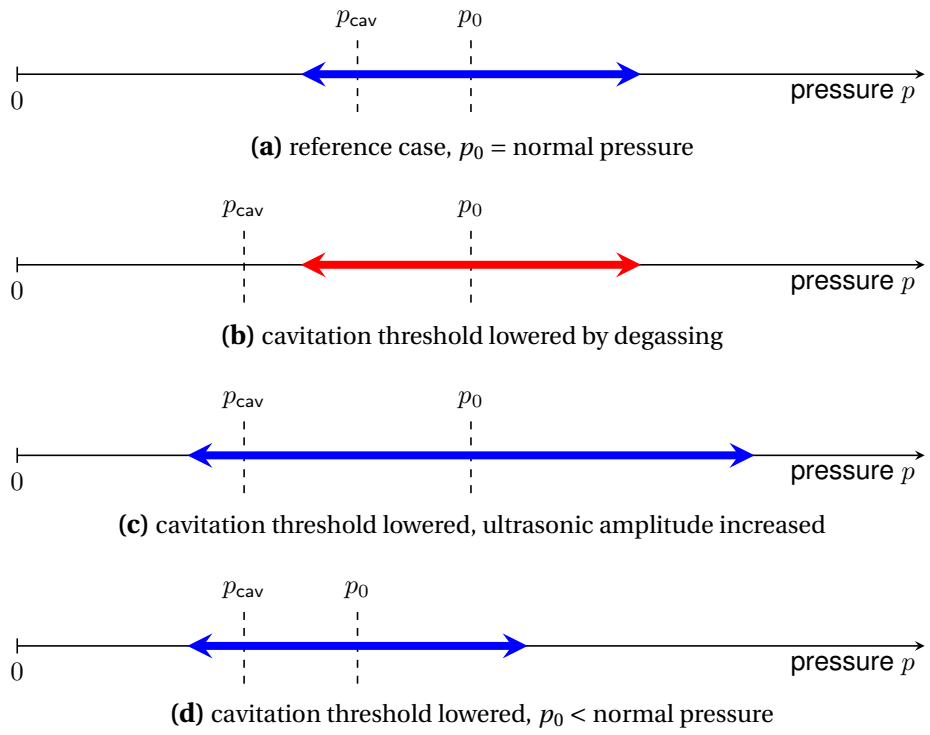

(a) reference case, p_0 = normal pressure

(b) cavitation threshold lowered by degassing

(c) cavitation threshold lowered, ultrasonic amplitude increased

(d) cavitation threshold lowered, p_0 < normal pressure

Figure 4.14.: Whether cavitation is generated by ultrasound or not depends on the cavitation threshold p_{cav}, the ambient pressure p_0, and the amplitude of the ultrasound.

generator at its lower limit does not cause cavitation, as sketched in figure 4.14b. There are two options to reactivate cavitation: Either the pressure amplitude is increased as sketched in figure 4.14c, or the ambient pressure is reduced as sketched in figure 4.14d. In experiment, both cases were observed.

Thus, when the cavitation threshold was lowered by degassing and the ultrasonic generator was operated at minimum amplitude, the role of cavitation on the nucleation could be observed directly. At a given temperature below the melting temperature but above the nucleation temperature, in fact whenever cavitation was absent, no nucleation was observed. Vice versa, whenever cavitation occurred in this temperature range, sononucleation was observed. It can therefore be clearly stated that cavitation is a necessary condition for sononucleation of water. This implies again that sononucleation is not a direct effect of the ultrasonic field induced in the sample.

While a change in cavitation threshold of the degassed water samples could be well observed, the sononucleation temperature was similar to that without degassing, as discussed in the next section. Also, the nucleation temperature in low pressure experiments without insonication was similar to the nucleation temperature at normal pressure. The number of these experiments is small, and thus might not be a solid proof considering the statistic nature of nucleation. The least that can be said is therefore

that no evidence nor hint was found that dissolved gases in the liquid would play a crucial role in nucleation of the solid, be it with or without ultrasonic treatment.

Impact of ultrasound on the nucleation temperature

An impact of ultrasound on the nucleation temperature could be clearly diagnosed for water. In figure 4.15, the accumulated nucleation frequencies of water are compared for the different experiments.

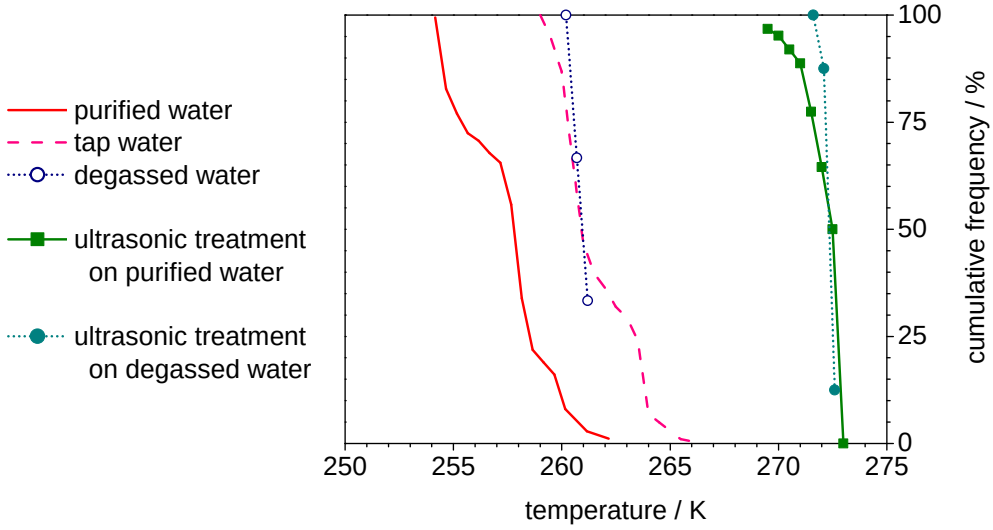

Figure 4.15.: Nucleation probability for water in different setups.

- ▷ The lowest nucleation temperature of about 258 K (at 50% frequency) was observed for purified water being cooled at normal pressure. Using tap water, the nucleation was observed already at 261 K. Those two values are well established due to the large number of experiments, namely over 170. For the reference measurements in a low pressure atmosphere with the ultrasonic horn dipped in the sample, nucleation was observed at 261 K as well. In that case, only a small number of experiments were carried out (namely 3), and the significance of this value is therefore lower.
- ▷ Ultrasonic treatment resulted in very good nucleation enhancement, independent from the static pressure of the setup. Over 90% of the sononucleation experiments resulted in a nucleation temperature above 271 K, i.e. subcooling was reduced to 2 K. The curve of the experiments on degassed water seems to be a bit flatter, but this is due to the different modes of operation: In all dynamic

experiments with irradiation, nucleation was observed at temperatures higher than 271 K. In all isothermal experiments, nucleation was observed as soon as the ultrasound was applied in the temperature range 268 K to 271 K.

As to the salt hydrates, an effect of the ultrasonic treatment on the nucleation temperature was not observed as described in section 3.4.2. Cavitation was however observed readily in all three salt hydrates. Nucleation of the irradiated samples was only triggered when cooling them to about the nucleation temperature as determined previously without the ultrasonic treatment. Considering the large difference between melting and nucleation temperatures at normal pressure, namely 22 K for $KF \cdot 4\,H_2O$, 31 K for $CaCl_2 \cdot 6\,H_2O$ and 78 K for $NaOAc \cdot 3\,H_2O$, even a moderate improvement of nucleation should have been clearly observed.

4.3. New insights in sononucleation

In this work, new experimental data on sononucleation of inorganic PCM was acquired. Pressure dependent melting and nucleation temperatures as well as temperature dependent crystal growth speeds were determined for three salt hydrates. Nucleation under ultrasonic treatment was investigated for the three salt hydrates and water. Successful sononucleation was observed for water only. In this section, based on the new facts, different possible nucleation mechanisms of water are analyzed, and a possible transfer to inorganic PCM is discussed in this section.

In table 4.6, a qualitative overview of data is given for the four investigated materials, and additionally for solutions. The list includes both own and literature data and serves as a reference for the further discussion.

Table 4.6.: Summary of data relevant for sononucleation. A qualitative scale is used where $--$ / $-$ / $\circ$ / $+$ / $++$ denote no / weak / some / strong / very strong subcooling or cavitation, no / slow / medium / fast / very fast solidification, not / a little / some / much / very much improved nucleation. Own data ($\bullet$) and literature data ($\circ$); "n.a.": no data available.

	water	KF $\cdot 4\,H_2O$	$CaCl_2$ $\cdot 6\,H_2O$	NaOAc $\cdot 3\,H_2O$	solutions
Subcooling	$-^{\bullet}$	$\circ^{\bullet}$	$+^{\bullet}$	$++^{\bullet}$	n.a.
Speed of solidification	$++^{\circ}$	$++^{\bullet}$	$+^{\bullet}$	$+^{\bullet}$	$--^{\circ}$
Cavitation by sonication	$+^{\bullet}$	$+^{\bullet}$	$+^{\bullet}$	$+^{\bullet}$	$+^{\circ}$
Nucleation by static pressure	$--^{\circ}$	$--^{\bullet}$	$++^{\bullet}$	$+^{\bullet}$	n.a.
Nucleation by ultrasound	$++^{\bullet}$	$-^{\bullet}$	$-^{\bullet}$	$-^{\bullet}$	$+^{\circ}$

4.3.1. Statistics in static nucleation and sononucleation

Statistics plays a prominent role in all nucleation problems, and particularly in sononucleation where two nucleation phenomena, namely cavitation and solidification, are relevant. The activity of nucleation sites and the active sample volume are discussed in the following.

Activity of nucleation sites

One main parameter that determines the nucleation barrier and thus the nucleation temperature is the surface tension σ. Whenever a sample is in contact with a container surface or with a surface of impurities, at this place the surface tension is changed compared to its bulk value and these surfaces can act as nucleation sites. Furthermore, it has been shown that sononucleation is always associated with cavitation in section 4.2.3. In the direct vicinity of the cavitation bubbles, pressure and temperature

are changed dynamically which is believed to cause sononucleation. The cavitation bubbles provide additional surfaces in the subcooled sample, which are potential nucleation sites, too.

The measurements at static pressure were intended to evaluate if the conditions next to a collapsing cavitation bubble favor nucleation in the ultrasonic experiments. However, only when the same kind of nucleation sites are active in two experimental setups, the nucleation barrier is necessarily comparable. Considering this, can the static pressure experiments be used to study the sononucleation experiments?

There are in fact three possible options:

1. Nucleation sites are active (or inactive) both in static and sononucleation experiments: the nucleation barrier in the two setups is similar.
2. Nucleation sites are active in static experiments, but not in sononucleation experiments: the nucleation barrier is higher for sononucleation.
3. Nucleation sites are active in sononucleation experiments, but not in static experiments: the nucleation barrier is lower for sononucleation.

Only in the first case, a direct transfer of the nucleation temperature determined in static experiments to sononucleation experiments can be valid. Two possible configurations of this situation are illustrated in figure 4.16.

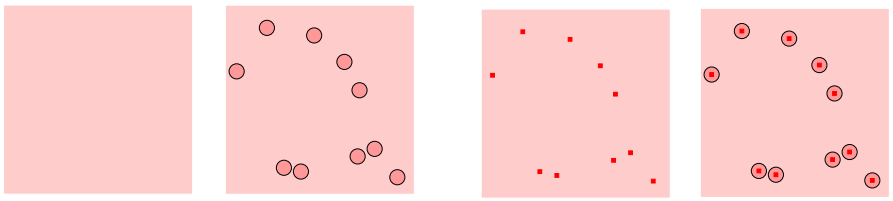

(a) homogeneous **(b)** heterogeneous

Figure 4.16.: If the activity of nucleation sites is similar for static nucleation and sononucleation depends on the local distribution of nucleation agents (■) and cavitation bubbles (○); see text.

If there are no seeds, i.e. in a case of homogeneous nucleation as sketched in figure 4.16a, the nucleation temperature in static and ultrasonic experiments is similar only if the cavitation bubbles don't change it. If there are seeds, i.e. in a case of heterogeneous nucleation as sketched in figure 4.16b, the same seeds are present in the static and sononucleation experiments. Supposing that the cavitation bubbles are formed at the same place where the seeds are, and that the seeds' activity is much higher than that of the bubble surface, again, a comparable nucleation temperature is expected. If the seeds act at the same time as nucleation sites for cavitation, this scenario is well possible.

The two other options are however possible, too. If the seeds do not have any impact on cavitation, and if they occupy a small fraction of the sample volume, the

number of seeds that locally coincide with a cavitation bubble is very low and the nucleation activity is reduced (case 2). If instead there are seeds that are only active in sononucleation, e.g. the cavitation bubbles as such, the nucleation activity is higher in the insonicated sample than in a static experiment (case 3).

In summary, based on the activity of nucleation sites, enhanced as well as inhibited nucleation is possible in sononucleation. A direct transfer of experimental data from static nucleation experiments is valid only under the following two assumptions:

- ▷ the nucleation activity of the cavitation bubbles is low compared to that of the seeds
- ▷ there are no seeds in the static experiments *or* the cavitation bubbles are nucleated at the location of the seeds

This is however not the whole picture, as nucleation theory suggests that not only the activity of the nucleation sites determines the macroscopic nucleation temperature, but also the active sample volume. This is discussed next.

Active sample volume

A second important parameter of nucleation theory is the sample volume. While in static setups the whole sample takes part in a nucleation experiment, in highly dynamic setups as in sononucleation, only a part of the sample volume is actually active. In fact, the whole sample is insonicated, but only in a small part of the sample cavitation bubbles develop, which are necessary for sononucleation. The nucleation rate being defined as number of nucleation events per time and volume, a reduced active volume may change the nucleation rate such that it is not observed in an experiment designed for larger volume and thus higher rates.

In the case of homogeneous nucleation, the active sample volume is clearly reduced in sononucleation to the immediate vicinity of the cavitation bubbles. For heterogeneous nucleation, the situation is more complicated. The numbers of particles that are in the vicinity of a seed is small compared to the whole sample volume anyway. Now, the seed activity determines the overall nucleation statistics. Figure 4.17 illustrates the following thoughts.

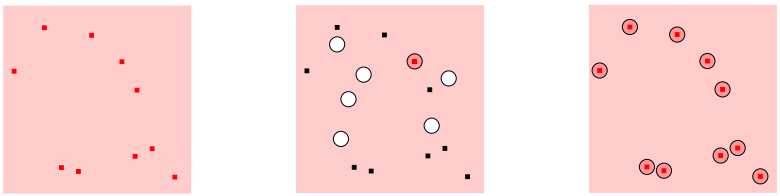

(a) uniform conditions **(b)** monoactive seeds **(c)** biactive seeds

Figure 4.17.: The active sample volume (dark areas) depends on the local distribution of seed sites (■) and bubbles (○); see text.

Under static conditions, i.e. isobaric isothermal nucleation experiments, the same thermodynamic conditions apply for the whole sample volume, and all seeds can act as center of nucleation for the solid phase figure 4.17a. In figure 4.17b, there are spatial variations of the thermodynamic conditions, such as small gas bubbles, here indicated by circles. Chances that the bubbles are found at the same spot as the seeds are low, if the density of the two types of inhomogeneities is low. This is different if the seeds are biactive as sketched in figure 4.17c, i.e. they act as center of nucleation both for the gas and the solid phase.

In addition, if the active volume around a bubble is in fact very small, nucleation could be prevented completely. Each bubble surrounding has to be considered as a single nucleation experiment in an isolated small volume. If this volume is smaller than the supercritical nucleus, sononucleation cannot occur at all, even if the overall active volume is large. The diameter of a cavitation bubble is typically in the range 0.01 mm to 1 mm, and the critical radius is rather in the range of 0.01 μm to 0.1 μm. However, the peak pressure in a cavitating liquid is created by the bubble collapse, and the activated volume could be thus much smaller than the maximum bubble volume.

In summary, after a close look on nucleation sites and active sample volume, quantitative comparisons between static and sononucleation experiments are based on a number of arguable assumptions. Both under- and overestimated nucleation probability can be well explained. Very different, microscopic experiments would be required to clarify these issues.

4.3.2. Theory of nucleation by a direct pressure mechanism

A pressure mechanism was believed to be effective in sononucleation, i.e. a nucleation mechanism which is fairly independent from specific material properties and can be applied to a wide range of inorganic PCM. This assumption is discussed in the light of the new data in this section.

Nucleation by high pressure

In contrast to the static high pressure experiments, the only successful sononucleation observed in this work was found for water. The equilibrium thermodynamic properties of water are well documented, and no own static pressure experiments were carried out. In general, literature data is precise and well established, with some limitations as described in section 4.1.3. The interpretation of this data with respect to high pressure nucleation is however not so straightforward.

In the basic study on sononucleation published by Hickling [103], experiments are reported also for a number of different materials, namely bismuth, germanium, silicon and gallium, which all have initially falling and later rising melting temperatures, as has water. If this shape of the melting curve is decisive for sononucleation, these materials should behave similarly as water does. In fact, failed sononucleation was observed in

all cases. Hickling argues that this is due to the fact that the melting curves of these materials reach their respective atmospheric melting temperature only at far higher pressures than water does. However, at a closer look, this cannot be the whole story.

Judging from the melting curves, a high pressure solid phase of water exists for temperatures above 273 K at pressures larger than 630 MPa, but this is not sufficient to permit nucleation by compression, as lined out in the following.

There is much less data available for the nucleation curve than for the melting curve, particularly at high pressures. Ice III was found to have similar subcooling than ice Ih, the stable solid at normal pressure, both from theoretic [150] and experimental works [144] as shown in figure 4.18.

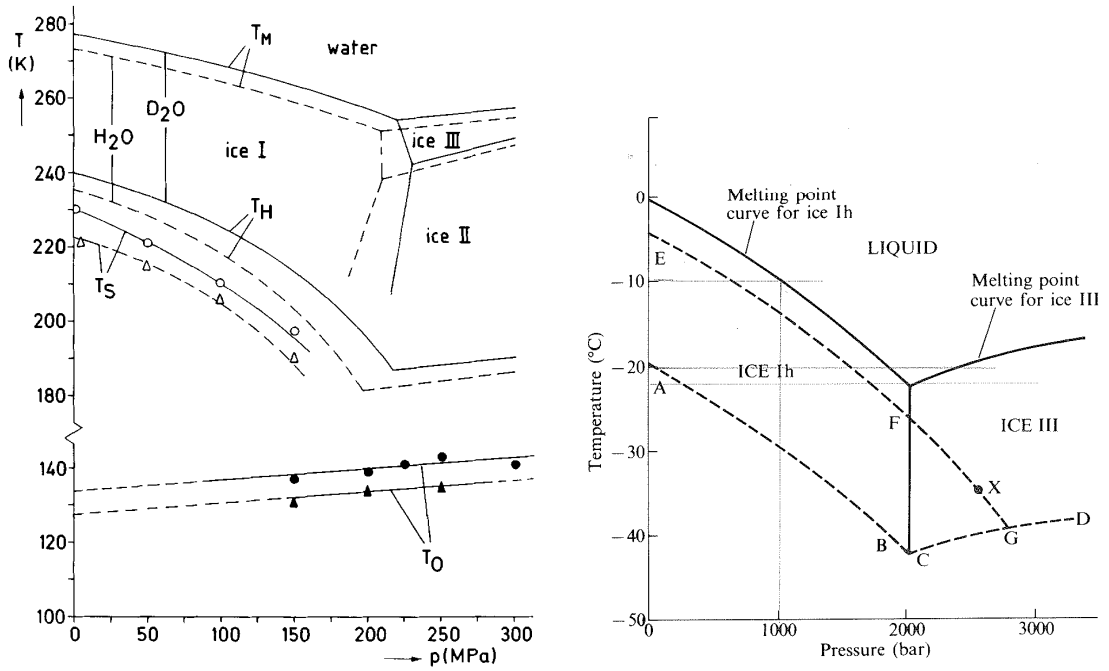

(a) Graph from Lang [150]

(b) Graph from Hobbs [144]

Figure 4.18.: Melting temperature T_M and homogeneous nucleation temperature T_H are shown for ordinary (——) and heavy water (– – – –) in (a). Experimental values of the melting (——) and nucleation (– – – –) curves of ordinary water are shown in (b).

In Lang's graph in figure 4.18a, the homogeneous nucleation temperature T_H for water and heavy water is shown. It is falling even steeper than the melting temperature T_M, i.e. maximum subcooling increases for high pressures. In Hobbs' graph in figure 4.18b, the melting and nucleation temperatures of the high pressure solid phases of water as observed experimentally and are basically parallel.

If the basically parallel melting and nucleation curves are extended over a wider pressure range, this results in a graph like figure 4.19. Using this extended nucleation curve, nucleation of ice VI is expected at 273 K and about 900 MPa. Fast compression

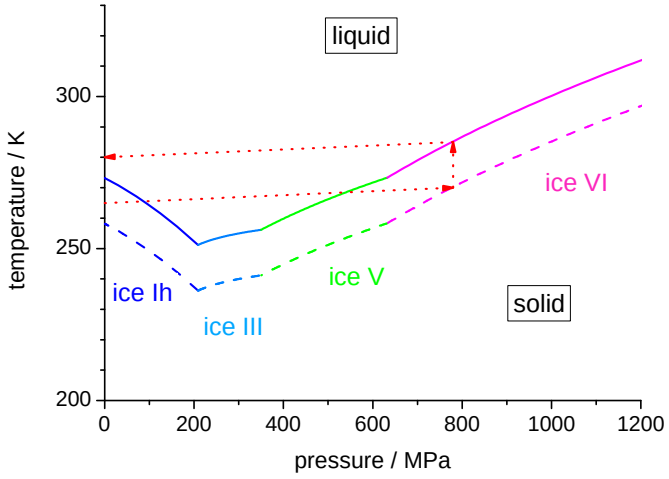

Figure 4.19.: Melting (——) and suggested nucleation (– – – –) curves of water, together with a path of nucleation by compression (·····). Data for the melting curve from IAPWS [151].

as in cavitation is rather adiabatic than isothermal and the temperature rises by about 5 K as explained in detail in section B.4. Considering that the room pressure nucleation temperature of 258 K is due to nucleating substances, it is not clear whether these or other substances nucleate the high pressure phases similarly. In addition, homogeneous nucleation of ice VI can be much different and could occur at lower subcooling than that of ice Ih. This is because surface and volume energies of the transition from liquid to ice VI are different than those of the transition from liquid to ice Ih. The simple extension using a constant subcooling for all phases is thus for sure a rough idea, but it should do to show an essential problem that is illustrated by the dotted line in figure 4.19.

If the nucleation curve is crossed by compression, and the solidification starts, latent heat of the phase change is set free. The temperature rises up to the melting temperature. When the sample is now decompressed, the sample enters a region in the phase diagram, where the liquid is the stable phase, and the solid nucleus would melt again. Even assuming that the decompression is fast and the solid has grown large enough to survive the crossing of the liquid region, in the end, a point in the phase diagram is reached which lies above the initial temperature before compression. If the initial temperature was at low subcooling, the final temperature is possibly above the room pressure melting temperature. To put it the other way round, in order to reach after compression, nucleation and decompression a point in the phase diagram where ice Ih is stable, the initial temperature has to be significantly lower than 273 K.

In the most favorable case, assuming that a small volume of solid ice VI is formed,

survives decompression, and ends at 0.1 MPa and something like 272 K, what happens next? A successful high pressure nucleation mechanism would require now a solid / solid phase conversion from ice VI to ice Ih. So again, nucleation of a new phase is necessary, now starting from a solid phase.

If ice VI is a nucleating agent for ice Ih, the pressure pulse would in fact have a positive impact on nucleation. Taking account of the fact that sononucleation was observed already at very small subcooling of less than 0.5 K in experiment, ice VI has to be very effective as nucleating agent. In figure 4.20, the crystal structure of the room pressure stable phase ice Ih and the high pressure phase ice VI are shown.

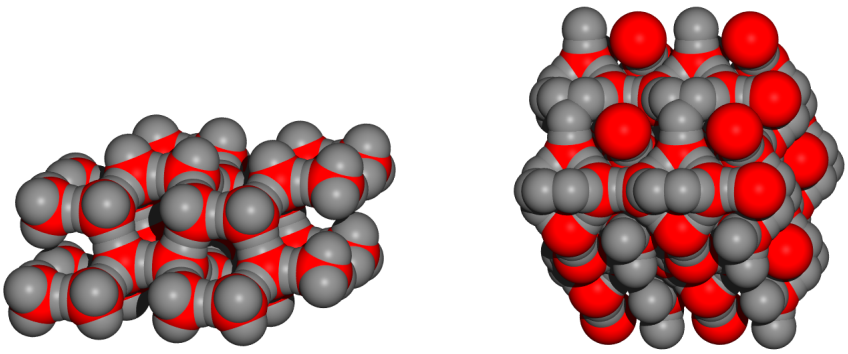

(a) ice Ih **(b)** ice VI

Figure 4.20.: The crystal structures of ice Ih (a) and ice VI (b) are not similar.

Decompressed ice VI should change its crystal shape to a small extend, i.e. the length of the unit cell probably increases. Therefore, it is very hard to judge whether ice VI can act as a nucleator for ice Ih. A theoretic prediction of the nucleating capabilities of two crystal structures is not yet reliably possible, as lined out in section 2.2.2.

To sum it up, a combination of several improbable assumptions is required for a high pressure nucleation mechanism that explains sononucleation of water:

- ▷ A peak pressure beyond about 900 MPa is reached.
- ▷ The high pressure is present long enough to allow the growth of a larger nucleus, that survives the liquid region during decompression.
- ▷ In spite of the latent heat set free during the growth of the solid, the temperature after decompression is below the melting temperature.
- ▷ Finally, ice VI acts as very effective nucleating agent for ice Ih.

While this process cannot be considered strictly impossible, it is extremely improbable.

Regardless of all the difficulties in analyzing the situation for water, if a high pressure mechanism explains the sononucleation of water, the situation for salt hydrates is much less complicated and in favor for nucleation. In the case of salt hydrates, there are no hints that the high pressure solid phase is different from the room pressure solid phase.

The pressure needed for the nucleation of $CaCl_2 \cdot 6\,H_2O$ is moderate compared to that of water. Similar cavitation was observed for all samples in the ultrasonic experiments, so in principle similar peak pressures should be reached in the salt hydrates as in water. Altogether, to put it the other way round, the fact that sononucleation does not occur in salt hydrates, but does occur readily in water, cannot be explained by the a high pressure mechanism only.

Nucleation by a low pressure mechanism

In the case of water – or other materials with a falling melting curve – nucleation by applying high pressures has been ruled out in the previous section because the solid phase which is stable at normal pressure is not accessible like this. But then, naturally, a reduction of the pressure could directly generate the correct solid phase and thus have a positive effect on nucleation. Is this *nucleation by low pressure* the cause for sononucleation of water? To judge on this issue, attainable low pressures are confronted with their impact on the degree of subcooling of water.

In a macroscopic, static setup, the lower limit of attainable pressure is given by the cavitation threshold as introduced in section 2.1.4. The value of the cavitation threshold in water is dependent on the boundary conditions, as discussed in section 2.2.3. Its theoretical limit is supposed to be at -120 MPa, and the largest reported values from experiments are -30 MPa.

In figure 4.21a, the melting and nucleating curves are linearly extrapolated to negative pressures.

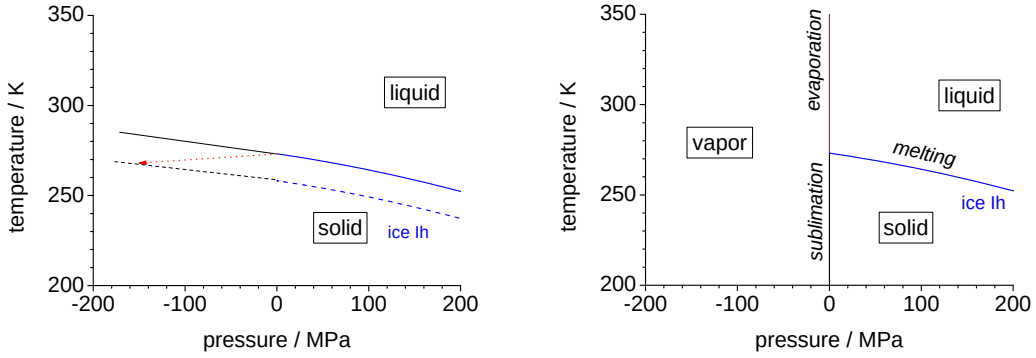

(a) extrapolated **(b)** equilibrium

Figure 4.21.: Linearly extrapolated melting and nucleation temperatures at low and negative pressure (a) and equilibrium phase change temperatures of water for low pressure (b). Data for the equilibrium curves from IAPWS [151].

The melting temperature rises by about 3 K by a decompression of 30 MPa. Compared to the subcooling of at least 10 K observed at atmospheric pressure, this is not

much. Taking the theoretic limit of tension, in the best case, a nucleation by decompression is possible for slightly subcooled water at about 271 K. This does not agree with the experimental observation of almost complete suppression of subcooling and strong sononucleation at 272.5 K already.

The difference is however not very large. Postulating that, in a highly dynamic setup, pressures of about -170 MPa are indeed reached in the liquid, if a new phase is nucleated in such a situation, is it the solid or the gaseous phase? This is in a region of the phase diagram far beyond the triple point, as shown in figure 4.21b. Instead of being a subcooled liquid, the liquid is now rather superheated with respect to the gaseous phase. As lined out in section 2.1.4, nucleation of the gaseous phase is much less complicated than nucleation of the solid phase. Therefore, if nucleation occurs, the gaseous phase will nucleate preferably. Then, the pressure increases rapidly due to the volume expansion during evaporation. Strong evaporative cooling takes place, and a region in the phase diagram at positive pressures but below the nucleation curve could be reached, where then nucleation of the solid phase is possible. This is then however not a direct pressure mechanism anymore.

Failed sononucleation for $CaCl_2 \cdot 6\,H_2O$ and $NaOAc \cdot 3\,H_2O$

For $CaCl_2 \cdot 6\,H_2O$ and $NaOAc \cdot 3\,H_2O$, the melting and nucleation curves rise with pressure, and the reasons that prohibit sononucleation by pressure in water do not apply. However, an improved nucleation by insonication was not observed for these substances. There are basically three options to explain this:

1. pressure is too low
2. temperature is too high
3. time of pulse is too short

Unfortunately, the sononucleation in water not being a pressure mechanism, direct deductions as to the form of the pressure pulse are not possible. An analysis of the failed sononucleation in $CaCl_2 \cdot 6\,H_2O$ and $NaOAc \cdot 3\,H_2O$ therefore can only be based on assumptions and estimations. In fact, too many open questions remain to allow an identification of the failing parameter.

The form of the cavitation pressure pulse and the temperature during the pulse are object to controversy as lined out in section 2.2.3. The range of discussed values is huge, namely 0-5000 K for the temperature rise and 10-30000 MPa for the pressure maximum. It is obvious that for the most favorable case, i.e. high pressure and low temperature, the equilibrium conditions for high-pressure nucleation are easily fulfilled for both substances. In the unfavorable high temperature and low pressure case, nucleation is not possible. In reality, high temperatures are caused by quick and strong compression, i.e. temperature and pressure maximums are interconnected. From this point of view, an identification of too high temperature or too low pressure as cause for failing sononucleation is not possible.

The assessment of the third parameter, time, is even more difficult. The speed of solidification was determined for the salt hydrates at different degrees of subcooling. Based on this data, the time span required for the growth of a supercritical nucleus should be estimated and confronted with the available time during the pulse. The available time span is in fact unknown, because information about the pressure/temperature pulse is too blurry as lined out above. Even for the required time span, there are many open questions:

- ▷ Is the microscopic growth of a nucleus well described by the measured macroscopic growth speed?
- ▷ What is the influence of pressure on speed of growth?
- ▷ What is the initial situation, i.e. the start of the growing process?
- ▷ Is there any time delay in the reaction of the system to changed boundary conditions?

In lack of basically all key parameters, it does not even seem to be helpful to set up a best case and worst case scenario. The only substantial conclusions are that the pressure pulse would need to be known much more precisely to allow an analysis.

4.3.3. Other mechanisms that could explain sononucleation

As shown in the previous sections, a pure pressure mechanism cannot explain sononucleation in water. However, as shown in the experimental part of this work, water can reliably be nucleated at very low subcooling by ultrasonic treatment. Similar results are reported for a number of solutions in literature. In this section, possible explanations for these observations are suggested that do not rely on a pressure mechanism and do not conflict with the failed sononucleation of the three investigated salt hydrates.

Nucleation by evaporative cooling

When a cavitation bubble grows in the ultrasonic field, evaporation from the surrounding liquid into the bubble volume can occur. The heat required for this evaporation could lead to a cooling of the liquid in the immediate vicinity of the bubble. Can this effect be large enough to cause nucleation by cooling? Two questions need to be answered: How much cooling is required for nucleation? And how much cooling can be expected from evaporation?

The temperature required for nucleation was determined experimentally, but in a cavitating liquid different boundary conditions could apply, such as deactivation of seeds or generation of new seeds, as lined out above in section 4.3.1. In order to see if nucleation could be a purely evaporative cooling effect, let's consider the lowest possible temperature, i.e. nucleation temperature of homogeneous nucleation, and the actually determined experimental value. For water, this is 233 K and 261 K, respective. The cooling effect depends on the amount of evaporated water and the liquid volume

that provides the required thermal energy, i.e. that is cooled. The specific heat of evaporation is well known, and the maximum bubble radius as well as the saturation pressure are known within an order of magnitude at least. However, the liquid volume from which this energy is extracted is unknown. An estimation of the cooling effect is presented in section B.5, but the results are vague. When gases are solved in the liquid, cavitation bubbles are nucleated preferably close to microbubbles of the gas, and thus the bubble content is rather gas than vapor. Gas inside the cavities hinders evaporation and thus reduces evaporative cooling, but at the same time, degassing also has an energetic effect. The ultrasonic experiments with degassed samples would show if nucleation occurs more readily when evaporation is favored. Unfortunately, sononucleation at atmospheric pressure with non-degassed water is so effective, that a further improvement could not be observed in any case.

Nucleation by induced surfaces

Irrespective of thermal or pressure effects which are hard to quantify as lined out above, the cavitation bubbles clearly create a large, strongly curved surface in the insonicated liquid. Could this induced surface be of any relevance for sononucleation? If so, why does it apparently not work in the salt hydrates?

Those are no trivial questions, and there is not much evidence to answer them. However, there are indeed some hints, and none of them contradicts with the experimental data.

Molecules on surfaces are known to arrange in a different way than in the bulk liquid [152], and in fact preferred nucleation of water at the liquid-air interface is reported [60]. A simple explanation why this surface induced nucleation could work in some substances, while it does not in others, is based on the chemical composition of the surface layer. For different substances, the chemical composition of the liquid surface layer that surrounds a cavitation bubble is different, as skteched in figure 4.22.

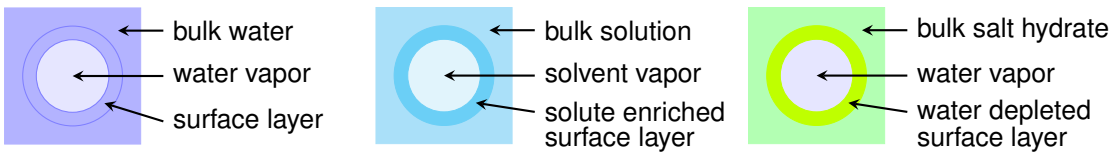

(a) water **(b)** solution **(c)** salt hydrate

Figure 4.22.: The composition of the surface layer between bubble and bulk volume is expected to be different in different systems.

If the surface somehow favors nucleation of the solid phase, be it by cooling or by providing a suitable template for the crystal, this is more or less effective depending on the composition of the liquid surface layer.

(a) For a pure substance such as water, the chemical composition of the liquid surrounding the bubble is similar to the bulk composition, or possibly even purified from solved gases. A nucleation of the solid on the surface layer is unhindered.

(b) For a solution, the surface layer can be particularly advantageous for nucleation. The solvent will evaporate preferably into the bubble, that is, the surface layer is enriched with the soluted substance. The supersaturation is increased, less solvent molecules interfere with the formation of the solid, and nucleation is favored.

(c) For salt hydrates, a similiar process is expected as for solutions: the water will preferably evaporate into the bubble, but in this case, this is counterproductive for nucleation. The depletion of water from the surface layer inhibits the formation of a stoichiometric salt hydrate solid.

The proposed "nucleation by induced surfaces" mechanism would thus agree with the experimental observation of successful sononucleation in water and solutions and failed sononucleation in salt hydrates.

Nucleation by disruption of "wrong" nuclei

A nucleation mechanism that profits from the disruption of wrong nuclei, i.e. nuclei that cannot grow to a macroscopic solid phase, is a third option to explain sononucleation without a direct pressure mechanism. There are some parallels to the case of "apparent sononucleation" discussed above in section 4.1.3.

A wrong solid phase could be present in materials that form two solid phases such as erythritol. If a metastable different solid phase is formed, a solid-solid phase transition is required to access the stable solid configuration. It is probable that this solid-solid transition is more difficult to nucleate than a liquid-solid transition, because of the stronger bonds between the particles. In such a situation, the disruption of solid particles might favor the formation of the stable solid phase. However, in order to really improve nucleation, the whole volume has to be solidified to the metastable phase first. This would have been noticed in a nucleation experiment, except if the wrong solid is not macroscopically visible.

For example, if subcritical clusters of the wrong solid bind the majority the particles, a macroscopic liquid appearance is still given, but the particles are not free to form supercritical clusters of the correct solid. The kind of situation could be possible in water. In water, clusters that are different in its molecular structure from the crystal phase are found [153]. The size of those clusters ranges up to several hundred molecules; an example of a water cluster is shown in figure 4.23.

These water clusters are highly ordered, but the molecules are not arranged in an extensible pattern such as in a crystal. Therefore, a water cluster cannot "grow", it can just dissolve and the molecules can then rearrange to a larger cluster with a different structure. If these clusters prevail in the liquid, their presence could in fact hinder the

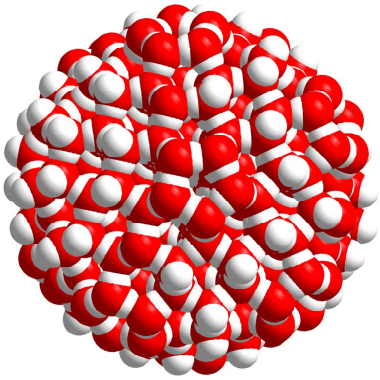

Figure 4.23.: A water cluster of 280 molecules.

forming of a crystalline solid. In that case, a destruction of the clusters by ultrasonic cavitation could “liberate” water molecules which then were free to arrange in the crystal pattern of the solid phase.

In order to judge on this issue, several difficult questions need clarification: What is the fraction of “free” water molecules compared to molecules that are part of a cluster in water at 273 K? Is the nucleation barrier for the formation of the solid indeed larger when starting from a cluster than from the liquid? Can indeed ultrasound or ultrasonic cavitation disrupt the clusters? Could this mechanism quantitatively explain or contribute to the observed effective sononucleation of water at very low subcooling? To answer these questions is beyond the scope of this work.

4.4. Conclusions and outlook

4.4.1. Conclusions

The scope of this work was to investigate sononucleation in inorganic phase change materials. The overall conclusions from analysis of theoretic work, literature review and own experiments as presented and discussed in the previous chapters are the following:

Nucleation of some salt hydrates can be triggered by high static pressure. It has been experimentally proved that the solidification of subcooled $CaCl_2 \cdot 6\,H_2O$ and $NaOAc \cdot 3\,H_2O$ can be triggered by applying static pressures in the range of several 100 MPa. For the third sample substance, $KF \cdot 4\,H_2O$, the melting and nucleation temperatures are falling with pressure and a high pressure nucleation does not work. This is a behavior similar to that of water with its pressure anomaly, as known from literature.

Sononucleation is observed only in combination with cavitation. Ultrasonic irradiation of liquids leads to cavitation, if the amplitude of the wave exceeds the cavitation threshold. In the reviewed literature, successful sononucleation is always associated with cavitation. This was also observed in the experiments, where sononucleation by ultrasonic treatment could in fact be suppressed when cavitation was avoided.

Sononucleation is a robust mechanism. Water can be sononucleated no matter if pure or with impurities, degassed or not, weakly or strongly subcooled. Also, the frequency and amplitude of the ultrasound does not influence whether sononucleation occurs or not, as long as cavitation is assured. For solutions, where more boundary conditions can be varied, sononucleation was stable even under a change of the solvent and the pH-value.

Ultrasonic nucleation of salt hydrates was not observed. Contrary to ultrasonic nucleation experiments on organic liquids, inorganic solutions and water, ultrasonic nucleation experiments on salt hydrates performed in this work were not successful. This failure of sononucleation is not due to missing cavitation, which was observed in all samples already at low insonication intensity.

Sononucleation is not a pressure mechanism The initial concept of a purely pressure based mechanism conflicts with the overall available data on nucleation and sononucleation. Instead, three possible other mechanisms, namely evaporative cooling, nucleation at induced surfaces and disruption of wrong nuclei, would provide satisfactory explanations for sononucleation in water and solutions and failed sononucleation in the investigated salt hydrates.

4.4.2. Outlook

As to possible future work, the following recommendations can be given from this investigation:

Is sononucleation of PCM to be expected in a different experimental setup? Judging from general properties of ultrasound and cavitation, combined with the presented analysis of the water phase diagram, it is extremely improbable that sononucleation is a pressure or thermal effect. It could be that in the investigated salt hydrates, high pressures are obtained during the bubble collapse, but probably at too high temperatures, and possibly during too short times. In any case, the thermodynamic conditions in an insonicated liquid cannot be controlled externally, because the peak values obtained during cavitation bubble collapse are primarily governed by the liquid's material properties. Therefore, while it cannot be excluded strictly that sononucleation occurs in other salt hydrates, chances for nucleation by ultrasonic irradiation of PCM are low independent from the experimental setup.

Is a different nucleation mechanism based on the pressure effect possible? The static high pressure experiments are a solid prove that a variation of pressure instead of temperature can in fact be used to trigger nucleation in some inorganic PCM. To profit from this effect, the most promising approach apparently is to use static pressure. While the large pressure cell used in this work is for sure not suitable in PCM applications, different high pressure generators such as an anvil cell setup could be a realistic option. Particularly for PCM melting below ambient temperature, where seeding with own crystals is troublesome, a pressure method could offer a way to make PCM usable which are not yet applied due to their subcooling.

What issues worthwhile future research have been identified? On the one hand, the supposed surface effect of sononucleation in water seems worth future research. A comparative study on the solidification of water in microscopic droplets with different surfaces, such as water in small pores, levitated droplets, or in emulsions, could shed more light on this issue. On the other hand, the nucleation and crystal growth kinetics of salt hydrates is yet poorly understood and could be object of future research. Material parameters of salt hydrates such as viscosity and surface energy as functions of temperature and pressure would be required for a deeper understanding and optimization of a pressure based nucleation mechanism. The cluster size distribution in subcooled melts, which determines the time span required for high pressure nucleation, could be investigated experimentally e.g. using neutron scattering technique.

5. Summary

Phase change materials (PCM) are used as storage materials in thermal energy storage technology. The main advantage of PCM compared to other thermal energy storage materials is their high storage density in narrow temperature intervals around the phase change temperature. In particular inorganic PCM are considered promising, but many of them suffer from considerable subcooling. The main current approach to reduce subcooling is to add nucleation seeds to the PCM, but suitable seeds are known only for some PCM. Inspired by reports of sononucleation in water, a new method to trigger solidification based on a pressure effect was investigated in this study.

Phase changes occur as a reaction to a change in boundary conditions of a thermodynamic system. The equilibrium transition temperature is a function of pressure due to the difference in specific volume of the two phases. The very first formation of a new phase amidst the old phase is associated with a large endothermic surface energy that hinders the phase change. Statistic thermal fluctuations allow to surpass this nucleation barrier, and determine the nucleation rate. Nucleation effects are found in many different fields of science, and thus a broad literature review was carried out to identify the current state of knowledge. In particular, investigations of sononucleation (nucleation by acoustic irradiation) were found for water, solutions, metals and organic materials, as well as for some inorganic PCM. While sononucleation is considered an established method to trigger solidification in water, some metals and solutions, for PCM there are only few and contradictory studies. A pressure effect is believed to cause sononucleation, but this approach is not shared by all authors and the exact mechanism is object of controversy.

Due to the many limitations and unknown input parameters of nucleation theory, a set of experiments was designed and carried out in order to establish a consistent data basis for selected PCM. The experiments were carried out on three salt hydrates ($KF \cdot 4\,H_2O$, $CaCl_2 \cdot 6\,H_2O$, $NaOAc \cdot 3\,H_2O$) and water. First, the melting and nucleation temperatures were determined at normal pressure and at high pressure up to 800 MPa. Compared to a linear extrapolation of normal pressure data, the pressure effect is considerably smaller than predicted. The nucleation curve is roughly parallel to the melting curve. Second, the effect of ultrasonic treatment on the samples was observed. While cavitation was readily obtained in all samples, a raised nucleation temperature was observed only in water. Third, the speed of solidification at different temperatures was determined. The speed increases as the temperature is lowered. The results of the new experiments have improved the data basis with respect to sononucleation of inorganic PCM. The same substances and similar setups were used for ambient

pressure, high pressure and ultrasonic experiments, such that the results can be directly compared.

A careful analysis of nucleation theory and experiments identified many doubtful assumptions and interpretations. Subcritical clusters are decisive in dynamic nucleation, because their properties and size distribution determine the time required for a pressure pulse to cause nucleation. They are however not well described by theory, and their properties cannot be extrapolated from macroscopic values. The solidification of inorganic PCM, liquids composed of water molecules, ions and hydrated ions, is not described by standard diffusion or condensation models. Real homogeneous nucleation as considered in theory is in fact not achievable in experiment. In sononucleation experiments on substances with slow crystal growth, such as solutions and highly viscous melts, primary nucleation is hard to identify. It is not possible to study the effect of pressure shocks in a cavitating liquid while suppressing the cavitation itself, and it is thus impossible to cross-check the postulated pressure mechanism directly.

As a consequence of the density anomaly of water, sononucleation of water cannot be a direct pressure effect. The physical conditions in the vicinity of cavitation bubbles can therefore not be deduced using water nucleation as calibration method. One possible explanation for the failed sononucleation in the materials that have shown nucleation under static high pressures is therefore that the required pressure and temperature is not reached by the ultrasonic treatment. However, failed sononucleation of salt hydrates could also be due to a reduced active volume. While in experiments with slowly changing temperature or pressure, the whole sample takes part in the experiment, the cavitation bubbles have an impact only on their direct vicinity, which reduces the active sample volume and thus the nucleation probability tremendously. Successful sononucleation in water could be due to the interface with the cavitation bubbles rather than the pressure peaks during their collapse. A bubble surface does not act similarly on the salt hydrates, because the liquid surrounding the bubble can have an altered chemical composition that prevents nucleation of the salt hydrate solid. Another possible sononucleation mechanism could be a disruption of clusters. If the particles of the subcooled liquid are bound to clusters which are unable to grow, an ultrasonic disruption of these clusters could promote solidification.

Contrary to the initial assumption, sononucleation in water is not a high pressure mechanism that can be transferred to salt hydrates. Instead, specific material properties play a key role in the sononucleation process, which, as a tendency, favor nucleation in pure substances and solutions, but hinder nucleation in salt hydrates. These material properties cannot be altered without degrading the thermal storage performance of inorganic PCM. As a consequence, nucleation by ultrasound has to be discarded for this group of materials. However, nucleation by static pressure was proved successful for two out of three investigated salt hydrates. This could be a starting point for future work and the development of a new pressure based trigger mechanism.

6. Acknowledgements

At last, I would like to add some personal words and acknowledge help and support on various levels.

Facilities! essential for an experimental work – thanks go to ZAE and E19 in general represented by Wolfgang Schölkopf and Prof. Stimming; Harald Mehling, Stefan Hiebler, Holger Köbel, Robert Redlich, Tobias Schmid for great help with the lab experiments in Garching; Matthias Werner of LFP / Weihenstephan and Uwe Schmidt of ZAE / Erlangen for assistance with their facilities; Christian Hilgers, Annemarie Löffler, Elfi Reischl and Friederike Kennett who kept the computers running and the administration going.

Money! urgently required to keep things moving – thanks go to the ZAE as employer, and thus the Bavarian State for their support of applied energy research, and the Federal Research Ministry for their funding of the LWSNet project.

Inspiration! invaluable for this work with its surprising traps and twists – thanks go to the PCM group, all the LWSNet project people, in particular Prof. Voigt and his group at University of Freiberg as well as Dr. Ebert and the team of ZAE / Würzburg; the group of Prof. Schembecker at University of Dortmund.

Encouragement! always welcome and sometimes crucial – thanks go to all my colleagues at ZAE for their very cooperative and human style of work, a group of PhD students for their shared experience and demonstrated feasibility, and people around the world for their compassion in PCM topics.

Ganz besonderen Dank möchte ich meiner Familie und meinen Freunden aussprechen, die mich all die Jahre hindurch unterstützt und an mich geglaubt haben, und die mich nicht haben vergessen lassen, dass es auch ein Leben außerhalb der Wissenschaft gibt.

إلى زوجي عزيز مروان، شكرا جزيلا لدعمك

A. Indexes

A.1. Publications

Parts of this work have been published as

- E. Günther, H. Mehling and M. Werner, *Bestimmung der Nukleations- und Schmelztemperaturen von Salzhydraten bei statischen Drücken bis zu 800 MPa* at: Statusseminar Thermische Energiespeicherung, Stuttgart, Germany (2006) [154]
- E. Günther, H. Mehling and M. Werner, *Nucleation and melting temperatures of salt hydrates used for heat and cold storage under static pressures up to 800 MPa* at: 12th ISSP – International Symposium on Solubility Phenomena and Related Equilibrium Processes, Freiberg, Germany (2006) [155]
- E. Günther, H. Mehling and M. Werner, *Melting and nucleation temperatures of three salt hydrate phase change materials under static pressures up to 800 MPa* J. Phys. D: Appl. Phys. **40**:4636-4641 (2007) [156]
- E. Günther, H. Mehling and S. Hiebler, *Simulation of subcooling and solidification in phase change materials* Modelling Simul. Mater. Sci. Eng. **15**:879-892 (2007) [14]
- H.-P. Ebert et al., *Schlussbericht – Netzwerk zur Überwindung grundlegender Probleme bei der Entwicklung hocheffizienter Latentwärmespeicher auf Basis anorganischer Speichermaterialien* ISBN 978-3-00-024699-9, ZAE Bayern e. V., Würzburg, Germany (2008) [77]
- E. Günther, H. Mehling and S. Hiebler, *Subcooling and solidification in modelling of heat transfer in phase change materials* at: 18th ECTP – European Conference of Thermophysical Properties, Pau, France (2008) [157]
- E. Günther, H. Mehling and S. Hiebler, *Nucleation by ultrasound in subcooled PCM* at: Effstock 2009 – 11th International Conference on Thermal Energy Storage, Stockholm, Sweden (2009) [16]

A.2. Nomenclature

The abbreviations, constants, greek and roman symbols as well as the sub- and superscripts used in this text are listed on the following pages together with an indication of their first appearance. In addition, some lowercase letters were used to denote specific values of variables listed here only in their uppercase variant.

Abbreviations

Constants

Greek letters

Ω number of microscopic configurations ..... p. 12

ρ density ..... p. 20

ρ' particle density ..... p. B-1

σ surface energy ..... p. 18

Roman letters

A surface area ..... p. 19

a constant coefficient ..... p. 19

b constant coefficient ..... p. 20

C number of components in a system ..... p. 14

c speed of sound ..... p. 38

c_p specific heat capacity ..... p. 4

D diffusion coefficient ..... p. 25

E energy ..... p. 22

F number of free variables in a system ..... p. 14

f degrees of freedom ..... p. 22

G Gibbs potential ..... p. 13

H enthalpy ..... p. 13

j nucleation rate ..... p. 25

J' flux ..... p. 25

M molar mass ..... p. B-1

m mass ..... p. 4

N number [of particles or experiments] ..... p. 12

P number of phases in a system ..... p. 14

p pressure ..... p. 12

p' momentum ..... p. B-1

Subscripts and superscripts

A.3. Bibliography

[1] M. Yamaha. In *IEA, ECES IA Annex 17 – Advanced Thermal Energy Storage Techniques : Feasbility Studies and Demonstration Projects*. Planning Workshop, Lleida, Spain (2001)

[2] *IEA - SHC Task 32 Handbook: Thermal energy storage for solar and low energy buildings* (2005). ISBN 84-8409-877-X

[3] Energiestatistiken des BMWi. *energy statistics of the german federal ministry for economics*, `http://www.bmwi.de/BMWi/Navigation/Energie/energiestatistiken,did=176656.html`

[4] İ. Dinçer and M. A. Rosen, eds. *Thermal Energy Storage – Systems and Applications*. Wiley (2002). ISBN 978-0-471-49573-4

[5] A. Sharma, V. Tyagi, C. Chen and D. Buddhi *Renewable and Sustainable Energy Reviews* **13**:318–345 (2009)

[6] FP7. *7th research framework programme of the European Union – activity energy.4: Renewables for heating and cooling*, `http://cordis.europa.eu/fp7/energy/about4_en.html`

[7] Ice Energy Corporation. *Colorado, USA*, `http://www.ice-energy.com`

[8] ZIEGRA-Eismaschinen GmbH. *Germany*, `http://www.ziegra.com`

[9] CALMAC Manufacturing Corporation. *New Jersey, USA*, `http://www.calmac.com`

[10] H. Mehling and L. F. Cabeza. *Heat and cold storage with PCM – An up to date introduction into basics and applications*. Springer (2008). ISBN 978-3-540-68556-2

[11] G. A. Lane. *Solar Heat Storage: Latent Heat Material*, vol. I: Background and Scientific Principles. CRC Press, Inc., Boca Raton, Florida (1983). ISBN 0-8493-6585-6

[12] G. A. Lane. *Solar Heat Storage: Latent Heat Material*, vol. II: Technology. CRC Press, Inc., Boca Raton, Florida (1983). ISBN 0-8493-6585-4

[13] B. Zalba, J. M. Marín, L. F. Cabeza and H. Mehling *Appl. Therm. Eng.* **23**(3):251–283 (2003)

[14] E. Günther, H. Mehling and S. Hiebler *Modelling Simul. Mater. Sci. Eng.* **15**:879–892 (2007)

[15] B. Zalba, J. M. Marín, L. F. Cabeza and H. Mehling *Int. J. Refrigeration* **27**:839–849 (2004)

[16] E. Günther, H. Mehling and S. Hiebler. In *Effstock 2009 – 11th International Conference on Energy Storage*. Stockholm, Sweden (2009)

[17] C. Rudolph. *Entwicklung einer Methode zur Suche nach Kristallisatoinsinitiatoren für Salzhydratschmelzen mittels High-Throughput-Screening*. Ph.D. thesis, Fakultät für Chemie und Physik, Technische Universität Bergakademie Freiberg (2002)

[18] J. W. Gibbs. *Elementary Principles in Statistical Mechanics*. C. Scribner's sons (1902)

[19] L. Boltzmann. *Entropie und Wahrscheinlichkeit*. Verlag Harri Deutsch (1872-1905). ISBN 978-3817132867

[20] P. Atkins and J. de Paula. *Physical Chemistry*. Oxford University Press, 7th ed. (2002). ISBN 978-0-716-73539-7

[21] H. Vogel, ed. *Gerthsen Physik*. Springer, 19. ed. (1997). ISBN 3-540-62988-2

[22] V. P. Skripov. *Metastable Liquids*. Halsted Press (1974). ISBN 0-470-79546-8

[23] W. Kurz and D. Fisher. *Fundamentals of Solidification*. Trans Tech Publications, 3rd ed. (1992). ISBN 0-87849-522-3

[24] D. Kashchiev. *Nucleation – Basic Theory with Applications*. Butterworth Heinemann (2000). ISBN 0-7506-4682-9

[25] J. Schmelzer *Mater. Phys. Mech.* **6**:21–33 (2003)

[26] C. E. Brennen. *Cavitation and Bubble Dynamics*. Oxford University Press (1995). ISBN 978-0195094091

[27] R. C. Tolman *J. Chem. Phys.* **17**(3):333–337 (1949)

[28] M. A. Larson and J. Garside *J. Cryst. Growth* **76**(1):88–92 (1986)

[29] V. M. Fokin, N. S. Yuritsyn, E. D. Zanotto, J. W. Schmelzer and A. A. Cabral *Journal of Non-Crystalline Solids* **354**:3785–3792 (2008)

[30] M. A. Rogerson and S. S. S. Cardoso *AIChE J.* **49**(2):505–515 (2003)

[31] D. Sette and F. Wanderlingh *Phys. Rev.* **125**(2):409–417 (1962)

[32] *12th ISSP – International Symposium on Solubility Phenomena and Related Equilibrium Processes*. TU Bergakademie Freiberg, Germany (2006)

[33] D. R. Lide, ed. *CRC Handbook of Chemistry and Physics: A Ready-reference Book of Chemical and Physical Data*. Chemical Rubber Publishing, 88th ed. (2008). ISBN 0-8493-0487-3

[34] National institute of standards and technology. *NIST chemistry webbook*, `http://webbook.nist.gov/chemistry/` (2008)

[35] *Journal of physical and chemical reference data:*, `http://scitation.aip.org/jpcrd/`

[36] P. W. Bridgman *The Physical Review* **3**:126–141 (1914)

[37] P. W. Bridgman *The Physical Review* **6**(1):1–33 (1915)

[38] P. W. Bridgman *Phys. Rev.* **6**(2):94 (1915)

[39] R. Feistel and W. Wagner. In *14th International Conference on the Properties of Water and Steam in Kyoto*, pp. 751–756. Kyoto (2004)

[40] W. Wagner and A. Pruss *J. Phys. Chem. Ref. Data* **31**(2):387–535 (2002)

[41] T. Sano, H. Mori, O. Sakata, E. Ohmura, I. Miyamoto, A. Hirose and K. F. Kobayashi *Appl. Surf. Sci.* **247**:571–576 (2005)

[42] D. Alfè, L. Vočadlo, G. D. Price and M. J. Gillan *J. Phys.: Condens. Matter* **16**:S973–S982 (2004)

[43] G. Q. Chen, T. J. Ahrens and E. Stopler *Phys. Earth Plan. In.* **134**:35–52 (2002)

[44] L. Otero and P. D. Sanz *J. Food Eng.* **72**(4):354–363 (2006)

[45] M. I. Eremets. *High Pressure Experimental Methods*. Oxford University Press, (1996). ISBN 978-0-19-856269-6

[46] G. Tammann. *Aggregatzustände*. Verlag von Leopold Voss, Leipzig (1922)

[47] P. Barrett and L. Naykalyk *Mater. Chem. Phys.* **21**(2):201–208 (1989)

[48] C. A. Angell and H. Kanno *Science* **193**:1121–1122 (1976)

[49] P. V. Hobbs. *Ice Physics*. Oxford University Press (1974). ISBN 0–19–851936–2

[50] D. M. Herlach, ed. *Solidification and Crystallization*. Wiley-VCH Verlag GmbH & Co. KGaA (2004). ISBN 3-527-31011-8

[51] M. J. Li, K. Nagashio and K. Kuribayashi *Scr. Mater.* **47**(4):213–218 (2002)

[52] A. Golpayegani, H.-O. Andren, H. Danielsen and J. Hald *Mater. Sci. Eng. A* **489**:310–318 (2008)

[53] R. P. Sear *J. Phys.: Condens. Matter* **19**(3):33101–33129 (2007)

[54] L. H. Seeley, G. T. Seidler and J. G. Dash *Rev. Sci. Instrum.* **70**(9):3664–3667 (1999)

[55] G. Vali *Atmos. Chem. Phys. Disc.* **8**(1):4059–4097 (2008)

[56] C. T. Avedisian *J. Phys. Chem. Ref. Data* **14**(3):695–729 (1985)

[57] T. Wada, K. Matsunaga and Y. Matsuo *Bull. Chem. Soc. Jpn.* **57**(2):557–560 (1984)

[58] C. A. Angell *Annu. Rev. Phys. Chem.* **34**:593–630 (1983)

[59] A. Heneghan, H. J. Moore, T. R. Lee and A. Haymet *Chem. Phys. Lett.* **385**(5–6):441–445 (2004)

[60] R. Shaw, A. Durant and Y. Mi *J. Phys. Chem. B* **109**(20):9865–9868 (2005)

[61] Y. Dai and J. S. Evans *J. Phys. Chem. B* **105**:10831–10837 (2001)

[62] J.-P. Sletta, D. Vuarnoz, O. Sari, D. Ata-Caesar, R. Lugo and P. W. Egolf. *Production de* Coulis de Glace *à germination spontanée: Système coldeco - résultats numériques et expérimentaux.* Tech. rep., École d'Ingénieurs du Canton du Vaud, CH-1401 Yverdon-les-Bains (2004)

[63] K. E. Zachariassen and E. Kristiansen *Cryobiology* **41**:257–279 (2000)

[64] Y. Tsuchiya, K. Sasaki and H. Hasegawa *J. Biosci. Bioeng.* **97**(1):71–74 (2004)

[65] S. Martin *Chem. Rev.* **100**(9):3403–3454 (2000)

[66] G. Vali. *Ice nucleation - theory: A tutorial*, `http://www-das.uwyo.edu/~vali/nucl_th.pdf` (1999)

[67] *Nevada state cloud seeding program*, `http://cloudseeding.dri.edu/`

[68] R. C. Schnell and G. Vali *Nature* **236**:163–165 (1972)

[69] B. C. Christner, C. E. Morris, C. M. Foreman, R. Cai and D. C. Sands *Science* **319**(5867):1214 (2008)

[70] C. Morris, D. Georgakopoulos and D. Sands *Journal de Physique IV* **121**:87 (2004)

[71] Snowmaking. *wikipedia*, `http://en.wikipedia.org/wiki/Snowmaking` (2008)

[72] B. Gerl. *Lautstark rieselt der Schnee*, `http://www.wissenschaft-online.de/artikel/859719` (2006)

[73] *Technische Beschneiung und Umwelt*. Tech. rep., Bayerisches Landesamt für Umweltschutz, `http://www.lfu.bayern.de/natur/fachinformationen/freizeitnutzung_wintersport/beschneiungsanlagen/doc/fachtagung_2006.pdf` (2000)

[74] EP1645821A2. *Lance head for a snow lance and nozzle assembly*, `http://v3.espacenet.com/textdoc?DB=EPODOC&IDX=EP1645821&F=0&QPN=EP1645821`. Patent (2006)

[75] M. A. Rogerson and S. S. S. Cardoso *AIChE J.* **49**(2):522–529 (2003)

[76] W. Voigt. *Institute for Inorganic Chemistry, TU Bergakademie Freiberg*, `http://www.chemie.tu-freiberg.de/~voigt`

[77] H.-P. Ebert, G. Reichenauer, R. Brandt, S. Braxmeier, T. Bauer, R. Tamme, W. Langer, B. Hudler, M. Christ, G. Sextl, G. Müller, U. Helbig, R. Houbertz, W. Voigt, H. Schmidt, T. Zehl, R. Mach, H.-E. Maneck, A. Meyer-Plath, F. Oleszak, M. Keuper, M. Reisert, H. Burkhardt, E. Günther and H. Mehling. *Schlussbericht - Netzwerk zur Überwindung grundlegender Probleme bei der Entwicklung hocheffizienter Latentwärmespeicher auf Basis anorganischer Speichermaterialien*. Tech. Rep. 03SF0307A-G, ZAE Bayern e. V., `http://www.lwsnet.info/Bericht/BMBF-Fkz-03SF0307A-G.pdf` (2008)

[78] P. A. Cziko, C. W. Evans, C.-H. C. Cheng and A. L. DeVries *J. Exp. Biol.* **209**(3):407–420 (2006)

[79] S. B. Pruss, F. A. Corsetti and W. W. Fischer *Sedimentary Geology* **207**(1-4):34 – 40 (2008)

[80] R. Montenegro, M. Antonietti, Y. Mastai and K. Landfester *J. Phys. Chem. B* **107**(21):5088–5094 (2003)

[81] A. Nahid, J. E. Bronlund, D. J. Cleland and B. Philpott *Int. J. Refrig.* **31**(1):152–160 (2008)

[82] H. Stöcker, ed. *Taschenbuch der Physik*. Harri Deutsch, 3 ed. (1998). ISBN 3-8171-1556-3

[83] E. A. Neppiras *Phys. Rep.* **61**:159–251 (1980)

[84] J.-P. Franc and J.-M. Michel. *Fundamentals of Cavitation*, vol. 76 of *Fluid Mechanics and its Applications*. Kluwer Academic Publishers, P.O. Box 322, 3300 AH Dordrecht, The Netherlands (2004)

[85] P. S. Epstein and M. S. Plesset *J. Chem. Phys.* **18**(11):1505–1509 (1950)

[86] E. Herbert, S. Balibar and F. Caupin *Phys. Rev. E* **74**(4):041603 (2006)

[87] S. D. Lubetkin *Langmuir* **19**(7):2575–2587 (2003)

[88] K. A. Mørch *Phys. Fluids* **19**(7):072104 (2007)

[89] J. Staudenraus and W. Eisenmenger *Ultrasonics* **31**(4):267–273 (1993)

[90] G. Iosilevskii and D. Weihs *Journal of The Royal Society Interface* **5**(20):329–338 (2008-03-06)

[91] U. Zimmermann, H. Schneider, L. H. Wegner and A. Haase *New Phytologist* **162**(3):575–615 (2004)

[92] A. Roth-Nebelsick *Biologie in unserer Zeit* **36**(2):110 – 118 (2006)

[93] L. Trilling *J. Appl. Phys.* **23**(1):14–17 (1952)

[94] Y. Qi. *Heterogeneous Nucleation And Influence Of Surface Structure And Wettability.* Ph.D. thesis, University Of Florida (2005)

[95] O. Behrend and H. Schubert *Ultrason. Sonochem.* **8**(3):271–276 (2001)

[96] D. Lohse and S. Hilgenfeldt *J. Chem. Phys.* **107**(17):6986–6997 (1997)

[97] M. Ashokkumar, M. Hodnett, B. Zeqiri, F. Grieser and G. J. Price *J. Am. Chem. Soc.* **129**(8):2250–2258 (2007)

[98] K. S. Suslick *Scientific American* **2**:80–86 (1989)

[99] E. B. Flint and K. S. Suslick *Science* **253**(5026):1397–1399 (1991)

[100] E. Ciawi, J. Rae, M. Ashokkumar and F. Grieser *J. Phys. Chem. B* **110**(27):13656–13660 (2006)

[101] A. Moshaii and R. Sadighi-Bonabi *Phys. Rev. E* **70**(1):016304 (2004)

[102] F. Faïd, M. Romdhane, C. Gourdon, A. Wilhelm and H. Delmas *Ultrason. Sonochem.* **5**(2):63–68 (1998)

[103] R. Hickling *Nature* **206**(4987):915–917 (1965)

[104] R. Chow, R. Blindt, R. Chivers and M. Povey *Ultrasonics* **41**:595–604 (2003)

[105] R. Chow, R. Blindt, R. Chivers and M. Povey *Ultrasonics* **43**:227–230 (2005)

[106] X. Zhang, T. Inada and A. Tezuka *Ultrason. Sonochem.* **10**:71–76 (2003)

[107] T. Inada, X. Zhang, A. Yabe and Y. Kozawa *Int. J. Heat Mass Transfer* **44**:4523–4531 (2001)

[108] X. Zhang, T. Inada, A. Yabe and Y. Kozawa *Int. J. Heat Mass Transfer* **44**:4533–4539 (2001)

[109] C. P. Lee and T. G. Wang *J. Appl. Phys.* **71**(11):5721–5723 (1992)

[110] G. Schembecker. *University of Dortmund, department of biochemical and chemical engineering (BCE), chair of plant and process design*, `http://www.bci.uni-dortmund.de/apt/modules/Udo/index.php?cid=6`

[111] DE1803420. *Kristallisationsverfahren.* Patent (1968)

[112] E. Miyasaka, S. Ebihara and I. Hirasawa *J. Cryst. Growth* **295**:97–101 (2006)

[113] C. Virone, H. Kramer, G. van Rosmalen, A. Stoop and T. Bakker *J. Cryst. Growth* **294**(1):9–15 (2006)

[114] W.-S. Chen and G.-C. Huang *Ultrason. Sonochem.* **15**(5):909 (2008)

[115] E. Miyasaka, M. Takai, H. Hidaka, Y. Kakimoto and I. Hirasawa *Ultrason. Sonochem.* **13**:308–312 (2006)

[116] M. A. Rogerson and S. S. S. Cardoso *AIChE J.* **49**(2):516–521 (2003)

[117] E. P. Ona, X. Zhang, S. Osawa, H. Matsuda, H. Kakiuchi, M. Yabe, M. Yamazaki and M. Sato *J. Chem. Eng. Jpn.* **35**(3):290–298 (2002)

[118] H. Matsuda, E. Ona, Y. Kojima, S. Ozawa, M. Yabe, H. Kakiuchi, S. Chihara and M. Sato. In *IEA ECES IA Annex 17 – Advanced thermal energy Storage through phase change materials and chemical reactions–feasbility studies and demonstration projects.* 3rd Workshop, Tokyo, Japan (2002)

[119] P. Günther, W. Zeil, W. Göring and J. F. Bornhardt *Z. Anorg. Allg. Chem.* **285**:191–204 (1956)

[120] US6630185. *Crystallization process using ultrasound.* Patent (2003)

[121] J. D. Hunt and K. A. Jackson *J. Appl. Phys.* **37**(1):254–257 (1966)

[122] L. J. McCausland, P. W. Cains and P. D. Martin *Chem. Eng. Progress* **97**(7) (2001)

[123] International Association for the Properties of Water and Steam. *The IAPWS formulation 1995 for the thermodynamic properties of ordinary water substance for general and scientific use*, `http://www.iapws.org`

[124] K. Röttger, A. Endriss, J. Ihringer, S. Doyle and W. F. Kuhs *Acta Cryst. B* **50**:644–648 (1994)

[125] A. Goto, T. Hondoh and S. Mae *J. Chem. Phys.* **93**:1412–1417 (1990)

[126] U. Birkbeck College. *Crystal space groups*, `http://img.chem.ucl.ac.uk/sgp/large/sgp.htm`

[127] Diamond. *Crystal and molecular structure visualization software*, `http://www.crystalimpact.com/diamond/`

[128] POV-Ray. *Ray tracing graphics software*, `http://www.povray.org/`

[129] A. Leclaire and M. M. Borel *Acta Cryst. B* **33**(5):1608–1610 (1977)

[130] G. Beurskens and G. A. Jeffrey *J. Chem. Phys.* **41**(4):917–923 (1964)

[131] K. M. Doxsee and R. C. Stevens *J.Inclusion Phenom.Macrocyclic Chem* **9**:327–336 (1990)

[132] T. Meister. *Aufbau und Regelung eines elektrostatischen Levitators*. Ph.D. thesis, Ruhr Universität Bochum (2001)

[133] P. Ryder and N. Warncke. In Herlach [50], chap. 12, pp. 103–109

[134] M. I. Kohira, A. Isomura, N. Magome, S. Mukai and K. Yoshikawa *Chem. Phys. Lett.* **414**:389–392 (2005)

[135] G. Brenn, L. Deviprasath, F. Durst and C. Fink *Int. J. Heat Mass Transfer* **50**:5073–5086 (2007)

[136] D. Holland-Moritz, O. Heinen, R. Bellissent and T. Schenk *Mater. Sci. Eng. A* **449–451**:42–45 (2007)

[137] D. M. Herlach *Annu. Rev. Mater. Sci.* **21**:23–44 (1991)

[138] L. Cabeza, J. Roca, M. Nogués, H. Mehling and S. Hiebler *Mater. Corros.* **53**:902–907 (2002)

[139] B. Wunderlich. In K. H. J. Buschow, R. W. Cahn, M. C. Flemings, B. Ilschner, E. J. Kramer, S. Mahajan and P. Veyssière, eds., *Encyclopedia of Materials: Science and Technology*, pp. 9134–9141. Elsevier, Oxford (2001)

[140] R. F. Speyer. *Thermal Analysis Of Materials*. Marcel Dekker, Inc. (1994). ISBN 978-0824789633

[141] *Meteorologic institute of Ludwig-Maximilians-Universität Munich*, `http://www.meteo.physik.uni-muenchen.de/mesomikro/garstat/plot.php`

[142] A. Delgado. *Lehrstuhl für Fluidmechanik und Prozessautomation, TU München, Weihenstephan.*

[143] M. Perez, M. Dumont and D. Acevedo-Reyes *Acta Mater.* **56**(9):2119–2132 (2008)

[144] P. V. Hobbs. *Nucleation of Ice*, chap. 7, pp. 461–523. In [49] (1974)

[145] V. Khvorostyanov and J. Curry *J. Phys. Chem. A* **108**(50):11073–11085 (2004)

[146] D. W. Oxtoby *J. Phys.: Condens. Matter* **4**(38):7627–7650 (1992)

[147] T. Schmid. *Theoretische und experimentelle Untersuchung von dynamischen und strukturellen Effekten auf Phasenübergänge 1. Ordnung.* Master's thesis, Technische Universität München (2008)

[148] E. P. Ona. *Studies on advanced heat storage technology for effective heat energy utilization using organic-based PCMs.* Ph.D. thesis, Graduate School of Engineering, Nagoya Universtiy (2005)

[149] A. Cucheval and R. Chow *Ultrason. Sonochem.* **15**(5):916–920 (2008)

[150] E. W. Lang and H.-D. Lüdemann *Angewandte Chemie Int. Ed.* **21**(5):315–329 (1982)

[151] International Association for the Properties of Water and Steam. *Revised release on the pressure along the melting and sublimation curves of ordinary water substance*, `http://www.iapws.org` (2008)

[152] S. I. Mamatkulov, P. K. Khabibullaev and R. R. Netz *Langmuir* **20**(11):4756–4763 (2004)

[153] M. Chaplin *Biol. Chem.* **83**(3):211–221 (1999)

[154] E. Günther, H. Mehling and M. Werner. In *Statusseminar Thermische Energiespeicherung*. Freiburg, Germany (2006)

[155] E. Günther, H. Mehling and M. Werner. [32]

[156] E. Günther, H. Mehling and M. Werner *J. Phys. D: Appl. Phys.* **40**:4636–4641 (2007)

[157] E. Günther, H. Mehling and S. Hiebler. In *18th ECTP – European Conference of Thermophysical Properties*. Pau, France (2008)

[158] F. Reif. *Fundamentals of Statistical and Thermal Physics.* McGraw Hill (1965)

[159] R. W. Goranson, D. Bancroft, B. L. Burton, T. Blechar, E. E. Houston, E. F. Gittings and S. A. Landeen *J. Appl. Phys.* **26**(12):1472–1479 (1955)

[160] R. A. Fine and F. J. Millero *J. Chem. Phys.* **59**(10):5529–5536 (1973)

[161] L. Ter Minassian, P. Pruzan and A. Soulard *J. Chem. Phys.* **75**:3064–3072 (1981)

[162] I. eFunda. *Saturation vapor pressure of water*, `http://www.efunda.com/materials/water/steamtable_sat.cfm`

[163] T. Wada, F. Yimura and R. Yamamoto *Bull. Chem. Soc. Jpn.* **56**:1223–1226 (1983)

B. Appendix

B.1. Are quantum effects relevant?

In nucleation theory, an energetic distribtion function is introduced to describe the energetic fluctuations in the thermodynamic system. Here, the Boltzmann function is used, while e.g. the description of the electron gas in metals or phonons in solids requires a different approach [158]. In this section, a justification is given why the classical formulation can be used for nucleation theory of salt hydrates and water.

The validity of classical formulations in physics in general and in statistical thermodynamics in this case is limited by the Heisenberg uncertainty principle. This principle states that a simultaneous specification of place x and momentum p' (denoted here by p' to avoid confusion with the pressure p) of a particle is limited in precision by

$$\delta x \, \delta p' \leq \frac{h}{2\pi} \tag{B.1a}$$

where h is Planck's constant, $h = 6.6256 \cdot 10^{-34}\,\mathrm{Js}$.

In another formulation, the de Broglie wavelength $\lambda_{\mathrm{dB}} = h/p$ of the particle is confronted with the mean separation of the particles $\mathrm{d}x$ (which limits the mean free path), and the condition for the validity of the classical formulation is

$$\mathrm{d}x \gg \lambda_{\mathrm{dB}} \tag{B.1b}$$

Particle masses involved in this work are all greater than the mass of the water molecule, so the following calculation is done for water.

Considering the density ρ of liquid water and its molar mass M

$$\rho = 1\,\mathrm{g/cm^3} \tag{B.2a}$$
$$M = 18\,\mathrm{g/mol} \tag{B.2b}$$

the mass of one particle is, using Avogadro's constant $N_{\mathrm{A}} = 6.022 \cdot 10^{23}\,\mathrm{mol^{-1}}$,

$$\begin{aligned} m &= M/N_{\mathrm{A}} \\ &\approx 3 \cdot 10^{-23}\,\mathrm{g} \end{aligned} \tag{B.2c}$$

and the particle density ρ' is given by

$$\begin{aligned} \rho' &= \rho/M \cdot N_{\mathrm{A}} \\ &= 1/18 \cdot 6.022 \cdot 10^{23}\,\mathrm{cm^{-3}} \\ &= 3.3 \cdot 10^{22}\,\mathrm{cm^{-3}} \end{aligned} \tag{B.2d}$$

corresponding to an intermolecular distance (with respect to their center of masses) of

$$\begin{aligned} \mathrm{d}x &= \sqrt[3]{1/\rho'} \\ &= 3.1 \cdot 10^{-8}\,\mathrm{cm} \end{aligned} \tag{B.2e}$$

In fact, the molecules of a liquid are far closer than the molecules in an [ideal] gas, such that the mean intermolecular distance with respect to the center of mass is not exactly the mean free path. In lack of a more precise formulation, we'll keep this limitation in mind and carry on with the de Broglie wavelength:

Using the ideal gas formulation for the determination of the mean momentum

$$p \approx \sqrt{3 m k_\mathrm{B} T} \tag{B.3a}$$

the de Broglie wavelength becomes at 273 K (equilibrium melting temperature of water)

$$\begin{aligned} \lambda_\mathrm{dB} &= h/p \\ &= 6.6 \cdot 10^{-34}\,\mathrm{Js} \cdot \sqrt{3 \cdot 3 \cdot 10^{-23}\,\mathrm{g} \cdot 1.4 \cdot 10^{-23}\,\mathrm{JK^{-1}} \cdot 273\,\mathrm{K}}^{-1} \\ &= 1.1 \cdot 10^{-12}\ \mathrm{Js}\left(\mathrm{g\ JK^{-1}\ K}\right)^{-1/2} \\ &= 1.1 \cdot 10^{-12} \frac{\mathrm{kg\,m^2\,sec^{-1}}}{\left(\left(10^{-3}\,\mathrm{kg}\right)^2\,\mathrm{m^2\,sec^{-2}}\right)^{1/2}} \\ &= 1.1 \cdot 10^{-9}\,\mathrm{cm} \end{aligned} \tag{B.3b}$$

and thus indeed

$$3.1 \cdot 10^{-8}\,\mathrm{cm} = \mathrm{d}x \gg \lambda_\mathrm{dB} = 1.1 \cdot 10^{-9}\,\mathrm{cm} \tag{B.4}$$

This inequality is however based on two rough assumptions: the formula for an ideal gas was applied to determine λ_dB in a liquid, and the finite size of the particles was neglected in the estimation of $\mathrm{d}x$.

For comparison, the critical radius of water is about 10^{-6} cm, as lined out in section B.2, which is already three orders of magnitude larger than the de Broglie wavelength[1] of a single particle.

[1] At 10 K subcooling, the de Broglie wavelength is only slightly increased with respect to the equilibrium melting temperature used here.

B.2. Pressure dependency of the critical radius

The critical radius as a function of temperature and pressure is given by

$$r_{\mathrm{crit}}(p,T) = \frac{2\sigma_o}{\Delta h\,\rho_{\mathrm{cm}}}\left(\frac{T}{T_{\mathrm{m}}^o\left(1+\Delta v/\Delta h\left(p-p_{\mathrm{m}}^0\right)\right)}-1\right)^{-1} \tag{B.5a}$$

The radius is thus proportional to

$$r_{\mathrm{crit}}(p,T) \propto \left(\frac{T}{T_{\mathrm{m}}^o\left(1+\Delta v/\Delta h\left(p-p_{\mathrm{m}}^0\right)\right)}-1\right)^{-1} \tag{B.5b}$$

For this equation, all parameters are available for the three investigated salt hydrates and water, as listed in table 3.2.

In the following, the critical radius in arbitrary units (a.u.) as a function of temperature is plotted for several isobars, using semi-logarithmic plots and covering the temperature range $T_{\mathrm{m}}^0 - 30\,\mathrm{K} \le T \le T_{\mathrm{m}}^0$.

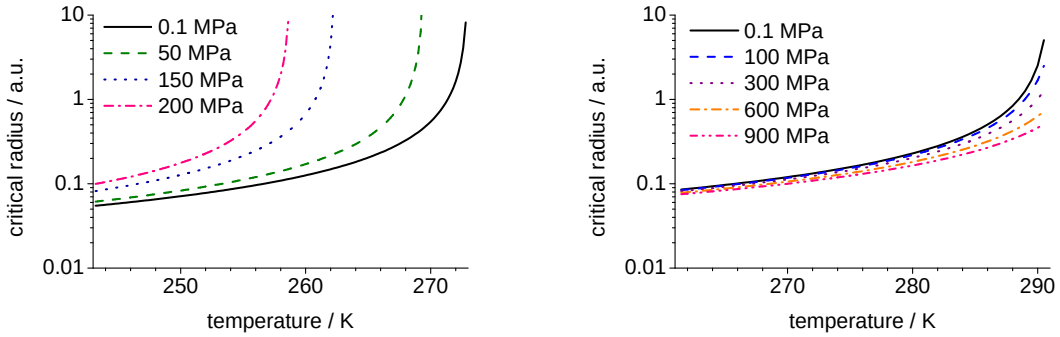

(a) H_2O **(b)** $KF \cdot 4\,H_2O$

Figure B.1.: Isobars of the critical radius in arbitrary units as function of temperature for H_2O and $KF \cdot 4\,H_2O$.

In general, the critical radius is sensible to pressure particuarly near the melting temperature at normal pressure T_{m}^0. Comparing the materials, $KF \cdot 4\,H_2O$ stands out with its very small Δv and therefore its almost insensible r_{crit}. The expected specific reduction of the critical radius at $T = T_{\mathrm{m}}^0 - 10\,\mathrm{K}$ for different pressures is summarized in table B.1.

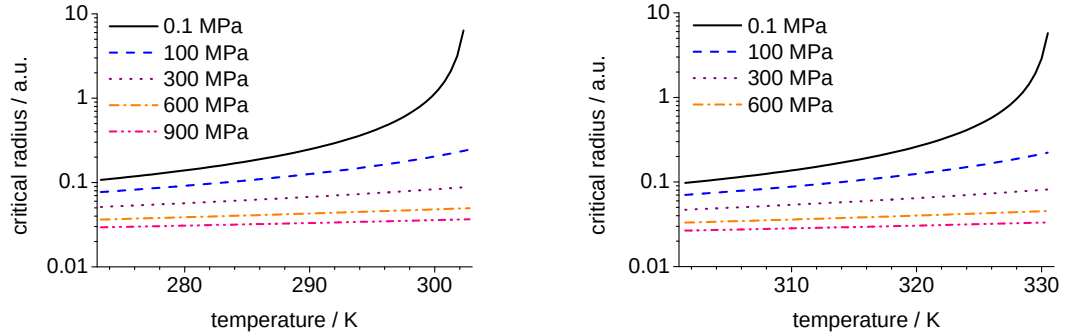

(a) $CaCl_2 \cdot 6\,H_2O$ **(b)** $NaOAc \cdot 3\,H_2O$

Figure B.2.: Isobars of the critical radius in arbitrary units as function of temperature for $CaCl_2 \cdot 6\,H_2O$ and $NaOAc \cdot 3\,H_2O$.

For water, the surface tension is known, and equation (B.5a) can be evaluated directly. At normal pressure, the critical radius as a function of temperature is

$$r^0_{\mathrm{crit}}(T) = \frac{2\sigma_0}{\Delta h\, \rho_{\mathrm{cm}}} \left(\frac{T}{T^o_{\mathrm{m}}} - 1 \right)^{-1} \tag{B.6}$$

At 10 K subcooling, i.e. at $T = 265\,\mathrm{K}$, using $\sigma_0 = -0.077\,\mathrm{Jm}^{-2}$ (extrapolated to 265 K, data from [82]) we get as a typical size of the critical radius of water

$$r^0_{\mathrm{crit}} = 16\,\mathrm{nm} \tag{B.7}$$

Table B.1.: Expected sensitivity of the critical radius to a change in pressure.

	$T^0_{\mathrm{m}} - 10\,\mathrm{K}$ / K	r^0_{crit} / AU	$r_{\mathrm{crit}}(p)/r^0_{\mathrm{crit}}$		
		at 0.1 MPa	at 100 MPa	at 600 MPa	at 900 MPa
H_2O	263	0.16	1.5	–	–
$KF \cdot 4\,H_2O$	281	0.25	0.95	0.78	0.70
$CaCl_2 \cdot 6\,H_2O$	293	0.32	0.45	0.14	0.11
$NaOAc \cdot 3\,H_2O$	321	0.29	0.45	0.14	0.11

B.3. Analysis of high pressure melting and nucleation curves

For the analysis of the high pressure melting and nucleation curves, the uncertainty of measurement data and theoretic curves is required. In this section, first the basics of error calculus are summarized, which are then applied to the high pressure curves. The interpretation of the results is given in the main text in section 4.2.2.

Error calculus

Uncertainty in interpolations

The standard derivation σ is used as a measure of the quality of an interpolation.

The deviation of one datapoint y_i from the mean value $< y >$ is given by

$$\delta y_i = \left| y_i - < y > \right| \tag{B.8a}$$

If not a mean value, but a fitted curve is regarded, the deviation of a data point (x_i, y_i) from the curve $f(x)$ is given by

$$\delta y_i = \left| y_i - f(x_i) \right| \tag{B.8b}$$

The squared mean deviation of all measurement points in one series is then given by the sum of the squared errors of each point

$$\sigma^2 = \frac{1}{n} \sum_{i=1}^{n} \left(y_i - f(x_i) \right)^2 \tag{B.9}$$

Uncertainty in functions

When a value f is determined as a function of uncertain parameters $\vec{x}$, the error in the parameters propagate.

The general formula for error propagation is

$$\delta f(\vec{x})^2 = \sum_i \left(\frac{\partial f}{\partial x_i} \right)^2 \cdot {\delta x_i}^2 \tag{B.10}$$

where all x_i are independent variables.

If f is a linear combination of $\vec{x}$, the summands are equal to the relative errors and

$$\frac{\partial f}{\partial x_i} \cdot \delta x_i = f(\vec{x}) \cdot \frac{\delta x_j}{x_j} \tag{B.11}$$

and thus

$$\frac{{\delta f(\vec{x})}^2}{f(\vec{x})} = \sum_j \left(\frac{\delta x_j}{x_j} \right)^2 \tag{B.12}$$

The absolute error is then

$$\delta f(\vec{x}) = f(\vec{x}) \cdot \sqrt{\sum_j {\frac{\delta x_j}{x_j}}^2} \tag{B.13}$$

Analysis of uncertainty of high pressure data

In this section, the uncertainty of the extrapolations from normal pressure data and the variance of the interpolated high pressure measurement data are determined.

Uncertainty of extrapolations from room data

The linearized Clausisus-Clapeyron as given in equation (2.9b) is used for the extrapolation. Considering the temperature lift only, equation (2.9b) is reduced to

$$\Delta T_\mathrm{m}(p) = T_\mathrm{m}^0 \frac{\Delta v}{\Delta h} \cdot p \tag{B.14}$$

The uncertainty of the melting curve is deduced by error propagation as described in section B.3. While T_m is known to a fraction of a degree for salt hydrate PCM, an uncertainty of at least 5% has to be assumed for both Δh and Δv. The pressure p is the free variable here and is assumed without error. The relative error in T_m is determined using equation (B.12).

For $\mathrm{NaOAc} \cdot 3\,\mathrm{H_2O}$, the calculation reads

$$\begin{aligned} \frac{\delta \Delta T_\mathrm{m}(p)}{\Delta T_\mathrm{m}(p)} &= \sqrt{\left(\frac{\delta T_\mathrm{m}^0}{T_\mathrm{m}^0}\right)^2 + \left(\frac{\delta \Delta v}{\Delta v}\right)^2 + \left(\frac{\delta \Delta h}{\Delta h}\right)^2} \\ &= \sqrt{\left(\frac{0.2}{330}\right)^2 + 0.05^2 + 0.05^2} \\ &\approx 7\% \end{aligned} \tag{B.15a}$$

The uncertainty of the extrapolated rise in the melting temperature is thus about 7% of its value. The contribution of the relative uncertainty in T_m^0 is very small compared to the uncertainties in Δv and Δh. At $p = 400\,\mathrm{MPa}$, the absolute error is

$$\delta \Delta T_\mathrm{m}(400\,\mathrm{MPa}) = 0.07 \cdot 57\,\mathrm{K} = 4\,\mathrm{K} \tag{B.15b}$$

For $\mathrm{CaCl_2} \cdot 6\,\mathrm{H_2O}$, the calculation is very similar and we get with $\Delta T_\mathrm{m}(400\,\mathrm{MPa}) = 54\,\mathrm{K}$ again

$$\delta \Delta T_\mathrm{m}(400\,\mathrm{MPa}) = 0.07 \cdot 54\,\mathrm{K} = 4\,\mathrm{K} \tag{B.16}$$

For $\mathrm{KF} \cdot 4\,\mathrm{H_2O}$, the situation is a bit different. Considering that the volume change for $\mathrm{KF} \cdot 4\,\mathrm{H_2O}$ is very small, a larger uncertainty of at least 20% in room pressure data for Δv seems more realistic. The relative error as in equation (B.12) is then dominated by the term $\delta \Delta v / \Delta v$ and sums up to 21%. In contrast to the other substances, the total change in melting temperature with pressure is very small for $\mathrm{KF} \cdot 4\,\mathrm{H_2O}$, i.e. $\Delta T_\mathrm{m}(400\,\mathrm{MPa}) = 1.9\,\mathrm{K}$. The absolute uncertainty in the rise of the melting temperature for $\mathrm{KF} \cdot 4\,\mathrm{H_2O}$ is then

$$\delta \Delta T_\mathrm{m}(400\,\mathrm{MPa}) = 0.21 \cdot 1.9\,\mathrm{K} = 0.4\,\mathrm{K} \tag{B.17}$$

Uncertainty of interpolations of high pressure data

As to the uncertainty of the measured curves, the uncertainties of the single data points are indicated in the measurement plots in figure 3.21 to figure 3.24. The experimental results do not lie on a linear curve (as supposed by the extrapolation) and are therefore interpolated by a cubic function of the form

$$T_\mathrm{m}(p) = T_\mathrm{m}(p = p_0) + a\,p - b\,p^2 \tag{B.18}$$

The uncertainty of the slope of the curve is determined by statistical analysis as described in section B.3. The coefficients for both melting and nucleation curves of the three sample materials are shown together with the standard deviations in table B.2.

Table B.2.: Values of the fit parameters used to interpolate the experimental results of the high pressure experiments by equation (4.3). Values indicated by *m* refer to melting, *n* to nucleating curves. σ denotes the standard derivation of the measured data with respect to the interpolation.

		a / $10^{-2}\,\mathrm{KMPa^{-1}}$	b / $10^{-5}\,\mathrm{KMPa^{-2}}$	σ / K
$KF \cdot 4\,H_2O$	m	−1.0	−1.4	0.74
	n	0.062	−3.2	2.6
$CaCl_2 \cdot 6\,H_2O$	m	11.9	−4.5	1.1
	n	9.2	−5.0	7.2
$NaOAc \cdot 3\,H_2O$	m	10.4	−3.4	3.8
	n	11	−5.4	2.6

B.4. Effect of variable compressibility on adiabatic heating

In this section, an estimation of adiabatic heating in a material with variable compressibility κ is given based on [103, 159].

For constant κ, adiabatic heating by compression $\Delta T = \Delta T_{\text{compression}}$ is given by

$$\Delta T(p) = \frac{\kappa^2 p^3}{\rho c_p} \tag{B.19}$$

For a large change in pressure, assuming invariable κ could introduce a significant error. In order to consider κ as a function of p [160, 161], a lengthy calculation is required as lined out in the following.

The derivative of equation (B.19) with respect to pressure is

$$\frac{\partial}{\partial p}\Delta T(p) = 3\frac{\kappa^2 p^2}{\rho c_p} \tag{B.20a}$$

i. e. a function of the form

$$\frac{\partial}{\partial p}\Delta T(p) = c\,\kappa^2 p^2 \tag{B.20b}$$

where $c = \frac{3}{\rho c_p}$. c is thus proportional to the thermal mass ρc_p. Postulating an invariance of the thermal mass with pressure, the integral can be evaluated.

The temperature lift caused by adiabatic compression is then given by

$$\Delta T(p) = c\int_0^p \kappa(p')^2 p'^2 \mathrm{d}p' \tag{B.21}$$

The compressibility is approximated by an exponential decay [161] of the form

$$\kappa(p) = a\cdot\exp(b\,p) + \kappa_o \tag{B.22}$$

as shown in figure B.3.

Then, the temperature lift due to adiabatic compression as a function of pressure can be written as

$$\begin{aligned}
\Delta T(p) &= c\int_0^p \left[a^2\cdot\exp(2b\,p') + \kappa_0^2 + 2\kappa_0\, a\cdot\exp(b\,p')\right] p'^2 \mathrm{d}p' && \text{(B.23a)}\\
&= \tau_0 + \frac{\kappa_0^2\, c}{3}p^3 + ac\,\kappa_0\int_0^p p'^2\exp(2b\,p')\mathrm{d}p' && \text{(B.23b)}\\
&\quad + a^2 c\int_0^p p'^2\exp(b\,p')\mathrm{d}p'
\end{aligned}$$

τ_0 is an integration constant to be determined later.

To evaluate this integral, integrals of the form

$$\int x^\alpha\, e^{\beta x} dx \tag{B.24}$$

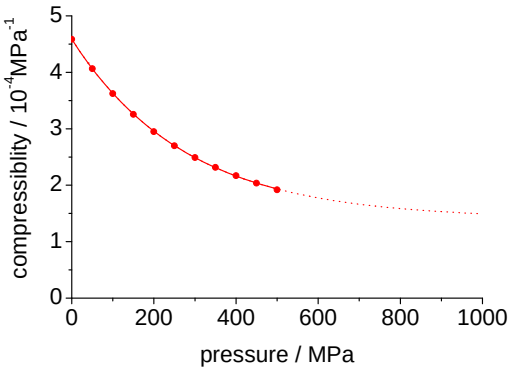

Figure B.3.: Compressibility of water using data from [161] and extrapolation to higher pressures.

have to be solved. For $\alpha \in (1,2)$, this is done by applying the integration by parts method, which results in

$$\int x^{\alpha}\, e^{\beta x} dx \;=\; x^{\alpha} \cdot \frac{1}{\beta} \cdot e^{\beta x} - \int \frac{1}{\beta} \cdot e^{\beta x} \alpha\, x^{\alpha-1} \mathrm{d}x \tag{B.25}$$

The exponent of x in the integral can thus be decremented stepwise until a simple exponential integral remains to be solved.

Using

$$\alpha_{1,2} \;=\; 2,1 \tag{B.26a}$$
$$\beta_{1,2} \;=\; b,2b \tag{B.26b}$$
$$x \;=\; p \tag{B.26c}$$

after two iterations and integration of a simple exponential term, the integral is

$$\begin{aligned} \Delta T(p) \;=\; & ac\,\kappa_0 \left[p^2 \cdot \frac{1}{2b} \cdot e^{2bp} - \frac{2}{2b} \left(p \cdot \frac{1}{2b} \cdot e^{2bp} - \frac{1}{4b^2} \cdot e^{2bp} \right) \right] \\ & + a^2 c \left[p^2 \cdot \frac{1}{b} \cdot e^{bp} - \frac{2}{b} \left(p \cdot \frac{1}{b} \cdot e^{bp} - \frac{1}{b^2} \cdot e^{bp} \right) \right] + \frac{\kappa_0^2\, c}{3} p^3 + \tau_1 \end{aligned} \tag{B.27a}$$

Introducing simple coefficients, this is

$$\begin{aligned} \Delta T(p) \;=\; & a_1 p^3 + a_2 + a_3 \left(a_4 p^2 + a_5 p + a_6 \right) e^{a_7 p} \\ & + a_8 \left(a_9 p^2 + a_{10} p + a_{11} \right) e^{a_{12} p} \end{aligned} \tag{B.27b}$$

The coefficients are listed in table B.3.

τ_1 is the overall integration constant, and has to fulfill the following relation

$$\Delta T(p=0) \;\stackrel{!}{=}\; 0 \tag{B.28a}$$

Table B.3.: Coefficients in equation (B.27b).

$a_1 = \frac{\kappa_0^2 c}{3}$	$a_5 = -\frac{1}{2b^2}$	$a_9 = \frac{1}{b}$
$a_2 = \tau_1$	$a_6 = \frac{1}{4b^3}$	$a_{10} = -\frac{2}{b^2}$
$a_3 = ac\,\kappa_0$	$a_7 = 2b$	$a_{11} = \frac{2}{b^3}$
$a_4 = \frac{1}{2b}$	$a_8 = a^2 c$	$a_{12} = b$

such that

$$\begin{aligned} \tau_1 &= -\frac{ac\kappa_0}{4b^3} - \frac{a^2 c}{b^3} \\ &= -\frac{ac}{b^3}\left(\kappa_0/4 + a\right) \end{aligned} \tag{B.28b}$$

The values for the constants in equation (B.27a) are for water

$$\rho c_p \approx 4.2 \cdot 10^{-6}\,\mathrm{J\,m^{-3}\,K^{-1}} \tag{B.29a}$$
$$c \approx 7.1 \cdot 10^{5}\,\mathrm{J^{-1}\,m^{3}\,K} \tag{B.29b}$$
$$\kappa_0 = 1.40 \cdot 10^{-4}\,\mathrm{MPa^{-1}} \tag{B.29c}$$
$$a = 3.18 \cdot 10^{-4}\,\mathrm{MPa^{-1}} \tag{B.29d}$$
$$b = -1/278\,\mathrm{MPa} \tag{B.29e}$$

This results in the coefficients as listed in table B.4.

Table B.4.: Values of coefficients in equation (B.27b). for water

$a_1 = 4.6 \cdot 10^{-3}\,\mathrm{K MPa^{-1}}$	$a_5 = -3.8 \cdot 10^{4}\,\mathrm{MPa^2}$	$a_9 = -278\,\mathrm{MPa}$
$a_2 = 3.3\,\mathrm{K}$	$a_6 = -5.4 \cdot 10^{6}\,\mathrm{MPa^3}$	$a_{10} = -1.5 \cdot 10^{5}\,\mathrm{MPa^2}$
$a_3 = 3.2 \cdot 10^{-4}\,\mathrm{K MPa^{-1}}$	$a_7 = -7.2 \cdot 10^{-3}\,\mathrm{MPa^{-1}}$	$a_{11} = -4.3 \cdot 10^{7}\,\mathrm{MPa^3}$
$a_4 = -139\,\mathrm{MPa}$	$a_8 = 7.2 \cdot 10^{-4}\,\mathrm{K MPa^{-1}}$	$a_{12} = -3.6 \cdot 10^{-3}\,\mathrm{MPa^{-1}}$

Substituting in equation (B.27b), and with $\pi = p/\,\mathrm{MPa}$, we finally get

$$\begin{aligned} \Delta T(\pi) = {} & 4.6 \cdot 10^{3}\,\mathrm{K}\,\pi^3 + 3.3\,\mathrm{K} \\ & + 3.2 \cdot 10^{2}\,\mathrm{K}\left(139\,\pi^2 - 3.8 \cdot 10^{4}\,\pi - 5.4 \cdot 10^{6}\right) e^{-7.2 \cdot 10^{-3}\,\pi} \\ & - 7.2 \cdot 10^{2}\,\mathrm{K}\left(278\,\pi^2 + 1.5 \cdot 10^{5}\,\pi + 4.3 \cdot 10^{7}\right) e^{-3.6 \cdot 10^{-3}\pi} \end{aligned} \tag{B.30}$$

This is plotted together with the results without taking account of variable compressivity in figure B.4.

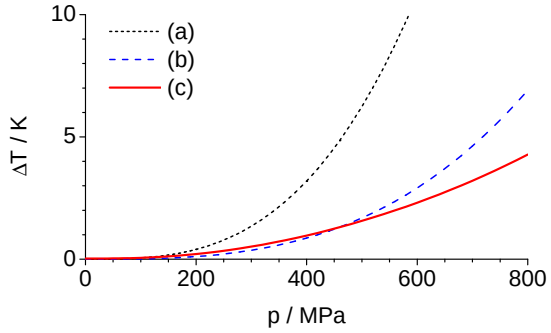

Figure B.4.: Adiabatic heating using constant (a,b) or variable (c) compressibility.

The value for the constant compressibility curves is taken as the compressiblity at normal pressure (a) and as the average value in the drawn range (b). In case (a), the heating is overestimated. In case (b), the heating is underestimated for low pressures and overestimated for high pressures. Although pressure dependent compressibility data for salt hydrates is missing, the results are probably in a similar order of magnitude.

B.5. Effect of evaporative cooling during cavitation

In this section, an estimate of the effect of evaporative cooling in a cavitation bubble is presented. The obtainable cooling effect is estimated for a simplified situation as sketched in figure B.5.

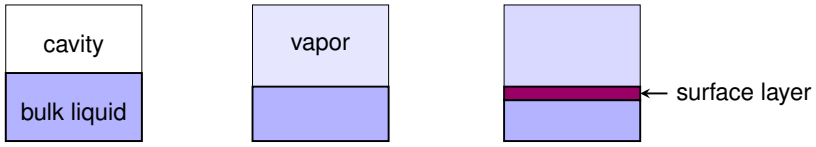

(a) stage 1 **(b)** stage 2 **(c)** stage 3

Figure B.5.: The cooling effect is estimated in two steps: a cavity (a) is filled with vapor from the bulk liquid (b). This evaporation cools the surface layer (c).

An empty cavity of radius r in water at 273 K is assumed. For simplicity, the surface is treated as planar[2]. Water from the surface evaporates into the cavity until the vapor pressure [162] is reached.

The energy required to evaporate enough water to fill the cavitation is given by

$$\Delta H = \Delta h \rho_{\text{vap}} \cdot \frac{4}{3}\pi r^3 \tag{B.31}$$

This heat is extracted from the bubble surface layer. The surface layer experiences a mean change in temperature ΔT

$$\Delta T = \frac{\Delta H}{c_{p,\text{liq}} m_{\text{liq}}} \tag{B.32}$$

where the surface layer mass m_{liq} is for a layer of thickness Δx

$$m_{\text{liq}} = \frac{4}{3}\pi \left[(r+\Delta x)^3 - r^3\right] \cdot \rho_{\text{liq}} \tag{B.33}$$

In order to reach a mean temperature T, the evaporative cooling should penetrate the liquid at most to

$$\begin{aligned} \Delta x &= \left(\frac{3 m_{\text{liq}}}{4\pi\rho_{\text{liq}}} + r^3\right)^{\frac{1}{3}} - r \\ &= \left(\frac{3}{4\pi} \cdot \frac{\Delta h \rho_{\text{vap}} \cdot \frac{4}{3}\pi r^3}{c_{p,\text{liq}} \rho_{\text{liq}} \Delta T} + r^3\right)^{\frac{1}{3}} - r \\ &= r \cdot \left(1 + \frac{\Delta h}{c_p \Delta T} \cdot \frac{\rho_{\text{vap}}}{\rho_{\text{liq}}}\right)^{\frac{1}{3}} - r \end{aligned} \tag{B.34}$$

[2] As lined out in section 2.1.2, this simplification is valid for water droplets larger than μm.

which, using the input paramaters

$$\rho_{\mathrm{vap}}(273\,\mathrm{K}) = 4.847\,\mathrm{kg/m^3} \tag{B.35a}$$
$$\rho_{\mathrm{liq}} = 1\cdot 10^3\,\mathrm{kg/m^3} \tag{B.35b}$$
$$\Delta h = 334\,\mathrm{J/g} \tag{B.35c}$$
$$c_{p,\mathrm{liq}} = 4.2\,\mathrm{J/gK} \tag{B.35d}$$
$$\Delta T = 40\,\mathrm{K} \tag{B.35e}$$

results in

$$\begin{aligned}\frac{\Delta x}{r} &= \left(1+\frac{334}{168}\cdot 4.847\cdot 10^{-3}\right)^{\frac{1}{3}}-1 \\ &= 3.2\cdot 10^{-3}\end{aligned} \tag{B.36}$$

Considering the size of the critical radius, which is supposed to in the range of some nm at this temperature according to equation (B.6), a bubble size of about $r \geq 5\,\mu$m would be large enough to deliver enough evaporative cooling.

The presented calculation considers only the energy balance. The required cavity sizes should be easily obtainable in ultrasonic cavitation. Therefore, the critical question is in fact rather about dynamics and heat transport.

B.6. Details of the observations of solidifying salt hydrates

In this section, details of the observations of the solidifying salt hydrates are presented. The speed of solidification was determined by evaluation of the movement of the phase boundary, which is clearly visible as a strong contrast in the graphs. Still images from the films that were recorded with the IR camera and the evaluated speeds of solidification are shown. A comparison to literature values is done for $NaOAc \cdot 3\,H_2O$, the only substance where published data was available.

$KF \cdot 4\,H_2O$

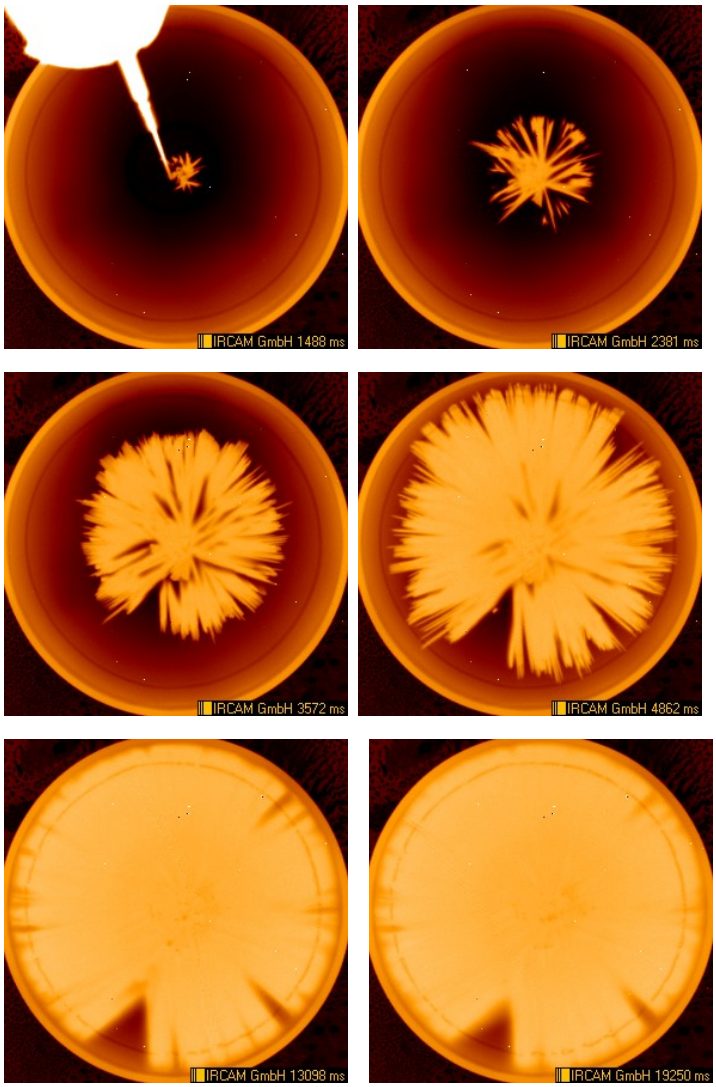

Figure B.6.: Stills from the IR camera recording of solidifying $KF \cdot 4\,H_2O$, sample 1, $T \approx 283\,K$.

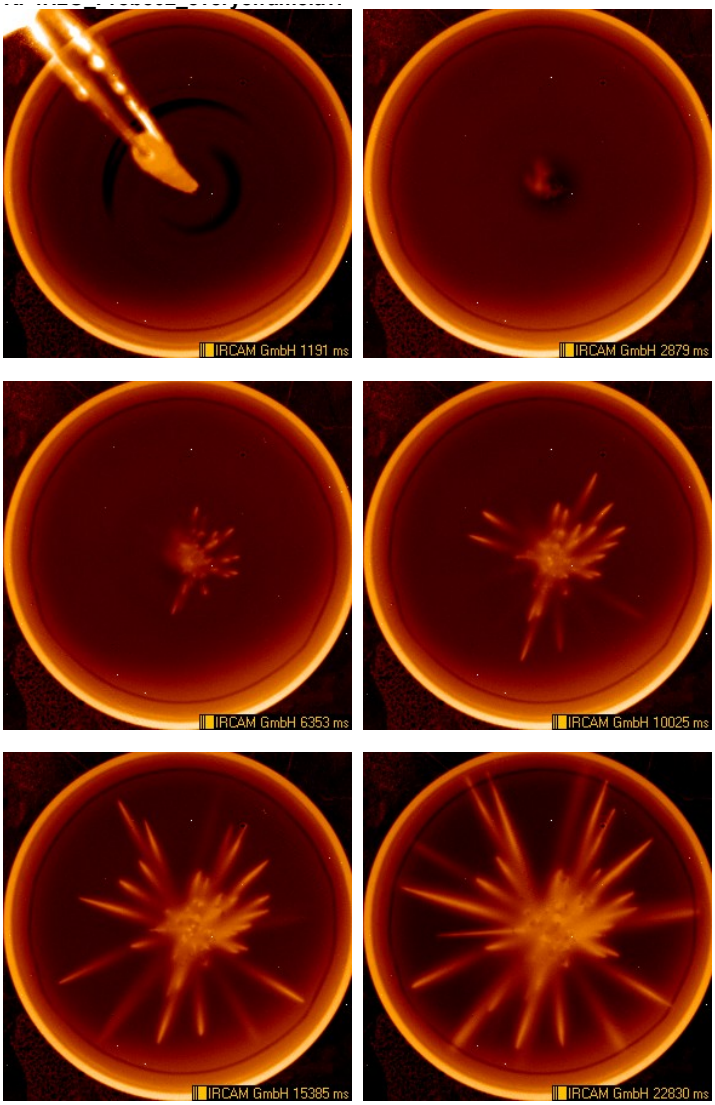

Figure B.7.: Stills from the IR camera recording of solidifying $KF \cdot 4\,H_2O$, sample 2, $T \approx 292\,K$.

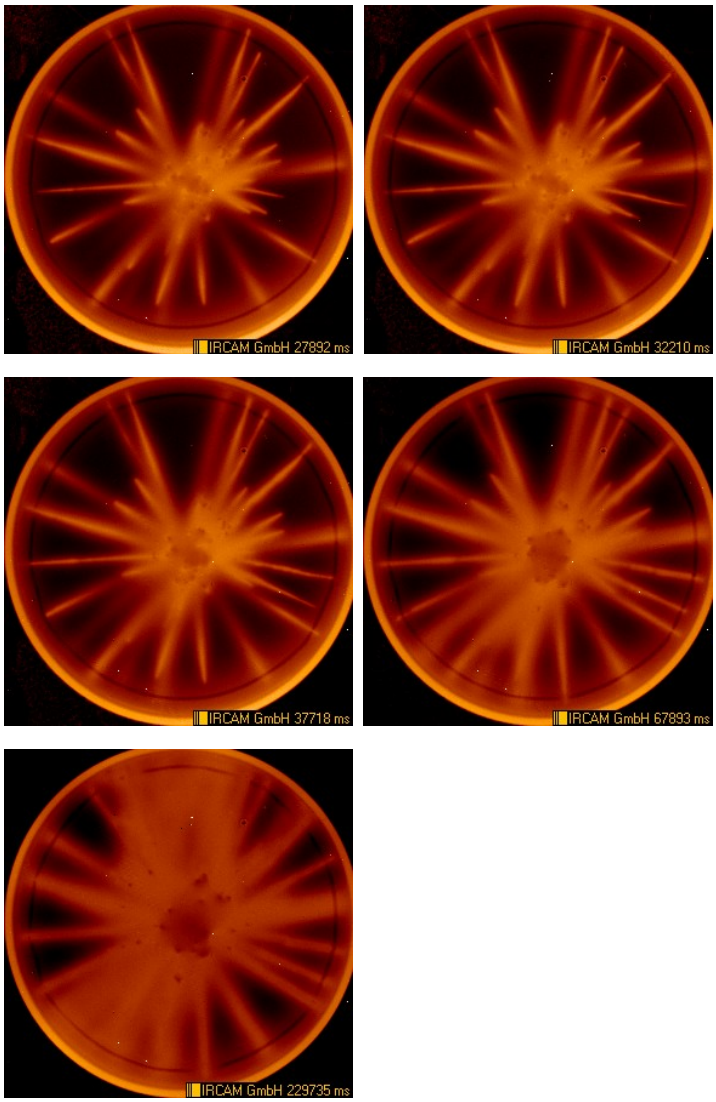

Figure B.8.: Stills from the IR camera recording of solidifying $KF \cdot 4\,H_2O$, sample 2 continued, $T \approx 292\,K$.

In figure B.9, the results are presented in a graph.

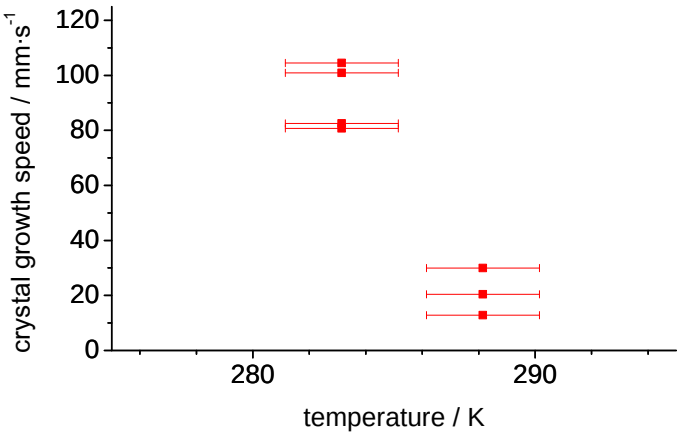

Figure B.9.: Speed of solidification of $KF \cdot 4\,H_2O$ as determined by the IR measurements.

Different needle tips were evaluated for each temperature level. The speeds of the individual needles show significant difference. The overall speed of solidification is fast compared to the other salt hydrates.

$CaCl_2 \cdot 6\,H_2O$

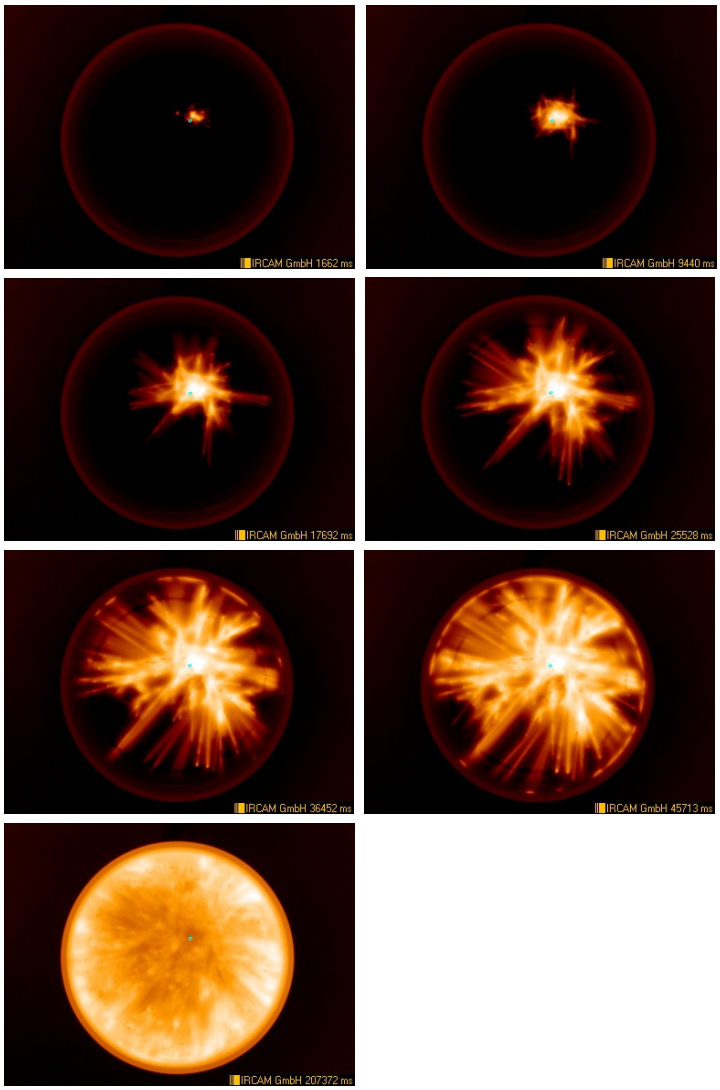

Figure B.10.: Stills from the IR camera recording of solidifying $CaCl_2 \cdot 6\,H_2O$, sample 1, $T \approx 293\,K$.

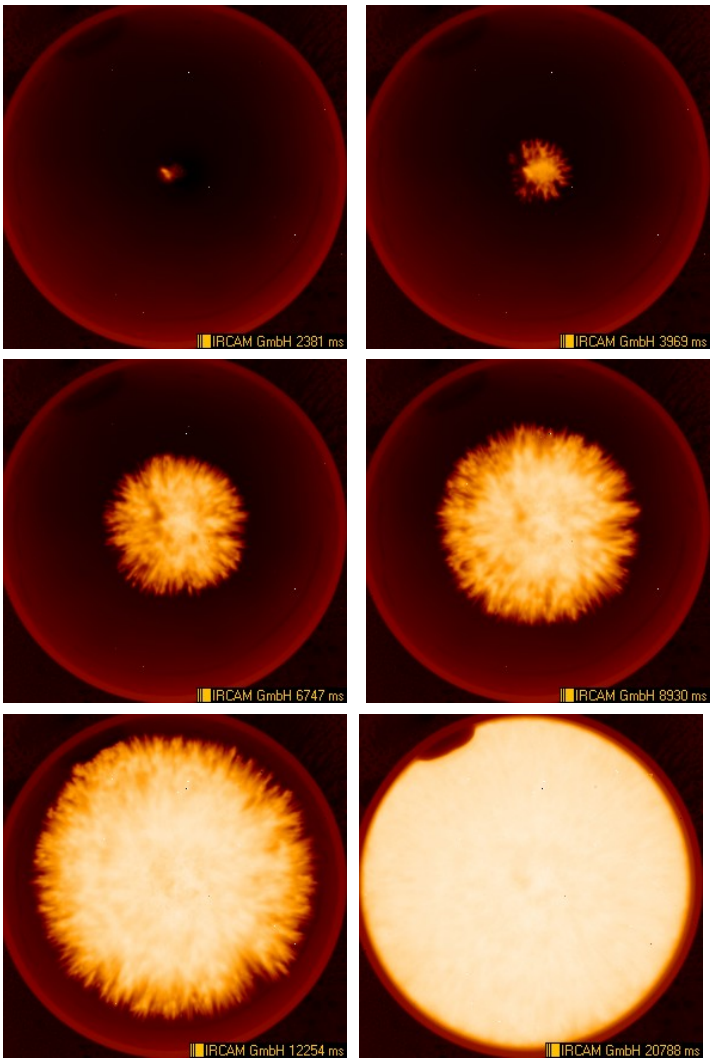

Figure B.11.: Stills from the IR camera recording of solidifying $CaCl_2 \cdot 6\,H_2O$, sample 3, $T \approx 283\,K$.

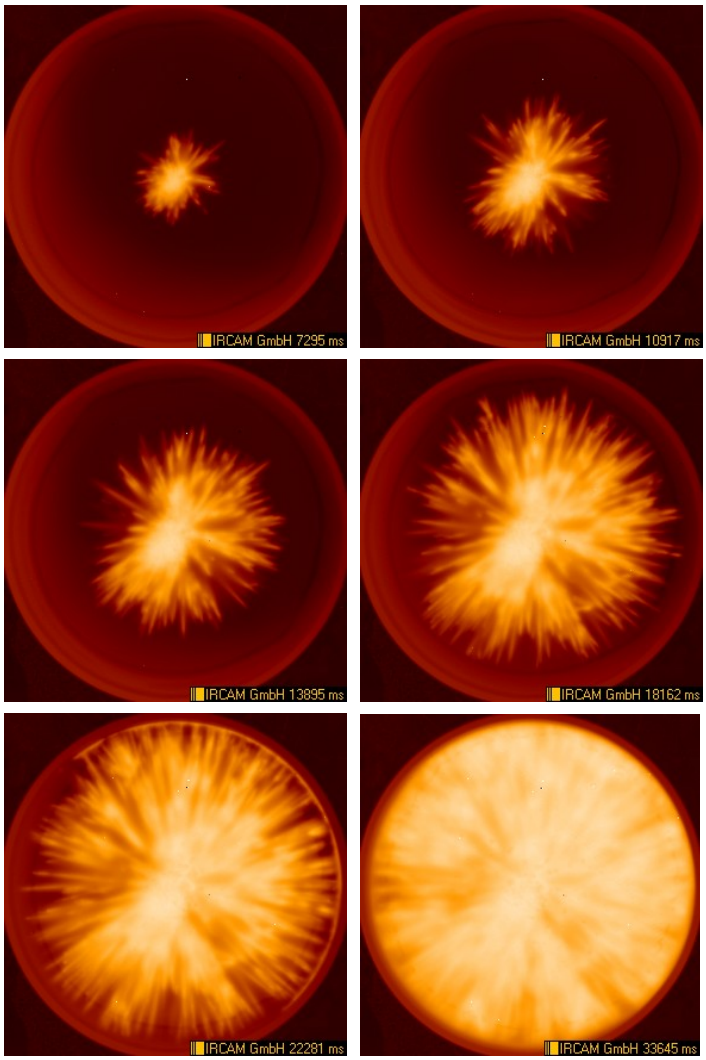

Figure B.12.: Stills from the IR camera recording of solidifying $CaCl_2 \cdot 6\,H_2O$, sample 4, $T \approx 288\,K$.

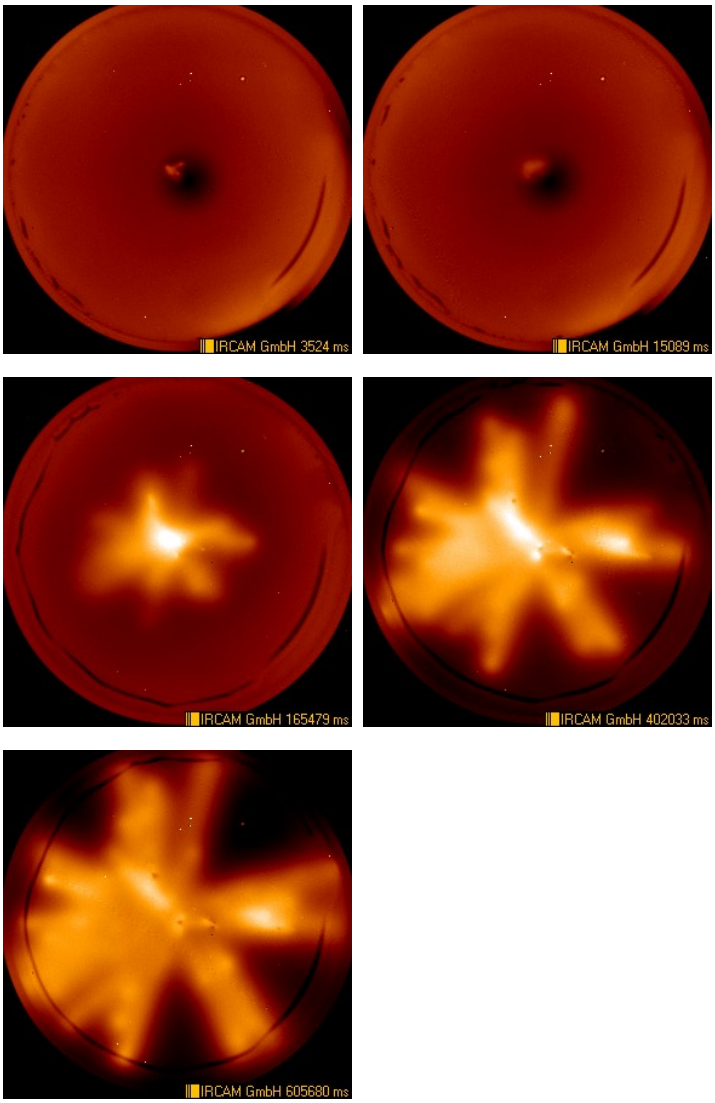

Figure B.13.: Stills from the IR camera recording of solidifying $CaCl_2 \cdot 6\,H_2O$, sample 5, $T \approx 297\,K$.

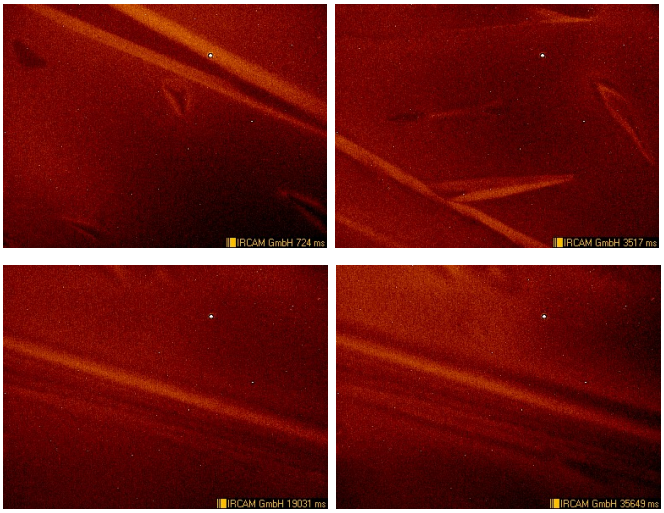

Figure B.14.: Stills from the IR camera recording of solidifying $CaCl_2 \cdot 6\,H_2O$, using a microscopic lens, part 1, $T \approx 283\,K$.

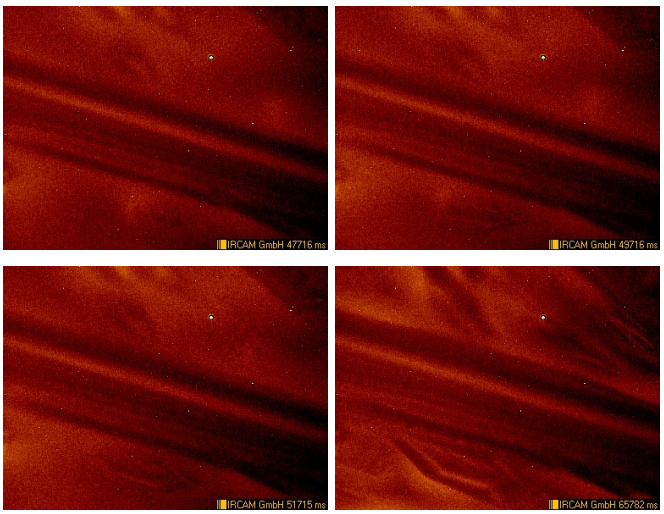

Figure B.15.: Stills from the IR camera recording of solidifying $CaCl_2 \cdot 6\,H_2O$, using a microscopic lens, part 2, $T \approx 283\,K$.

In figure B.16, the results are presented in a graph.

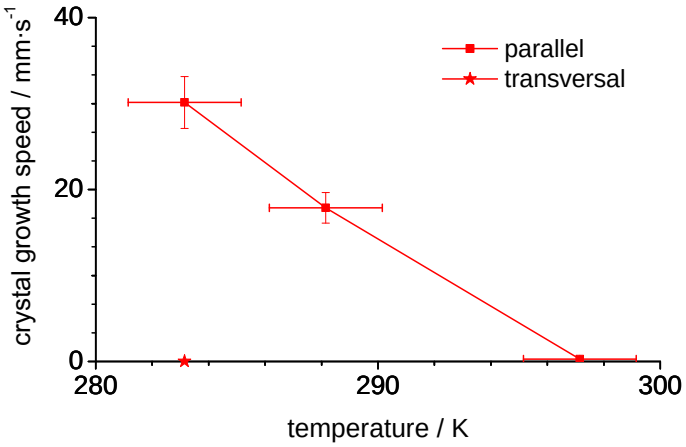

Figure B.16.: Speed of solidification of $CaCl_2 \cdot 6\,H_2O$.

The speed of solidification was evaluated for the direction of needle growth (“parallel”) and perpendicular to the needle growth (“transversal”), as shown in figure B.14 and B.15. The recordings using the microscopic lens were difficult to carry out and evaluate, because the needles move in the solidifying liquid and thus move out of focus continuously.

$NaOAc \cdot 3\,H_2O$

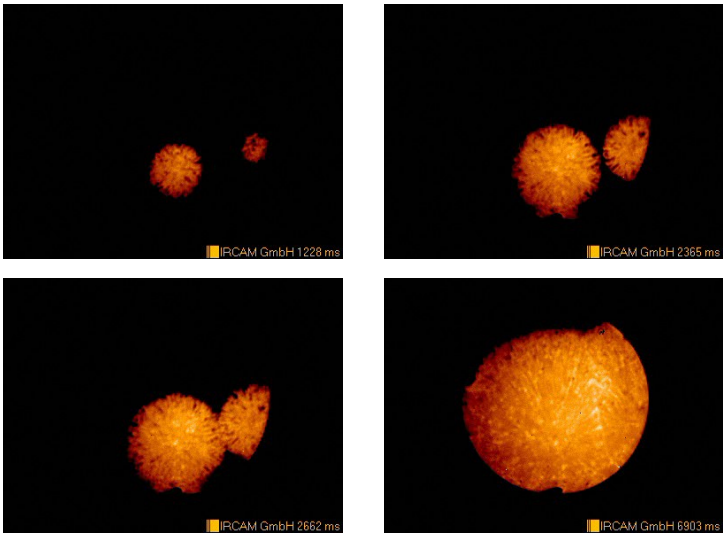

Figure B.17.: Stills from the IR camera recording of solidifying $NaOAc \cdot 3\,H_2O$, sample 1, $T \approx 313\,K$. Here, two seed crystals in asymmetric position were dropped in the subcooled sample. It can be observed in the last image, that the "grain boundary" is linear. This is a clear indication of a constant speed from both seed locations.

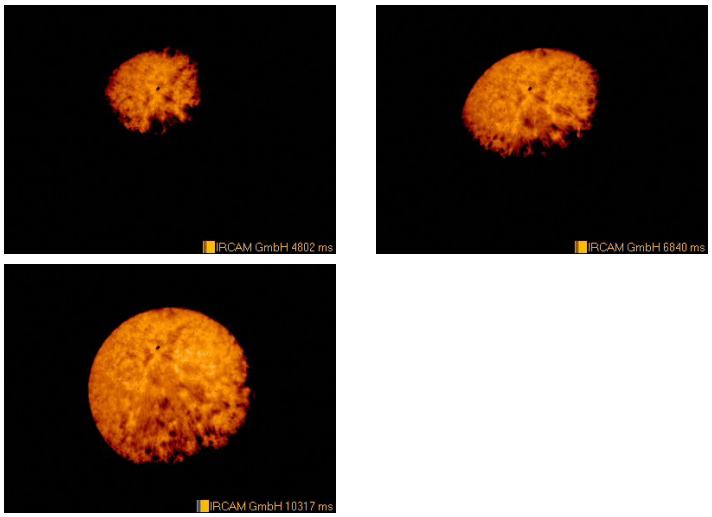

Figure B.18.: Stills from the IR camera recording of solidifying $NaOAc \cdot 3\,H_2O$, sample 2, $T \approx 313\,K$.

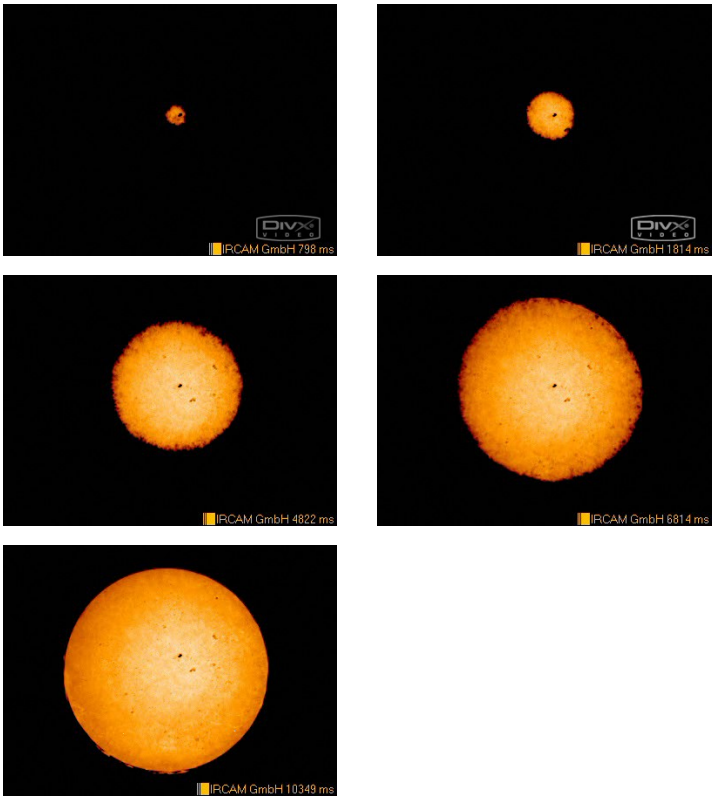

Figure B.19.: Stills from the IR camera recording of solidifying $NaOAc \cdot 3\,H_2O$, sample 3, $T \approx 313\,K$.

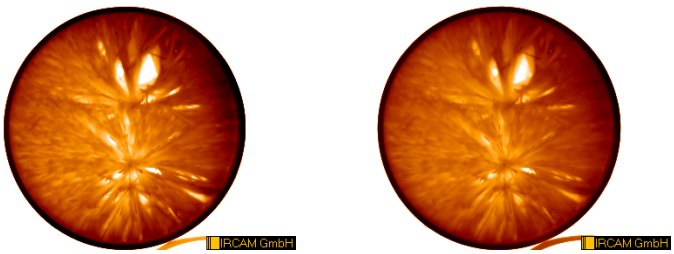

Figure B.20.: Stills from the IR camera recording of solidifying $NaOAc \cdot 3\,H_2O$, sample 4, $T \approx 313\,K$.

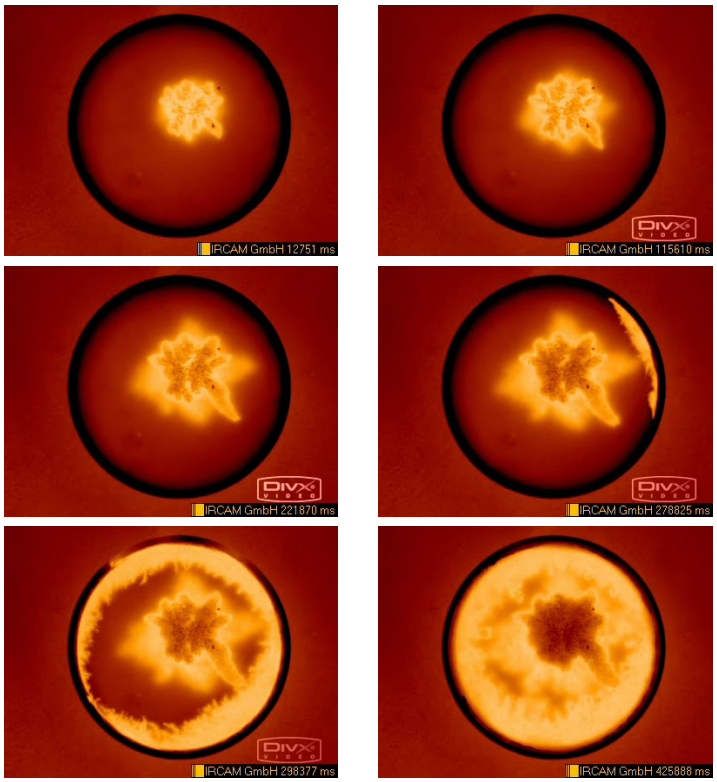

Figure B.21.: Stills from the IR camera recording of solidifying $NaOAc \cdot 3\,H_2O$, sample 5, $T \approx 328\,K$.

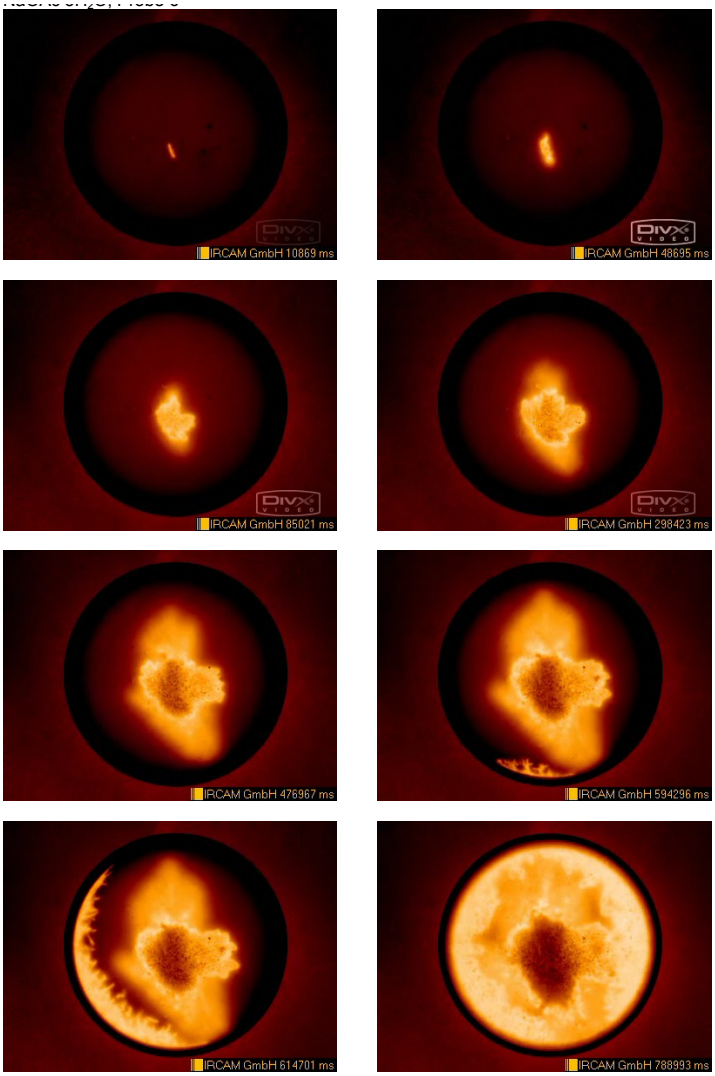

Figure B.22.: Stills from the IR camera recording of solidifying $NaOAc \cdot 3\,H_2O$, sample 6, $T \approx 328\,K$.

In figure B.23, the results are compared to literature data and preliminary measurements. Data from the presented IR measurements (line 1) is compared to preliminary measurments using a different IR camera (line 2) and a video camera (line 3), and to literature data from Wada et al. [163] and Rogerson and Cardoso [75].

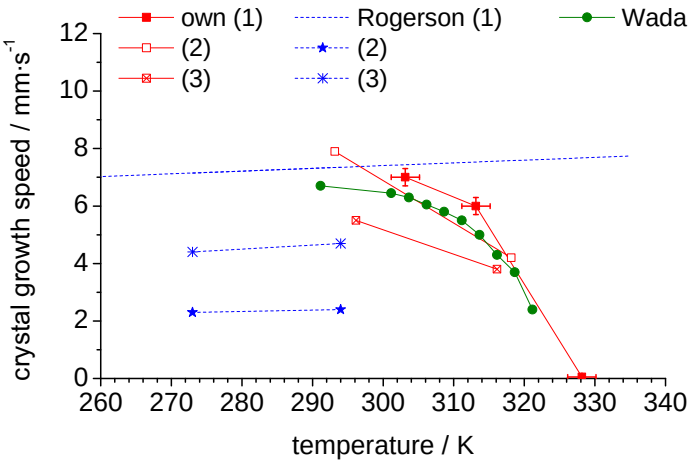

Figure B.23.: Speed of solidification of $NaOAc \cdot 3\,H_2O$ as determined in this study and literature data from Wada et al. [163] and Rogerson and Cardoso [75]; see text below.

In the work of Rogerson, the speed of crystal growth was measured on diluted $NaOAc \cdot 3\,H_2O$ (lines 1,2 in the graph) and the data for the stoichiometric trihydrate was determined by extrapolation (line 3 in the graph). The data of Rogerson does not show a reduced speed of crystallization for temperatures close to the melting temperature. This is due to the extrapolation from only two temperatures far away from the melting temperature. The extrapolation with respect to the water content is however rather successful.

The preliminary measurements using a video camera were very difficult to evaluate because of low contrast and difficult location of the phase front. This is particularly a problem for $NaOAc \cdot 3\,H_2O$ which tends to form an opaque layer of dehydrated salt on the sample surface. Therefore, an IR camera available at the chair of Prof. Voigt [76] was tested for better contrast. These test were successful and another IR camera available at ZAE division 3 in Erlangen could be used for the following experiments. The data acquired in this final setup are in good agreement with data by Wada.